bioengineering

Advances in Polyhydroxyalkanoate (PHA) Production, Volume 2

Edited by
Martin Koller

Printed Edition of the Special Issue Published in *Bioengineering*

www.mdpi.com/journal/bioengineering

MDPI

Advances in Polyhydroxyalkanoate (PHA) Production, Volume 2

Advances in Polyhydroxyalkanoate (PHA) Production, Volume 2

Special Issue Editor

Martin Koller

MDPI • Basel • Beijing • Wuhan • Barcelona • Belgrade

Special Issue Editor
Martin Koller
Office of Research Management
and Service, c/o Institute of
Chemistry, University of Graz
Austria

Editorial Office
MDPI
St. Alban-Anlage 66
4052 Basel, Switzerland

This is a reprint of articles from the Special Issue published online in the open access journal *Bioengineering* (ISSN 2306-5354) from 2018 to 2020 (available at: https://www.mdpi.com/journal/bioengineering/special_issues/PHA2).

For citation purposes, cite each article independently as indicated on the article page online and as indicated below:

LastName, A.A.; LastName, B.B.; LastName, C.C. Article Title. *Journal Name* **Year**, *Article Number*, Page Range.

ISBN 978-3-03928-640-9 (Pbk)
ISBN 978-3-03928-641-6 (PDF)

Cover image courtesy of Martin Koller.

Contents

About the Special Issue Editor

Martin Koller completed his doctoral thesis under the supervision of one of the most eminent PHA pioneers, Prof. Gerhart Braunegg, on PHA production from dairy surplus streams; these activities were part of the EU-FP5 project WHEYPOL. Afterwards, he became an experienced researcher in the PHA field, working on the development of continuous and discontinuous fermentation processes and novel downstream processes for sustainable PHA recovery.

His research is focused on the cost-efficiency of PHA production from surplus materials by eubacteria and haloarchaea. He has numerous articles in high-ranked scientific journals, has authored several chapters in scientific books, has given numerous lectures at international conferences, and is an active member of the Editorial Board of numerous distinguished scientific journals. From 2010 to 2012, he acted as coordinator of the EU-FP7 project ANIMPOL, which investigated the conversion of waste streams from the animal processing industry towards structurally diversified PHAs and marketable follow-up products.

bioengineering

MDPI

Editorial

Advances in Polyhydroxyalkanoate (PHA) Production, Volume 2

Martin Koller [1,2]

[1] Institute of Chemistry, University of Graz, NAWI Graz, Heinrichstrasse 28/VI, 8010 Graz, Austria; martin.koller@uni-graz.at; Tel.: +43-316-380-5463

[2] ARENA—Association for Resource Efficient and Sustainable Technologies, Inffeldgasse 21b, 8010 Graz, Austria

Received: 19 February 2020; Accepted: 2 March 2020; Published: 4 March 2020

Abstract: During the two years that have passed since the first volume of "Advances in Polyhydroxyalkanoate (PHA) production" was published, the progress in PHA-related research was indeed tremendous, calling for the next, highly bioprocess- and bioengineering-oriented volume. This editorial paper summarizes and puts into context the contributions to this second volume of the *Bioengineering* Special Issue; it covers highly topical fields of PHA-related R&D activities, covering, beside the pronounced bioengineering-related articles, the fields of the microbiology of underexplored, but probably emerging, PHA production strains from the groups of *Pseudomonas*, cyanobacteria, methanotrophs, and from the extremophilic domain of haloarchaea. Moreover, novel second-generation lignocellulose feedstocks for PHA production from agriculture to be used in biorefinery concepts, new approaches for fine-tuning the composition of PHA co- and terpolyesters, process simulation for PHA production from methane-rich natural gas, the challenges associated with rheology-governed oxygen transfer in high cell density cultivations, rapid spectroscopic in-line analytics for process monitoring, and the biomedical application of PHA biopolyesters after appropriate advanced processing are the subjects of the presented studies.

Keywords: biomedical application; cyanobacteria; feedstocks; gaseous substrates; haloarchaea; high cell density cultivation; in-line monitoring; PHA composition; PHA processing; polyhydroxyalkanoate; process engineering; process simulation; *Pseudomonas* sp.; rheology; terpolyester; waste streams

1. Introduction

Nowadays, we are witnessing highly dynamic research activities in the captivating field of biodegradable materials with plastic-like properties. These activities are indeed boosted by an increasing public awareness of prevailing ecological issues connected to growing piles of plastic waste, the microplastic predicament, new regulations for plastic use and management, and increasing greenhouse gas emissions contributing to global warming and climate change. These environmental concerns go in parallel with the continuing depletion of fossil feedstocks, which are used at present to produce established full carbon backbone plastics. To a gradually increasing extend, polyhydroxyalkanoate (PHA) biopolyesters, a family of microbial storage compounds with versatile plastic-like material properties, are considered a future-oriented answer to these problems. Bio-catalyzed PHA production is based on renewable resources, and occurs in vivo by the action of living prokaryotic cells. If performed in an optimized way, both PHA production and the entire lifecycle of PHA-based products are embedded into nature´s closed carbon cycle [1]. Still, experts in this field emphasize that sustainable and efficient PHA production requires the understanding and optimization of all individual process steps [2]. The holistic improvement of PHA production, applicable also on an industrial scale, *inter alia* calls for: optimized bioprocess engineering and adapted

fermentation modes [3], consolidated knowledge about the enzymatic, metabolic, and genetic ongoings in PHA accumulating organisms in the context of "Next Generation Industrial Biotechnology" [4], the multi-facetted role of PHA granules in living cells and the impact of environmental stress factors on PHA formation [5], an in-depth understanding of the kinetics of the bioprocess [6], the selection of ethically clear, inexpensive feedstocks [7,8], tailoring the composition of PHA on the level of the monomeric constituents [9], and efficient and ecologically benign strategies for PHA recovery from biomass [10].

Since the publication of the first *Bioengineering* Special Issue, "Advances in Polyhydroxyalkanoate (PHA) production", two years have passed [11]. During this period, global R&D activities in the field of PHA biopolyesters have increased at a breathtaking pace, with several new ambitious and highly specialized research groups now having succeeded to become global trendsetters in this scientific field. In view of the apparently exponentially growing number of relevant publications, it is actually a challenging task to completely and permanently keep up with all the ongoing developments in PHA research. Hence, it is definitely time for an update on the *status quo* of PHA research! Therefore, this Special Issue of articles addresses several distinguished aspects of the PHA production chain; it consists of a total of eleven original articles and specialized review papers written by globally recognized experts who have had a significant impact on this research area already for a long time, and by emerging groups who have only recently consolidated their scientific position in the PHA community.

2. Individual Contributions

The search for novel, inexpensive, and amply available feedstocks for ethically clear and economic PHA production is a research direction that is still heavily pursued. In this context, the Mexican research group of Yolanda González-García and colleagues resorted to tequila agave bagasse (TAB), which constitutes the lignocellulosic, fibrous waste stream originating from tequila production. TAB accrues in large amounts and currently has to be disposed of somehow. Therefore, the use of hydrolyzed TAB as a source of hexose and pentose sugars for the production of poly(3-hydroxybutyrate) (PHB) homopolyester by the strain *Burkholderia sacchari* was studied. For this purpose, TAB was chemically hydrolyzed to xylose (pentose) and glucose (hexose) as the main sugars. Next, the effect of hydrolysis by-products, such as phenolic compounds, on *B. sacchari* growth was evaluated. After the removal of those inhibiting phenolics by convenient methods, the detoxified hydrolysate was used as feedstock for PHB production in a two-step batch cultivation process, resulting in a PHB concentration of almost 3 g/L after 122 h of cultivation. This study provides another example how PHA production can be integrated into the production lines of existing agricultural and food-processing industries in order to upgrade existing waste streams to feedstocks for biopolymer production [12].

Dan Kucera and co-workers optimized the production of PHA terpolymers with enhanced material properties consisting of 3-hydroxybutyrate (3HB), 3-hydroxyvalerate (3HV), and 4-hydroxybutyrate (4HB) using the short-chain length (*scl*-) PHA producer *Cupriavidus* sp. DSM 19379. Cultivations in presence of the 4HB-precursor compounds γ-butyrolactone (GBL), ε-caprolactone, 1,4-butanediol, and 1,6-hexanediol resulted in the biosynthesis of PHA copolyesters consisting of 3HB and 4HB building blocks. Furthermore, single- and two-stage production strategies were tested for the production of terpolyesters consisting of 3HB, 3HV, and 4HB monomers. During single-stage cultivation, GBL and 1,4-butanediol served as the main substrates, while propionic and valeric acid acted as 3HV-precursors. During two-stage production, glycerol was used in the phase of biomass growth, while 3HV- and 4HB-precursors for terpolyester formation were used in the second, nitrogen-limited, cultivation phase. The obtained terpolyesters contained 0%–29% mol 3HV and 16%–32% mol 4HB and were thoroughly characterized by state-of-the art analytical tools in order to assess their thermo-mechanical properties and molecular mass distribution in dependence on the PHA composition [13].

Warren Blunt and associate researchers addressed the important topic of high-cell-density cultivations, which are a pre-condition for high-throughput, high-productivity PHA production.

However, high-cell-density cultivations pose bioengineering challenges; in the bioreactor, the increasing viscosity severely impacts oxygen import by making mixing and sparging more difficult. To get detailed knowledge about the impact of high-cell-density fed-batch cultivation on the kinetics of PHA-accumulating strain *Pseudomonas putida* LS46, the time-dependent rheological properties of the microbial cultures were followed during cultivations. It was shown that increasing cell density drastically increases culture viscosity, making the cultivation broth increasingly shear-thinning. However, at increasing shearing rates, shear-thickening behavior was observed. It was shown that the cell-free supernatant contributed more to observed viscosity than the cells themselves. As a consequence, the oxygen transfer performance of the bioreactor system dropped to only 50% of the performance at the beginning of the cultivation, showing that the dynamic rheological behavior of high-cell-density cultures is a pivotal process engineering parameter to be considered, which severely impacts the success of PHA production processes in terms of the productivity, scalability, and efficiency of downstream processing [14].

High-cell-density fed-batch cultures of *Pseudomonas putida* LS46 were also studied in the second article by W. Blunt et al., who tested a reactive pulse feeding approach based on real-time measurements of CO_2 and dissolved oxygen (DO) as feedback variables. This way, an oxygen-limited fed-batch process for enhanced medium chain length (*mcl*-) PHA productivity was developed. Using octanoic acid as the sole carbon source in a bioreactor operated under atmospheric conditions, about 30 g/L cell dry mass (CDM), containing about 60 wt.% of *mcl*-PHA (volumetric productivity: about 0.7 g/(L·h)) was obtained within 27 h of operation, although the onset of oxygen limitation occurred already 14 h after start of the process. While supplying the carbon source via a "continuous drip feed process" (determined as a "proactive feeding strategy" in contrast to pulse feeding) did not significantly impact the final volumetric productivity, it favored the production of non-PHA biomass during bacterial growth, while pulse feeding boosted *mcl*-PHA concentration and product yield during the accumulation phase. Hence, intrinsic O_2-limitation in high-cell-density cultivation setups can be implemented as a convenient and efficient control tool for enhanced *mcl*-PHA synthesis from long chain carboxylic acids. Furthermore, the pulse feed strategy turned out as a reliable and relatively easy strategy for quick optimization of fed-batch processes, especially in the case of rather toxic substrates like octanoic acid [15].

In the context of *mcl*-PHA, Grazia Licciardello and associated scientists comprehensively reviewed the co-production of elastomeric *mcl*-PHA and extracellular products (EPS, mainly alginates) both on related and unrelated carbon sources by strains of *Pseudomonas corrugata* and *P. mediterranea*. It is shown that product yield and product composition are dependent on the production strain, the carbon source, the cultivation process, and fermentation additives. Selected *P. corrugata* strains accumulate amorphous and sticky *mcl*-PHA from high-grade and partially refined glycerol, a by-product of the biodiesel production process. In contrast, *P. mediterranea* strains produce a characteristic filmable PHA, very different from typical microbial *mcl*-PHA. These novel *mcl*-PHA films are suitable for manufacturing biopolymer blends with polylactic acid (PLA). As a drawback, *mcl*-PHA yields still need to be increased, and production costs to be reduced. Furthermore, an integrated process is presented in this review to conveniently recover intracellular *mcl*-PHA by the halogen-free solvent acetone and bioactive EPS by chloroform/methanol mixtures. Moreover, available transcriptional regulation studies during PHA production contribute to better understand the metabolic potential of *P. corrugata* and *P. mediterranea* strains; here, the available data suggest that regulating of PHA biosynthesis genes will enable to develop new, integrated strategies for cost-effective *mcl*-PHA and EPS production in the future [16].

Björn Gutschelmann and colleagues addressed the fact that effective process development and monitoring is needed for competitive PHA production; this can be achieved by appropriate on-line or in-line monitoring devices. In this context, photon density wave (PDW) spectroscopy was tested for the first time as a new process analytical tool (PAT) for the cultivation of *Cupriavidus necator* H16 on plant oils for PHA production. PDW spectroscopy was used for the in-line monitoring of the reduced

scattering coefficient μ_s' and the absorption coefficient μ_a at 638 nm. A correlation of μ_s' with CDM and μ_a with the non-PHA biomass was observed during the phases of growth, PHA accumulation, and PHA degradation in batch and fed-batch cultivation setups. These correlations were successfully used to forecast CDM and the PHA content in a high cell density fed-batch cultivation process with a volumetric PHA productivity of 1.65 g/(L·h), a CDM of 106 g/L, and a PHA content in biomass of 73 wt.% [17].

Mohsen Moradi and associate researchers simulated the ability of special microorganisms for PHB production using methane-rich natural gas as a carbon source in a bubble column bioreactor. Using the Taguchi algorithm, the optimum dimensions (length and diameter) of the bubble column and process conditions for PHB production from natural gas were evaluated as 30 cm length, 1.5 cm diameter, and a temperature of 32 °C. Moreover, an optimum volume ratio of air-to-methane of 1:1 was calculated. The simulation was carried out by using the COMSOL software tool with the two-dimensional symmetric mode. Mass transfer, momentum, density-time, and density-place were studied. The maximum biomass concentration amounted to 1.63 g/L, which shows a difference of only 10% in comparison to elaborated experimental results. Moreover, the impact of the inlet gas rate on product concentration and gas hold up was studied, and the simulated results were compared to experimental data; a high prediction performance of the simulation was demonstrated by a deviation of less than 20% [18].

Donya Kamravamanesh and colleagues reviewed PHA production from another gaseous substrate, namely CO_2-based, solar-driven PHA production by cyanobacteria. Cyanobacteria can accumulate PHA under photoautotrophic growth conditions using CO_2 and sunlight. It is demonstrated that the productivity of photoautotrophic PHA production from cyanobacteria is considerably lower than that described for the PHA production process by many chemoheterotrophic microbes. Therefore, a lot of effort has been dedicated during the last years to decrease PHA production cost, mainly by developing optimized microbial production strains and more effective cultivation and downstream processes. It is shown that a reduction in the PHA production cost can only be achieved by considering the process design and by a complete, holistic analysis of the entire PHA production process. With the final aim being the market success of PHA, this review discusses the benefits and the challenges associated with the upstream processing of cyanobacterial PHA production with a focus on process engineering aspects, in order to support and accelerate the realization of this promising PHA production approach on an industrial scale. Most of all, it is suggested that cyanobacterial PHA production plants have to be installed next to CO_2-emmiters, such as power plants or other factories, and should resort to the use of nutrient-rich wastewater. Moreover, robust cyanobacteria should be the production strains of choice to allow their cultivation under septic conditions in open tanks and ponds. Finally, PHA should not be the only product recovered from cyanobacteria; profiting also from other marketable products, such as pigments or bioactive compounds, cyanobacteria should emerge as whole-cell bio-factories and get embedded into biorefinery concepts [19].

Haloarchaea are another particular group of microbes deserving of specific consideration when it comes to PHA biosynthesis. Among them, we find a gradually growing number of microbes that accumulate significant quantities of PHA. These earliest organisms on earth live in challenging habitats at salinities between 100 and 300 g/L NaCl and could potentially beat established PHA production strains in future due to several benefits: cultivations in highly saline media can be run at reduced sterility by preventing the growth of non-halophilic contaminants; the high intra-cellular osmotic pressure of haloarchaea simplifies the release of intracellular PHA granules by hypo-osmotic cell disintegration; many haloarchaea convert diverse inexpensive carbonaceous waste materials as feedstocks for growth and PHA production, which combines PHA production with waste upcycling; some haloarchaea are even said to produce high-quality copolyesters from simple, structurally unrelated inexpensive substrates; finally, PHA biosynthesis often takes place in parallel to the biosynthesis of additional marketable compounds, such as polysaccharides, antibiotics, or pigments. The current knowledge on PHA production by haloarchaea is reviewed in this article, covering the quest for new

PHA-producing haloarchaea, their genetic and enzymatic idiosyncrasies, the properties of haloarchaeal PHA, successful attempts for upscaling PHA production by haloarchaea, and techno-economic and life cycle assessments of selected processes [20].

In the context of emerging biomedical applications of PHA, Alejandra Rodríguez-Contreras reviewed that their central characteristics biocompatibility, biodegradability, and non-toxicity are the pivotal properties that make them suitable for applications as biomaterials. It is discussed how PHA has been used as bone graft substitutes, in tissue engineering, as sutures, as valves in implantology, for cartilage repair, to develop new biological stents for nerve repair, and for cardiovascular patches. Based on their expedient in vivo biodegradability and the fact that the products of their in vivo degradation are non-toxic, PHA have also been broadly used as biological carriers for fine-tuned drug-release systems. Due to the fact that global interest in the biomedical application of PHA is steadily increasing, this review shines a light on the most recent scientific outcomes and advances in the exploitation of PHA and their follow-up products as biomaterials in diverse medical fields [21].

Finally, Dario Puppi and colleagues addressed the fact that this quickly growing interest on PHA processing for biomedical applications is based on the unique combinations of their characteristics in terms of biocompatibility, biodegradability, processing properties, and mechanical behavior; these indisputable benefits, however, need to go in parallel with their sustainable production. The comprehensive review article presents the best exploited processing techniques up to date employed in the biomedical area to develop devices and other biomedical PHA-based items, both for experimental and commercial applications. To this end, PHA's physical, thermomechanical, and processing properties are linked to the requirements of processing techniques conventionally employed to process plastics, such as solvent casting or melt-spinning, and to advanced, currently emerging manufacturing techniques, such as electrospinning or additive manufacturing (3D-printing). Key publications on different aspects affecting the workability of differently composed PHA homo- and copolyesters are summarized [22].

3. Conclusions

The respected reader will get an insight into current research activities dedicated to the individual scientific fields involved in making PHA biopolyesters market-fit, starting from the exploration of novel microbial production strains, switching to the challenges associated with bioprocess engineering for PHA production, and ending with advanced manufacturing techniques to produce high-performance biomaterials. I am confident that reading this second PHA-related *Bioengineering* Special Issue at hand will lead to a real motivation and inspiration boost for researchers all over the planet; expected future research activities will further deepen our understanding of PHA metabolism, biosynthesis, and its functional role. Most of all, additional efforts will hopefully be dedicated to the improvement of the PHA-related bioengineering as the *conditio sine qua non* for making PHA ultimately competitive on the plastic market.

Conflicts of Interest: The author declares no conflict of interest.

References

1. Narodoslawsky, M.; Shazad, K.; Kollmann, R.; Schnitzer, H. LCA of PHA production–Identifying the ecological potential of bio-plastic. *Chem. Biochem. Eng. Q.* **2015**, *29*, 299–305. [CrossRef]
2. Koller, M.; Maršálek, L.; Miranda de Sousa Dias, M.; Braunegg, G. Producing microbial polyhydroxyalkanoate (PHA) biopolyesters in a sustainable manner. *New Biotechnol.* **2017**, *37*, 24–38. [CrossRef]
3. Koller, M. A review on established and emerging fermentation schemes for microbial production of Polyhydroxyalkanoate (PHA) biopolyesters. *Fermentation* **2018**, *4*, 30. [CrossRef]
4. Chen, G.Q.; Jiang, X.R. Next generation industrial biotechnology based on extremophilic bacteria. *Curr. Opin. Biotechnol.* **2018**, *50*, 94–100. [CrossRef] [PubMed]

5. Obruca, S.; Sedlacek, P.; Koller, M.; Kucera, D.; Pernicova, I. Involvement of polyhydroxyalkanoates in stress resistance of microbial cells: Biotechnological consequences and applications. *Biotechnol. Adv.* **2018**, *36*, 856–870. [CrossRef] [PubMed]
6. Novak, M.; Koller, M.; Braunegg, M.; Horvat, P. Mathematical modelling as a tool for optimized PHA production. *Chem. Biochem. Eng. Q.* **2015**, *29*, 183–220. [CrossRef]
7. Brigham, C.J.; Riedel, S.L. The potential of polyhydroxyalkanoate production from food wastes. *Appl. Food Biotechnol.* **2018**, *6*, 7–18. [CrossRef]
8. Koller, M. Linking food industry to "green plastics"—Polyhydroxyalkanoate (PHA) biopolyesters from agro-industrial by-products for securing food safety. *Appl. Food Biotechnol.* **2018**, *6*, 1–6. [CrossRef]
9. Koller, M. Chemical and biochemical engineering approaches in manufacturing polyhydroxyalkanoate (PHA) biopolyesters of tailored structure with focus on the diversity of building blocks. *Chem. Biochem. Eng. Q.* **2018**, *32*, 413–438. [CrossRef]
10. Pérez-Rivero, C.; López-Gómez, J.P.; Roy, I. A sustainable approach for the downstream processing of bacterial polyhydroxyalkanoates: State-of-the-art and latest developments. *Biochem. Eng. J.* **2019**, *150*, 107283. [CrossRef]
11. Koller, M. Advances in polyhydroxyalkanoate (PHA) production. *Bioengineering* **2017**, *4*, 88. [CrossRef] [PubMed]
12. González-García, Y.; Grieve, J.; Meza-Contreras, J.C.; Clifton-García, B.; Silva-Guzman, J.A. Tequila agave bagasse hydrolysate for the production of polyhydroxybutyrate by *Burkholderia sacchari*. *Bioengineering* **2019**, *6*, 115. [CrossRef]
13. Kucera, D.; Novackova, I.; Pernicova, I.; Sedlacek, P.; Obruca, S. Biotechnological production of poly(3-hydroxybutyrate-*co*-4-hydroxybutyrate-*co*-3-hydroxyvalerate) terpolymer by *Cupriavidus* sp. DSM 19379. *Bioengineering* **2019**, *6*, 74. [CrossRef] [PubMed]
14. Blunt, W.; Gaugler, M.; Collet, C.; Sparling, R.; Gapes, D.J.; Levin, D.B.; Cicek, N. Rheological behavior of high cell density *Pseudomonas putida* LS46 cultures during production of medium chain length polyhydroxyalkanoate (PHA) polymers. *Bioengineering* **2019**, *6*, 93. [CrossRef]
15. Blunt, W.; Dartiailh, C.; Sparling, R.; Gapes, D.J.; Levin, D.B.; Cicek, N. Development of high cell density cultivation strategies for improved medium chain length polyhydroxyalkanoate productivity using *Pseudomonas putida* LS46. *Bioengineering* **2019**, *6*, 89. [CrossRef]
16. Licciardello, G.; Catara, A.F.; Catara, V. Production of polyhydroxyalkanoates and extracellular products using *Pseudomonas corrugata* and *P. mediterranea*: A review. *Bioengineering* **2019**, *6*, 105. [CrossRef]
17. Gutschmann, B.; Schiewe, T.; Weiske, M.T.; Neubauer, P.; Hass, R.; Riedel, S.L. In-line monitoring of polyhydroxyalkanoate (PHA) production during high-cell-density plant oil cultivations using photon density wave spectroscopy. *Bioengineering* **2019**, *6*, 85. [CrossRef]
18. Moradi, M.; Rashedi, H.; Mofradnia, S.R.; Khosravi-Darani, K.; Ashouri, R.; Yazdian, F. Polyhydroxybutyrate production from natural gas in a bubble column bioreactor: Simulation using COMSOL. *Bioengineering* **2019**, *6*, 84. [CrossRef]
19. Kamravamanesh, D.; Lackner, M.; Herwig, C. Bioprocess engineering aspects of sustainable polyhydroxyalkanoate production in cyanobacteria. *Bioengineering* **2018**, *5*, 111. [CrossRef]
20. Koller, M. Polyhydroxyalkanoate biosynthesis at the edge of water activity-haloarchaea as biopolyester factories. *Bioengineering* **2019**, *6*, 34. [CrossRef]
21. Rodríguez-Contreras, A. Recent advances in the use of polyhydroyalkanoates in biomedicine. *Bioengineering* **2019**, *6*, 82. [CrossRef]
22. Puppi, D.; Pecorini, G.; Chiellini, F. Biomedical processing of polyhydroxyalkanoates. *Bioengineering* **2019**, *6*, 108. [CrossRef]

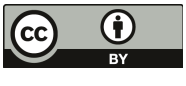

bioengineering

MDPI

Review

Polyhydroxyalkanoate Biosynthesis at the Edge of Water Activity-Haloarchaea as Biopolyester Factories

Martin Koller [1,2]

[1] Office of Research Management and Service, c/o Institute of Chemistry, University of Graz, NAWI Graz, Heinrichstrasse 28/III, 8010 Graz, Austria; martin.koller@uni-graz.at; Tel.: +43-316-380-5463

[2] ARENA—Association for Resource Efficient and Sustainable Technologies, Inffeldgasse 21b, 8010 Graz, Austria

Received: 20 March 2019; Accepted: 4 April 2019; Published: 16 April 2019

Abstract: Haloarchaea, the extremely halophilic branch of the Archaea domain, encompass a steadily increasing number of genera and associated species which accumulate polyhydroxyalkanoate biopolyesters in their cytoplasm. Such ancient organisms, which thrive in highly challenging, often hostile habitats characterized by salinities between 100 and 300 g/L NaCl, have the potential to outperform established polyhydroxyalkanoate production strains. As detailed in the review, this optimization presents due to multifarious reasons, including: cultivation setups at extreme salinities can be performed at minimized sterility precautions by excluding the growth of microbial contaminants; the high inner-osmotic pressure in haloarchaea cells facilitates the recovery of intracellular biopolyester granules by cell disintegration in hypo-osmotic media; many haloarchaea utilize carbon-rich waste streams as main substrates for growth and polyhydroxyalkanoate biosynthesis, which allows coupling polyhydroxyalkanoate production with bio-economic waste management; finally, in many cases, haloarchaea are reported to produce copolyesters from structurally unrelated inexpensive substrates, and polyhydroxyalkanoate biosynthesis often occurs in parallel to the production of additional marketable bio-products like pigments or polysaccharides. This review summarizes the current knowledge about polyhydroxyalkanoate production by diverse haloarchaea; this covers the detection of new haloarchaea producing polyhydroxyalkanoates, understanding the genetic and enzymatic particularities of such organisms, kinetic aspects, material characterization, upscaling and techno-economic and life cycle assessment.

Keywords: Archaea; bioeconomy; biopolyester; downstream processing; extremophiles; haloarchaea; *Haloferax*; halophiles; polyhydroxyalkanoates; salinity

1. Introduction

The first description of a biological polymer with plastic-like properties was published in the 1920s, when Maurice Lemoigne detected light-refractive intracellular inclusion bodies [1], today referred to as "granules"—or, more recently "carbonosomes" [2]—n resting cultures of the Gram-positive bacterium *Bacillus megaterium*. Based on the acidic degradation product of these inclusions, 3-hydroxybutyrate (3HB), Lemoigne correctly assumed the microscopically observed intracellular product to be the polymer of 3HB, namely poly(3-hydroxybutyrate) (PHB). In the meantime, PHB and its related homo- and heteropolyesters, as a group labelled as polyhydroxyalkanoates (PHA), have attracted global attention as biological, bio-based, biocompatible and biodegradable alternatives to established plastics of petrochemical origin in many sectors of the rocketing plastic market [3,4]. PHA consist of a variety of diverse building blocks, which make their material properties highly versatile [5], and can be produced biotechnologically by different continuous or discontinuous fermentation approaches and feeding strategies [6]. In principle, short chain length PHA (*scl*-PHA) are distinguished from medium chain length PHA (*mcl*-PHA). While *scl*-PHA typically constitute thermoplastic materials, *mcl*-PHA are

known as materials with elastomeric and latex-like properties and are often of a sticky nature. Among *scl*-PHA, the homopolyester PHB and the copolyester poly(3-hydroxybutyrate-*co*-3-hydroxyvalerate) (PHBHV) are best described; in this context, increasing 3-hydroxyvalerate (3HV) fractions in the copolyester decreases melting temperature and crystallinity, which makes such PHBHV copolyesters easier to process than the rather crystalline and brittle PHB, a material of restricted applicability [3,4].

Apart from wild-type and genetically engineered eubacteria and recombinant yeasts, plants, and microalgae, PHA biosynthesis takes place also in the cytoplasm of various extremely halophilic species from the Archaea domain, the so called "haloarchaea". Exclusively *scl*-PHA production is reported for haloarchaea, while for eubacteria, both *scl*- and *mcl*-PHA production is reported [3,4]. Extremely challenging habitats include environments where such highly adaptive survivalists are typically isolated; illustrative examples are the Great Salt Lake, the Dead Sea, hypersaline anoxic deep-sea basins, solar saltern crystallizers, hypersaline soil samples, salt mine boreholes, salt production pans, or even alpine dry salt rocks. The taxonomic classification of these extremely salt-demanding, typically aerobic organisms is by no means a trivial task and is based on steadily refined knowledge about the genomics, proteomics, metabolomics, and lipidomics of these organisms. Traditionally, haloarchaea are members of the family Halobacteriaceae, which belongs to the order Halobacteriales, which in turn is part of class III (*Halobacteria*) consisting of two major clades A and B, of the phylum and (sub)kingdom of Euryarchaeota, which belongs to the domain of Archaea (according to International Committee on Systematics of Prokaryotes, Subcommittee on the taxonomy of Halobacteriaceae; cited by [7]). Later, members of the class *Halobacteria* were re-grouped into three orders: a revised order Halobacteriales and two new orders, Haloferacales and Natrialbales, which encompass the novel families Haloferacaceae and Natrialbaceae [8]. More recently, based on phylogenetic analyses and conserved molecular characteristics, it was suggested to divide the order "Halobacteriales" into the families Halobacteriaceae, Haloarculaceae, and Halococcaceae, and the order "Haloferacales" into the families Haloferacaceae and Halorubraceae [9]. These are the currently valid designations of the families where haloarchaea demonstrated to produce PHA are grouped. Figure 1 provides a schematic overview about the phylogenetic classification of the haloarchaeal species discussed in the present review.

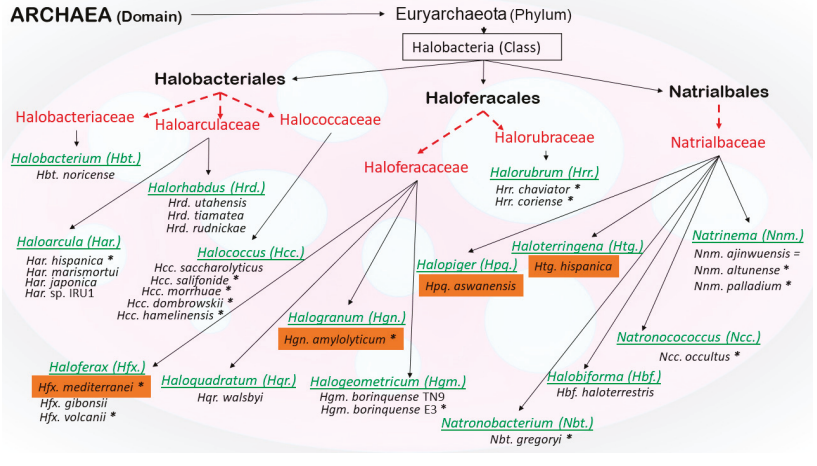

Figure 1. Extract from the phylogenetic tree of haloarchaea, selecting those species reported to accumulate PHA biopolyesters. Colored (orange) background highlights the limited number of species to date cultivated on bioreactor scale to study PHA production. The asterisks indicate 3-hydroxyvalerate production by the strain from structurally unrelated substrates. (Bold: orders; red: families; *italics and underlined*: genera; *italics*: species).

Talking about PHA biosynthesis by haloarchaea, it took the scientific community until 1972, when Kirk and Ginzburg carried out morphological characterizations of a Dead Sea isolate, which was labeled "*Halomonas* sp." by these authors. This organism was cultivated on a highly saline medium containing 200 g/L NaCl. By using freeze-fracture and freeze-etch techniques, the authors revealed plastic-like cytoplasmic inclusion bodies, which were extracted from microbial biomass and investigated by X-ray diffractometry. Grounded solely on these examinations, the authors correctly recognized this material as the biopolyester PHB, the material already known at the time as a carbon and energy storage product for many eubacteria, as reported by Lemoigne [1] and succeeding generations of scholars. In any case, this study by Kirk and Ginzburg was the very first unambiguous description of PHA production by an archaeon [10]. Regarding the production strain "*Halomonas* sp.", it took nearly three decades until this isolate was classified as *Haloarcula* (*Har.*) *marismortui*, its currently valid species name, in a report published by Nicolaus et al. [11].

2. Genetic and Enzymatic Particularities of Haloarchaeal PHA Biosynthesis

Generally, PHA synthases, the enzymes catalyzing the polymerization of PHA precursors (hydroxyacyl-CoAs like acetyl-CoA, propionyl-CoA, etc.) found in haloarchaea are grouped in the Class III of PHA synthases [12]. Class III PHA synthases were identified in several eubacteria such as *Allochromatium vinosum* (previously known as *Chromatium vinosum*) or *Thiocapsa pfennigii*; Class III PHA synthases polymerize short hydroxyacyl-CoAs, namely those not longer than 3-hydroxyvaleryl-CoA; moreover, such synthases are typically composed of two subunits: the catalytically active subunit PhaC (molar mass ranging from 40–53 kDa) and the structural subunit PhaE (molar mass 20–40 kDa), which is also indispensable for polymerization. Together, the two subunits form a biocatalytic cluster, the so called "PhaEC complex" [13]. Hezayen et al. were the first scientists who revealed the special features of PHA synthases in haloarchaea. When studying "strain 56" (today classified as *Halopiger* (*Hpq.*) *aswanensis*), a species isolated from hypersaline soil collected near Aswan, Egypt, which thrives best with 250 g/L NaCl, Hezayen et al. discovered a PHA synthase covalently bound to the PHA granules. This enzyme exposed particular features in comparison to PHA synthases in eubacteria described earlier; the new enzyme displayed high thermostability up to 60 °C, with strongly increasing activity at higher salinity; especially, Mg^{2+} ion concentration had a significant effect on synthase activity. In addition, this halophilic biocatalyst exhibited a remarkably narrow spectrum of PHA-precursors: the enzyme polymerized only 3-hydroxybutyryl-CoA, but neither 3-hydroxyvaleryl-CoA, 4-hydroxybutyryl-CoA, nor 3-hydroxyhexanoyl-CoA. Most extraordinarily, no other PHB biosynthesis enzymes typically needed for PHA biosynthesis in bacterial PHA production strains, namely 3-ketothiolase or NADH/NADPH-dependent acetoacetyl–CoA reductase, were produced by *Hpq. aswanensis*; this evidenced for the first time that haloarchaea use a metabolic route for PHA biosynthesis different to eubacteria [14].

To better comprehend and to enhance PHA production by haloarchaea, various subsequent genomic and enzymatic investigations were carried out. Similar to the studies with *Hpq. aswanensis*, the haloarchaeal genes encoding for homologues of bacterial Class III PhaC synthase enzymes were identified by Baliga et al. also in the genomes of *Har. marismortui* isolated from the Dead Sea [15], or by Bolhuis et al. in "Walsby's square bacterium" *Haloquadratum* (*Hqr.*) *walsbyi* isolated from different saltern crystallizers [16]. Han and colleagues, active at Professor Xiang´s laboratories, which are world-leading in the study of PHA biosynthesis genes in haloarchaea, explored for the first time the expression profile of genes encoding haloarchaeal PHA synthases. In this work, *Har. marismortui*, when cultivated in defined saline medium containing high amounts of glucose as carbon source, is able to accumulate PHB fractions in cell dry mass (CDM) up to 21 wt.%. As a major result, the neighboring genes $phaE_{Hm}$ and $phaC_{Hm}$ were identified by molecular characterization of the $phaEC_{Hm}$ operon; these two genes encode two Class III PHA synthase subunits, and are triggered by only one single promoter. It was shown that these genes are constitutively expressed, both under balanced and nutrient-limited cultivation conditions. Remarkably, in contrast to the non-granule associated gene $PhaE_{Hm}$, $PhaC_{Hm}$ is

strongly connected to the PHA granules. Inserting $phaE_{Hm}$ or $phaC_{Hm}$ genes into the closely related strain *Har. hispanica*, which contains highly homologue $phaEC_{Hh}$ genes, considerably increased PHB biosynthesis. Particularly, the co-expression of both genes resulted in the highest PHB productivity; in contrast, deleting $phaEC_{Hh}$ genes from the *Har. hispanica* genome ("knocking out") totally terminates PHA production. By transferring $phaEC_{Hm}$ genes into such knockout mutants fully restored the activity of PHA synthase and PHA accumulation. These studies validated for the first time the high significance of *phaEC* genes for PHA biosynthesis in haloarchaea [17].

Lu et al. carried out groundbreaking work with *Haloferax* (*Hfx.*) *mediterranei* to elucidate the genetic and enzymatic PHA biosynthesis background of this strain. Using thermal asymmetric interlaced PCR, these authors were able to clone the $phaEC_{Hme}$ gene cluster of strain *Hfx. mediterranei* CGMCC 1.2087. By Western blotting, it was shown that, analogous to the above described findings for *Har. marismortui*, both $phaE_{Hme}$ (about 21 kDa) and $phaC_{Hme}$ (about 53 kDa) genes were constitutively expressed, and both synthases were strongly connected to the PHA granules. Interestingly, the strain synthesized poly(3-hydroxybutyrate-*co*-3-hydroxyvalerate) (PHBHV) copolyesters in both nutrient-limited (supplemented with 1% starch, production of up to 24 wt.% PHBHV in CDM) and nutrient-rich (up to 18 wt.% PHBHV in CDM) media in shaking flask experiments. Knockout of $phaEC_{Hme}$ genes in this strain completely stopped PHBHV biosynthesis; PHBHV biosynthesis capability was re-established only after complementation with the complete $phaEC_{Hme}$ gene cluster, but not when transferring either $phaE_{Hme}$ or $phaC_{Hme}$ alone. It is worth noting that the described PhaC synthase subunits were considerably longer at their carbon-end than reported for bacterial PHA synthases; this C-terminal extension of $PhaC_{Hme}$ was shown to be indispensable for the enzymes´ in vivo activity at high salinity. Moreover, a 1:1 mixture of isolated $PhaE_{Hme}$/$PhaC_{Hme}$ enzymes displayed substantial PHA synthesis activity in vitro. These outcomes showed that also *Hfx. mediterranei* possesses the novel type of class III PHA synthases typical for haloarchaea, which are assembled by $PhaC_{Hme}$ and $PhaE_{Hme}$ subunits [18]; this corresponds to the above described discoveries for PHA synthases in *Har. hispanica* and *Har. marismortui* [17].

By further sequencing of the *Hfx. mediterranei* CGMCC 1.2087 genome, Han and colleagues identified three more "hidden" *phaC* genes (*phaC1*, *phaC2*, and *phaC3*), which encode possible PhaC synthases. The three "cryptic" genes were distributed all over the whole *Hfx. mediterranei* genome. Similar to $PhaC_{Hme}$ (molar mass 54.8 kDa), PhaC1 (49.7 kDa) and PhaC3 (62.5 kDa) exhibited conserved Class III PHA synthase motifs, which was not the case for PhaC2 (40.4 kDa). Moreover, the longer C-terminus of the other three PhaC enzymes was not found in PhaC2. It was revealed via reverse transcription PCR (RT-PCR) that among all four genes, only $phaC_{Hme}$ was transcribed in the wild-type strain under conditions supporting PHA biosynthesis. Astonishingly, heterologous co-expression of $phaE_{Hme}$ with each *phaC* gene in the PHA-negative mutant *Har. hispanica* PHB-1 revealed that all PhaCs, except PhaC2, effect PHBHV synthesis, though with different 3HV portions in the copolyesters. These products were characterized, revealing that thermal properties (melting point, crystallinity, glass transition temperature, etc.) and molecular mass strongly depend on the 3HV fraction in the copolyester. Briefly, the study defined three novel "hidden" *phaC* genes in *Hfx. mediterranei*, and suggested that genetic engineering of these "cryptic" *phaC* genes might have biotechnological applicability in terms of designing PHBHV copolyesters of tailored material properties based on the fine-tuning 3HV contents [19]. In 2012, Han et al. were able to report the complete genome sequence of *Hfx. mediterranei* CGMCC 1.2087, which has a size of 3,904,707 bp and consists of one chromosome and three mega-plasmids, by using a combination of 454 pyrosequencing and Sanger sequencing [20]. Shortly thereafter, Ding et al. deciphered the complete sequence of the *Har. hispanica* ATCC 43049 genome; unexpectedly, these authors noticed substantial differences when comparing this sequence with the gene sequence of *Har. hispanica* ATCC 33960 [21], the model organism used for molecular characterization studies by Han et al. described above [19]. In any case, the works presented by Han et al. [19] and Ding et al. [21] demonstrate that clustered *phaEC* genes encoding Class III PHA synthases are typical features of PHA-producing haloarchaea. This was substantiated by Han

and colleagues, who screened PHA synthase genes in haloarchaeal PHA producers from 12 genera; the authors demonstrated the wide distribution of *phaEC* genes among haloarchaea. Compared to their bacterial counterparts, haloarchaeal PHA synthases differ significantly in both molecular weight and some conserved motifs. Therefore, Han and colleagues proposed to classify haloarchaeal PHA synthases as "subtype IIIA", while type III PHA synthases from bacteria were proposed as "subtype IIIB" [22].

Genome analysis of *Hfx. mediterranei* has also evidenced eight potential 3-ketothiolase genes in *H. mediterranei*, which might express enzymes responsible for the condensation of two acetyl-CoA molecules to acetoacetyl-CoA, or one acetyl-CoA and one propionyl-CoA to 3-ketovaleryl-CoA. It was shown that only the 3-ketothiolases encoded by *HFX_6004-HFX_6003* and *HFX_1023-HFX_1022* are involved in the biosynthesis of PHBHV. Knockout of *HFX_6004-6003* leads to the accumulation of PHB homopolyester without the 3HV building blocks, while simultaneous knockout of *HFX_6004-6003* and *HFX_1023-1022* stopped the strain´s ability to produce PHA. This was the first report on haloarchaeal 3-ketothiolases, which reveled considerable differences to their bacterial relatives in subunit composition and catalytic residue [23]. Finally, genes encoding for PHA-specific acetoacetyl-CoA reductases, catalyzing the reduction of ketoacyl-CoAs to hydroxyacyl-CoAs as the substrates of PHA synthases were discovered and characterized in *Har. hispanica* [24] and *Hfx. mediterranei* [25]. Further, these enzymes displayed considerable differences to their eubacterial counterparts encoded by *phaB* genes. Only recently, Xiang summarized the genomic and enzymatic particularities of PHA biosynthesis by *Hfx. mediterranei* in a comprehensive way [26]. Figure 2 provides a simplified schematic of the pathways leading to PHB and PHBHV by eubacteria and haloarchaea, respectively. For haloarchaea, especially the multiple propionyl-CoA supplying pathways are highlighted.

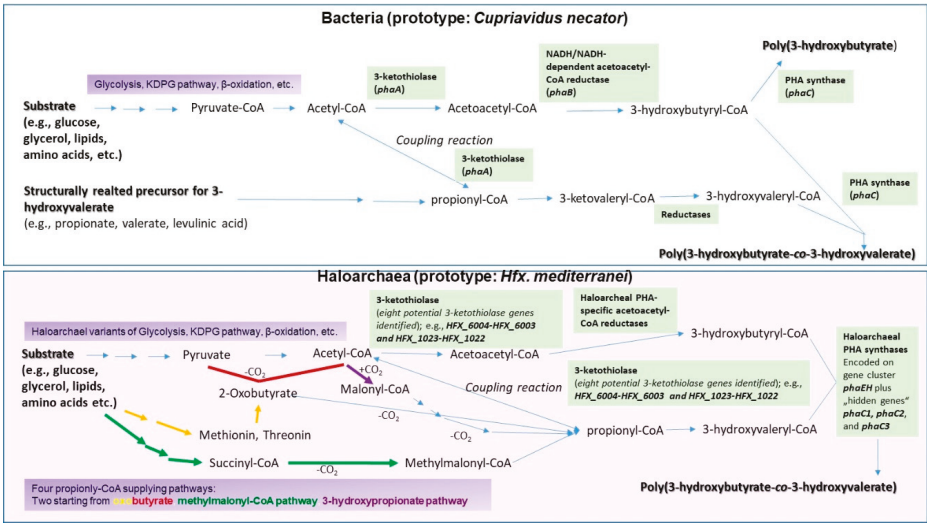

Figure 2. Simplified illustration of PHB and PHBHV biosynthesis by eubacteria (upper part, in grey; prototype organism: *C. necator*) and haloarchaea (lower part, in pink; prototype: *Hfx. mediterranei*). Enzymes and genes (in italics) involved in the PHA biosynthesis steps (starting from acetyl-CoA and propionyl-CoA) are in green text boxes. Special emphasis is dedicated to the propionyl-CoA supplying pathways in haloarchaea: Propionyl-CoA is generated (a) beginning with the coupling of pyruvate and acetyl-CoA, and the decarboxylation of 2-oxobutyrate (marked in brown), (b) starting from the conversion of the amino acids methionine or threonine to 2-oxobutyrate (marked in yellow), (c) starting from succinyl-CoA via methlymalonyl-CoA (marked in green), or (d) starting with carboxylation of acetyl-CoA to malonyl-CoA (marked in purple). Based on [26].

3. *Haloferax mediterranei*—The Prototype PHA Production Strain among Haloarchaea

Hfx. mediterranei was the first haloarchaeon for which PHA-accumulation kinetics were studied in detail. *Hfx. mediterranei* was among the 19 organisms first isolated in 1980 by Rodriguez-Valera et al. from samples collected from the evaporation ponds of solar salterns near Alicante, Spain, and designated as strain "Q4". In this publication, the authors reported on the isolation of "moderate and extremophile bacteria", without discriminating between halophilic eubacteria and haloarchaea. However, this study already proposed the possibility to enrich slowly growing extremophiles from mixed microbial cultures by carrying out chemostat continuous cultivations at a low dilution rate (D) and high substrate concentration. Moreover, the authors supposed that moderate halophiles by trend prefer a rather low temperature for growth, while extreme halophiles grow best at higher temperatures. Further, this study showed for the first time that the pigmentation of extremely halophilic organisms is more pronounced at elevated temperatures, and especially so at high salinity. In their study, Rodriguez-Valera et al. described already crucial characteristics of the most outstanding among the isolates, strain "Q4", namely negative Gram-staining, pinkish pigmentation, formation of pleomorphic rods, an optimum salinity of 250 g/L NaCl with salinity range of 100–300 g/L, and a maximum specific growth rate ($\mu_{max.}$) of 0.05 1/h. Yet, this study did not search for PHA accumulation by this strain [27]. In a subsequent study, these researchers mentioned that this new isolate exhibited substantial physiological and morphological differences to other "halobacteria" described, and recommended that "R-4" (previously strain "Q4") should be grouped into the new species *Halobacterium (Hbt.) mediterranei* [28].

In 1986, Fernandez-Castillo et al. recognized for the first time granular PHA inclusions in cells of this intriguing strain when exploring it in an experimental series with other extremely halophilic isolates (in this study termed "halobacteria"), viz. *Hbt. gibonsii*, *Hbt. halobium*, *Hbt. hispanicum*, and *Hbt. volcanii*, which were farmed in rather simple cultivation setups performed in aerated and magnetically stirred glass vessels. All these strains except *Hbt. halobium* showed PHA accumulation when growing on media containing 250 g/L salts, 10 g/L glucose, and 1 g/L yeast extract; however, *Hbt. mediterranei* by far outperformed the other strains in terms of PHA formation [29]. Today, these isolates are classified as the strains *Hfx. gibbonsii*, *Hfx. volcanii*, *Har. hispanica*, and *Har. marismortui*. These updated species names are based on a new numerical taxonomic classification based on the polar lipids of "halobacteria"; this classification was performed during the studies of Torreblanca et al.; as result, the original genus *Halobacterium* was divided into the three new genera *Haloarcula*, *Halobacterium*, and *Haloferax*; strain "*Halobacterium mediterranei*" (isolate R-4, originally "Q4") got the new species name "*Haloferax mediterranei*" [30]. For this strain, higher PHA contents in biomass of 17 wt.% were obtained using glucose than with other substrates (citrate, cellobiose, and glycerol). Further isolates used in the study (*Hfx. volcanii*, *Hfx. gibbonsii*, and *Har. hispanica*) exhibited only minor PHA fractions in CDM of 7 wt.%, 12 wt.%, and 24 wt.%, respectively, when thriving in a medium with 250 g/L NaCl, 10 g/L glucose, and 1 g/L yeast extract. Notably, in this study, authors reported that exclusively PHB homopolyester ("poly-β-butyric acid") was produced of by all of these strains, despite the fact that the products were subjected towards ^{13}C-NMR characterization, which revealed that PHA constituents other than 3HB were present in some of the isolated PHA samples [29]. According to today´s knowledge, particularly *Hfx. mediterranei* synthetizes PHBHV copolyesters under the described cultivation conditions (sufficient supply of sugars or glycerol) [31]. Importantly, this study suggested for the first time the disruption of haloarchaeal cells by exposing them to hypotonic media (distilled water) for the facile recovery of PHA granules without the use of organic solvents, which substantially facilitates downstream processing in economic and environmental terms [29]. This study can be considered the ignition spark for setting *Hfx. mediaterranei* at the pole position of research activity with respect to PHA production by haloarchaea.

Data on the detailed exploration of PHA production by other haloarchaea are still rather scarce because, as reported by Lillo and Rodriguez-Valera [32] and Rodriguez-Valera and Lillo [31], *Hfx. mediterranei* displays higher specific growth and PHA production rates in comparison to other

haloarchaea reported to accumulate PHA; this consequently is beneficial for the volumetric productivity of the bioprocess. Detailed insights into kinetics and optimized cultivation process parameters for PHA production with this strain were provided by a key publication by Lillo and Rodriguez-Valera. These authors studied continuous chemostat cultivations performed at a dilution rate D of 0.12 1/h at 38 °C. Using 20 g/L glucose and high salinity (250 g/L marine salts), 3.5 g/L PHA were produced. Replacing glucose with inexpensive starch resulted in an almost duplication of the PHA concentration (6.5 g/L), and also demonstrated the high α-amylase activity of the strain. These authors already determined that the temperature optima for growth and PHA biosynthesis by this strain are not identical [32]. Further, Antón et al. demonstrated experimentally that the organism requires highly saline nutrient media containing at least 200 g/L NaCl for optimum growth; such high salinity de facto excludes the risk of contamination with foreign germs, which is a significant gain when carrying out large-scale production setups under reduced sterility precautions [33]. This high robustness of *Hfx. mediterranei* cultivation setups against microbial rivals was later substantiated by Hermann-Krauss and colleagues, who carried out fed-batch cultivations with this strain without any sterilization provisions neither for the cultivation medium nor the bioreactor; even after several days, no infection by other microbes was detectable [34]. In contrast to high medium salinity, the cytoplasm of *Hfx. mediterranei* contains high quantities of KCl to generate high inner osmotic pressure, hence, to balance the outer osmotic pressure; this strategy of the strain to cope with such extremely high extracellular salinity [20], the so-called "salt-in" strategy, is a typical feature of haloarchaea. This requires an adaptation of the proteome, e.g., high surface charge of enzymes, to conserve the proper conformation and activity of enzymes at the edge of salt saturation. This approach drastically differs from strategies known of halophilic eubacteria, which accumulate soluble osmolytes such as ectoins as a reaction to excessive extracellular salinity [35].

PHA is not the only intriguing polymeric product produced by *Hfx. mediterranei*. In 1988, Antón et al. reported that the strain excretes also an extracellular polymer, which can be recovered from solution by precipitation with cold ethanol. This extracellular polysaccharide (EPS) causes the typical mucous appearance of *Hfx. mediterranei* colonies grown on solid nutrients [33]. This EPS is an anionic, sulfated polymer, consisting of a regular trisaccharide-repeating unit with one mannose and two 2-acetamido-2-deoxyglucuronic acid monomers and one sulfate ester bond per trisaccharide unit. Rheologically, the polymer displays xanthan-like characteristics, which has attracted interest in it as a thickening and gelling agent in food technology [36]. Later, the interrelation between parallel production and in vivo degradation of the two polymers (PHA and EPS) was investigated. It was revealed that intracellular PHA degradation is a rather slow process, even under carbon-limited conditions; technologically, this allows postponing cell inactivation and harvest after complete depletion of the carbon source without risking significant product degradation. In this study, it was also demonstrated that pronounced EPS production takes place when feeding the strain with defined carbon sources like carbohydrates, but not when supplying complex substrates like yeast extract; this trend is analogous to the strain's PHA accumulation profile: defined carbon sources result in high PHA biosynthesis, while complex substrates favor biomass growth [37]. More details were reported by Cui et al., who studied the salinity effect on PHA and/or EPS biosynthesis as a tool to direct the carbon flux towards one product or another. These cultivations were performed in 1.2 L airlift bioreactors. In a nutshell, high salinity inhibited EPS biosynthesis, but preferred PHA accumulation. Increasing NaCl concentration from 75 g/L to 250 g/L, EPS production slightly dropped from 37 wt.% to 32 wt.%. With 71 wt.%, the PHA fraction in biomass reached its highest value at a salinity of 250 g/L NaCl; this demonstrated that a high salinity boosts PHA production at the expense of EPS formation. Technologically, these results enable a regulation of the carbon flux in *Hfx. mediterranei* by adapting the salinity of the cultivation medium in order to enhance the biosynthesis of either PHA or EPS, both constituting industrially applicable products [38].

Figure 3a shows *Hfx. mediterranei* colonies grown on solid agar medium with yeast extract and enzymatically hydrolyzed whey permeate as substrates; the mucous and pinkish character of colonies due to the production of EPS and pigments (C50 carotenoids) is apparent. Figure 3b presents liquid

samples taken from the beginning through to the end of a bioreactor cultivation of *Hfx. mediterranei* under controlled conditions in a 200 L (working volume; total volume: 300 L) pilot scale bioreactor (L 1523, Bioengineering, Wald, CH) using the same substrates: yeast extract (initial concentration 6.25 g/L) and enzymatically hydrolyzed whey permeate (initial concentration 50 g/L, corresponds to 10 g/L of an equimolar glucose/galactose mixture); a refeed of hydrolyzed whey permeate was done according to HPLC analysis of the cultivation broth after each sampling, while a re-feed of yeast extract solution was done drop-wise according to the reaction of the dissolved oxygen probe during the first phase of the cultivation (until t = 28 h) in order to provoke enhanced PHA biosynthesis. The pH-value and dissolved oxygen were permanently controlled and recorded online and PHA, EPS and protein concentrations were determined after each sampling. The samples show increasing coloration and viscosity until the end of the cultivation, when the mass fraction of PHA (a PHBHV copolyester containing 10 mol.% of 3HV amounted to 67 wt.%; final concentrations of 7.2 g/L and 1 g/L were obtained for PHBHV and EPS, respectively.

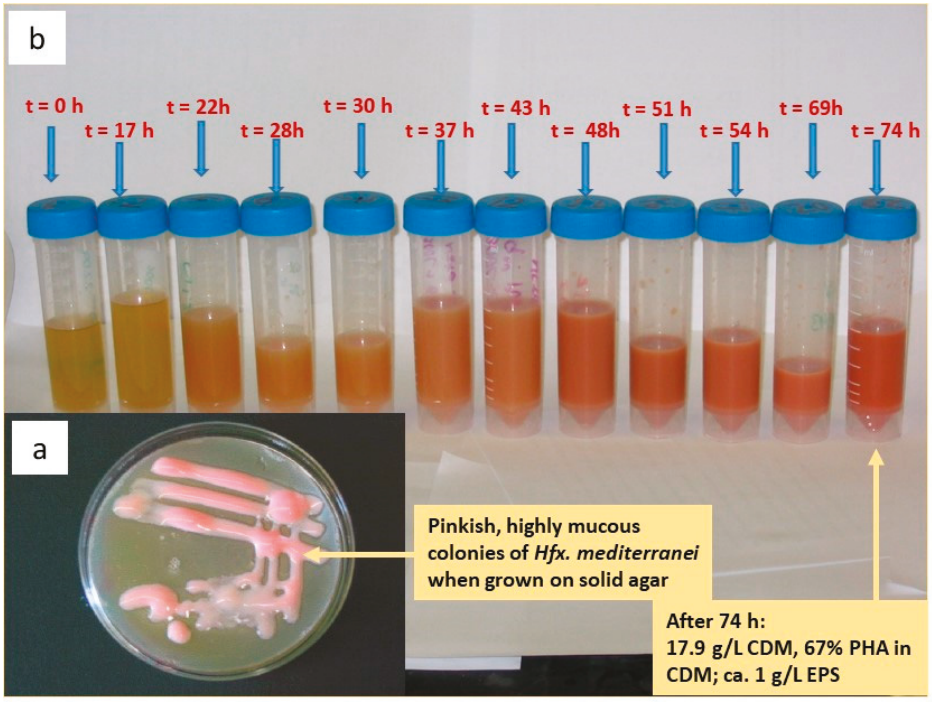

Figure 3. (**a**) Pinkish, mucous *Hfx. mediterranei* colonies grown on solid medium. (**b**) Macroscopic appearance of samples taken from a *Hfx. mediterranei* bioreactor cultivation from the beginning (t = 0 h) until the end (t = 74 h) of the process. Own pictures of the author M. Koller.

As stated above, when using simple carbon sources like carbohydrates, *Hfx. mediterranei* does not produce the homopolyester PHB as typical for the majority of wild type eubacteria, but a PHBHV copolyester. *Hfx. mediterranei* was the first strain at all, for which PHBHV copolyester production from structurally unrelated carbon sources was reported. For other strains, in vivo incorporation of 3-hydroxyvalerate (3HV) in growing PHA chains is dependent on the supply of precursors structurally related to 3HV, such as propionic acid, valeric acid, or levulinic acid. These precursors contribute considerably to the costs of PHBHV production [4]. Only decades later, the metabolic background of this particular feature was revealed by bioinformatic analysis of the *Hfx. mediterranei* genome sequence,

when Han et al. proposed four active pathways in *Hfx. mediterranei*, which synthesize the 3HV-precursor propionyl-CoA. The first two pathways involve the conversion of 2-oxobutyrate (either from starting pyruvate and acetyl-CoA or starting from threonine and methionine) to propionyl-CoA. The third pathway, the so called methylmalonyl-CoA pathway, starts from the isomerization of succinyl-CoA to methylmalonyl-CoA, which gets decarboxylated to propionyl-CoA. Finally, the 3-hydroxypropionate pathway starts with carboxylation of acetyl-CoA forming malonyl-CoA, which gets reduced in a cascade of catalytic steps to propionyl-CoA. In this context, coupling of propionyl-CoA and acetyl-CoA generates 3-ketovaleryl-CoA, while condensation of two acetyl-CoA molecules, the universal, central metabolite, generates acetoacetyl-CoA. Both reactions are catalyzed by the enzyme 3-ketothioase (in older literature: β-ketothiolase). Subsequently, 3-ketovaleryl-CoA is reduced by reductases to 3HV-CoA, which acts as substrate of PHA synthases for 3HV polymerization in growing PHA chains, while acetoacetyl-CoA is transformed into 3-hydroxybuytryl-CoA, the active form of the PHB monomer 3HB [39]. Technologically important: PHBHV copolyesters, characterized by their lower crystallinity and higher difference between meting temperature and degradation temperature, are more easily processed by injection molding, melt extrusion, or other polymer processing techniques if compared with the typically highly crystalline and brittle PHB homopolyester. Moreover, due to their pronounced amorphous domains, PHBHV copolyesters are more prone to (bio)degradation in vivo and during composting if compared with PHB [40]. In particular, the PHBHV copolyester produced by *Hfx. mediterranei* typically exhibits material features desired for processing, such as a low melting temperature (T_m), low degree of crystallinity (X_c), high molecular mass up to the MDa range, and low polydispersity ($Đ_i$), hence a high uniformity of polyester chains in one and the same sample [41].

As described, it was only during the last decade, when profound information about the enzymatic and genomic particularities of *Hfx. mediterranei*, with special emphasis dedicated to the mechanisms involved in PHA biosynthesis, was elaborated [26]. This covers studies on the special *Hfx. mediterranei* PHA synthase enzymes [18], haloarchaeal phasins as enzymes essential for PHA granule formation [42], the identification and mapping of the phaB genes encoding PHA biosynthetic enzymes in *Hfx. mediterranei* [25], the multiple pathways generating the 3HV-precursor propionyl-CoA [39,43], or patatin, the first haloarchaeal enzyme identified to serve the in vivo mobilization (depolymerization) of native *Hfx. mediterranei* granules [43].

4. Process Parameters for Optimized *Hfx. mediterranei*-Mediated PHA Production

In 2017, Ferre-Güell and Winterburn investigated the impact of the nitrogen sources NH_4^+ and NO_3^- on biomass formation and PHA production by *Hfx. mediterranei*. In a N-rich medium based on glucose, yeast extract and 156 g/L NaCl, CDM and PHA content in CDM reached 10.7 g/L and 4.6 wt.%, respectively when using NH_4^+; with NO_3^-, only 5.6 g/L CDM, but 9.3 wt.% PHA in CDM were produced. Astonishingly, the type of N-source affected the composition of PHBHV copolyesters. While 16.9 mol.% 3HV were present in PHBHV when using NH_4^+, the 3HV fraction dropped to 12.5 mol.% when using NO_3^-. With NH_4^+, a low C/N-ratio of 42/1 resulted in reduced formation of active biomass, but increased the PHBHV share in CDM to 6.6 wt.%; the effect of the C/N-ratio was less pronounced when using NO_3^-. Remarkably, a lower C/N-ratio increased the 3HV share in PHBHV, which suggests an effect of the C/N-ratio on the activity of the propionyl-CoA generating pathways. Interestingly, no 3HV was detected in PHA before the polyester concentration reached 0.45 g/L. Hence, detailed understanding of the effect of type and concentration of different N-sources can contribute to the enhanced production of PHBHV copolyesters by haloarchaea with pre-defined composition and characteristics [44]. As a follow-up study, Melanie and colleagues examined the impact of the initial phosphate concentration on PHA production by *Hfx. mediterranei*; 0.95 g/L PHBHV (15.6% in CDM) with unexpectedly high 3HV content (22.36 mol.%) was produced after seven days of cultivation with 156 g/L NaCl and 0.5 g/L KH_2PO_4 as P-source in 500 mL shaking flasks. Lower initial KH_2PO_4 concentrations (0.25 or 0.00375 g/L) caused lower PHA productivity and lower 3HV fractions in PHBHV copolyesters. Thermal characterization of the products revealed data typical for PHA produced by *Hfx.*

mediterranei [45]. Moreover, Cui et al. studied the temperature effect on biomass and PHA formation by *Hfx. mediterranei*. This was done by developing, calibrating, and validating a mathematical model for growth and PHA production kinetics at 15, 20, 25, and 35 °C. The kinetic coefficients implemented into the model were obtained by experimental results from cultivations carried out in stirred and aerated flasks in a medium of similar composition to molasses wastewater. As a result, it was shown that the cultivation temperature considerably effects PHA production by *Hfx. mediterranei*; at 15 °C, the volumetric PHA productivity amounted to only 390 mg/(L·h), while 620 mg/(L·h) were obtained in cultivations at 35 °C. An Arrhenius equation plot was drawn that revealed the maximum specific growth rate ($\mu_{max.}$; 0.009 1/h at 15 °C, 0.033 1/h at 35 °C), maximum specific substrate uptake rate ($q_{Smax.}$; 0.018 g/(g·h) at 15°C, 0.037 g/(g·h) at 35 °C), and specific decay rate (k_d; 0.0048 1/h at 15 °C, 0.0089 1/h at 35 °C) were higher at increased temperature. The calculated activation energy for biomass growth, decay, and substrate uptake were 58.31 kJ/mol, 22.38 kJ/mol, and 25.59 kJ/mol, respectively. For all investigated temperatures, the developed model was of high predictive power. Even with sufficient supply with nitrogen source, the elevated temperature level of 35 °C significantly improved PHA productivity; this temperature was therefore recommended as the optimal cultivation temperature to be used for this strain. Furthermore, the 3HV fraction in PHBHV turned out to be independent from temperature; under all temperature conditions, the PHBHV copolyesters contained 16.7 mol.% 3HV. These data are of high importance, because information in older literature for the temperature optimum of *Hfx. mediterranei* were inconsistent and even contradictory [46]. Unfortunately, the authors did not study higher temperatures, which were reported in the basic publications for *Hfx. mediterranei* as optimum for growth and PHA-biosynthesis (50 °C and 45 °C, respectively) [32].

5. Use of Different Feedstocks for PHA Biosynthesis by *Hfx. mediterranei*

A range of diverse inexpensive carbon-rich food and agro-industrial waste and side products have already been tested as feedstocks for PHA production by *Hfx. mediterranei*. This encompasses surplus whey from cheese and the dairy industry [41,47,48], crude glycerol phase (CGP) as the main by-product of biodiesel production [33], extruded corn starch [49], extruded rice bran [50], stillage from bioethanol manufacturing [51,52], molasses wastewater form sugar industry [48], olive mills wastewater [53], vinasse from molasses-based ethanol production [54], or macroalgae (seaweeds) hydrolyzed by advanced techniques [55].

5.1. Hfx. mediterranei on Hydrolyzed Whey Permeate

Indeed, *Hfx. mediterranei* is considered one of the most auspicious organisms for whey-based PHA production on a large scale because of its high production rates, high robustness and the stability of fermentation batches, as well as convenient product recovery via hypo-osmotic cell disintegration [41]. The strain grows excellently on both acidic or enzymatically hydrolyzed whey permeate (equimolar mixtures of glucose and galactose as main carbon source; permeate generally separated from whey retentate via ultrafiltration) but does not utilize intact lactose [56]. In bioreactor cultivation setups, high maximum specific growth rates ($\mu_{max.}$) of 0.11 1/h were reported when using hydrolyzed whey permeate as a substrate; this is substantially higher than specific growth values reported for other haloarchaea. Maximum values for specific PHA production (q_P) amounted to 0.08 g/(g·h). When optimizing the cultivation conditions (inoculum preparation, medium composition), these values were even enhanced to $\mu_{max.}$ = 0.09 g/(L·h) and q_P = 0.15 g/(g·h), respectively. Biomass concentration and PHA fractions in biomass reached 16.8 g/L and 73 wt.%, respectively [57]. Importantly, when cultivated on hydrolyzed whey lactose (equimolar mixture of glucose and galactose), *Hfx. mediterranei* has a clear preference for glucose, which results in the accumulation of galactose in the fermentation medium, thus drastically increasing the biochemical oxygen demand of spent fermentation broth and causing the loss of a substantial part of the substrate. Suggested solutions to solve this ecological and economic shortcoming involve separating galactose from spent fermentation broth for further use, e.g., as a sweetener or nutritional and pharmaceutical additive; yet, this approach is economically rather

doubtful. In this context, Pais et al. discovered that the activity of the strain´s enzymes involved in galactose conversion can be increased by adaptation of the trace elements supply to the cultivation medium; this way, a more complete substrate conversion was achieved. Remarkably, the PHBHV copolyesters obtained in this study had a very low 3HV fraction of only 2 mol.% 3HV [48].

Attempts to further increase the material features of whey-based PHA produced by *Hfx. mediterranei*, the precursor substrates valeric acid and γ-butyrolactone (GBL) were supplied in bioreactor cultivations with 200 g/L NaCl and hydrolyzed whey permeate as main carbon source. These precursors were added in order to achieve higher 3HV fraction in PHA, and to introduce 4HB as an additional PHA building block. This way, a poly(3HB-*co*-21.8%-3HV-*co*-5.1%-4HB) terpolyester with encouraging material properties (low melting points, high molecular mass and low crystallinity) was produced, and suggested for further use in the medical field [47].

It is obvious that the highly saline waste streams of *Hfx. mediterranei* cultivations need appropriate handling, hence sustainable disposal or re-utilization in order to reduce process costs and to minimize the risk of environmental pollution. Importantly, disposing salt-rich materials after cell harvest and PHA recovery constitutes a real environmental threat, especially for large cultivation setups; the concentration of total dissolved solids (TDS) in disposed wastewater is limited with 2 g/L according to valid environmental norms. Therefore, the possibility of re-using saline cell debris, which remains after PHA recovery, as well as recycling the salt-rich spent fermentation broth by using it as mineral source in new cultivation setups was studied. Experiments with spent fermentation broth and saline cell debris were carried out; the results underlined the viability of recycling these waste streams. It was demonstrated that re-using spent fermentation broth for the preparation of new saline mineral medium drastically reduces the need for fresh salts. Furthermore, substituting up to 29% of yeast extract, typically a costly component used in *Hfx. mediterranei* cultivation media, for saline PHA-free cell debris gave growth rates similar to those obtained in the original cultivations [58].

Data from fed-batch cultivations on 200 L pilot scale, which are as yet the only results for large-scale PHA production using haloarchaea and inexpensive feedstock, were used for the cost assessment of PHBHV production on hydrolyzed whey by *Hfx. mediterranei*. This assessment encompassed the profits of solvent-free PHA recovery in distilled water, inexpensive acidic whey hydrolysis by mineral acids, abandoning any sterility provisions, copolyester production without the need for 3HV precursors, and the re-use of saline cell debris and spent fermentation broth in subsequent fermentation batches. A price of less than € 3 was estimated for the production of 1 kg PHA, which is significantly less than is typically reported PHA production prices of 5–10 €/kg. This pilot scale calculation delivered 7.2 g/L PHA and a volumetric productivity of 0.11 g/(L·h). The study also compared value creation for converting whey to, on the one hand, PHA, with, on the other hand, to whey powder, the currently most common application. In addition to cost assessment, a life cycle assessment (LCA) using the "sustainable process index" (SPI) as indicator for sustainability was carried out. A significant result of this process suggested that the estimated ecological footprint of whey-based PHA produced by *Hfx. mediterranei* is superior to fossil-based plastics if all process side streams are recycled [59]. This is in accordance with more recent considerations published by Narodoslawsky and colleagues, who concluded that the ecological footprint of "bioplastics" outperforms established plastics only when considering and optimizing the entire life cycle of the polymer [60].

5.2. Hfx. mediterranei on Crude Glycerol Phase from Biodiesel Industry

Beside hydrolyzed whey, strain *Hfx. mediterranei* accumulates PHA heteropolyesters (co- and terpolyesters) also when being fed with crude glycerol phase (CGP). CGP constitutes the main side-product of biodiesel production, which is steadily emerging in many global areas. In this context, CGP was used as feedstock for fed-batch bioreactor cultivations of *Hfx. mediterranei* in media containing 150 g/L NaCl; in these experiments, a volumetric PHBHV productivity of 0.12 g/(L·h) and a product fraction of 75 wt.% PHBHV (10 mol.% 3HV) in CDM were reached. Co-feeding the 4HB-precursor GBL together with the main substrate CGP, a PHA terpolyester containing 3HB (83 mol.%), 3HV (12 mol.%),

and 4HB (5 mol.%) was synthesized [32]. Here, it should be added that the utilization of glycerol for PHA biosynthesis is not a typical feature for other haloarchaea; many of them use this substrate for the production of non-PHA biomass and maintenance energy, but not for PHA biosynthesis [61].

5.3. Hfx. mediterranei on Processed Starchy Materials

Extruded rice bran (ERB) and extruded cornstarch (ECS) were applied by Huang et al. as additional inexpensive substrates for PHA production by *Hfx. mediterranei*. For this purpose, 5 L scale bioreactor cultivations were performed in repeated fed-batch mode under pH-stat conditions with a medium containing 234 g/L NaCl and all other compounds required by the strain. Due to the insufficient utilization of non-processed ERB and ESC, these feedstocks were extruded before being supplied as substrate as ERB/ECS mixtures in a ratio of 1/8 (g/g). High values for CDM, PHA, and PHA content in biomass were reported: 140 g/L, 77.8 g/L, and 56 wt.%, respectively [51]. In a similar way, Chen and colleagues used cornstarch treated by an enzymatic (α-amylase) reactive extrusion process for PHA production by *Hfx. mediterranei*. The cultivation was performed in a 6 L bioreactor under pH-stat fed-batch cultivation conditions and a salinity of 234 g/L NaCl. Carbon and nitrogen concentration in the cultivation broth was kept constant by feeding a stream containing a 1/1.7 (g/g) mixture of extruded ECS (carbon source) and yeast extract (nitrogen source). After 70 h, the PHA concentration and PHA content in CDM reached 20 g/L and 51 wt.%, respectively. Similar to other PHA production setups carried out with *Hfx. mediterranei*, a PHBHV copolyester with 10.4 mol.% 3HV was produced by the strain without supply with 3HV precursor compounds. This process reached the as yet highest volumetric PHA productivity with *Hfx. mediterranei* with around 0.28 g/(L·h) [49].

5.4. Hfx. mediterranei on Waste Streams of Bioethanol Production

Vinasse constitutes a recalcitrant waste of ethanol production based on molasses. On shaking the flask scale, this waste product was studied as a potential substrate for PHA production by *Hfx. mediterranei*. Pre-treatment by adsorption on charcoal was carried out to remove inhibiting compounds from vinasse, mainly phenolic compounds. Using 25–50% (v/v) pre-treated vinasse delivered a maximum PHA content in biomass of 70 wt.%, a maximum PHA concentration of 19.7 g/L, a volumetric productivity for PHA of 0.21 g/(L·h), and a substrate conversion yield of 0.87 g/g. By this process, about 80% of the (bio)chemical oxygen demand of pre-treated vinasse were removed. Further, in these experiments PHA was recovered from biomass by cell lysis in a hypotonic medium and further purified by treatment with sodium hypochlorite and organic solvent. Again, the product was characterized as a PHBHV copolyester. Using 25% pre-treated vinasse, the 3HV fraction in PHBHV amounted to 12.4 mol.% and increased to 14.1 mol.% when using 50% pre-treated vinasse. The high medium salinity allowed the performance of the cultivation without prior sterilization of the bioreactor and medium, which contributes to production cost reduction. The authors underlined that the simple use of charcoal for vinasse detoxification was more economical than the above described processes using other waste materials as substrates; ultrafiltration to concentrate whey, or extrusion and enzymatic treatment of starchy materials contribute more to the production cost than charcoal pre-treatment. Analogous to the processes based on whey, which can be integrated into the production lines of dairies and cheese factories, where whey directly accrues as waste stream, the vinasse-based process can easily be integrated into distilleries, where it even contributes to the treatment of process wastewater [54].

As the main waste material stemming from ethanol manufacture based on rice, raw stillage was applied without pre-treatment by the same team of researchers as another inexpensive substrate for PHA biosynthesis by *Hfx. mediterranei*. These experiments strongly focused at closing material cycles within the process, and to reduce its environmental impact; for this purpose, medium salts from previous cultivation batches were directly recycled. 16.4 g/L PHA, about 70 wt.% PHA in biomass, a substrate conversion yield of 0.35 g/g, and a volumetric PHA productivity of 0.17 g/(L·h) were achieved in shaking flask experiments. In analogy to above described experiments performed using whey, a PHBHV copolyester with 15.3 mol.% 3HV was produced. A reduction of the (bio)chemical

oxygen demand in feedstock stillage by about 85%, and a decrease of total dissolved solids (TDS) in spent fermentation broth to only 0.67 g/L were reached [50].

As follow up study, Bhattacharyya et al. performed a techno-economic assessment of *Hfx. mediterranei*-mediated PHA production on unsterile waste stillage from rice-based ethanol manufacturing. This process was performed in a plug-flow bioreactor made of plastic, which is normally used to study and optimize activated sludge processes. *Hfx. mediterranei* successfully utilized stillage, and produced 63 wt.% PHA in biomass, while PHA concentration, product yield, and volumetric productivity amounted to 13 g/L, 0.27 g/g, and 0.14 g/(L·h), respectively. A significant reduction of the (bio)chemical oxygen demand of stillage by 82% was reached. The accumulated PHA was identified as PHBHV copolyester with a molar 3HV fraction of 18%. An innovative desalination process of the supernatant of spent fermentation broth, consisting of two steps, was developed; this process involved stirring and heating the spent supernatant with decanoic acid. After cooling and settling, the mixture separated into three phases: salts precipitated and became available for subsequent fermentation batches, an organic phase of lower density (decanoic acid; to be applied for subsequent desalination cycles), and the heavier water phase. By this simple approach, it was possible to recover 99.3% of the medium salts and to re-use them in next PHA production batches. An assessment of cost for PHBHV produced via this process, which was suggested by the authors as the basis for the design of a pilot plant, estimated US $ 2.05 per kg of product; this calculation refers to a production plant with a production capacity of 1890 annual tons. It is important to note that desalination particularly contributed considerably to this low-cost estimate. Further, this techno-economic analysis holds promise for the realization of PHA production integrated in existing industrial production plants, in the case of rice-based stillage especially in emerging countries like India [52].

5.5. Hfx. mediterranei on Wastewater of Olive Oil Production

Using olive oil wastewater (OMW), a highly contaminated side stream of the olive processing industry, *Hfx. mediterranei* was cultivated in a one-stage cultivation process aiming at PHBHV production. In this process presented by Alsafadi and Al-Mashaqbeh, the inexpensive feedstock OMW was supplied to the culture without pre-treatment, which saved costly steps, e.g., for dephenolization. When the entire cultivation medium contained up to 25% OMW, the present phenolic compounds did not inhibit grow of the strain. The cultivation conditions were optimized to achieve maximum polymer yield and PHA fraction in biomass; this encompassed fine-tuning salinity, temperature, and oxygen supply. A salt concentration of 220 g/L NaCl and a temperature of 37 °C turned out to be best values for optimum PHA productivity. The accumulated biopolyester was recovered from biomass by hypotonic cell lysis assisted by SDS and vortexing, and further purified with sodium hypochlorite, thus using only minor amounts of organic solvents. The relative content of 3HV in the generated PHBHV copolyester amounted to 6%, which is significantly lower than 3HV fraction for *Hfx. mediterranei* PHBHV produced on other substrates as described above for whey, stillage, starchy materials, or vinasse. This process was suggested by the authors to enhance OMW valorization, and to reduce production cost of desired bioproducts. However, taking into account that the cultivations were performed only on a small shaking flask scale, upscaling to the bioreactor scale, to be carried out under controlled cultivation conditions, it will be necessary to assess industrial viability [53].

5.6. Hfx. mediterranei on Hydrolyzed Macroalgae

The green seaweed (microalga) *Ulva* sp., an organism typically producing unwanted algal blooms at coastal areas, was hydrolyzed by alkaline (4.8 mM KOH) and thermal (180 °C) batch treatment and used as substrate for shaking flask cultivations of *Hfx. mediterranei* at 42 °C and pH 7.2. PHA concentration, CDM, PHA content in biomass and 3HV fraction in PHA obtained when using 25% of Ulva hydrolysate reached 2.2 g/L, 3.8 g/L, 58 wt.%, and 0.08 mol/mol, respectively [55].

6. Microstructure of *Hfx. mediterranei* PHA Copolyesters

Hfx. mediterranei produces PHBHV copolyesters, which are not homogenous materials, but consist of diverse fractions of varying molecular mass and monomeric composition. PHBHV produced by *Hfx. mediterranei* using glucose and yeast extract was separated into two fractions with different 3HV contents by using a mixture of chloroform and acetone. The predominant fraction, which amounts to about 93% of the entire polymer had a 3HV fraction of 10.7 mol.% and a molecular mass of about 570 kDa, while the minor fraction contained considerably lower amounts of 3HV (12.3 mol.%) and had a significantly lower molecular mass of 78.2 kDa. This low-molecular mass fraction was soluble even in acetone, which typically is reported as an "anti-solvent" for short-chain-length PHA like PHB or PHBHV at temperatures below the boiling point of the solvent. T_m and T_g of both fractions were similar, and both had rather low $Đ_i$ values. By DSC characterization at heating rates below 20 °C/min, two overlapping melting peaks became visible in the DSC traces, with varying relative peak intensities when changing the heating rate; the authors supposed that this effect might originate from melt-and-recrystallization phenomena in PHA [62]. In another study, a low-molecular mass (209 kDa) fraction of a *Hfx. mediterranei* poly(3-hydroxybutyrate-*co*-3-hydroxyvalerate-*co*-4-hydroxybutyrate) terpolyester was extracted by acetone under reflux conditions in a Soxleth apparatus, while the major part of the product amounting to about 99%, which had a considerably higher molecular mass exceeding 1 MDa, was soluble in acetone only at a temperature exceeding acetone´s boiling point [63]. Both studies confirmed the presence of intracellular PHA blends in *Hfx. mediterranei*. More detailed insights into the microstructure of PHBHV produced by *Hfx. mediterranei* were disclosed by Han et al., who described the complex blocky structure of the biopolyester (*b*-PHA), which consists of alternating PHB and poly(3-hydroxyvalerate) (PHV) blocks, which are linked to blocks of randomly distributed PHBHV copolyesters. These researchers also demonstrated that *b*-PHA production by *Hfx. mediterranei* could be fine-tuned via the co-feeding of glucose and valerate. Because of this "blocky" structure and its high 3HV content, *Hfx. mediterranei b*-PHA displays exciting material features such as low degree of crystallinity and improved Young's modulus. Films of this polyester showed unique foveolar cluster-like surface morphology with high roughness. This enables a possible biomedical application of this *b*-PHA, as revealed by its better blood platelet adhesion and faster blood clotting behavior in comparison to randomly distributed PHBHV [64].

A fed-batch process using mixtures of butyric and valeric acid as substrate for *Hfx. mediterranei* was described by Ferre-Güell and Winterburn; this process was designed to synthesize PHBHV copolyesters with pre-defined composition in a reproducible way. Tween 80 added as emulsifier at a temperature of 37 °C improved the bioavailability of the substrates; the highest PHBV contents in biomass (59 wt.%) and volumetric productivity (10.2 mg/(L·h)) were reported for a butyric/valeric acid mix of 56/44. The biopolyester had a pre-defined 3HV fraction of 43 mol.%. This triggering of the PHBHV composition by adapting the composition of the substrate mix was realized both on shaking flask and bioreactor scale under different temperatures and emulsifier concentrations. Only insignificant variances in PHBHV product quality (molecular mass, thermo-mechanical properties) were observed for different production scales (bioreactor or shaking flask, respectively), which demonstrated the convenient scalability of this process [65]. A similar study aimed also at manufacturing *Hfx. mediterranei* PHBHV copolyesters of controlled composition and microstructure. Both *b*-PHBHV and PHBHV of random distribution were produced by supplying cultures with different fatty acids with an even (acetic, butyric, hexanoic, octatonic, and decanoic acid) or an odd number (propionic, valeric, heptanoic, nonanoic, undecanoic acid) of carbon atoms. Only those fatty acids with less than seven carbon atoms were accepted by the strain as a substrate for growth and PHA production. When feeding acetic acid, a PHBHV copolyester with about 10 mol.% 3HV was produced, which is in accordance to the 3HV fraction typically obtained when using glucose, glycerol, etc., while in the case of butyric acid, almost no 3HV was found in the copolyesters. Valeric acid used as sole carbon source resulted in an exceptionally high 3HV content of more than 90 mol.%. When using propionic acid, the 3HV content was lower than in the case of valeric because of the partial oxidative propionyl-CoA

decarboxylation, which converts propionyl-CoA to CO_2 and acetyl-CoA, which acts as 3HB precursor. Applying different feeding strategies for butyric acid, valeric acid and mixtures of these acids, it was shown that sequential feeding creates *b*-PHBHV containing alternating PHB and PHV blocks, while random distribution of 3HB and 3HV occurs when co-feeding the substrates. Furthermore, higher 3HV fractions in randomly distributed PHBHV resulted in higher PHA chain mobility in the amorphous phase of the polyesters, which was evidenced by lower T_g values. In general, higher 3HV fractions in random PHBHV resulted in decreased polyester crystallinity, lower T_m, improved ductility, and higher elasticity, which consequently enhances processibility of the polymers [66].

7. Further Haloarchaeal Genera Encompassing PHA Producers

7.1. Haloarcula sp.

Beside the broadly described strain *Hfx. mediterranei*, other haloarchaea with more or less pronounced PHA production capacity were isolated from different saline environments. In this context, Altekar and Rajagopalan exposed the interrelation between PHA accumulation by the haloarchaea *Hfx. mediterranei*, *Hfx. volcanii* and *Har. marismortui*, and CO_2-fixation activity catalyzed by ribulose bisphosphate carboxylase (RuBisCo) present in the cell extracts of these strains [67]. Later, Nicolaus and colleagues isolated three previously unknown organisms from Tunesian marine salterns. These isolates grew well under extremely saline conditions (3.5 M NaCl, ~200 g/L). All three strains displayed parallel PHB production and EPS excretion when supplied with different carbon sources. By analyzing the strains´ lipid patterns, it was concluded that all of them belong to the genus *Haloarcula* (*Har.*). All of them grew on starch, and one (isolate "T5") grew expediently on the inexpensive substrate molasses. After growing about ten days on starch or glucose, this strain T5 accumulated 0.5 wt.% PHB in CDM, and 1 wt.% when growing on molasses. DNA-DNA hybridization tests and other biochemical studies identified strain T5 as a new *Har. japonica* ssp. [11]. Legat and colleagues later revealed by means of Nile Blue and Sudan Black staining and ^{1}H-NMR investigation of freeze-dried cells that also *Har. hispanica* strain DSM 4426^T constitutes a producer of PHA, more precisely of PHBHV copolyesters [68].

Haloarcula sp. IRU1 was isolated from the hypersaline Iranian Urmia lake. In shaking flask cultivations, PHB production was optimized by using varying carbon, nitrogen, and phosphate source concentrations and by studying the effect of temperature in between 37 °C and 55 °C. Highest PHB contents in biomass of 63 wt.% were reported for 42 °C when using 2 g/L glucose, 0.2 g/L NH_4Cl, and 0.004 g/L KH_2PO_4 [69]. Later, glucose, fructose, sucrose, starch, acetate, and palmitic acid were tested as substrates for *Har.* sp. IRU1. Using glucose, CDM and PHB concentration substantially increased compared to all other carbon sources, while lowest CDM and PHB concentration were reported for acetate and palmitic acid [70]. The same organism, *Har.* sp. IRU1, was also cultivated on a medium containing petrochemical wastewater as carbon source; as determined by a Taguchi experimental design, highest PHB fractions in biomass (47 wt.%) were obtained with 2% wastewater, 0.8% tryptone, 0.001% KH_2PO_4 and a temperature of 47 °C [71]. In addition, *Har.* sp. IRU1 was also cultivated in minimal media containing crude oil as sole carbon source; axenic cultivations for five days with 2% crude oil, 0.4% yeast extract, and 0.016% NaH_2PO_4 at 47 °C were carried out. Unfortunately, only the highest PHB fraction in CDM (41 wt.%) was reported in this article, but no data for productivity or PHB concentration were reported. Still, *Har.* sp. IRU1 was proposed as promising organism for bioremediation of petrochemically polluted environments, combined with value-added PHB biosynthesis [72]. Finally, even textile wastewater was investigated as a substrate for this strain to thrive; in this study, PHA biosynthesis was not monitored [73].

Vinasse, a side-product of molasses-based ethanol manufacturing, comprises non-volatile phenolic compounds, which remain in the residue after distillative ethanol removal; these phenolic compounds are known inhibitors of microbial growth. In 2012, vinasse was studied by Pramanik and colleagues as a substrate to cultivate the extremely halophile *Har. marismortui* [74], the first haloarchaeon unambiguously shown to produce PHB by Kirk and Ginzburg already in the early 1970ies [10]. Using

a highly saline (200 g/L NaCl) cultivation medium containing 10% raw vinasse, *Har. marismortui* accumulated 26 wt.% PHB in CDM and reached a volumetric PHB productivity of 0.015 g/(L·h) in shaking flask experiments. These values became considerably better after removing the phenolic compounds by well-established absorption on charcoal; in a medium consisting of 100% dephenolized vinasse, 30 wt.% PHB in CDM and a volumetric productivity of 0.02 g/(L·h) were reached [66]. However, it should be noticed that PHA biosynthesis is not observed in all *Har.* sp.; e.g., Oren and colleagues did not detect any PHA inclusions when investigating the red, square-shaped Egyptian brine-pool isolate *Har. quadrata* in details [75].

7.2. Halogeometricum sp.

In 2013, Salgaonkar et al. screened seven extremely halophilic Archaea isolated from brine and sediments of solar salterns in India. Defined saline cultivation media with 200 g/L NaCl turned out to be suitable for the growth of all seven microbial isolates; all of them also accumulated PHA. Based on phenotypic and genotypic tests, six strains out of them were grouped into the genus *Haloferax*, and named as strains TN4, TN5, TN6, TN7, TN10, and BBK2, while isolate TN9 was described as the new taxonomic species *Halogeometricum (Hgm.) borinquense*. This new organism performed most auspiciously among the seven isolates, and was investigated in more detail regarding its growth and PHA accumulation kinetics. It was revealed that highest PHA accumulation rates for strain *Hgm. borinquense* TN9 already take place during the exponential phase of growth, hence prior to depletion of growth-essential nutrients. This "growth-associated PHA-production" characteristic differs from most other reported PHA production strains, which typically display maximum PHA productivity not before nutrient deprivation. In biomass, 14 wt.% PHB homopolyester was produced after a cultivation period of five days [76]. Later, the same researchers isolated another haloarchaeon from the Marakkanam solar salterns in Tamil Nadu, India. This new organism was labeled *Hgm. borinquense* E3; the strain produced PHBHV copolyesters when growing in a highly saline medium on glucose as the sole carbon substrate. This copolyester production is similar to the findings discussed above for *Hfx. mediterranei*, but in contrast to the strain´s close relative *Hgm. borinquense* TN9, a strain which produced only PHB homopolyester on glucose. Shaking flask cultivation experiments lasting four days resulted in a high intracellular polymer content of 74 wt.% PHBHV (with 22 mol.% 3HV) in biomass [77]. Additionally, the same research team cultivated four wildtype haloarchaea on hydrolyzed sugarcane bagasse (hSCB), which constitutes an amply available by-product of sugar manufacturing mainly consisting of lignocelluloses. Among these organisms, *Hgm. borinquense* E3 exhibited the highest PHA productivity according to fluorescence measurements after Nile Red staining. The organisms were identified as *Haloferax volcanii* BBK2 (one of the strains isolated in [70]), *Haloarcula japonica* BS2, and *Halococcus salifodinae* BK6. As also described for *Hfx. mediterranei*, strain *Hgm. borinquense* E3 forms slightly pink colored colonies with a slimy appearance, which demonstrated pigment and EPS biosynthesis. In a medium containing 200 g/L NaCl at 37°C and 25% or 50% hSCB, *Hgm. borinquense* E3 was cultivated for six days in shaking flasks. The PHA fractions in biomass amounted to 50 wt.% (25% SCB) and 46 wt.% (50% hSBC), respectively, while specific production rates (q_p) were reported with 3.0 mg/(g·h) for 25% hSCB, and with 2.7 mg/(g·h) for 50% hSBC. A PHBHV copolyester with 13.3 mol.% 3HV was isolated from biomass [78]. Subsequent studies with *Hgm. borinquense* E3 resorted to starch-based waste materials used as substrates for PHA production. In this context, pure starch and acid-hydrolyzed cassava waste were used in parallel shaking flask cultivation experiments at a salinity of 200 g/L NaCl. After ten days, 4.6 g/L PHBHV (13.1 mol.% 3HV) were produced on pure starch, while the use of cassava waste delivered 1.5 g/L PHBHV (19.7 mol.% 3HV) [79]. It is noteworthy that, unfortunately, all cultivations with *Hgm. borinquense* were carried out on a shaking flask scale; scale up experiments under controlled conditions in bioreactors are still missing in the literature.

7.3. Halopiger sp.

A corrosion-resistant bioreactor consisting of polyether ether ketone (PEEK), tech glass and silicium nitrite ceramics was constructed by Hezayen and colleagues [80]. This new composite bioreactor was used for the cultivation of two new extremely halophilic isolates. One of them, "strain 56", today known as *Halopiger (Hpg.) aswanensis* DSM 13151, was studied for PHB production in a medium containing more than 200 g/L NaCl. The other strain, *Natrialba* (*Nab.*) sp., was used to synthesize poly(γ-glutamic acid) as target product in a medium of the same salinity. Both organisms were isolated from hypersaline samples taken from the soil of the Egyptian city Aswan. PHB production by "strain 56" (*Hpg. aswanensis*) on acetate and n-butyric acid as mixed substrate amounted to 4.6 g/L, and the PHB content in CDM to 53 wt.% after 12 days cultivation in batch-mode. It was determined that 40 °C was the optimal temperature to cultivate this strain. The isolated biopolyester had a M_w of 230,000 g/mol and a $Đ_i$ of about 1.4 [80]. In a follow-up study, Hezayen et al. reported for the first time on a PHA synthase of haloarchaea; here, the authors investigated crude extracts of "strain 56" in environments supporting PHA biosynthesis. A protocol for release of PHA granules by cell lysis in hypotonic medium and separation of granules by differential centrifugation was developed, and the granule-associated PHA synthase was studied and characterized [14]. Later, this strain, which forms Gram-negative, motile, pleomorphic pink rods, was biochemically and taxonomically categorized, and is nowadays known as *Hpg. aswanensis* DSM 13151. The organism was reported to produce large amounts of PHB; it also excretes an EPS, which causes high viscosity of the cultivation broth. High salinity of 220–250 g/L NaCl, pH-value 7.5 (range: 6–9.2) and a temperature of 40 °C (maximum accepted temperature: 55 °C) were determined as the optimum condition for this extreme halophilic species to thrive [81].

7.4. Halobiforma sp.

In the study published by Hezayen and colleagues [14], another red pigmented (carotenoid-rich) aerobic organism was isolated from hypersaline Egyptian soil in Aswan. When cultivated for eight days in shaking flasks on butyric acid, this "strain 135^T" accumulated up to 40 wt.% PHB in biomass; on complex substrates like casamino acids, peptone, or yeast extract, even 15 wt.% PHB in biomass were accumulated. This organism requires at least 130 g/L NaCl for biomass growth, and a temperature of 42 °C revealed best growth. The authors classified the new isolate as species *Halobiforma (Hbf.) haloterrestris* sp. nov. (DSM 13078^T) [82]. *Hbf. lacisalsi* sp. nov., a close microbial relative from the genus *Halobiforma*, was later isolated by Xu and associates from a salt lake in China. This organism was shown to grow optimally at 100 g/L NaCl; unfortunately, no tests were reported that refer to PHA biosynthesis [83].

7.5. Natrinema sp.

Danis et al. investigated five extremely halophilic archaeal isolates in order to identify new extremophilic strains with high capacity for PHA biosynthesis; the conversion of different inexpensive raw materials such as cornstarch, melon, apple, and tomato processing waste, sucrose, and whey. Among these materials, cornstarch appeared as the most encouraging substrate for PHA biosynthesis, while among the five isolated haloarchaea, strain 1KYS1 showed highest PHA production capacity. Via comparative 16S rRNA gene sequence analysis, it was revealed that strain 1KYS1 was closely related to the extremely halophilic genus *Natrinema* (*Nnm.*), and, within this genus, to the strain *Nnm. pallidum* JCM 8980. When cultivated on starch as single carbon source and a salinity of 250 g/L NaCl, strain 1KYS1 accumulated 0.53 g PHA per g of its biomass. Transmission electron microscopy (TEM) revealed that the accumulated material, a PHBHV copolyester, forms large, uniform granules ("carbonosomes"), which, after cell lysis, is a considerable benefit for the convenient separation of PHA granules via floatation or centrifugation. In addition, this biopolyester was blended with low molar mass poly(ethylene glycol), which resulted in the preparation of a new type of biocompatible polymer

film, which has been applied for drug release studies using the antibiotic Rifampicin [84]. In 2018, the haloarchaeon *Natrinema ajinwuensis* RM-G10 (synonym: *Natrinema altunense* strain RM-G10) was isolated from salt production pans in India. *Nnm. ajinwuensis* accumulated about 61 wt.% PHA in biomass and showed high volumetric PHA productivity of 0.21 g/(L·h) when cultivated for 72 h in repeated batch shaking flask cultivation setups on glucose. Using glycerol instead of glucose resulted in biomass formation, but not in PHA biosynthesis. The product based on glucose turned out to be a PHBHV copolyester with a 3HV fraction in PHBHV of 0.14 mol/mol, which is a value similar to those reported for other haloarchaeal strains (*vide supra*). When analyzed by DSC, the biopolyesters showed two separated melting endotherms (T_m 143 °C and 157.5 °C), T_g of −12.3 °C, an onset of decomposition temperature (T_d) of 284 °C, and a degree of crystallinity (X_c) of 35.45%. 200 g/L NaCl were reported as optimal salinity for both biomass growth and PHA production by this organism [61].

7.6. Haloquadratum sp.

Unusual organisms, originally isolated at the Egyptian Sinai Peninsula, were described in 1980 by Walsby, who was interested in the highly refractive gas vesicles produced by the microbes; this researcher described his isolates as "ultra-thin square bacteria" [85]. A quarter of a century later, Walsby reported that cells of this strain resemble "thin, square or rectangular sheets with sharp corners", and reported their dimensions being 2–5 μm wide but not even 0.2 μm thick. The outstanding low thickness of sheets makes them bulge slightly, with gas vesicles visible along their edges; he also noted that this organism thrives "at the edge of water activity". Importantly, Walsh also observed "poly-β-hydroxybutyrate granules in the corners" [86]. The organism was for a long time believed to be not culturable in monoseptic cultures, and its genome was deciphered not before 2006 by Bolhuis et al.; these researchers revealed that the strain´s genome encodes photoactive retinal proteins of the membrane and S-layer glycoproteins of the cell wall. In this study, the species name *Haloquadratum (Hqr.) walsbyi* was used [16]. Later, Burns et al. investigated two closely related novel square-shaped aerobic, extremely halophilic members of the haloarchaea, isolated from saltern crystallizers in Australia and Spain, and classified both of them as members of the new species *Hqr. walsbyi*. In this study, the authors described that growth of this occurs at pH 6.0–8.5, 25–45 °C and 14–360 g/L NaCl. The extremely halophilic cells lyse immediately in distilled water and a minimum of ~140 g/L salts is required for growth. Optimal growth occurs under neutral to alkaline conditions, above 180 g/L NaCl. By electron cryomicroscopy, PHA inclusions were reported by the authors, but not further studied or quantified [87]. Nile Blue A and Sudan Black staining of *Hqr. walsbyi* DSM 16790 grown in complex medium further substantiated PHA accumulation by this strain, which was confirmed by ^{1}H-NMR studies of fresh cells, evidencing the accumulation of PHB homopolyester, which, however, did not exceed 0.1% of CDM [69]. In 2011, the strain was grown aerobically with illumination on a medium containing 195 g/L NaCl and 0.5 g glycerol, 0.1 g yeast extract and 1 g sodium pyruvate as carbon sources; atomic force microscopy (AFM) was used for a detailed study of the cellular morphology. Importantly, these AFM studies showed corrugation of the cellular surface due to the presence of PHA granules, which were of almost uniform size within a single cell, and were packaged in tight bags. It was assumed that the primary function of these PHA granules was to reduce the cytosol volume, thus reducing the cellular energy demand for osmotic homeostasis; hence, they play a pivotal role for the strain to cope with the high salinity. In the supplementary material, the authors provided also impressing fluorescence microscope pictures of the cells with PHA granules visible as stained inclusions [88].

7.7. Halococcus sp.

A total of 20 haloarchaeal strains from strain collections were screened by Legat et al. via different PHA-staining techniques (Sudan Black B, Nile Blue A, and Nile Red). Both complex and defined cultivation media were used for the experiments. Further, PHA granules were visualized via TEM, while ^{1}H-NMR spectroscopy was applied to determine PHA composition. Beside strains known before as PHA producers like *Har. hispanica* DSM 4426^T or *Hgr. walsbyi* DSM 16790, other organism like *Hbt.*

noricense DSM 9758^T, *Halococcus (Hcc.) dombrowskii* DSM 14522^T, *Hcc. hamelinensis* JCM 12892^T, *Hcc. morrhuae* DSM 1307^T, *Hcc. qingdaonensis* JCM 13587^T, *Hcc. saccharolyticus* DSM 5350^T, *Hcc. salifodinae* DSM 8989^T, *Hfx. volcanii* DSM 3757^T, *Halorubrum (Hrr.) chaoviator* DSM 19316^T, *Hrr. coriense* DSM 10284^T, *Natronococcus (Ncc.) occultus* DSM 3396^T, and *Natronobacterium (Nbt.) gregoryi* NCMB 2189^T showed for the very first time accumulation of PHA when cultured in defined media with 200 g/L NaCl. By these tests, *Halococcus (Hcc.)* was identified as a new genus of PHA-producing microbes. While *Hcc. saccharolyticus* produced PHB homopolyester, all other strains produced PHBHV copolyesters without a supply of 3HV precursors. In this study, TEM pictures were produced for *Hcc. morrhue* and *Hcc. salifodine*, which showed the presence of at least one PHA carbonosome per cell, each about 0.05 to 0.3 μm in diameter [68].

7.8. Halogranum sp.

The haloarchaeon *Halogranum (Hgn.) amylolyticum* TNN58 was isolated in 2015 by Zhao and colleagues from marine solar salterns near Lianyungang in PR China. This organism was described to be a proficient producer of PHBHV copolyesters from simple, structurally unrelated substrates without being supplied with 3HV-related precursor compounds. Observed by TEM, a high number of PHA granules were visible inside the cells. High 3HV fractions in PHBHV exceeding 0.2 mol/mol are the up to now highest 3HV content in PHBHV reported for PHBHV copolyester production by wild-type organisms from unrelated carbon sources. Nitrogen limitation turned out to support PHBHV production by the strain *Hgn. amylolyticum* TNN58, though PHBHV accumulation occurred in an at least partially growth-associated way. Among the substrates acetate, benzoic acid, butyric acid, casamino acids, glucose, glycerol, lauric acid, and starch, the use of glucose allowed best biomass growth and highest PHA productivity. Fed-batch cultivations under controlled conditions in 7.5 L bioreactors were performed to investigate PHBHV production by *Hgn. amylolyticum* in more details. After 188 h of cultivation, CDM, PHBHV concentration, PHBHV fraction in biomass, and volumetric PHBHV productivity amounted to 29 g/L, 14 g/L, 48 wt.%, and 0.074 g/(L·h), respectively [89].

7.9. Haloterrigena sp.

The haloarchaeon *Haloterrigena (Htg.) hispanica* DSM 18328^T was originally isolated as strain "FP1", and was the dominant organism thriving in a saltern crystallizer pond at Fuente dePiedra in the south of Spain. Romano and colleagues were the first who described this strain. The strain needs a minimum salinity of 150 g/L NaCl to grow optimally; growth occurs in a salinity range of 130–230 g/L NaCl, at pH-values between 6.5 and 8.5, and at temperatures between 37 °C and 60 °C. These authors also mentioned accumulation of "PHB" in this organism under nutritionally optimal cultivation conditions; corresponding to their publication, this postulation was made merely based on observation of PHA inclusions in the phase contrast microscope without characterizing the composition of the material at the level of monomers [90]. Later, *Htg. hispanica* DSM 18328^T was cultivated by Di Donato and colleagues in a highly saline medium containing 200 g/L NaCl using carrot- or tomato waste, which accrues at enormous quantities in many countries like Italy, as sole carbon sources. This study confirmed that this thermophilic strain grows optimally at 50 °C; using this temperature, the organism was cultivated in batch bioreactor fermentation setups, which lasted five days, and also in dialysis fermentations, where bioreactors were equipped with a dialysis tube. Using a complex cultivation medium, the PHB homopolyester was produced at a quantity of 0.135 wt.% PHB in biomass; product composition was determined by ^{1}H-NMR analysis. When using carrot waste as substrate, 0.125 wt.% PHB in biomass were accumulated by *Htg. hispanica*, which is a quantity comparable to results obtained by cultivations on expensive media based on casamino acids and yeast extract. Astonishingly, ^{1}H-NMR analysis of this biopolyesters produced from carrot waste medium disclosed that the homopolyester poly(4-hydroxybutyrate), a highly flexible material with broad use in the surgical field, was produced instead of expected PHB [91].

7.10. Halorhabdus sp.

In 2000, the aerobic organism AX-2T was isolated by Wainø and colleagues from sediments of the Great Salt Lake in Utah, USA. This thermophilic strain grew optimally at extremely high NaCl concentrations of 270 g/L, which that time constituted the highest salinity optimum at all reported for any living species. Further, 50 °C and a neutral pH-value were determined as optimum growth parameters. Only a limited number of carbohydrates, namely glucose, fructose, and xylose, were accepted by the strain for biomass formation, while neither fatty acids nor complex substrates like peptone or yeast extract enabled microbial growth of this strain. Cells of this isolate lyse instantly when exposed to distilled water, and were tested positively for PHA biosynthesis ("PHB is produced"); however, neither quantitative data for PHA production nor PHA composition were reported. Based on the outcomes of 16S rRNA analysis, the strain was classified as member of the Halobacteriaceae, but showed only limited similarity to other described species of this family. The new taxon name *Halorhabdus (Hrd.) utahensis* was selected for this new strain, which is now deposited as DSM 12940^{T} [92]. *Hrd. tiamatea* is another representative of this genus. This extremely halophilic, non-pigmented archaeon was isolated in 2008 by Antunes and colleagues from a hypersaline, anoxic deep-sea brine-sediment interface of the Northern Red Sea, an unusual athalassohaline environment associated with tectonic activity. Also *Hrd. tiamatea* revealed optimal growth at a salinity of 270 g/L NaCl, neutral pH-value, a temperature of 45 °C, and the conversion of starch for biomass formation. In contrast to *Hrd. utahensis*, which can be cultivated under both aerobic and anaerobic conditions, *Hrd. tiamatea* shows a clear preference for microaerophilic environments. However, the fact that *Hrd. tiamatea* accumulates PHA was revealed merely as a short annotation in this publication ("Poly-β-hydroxybutyrate is produced"); for this PHA-production test, based only on observation in phase-contrast microscope, cells were cultivated in HBM minimal medium supplemented with 0.005% (*w*/*v*) NH_4Cl and 0.5 to 1% (*w*/*v*) maltose [93]. Later, the same group of authors deciphered the complete genome of *Hrd. tiamatea*, which disclosed significant differences to the genome of *Hrd. utahensis*; for example, it was revealed that *Hrd. tiamatea* possesses putative trehalose and lactate dehydrogenase synthase genes, which are not found in *Hrd. utahensis* [94]. Finally, the facultative anaerobic strain *Hrd. rudnickae*, isolated from a borehole sample taken at a Polish salt mine, is the third member of the genus *Halorhabdus*, which was described to accumulate PHA. This organism forms non-motile Gram-negative cocci, is red pigmented, und thrives best at a salinity of 200 g/L NaCl, a temperature of 40 °C and a neutral pH-range. Again, PHA inclusions in cells were spotted by TEM, but neither quantified nor characterized ("Poly-β-hydroxybutyrate is produced") [95]. Hence, production of PHA biopolyesters by the *Halorhabdus* genus is still awaiting its kinetic analysis and characterization at the monomeric level.

8. Conclusions

As detailed in the present review, a two-digit number of different haloarchaeal species were already described as potential PHA producers. However, most of these studies were restricted to modest cultivation scales, often merely reporting on microscopic observation and fluorescence staining of PHA granules. To the best of the author´s knowledge gained from the open literature and discussions with other scientists active in this field, there are not more than four haloarchaeal species (*Hfx. mediterranei*, *Hpg. aswanesnsis*, *Hgn. amylolyticum*, and *Htg. hispanica*), for which PHA accumulation was studied in cultivations performed under controlled conditions in bioreactors. However, such bioreactor cultivation setups are the conditio sine qua non to get reliable kinetic data, and reasonable amounts of product for in-depth characterization. Most of all, sufficient amounts of product are needed for processing it to marketable prototype specimens; such processing is completely lacking in the case of haloarchael PHA. Moreover, techno-economic assessment of PHA production by haloarchaea, based on solid experimental data and holistic consideration of the entire production cycle, is only available for *Hfx. mediterranei*, for which economic and life cycle considerations were carried out based on the surplus substrates whey and waste stillage. Nevertheless, exactly these early techno-economic assessments already indicate the high potential of the extremely halophilic members of the Archaea domain for bio-economic biopolyester production of the future. Taking advantage of the broad substrate spectrum, the formation of PHA heteropolyesters of tunable composition and microstructure in dependence on the cultivation strategy, the accessibility of haloarchaea towards inexpensive and convenient product recovery from biomass, the recyclability of process side-streams (spent fermentation broth and cell debris), the detailed knowledge about the complete genome of an increasing number of haloarchaea, and the expedient robustness of such cultivation batches sets haloarchaea at the forefront of efforts dedicated to finally make PHA economically competitive polymers with plastic-like properties, which also match the end-consumer´s expectations. What is needed now is upscaling those processes at a promising lab-scale, and to tap the wealth of haloarchaea reported to produce PHA merely on a qualitative basis, or which have not yet been studied for PHA biosynthesis. In addition, one should be aware of parallel R&D activities with halophilic eubacteria as PHA production strains; here, especially the seminal works with *Halomonas bluephagenensis* TD01 should be mentioned, a proficient PHA production strain which can be cultivated in open bioreactor facilities [96], and which is well studied in terms of genetic manipulation [97,98]. Other examples for promising halophilic eubacteria as PHA producers encompass *Halomonas halophila* [99], or *Halomonas campaniensis* [100]. However, these organisms thrive best under salinities of about 60–70 g/L, which is drastically below the optimum salinity of haloarchaea, which makes the long-term stability of fermentation batches with *Halomonas* sp. uncertain compared with their "competitors" from the realm of haloarchaea.

To summarize the aforementioned, Tables 1 and 2 provide an overview of the PHA production processes by the individual haloarchaea discussed in the review, indicating the productivities, type of biopolyester produced, and studied production scale. While Table 1 collects the setups on smaller scale, Table 2 refers to the rather scarce number of setups carried out under controlled conditions in laboratory and pilot scale bioreactors.

Table 1. PHA production by haloarchaea on shaking flask and stirred flask scale–collected data from literature.

Species	Strain Isolation	Salinity in Medium, Substrates, T	Product	Production Scale/Productivity	Ref.
Hfx. mediterranei	Salt pond at the coast near Alicante, Spain	150 g/L NaCl Molasses wastewater T = 15, 20, 25, and 35 °C	PHBHV (16.7 mol.% 3HV)	2.5 L aerated and stirred flasks 0.62 (g/L·h), $q_{Pmax.}$ = 0.037 1/h (35 °C)	[46]
,,	,,	200 g/L NaCl; T = 37 °C 25–50% pre-treated vinasse	PHBHV (12.4 mol.% 3HV using 25% vinasse) (14.1 mol.% 3HV using 50% vinasse)	Shaking flask scale; 19.7 g/L PHA, 70 wt.% PHA in CDM, 0.21 g/(L·h)	[54]
,,	,,	200 g/L NaCl; T = 37 °C Rice-based stillage	PHBHV (15.3 mol.% 3HV)	Shaking flask scale; 16.4 g/L PHA, 70 wt.% PHA in CDM, 0.17 g/(L·h)	[51]
,,	,,	190 g/L total salts; 144 g/L NaCl; Alkaline hydrolyzed *Ulva* sp. (macroalgae) as substrate T = 42 °C	PHBHV (3 mol.% 3HV)	Shaking flask scale; batch cultivation; 2.2 g/L, 58% PHA in CDM, 0.035 g/(L·h)	[55]
,,	,,	220 g/L NaCl Dephenolized and native olive mill waste water (OMW) T = 37 °C	PHBHV (6.5 mol.% 3HV)	Shaking flask scale, batch cultivation; 43 wt.% PHA in CDM (concentration and productivity data inconsistent in publication)	[53]
,,	,,	156 g/L NaCl; Glucose; nitrate or ammonia as N-source T = 37 °C	PHBHV (12.5 mol.% 3HV using nitrate) (16.9 mol.% 3HV using ammonia)	Shaking flask scale, batch cultivation; 0.63 g/L, 4.6% PHA in CDM, 0.035 g/(L·h) with ammonia (C/N = 8) 0.80 g/L, 9.3% PHA in CDM, 0.035 g/(L·h) with ammonia (C/N =8)	[44]
,,	,,	156 g/L NaCl; T = 37 °C Glucose; varying phosphate concentrations	PHBHV (22.4 mol.% 3HV)	500 mL shaking flasks, batch 0.95 g/L PHA, 15.6 % PHA in CDM; 0.007 g/(L·h) with optimum phosphate concentration 0.5 g/L KH_2PO_4	[45]
,,	,,	156 g/L NaCl; Different even- or add-numbered fatty acids T = 37 °C	PHBHV (random or *b*-PHBHV) (<10 mol.% 3HV using even-numbered acids) (>87 mol.% 3HV using odd-numbered acids)	Shaking flask scale; batch and fed-batch 0.4–1.5 g/L PHA, 10.3–27.1 wt.% PHA in CDM, 0.003–0.010 g/(L·h) (fed-batch, dependent on C-source)	[66]
Hfx. volcanii	Dead Sea	200 g/L NaCl; T = 37 °C Glucose	?	Shaking flask scale; Below detection limit	[68]

Table 1. *Cont.*

Species	Strain Isolation	Salinity in Medium, Substrates, T	Product	Production Scale/Productivity	Ref.
,,	,,	250 g/L NaCl; T = 37 °C Glucose + yeast extract	"PHB"	Shaking flask scale; 7 wt.% PHA in CDM	[29]
,, (strain BBK2)	Solar salterns of Ribandar in Goa, India	200 g/L NaCl; T = 37 °C Sugarcane bagasse hydrolysate	? (not identified)	Shaking flask scale; Not quantified	[78]
Hfx. gibbonsii	Salt pond at the coast near Alicante, Spain		"PHB"	Shaking flask scale; 1.2 wt.% PHA in CDM	[29]
Har. marismortui	Dead Sea	200 g/L NaCl; Raw and charcoal-pretreated vinasse from bioethanol production	PHB	Shaking flak scale; PHA content in CDM between 23 wt.% (10% non-detoxified vinasse) and 30 wt.% (100% charcoal-detoxified vinasse); 0.015 (non-detoxified) and 0.02 (detoxified) g/(L·h) PHB (2.8 and 4.5 g/L PHB, respectively)	[74]
Har. hispanica	Salt pond at the coast near Alicante, Spain	250 g/L NaCl; T = 37 °C Glucose + yeast extract	"PHB"	Shaking flask scale; PHA content: 2.6 wt.% PHA in CDM	[29]
,,	,,	200 g/L NaCl; T = 37 °C Glucose	PHBHV	0.09 wt.% PHA in CDM	[68]
***Har.*sp. IRU1**	Hypersaline Urmia lake, Iran	250 g/L NaCl 42 °C (other T tested) Glucose (other substrates tested)	PHB	Shaking flask scale; 66 wt.% PHB in CDM	[69]
,,	,,	250 g/L NaCl 42 °C (other T tested) Glucose (other substrates tested)	PHB	Shaking flask scale; 62 (glucose), 57 (starch), 56 (sucrose), 55 (fructose), 40 (acetate), 39 (palmitic acid) wt.% PHB in CDM Max. PHA concentration and productivity: 0.98 g/L, 0.016 g/(L·h) (glucose)	[70]
		250 g/L NaCl 47 °C (other T tested) Petrochemical wastewater, tryptone	PHB	Shaking flask scale; Max. 46.6 wt.% PHB in CDM (2% petrochemical wastewater, yeast extract, 47 °C	[71]
,,	,,	250 g/L NaCl 47 °C (other T tested) Crude oil, yeast extract (other N-sources tested)	PHB	Shaking flask scale; Max. 41.3 wt.% PHB in CDM (2% crude oil, yeast extract, 47 °C)	[72]

Table 1. *Cont.*

Species	Strain Isolation	Salinity in Medium, Substrates, T	Product	Production Scale/Productivity	Ref.
Har. Japonica (strain BS2)	Solar salterns of Ribandar in Goa, India	200 g/L NaCl; T = 37 °C Sugarcane bagasse hydrolysate	? (not identified)	Shaking flask scale; Not quantified	[78]
Hgm. borinquense (strain TN9)	Solar salterns of Marakkanam in Tamil Nadu, India	200 g/L NaCl; T = 37 °C Glucose	PHB	Shaking flask scale; PHA content in CDM 14 wt.%; ca. 3 mg/(L·h) PHA	[76]
Hgm. Borinquense (strain E3)	Solar salterns of Marakkanam in Tamil Nadu, India	200 g/L NaCl; T = 37 °C Glucose	PHBHV (21.5 mol.% 3HV)	Shaking flask scale; PHA content in CDM 74 wt.%; 0.21 g/(L·h) PHA	[77]
´´	´´	200 g/L NaCl; T = 37 °C 25% and 50% hydrolyzed sugarcane bagasse	PHBHV (13.3 mol.% 3HV)	Shaking flak scale; PHA content in CDM between 45 and 50 wt.%; 0.0113 g/(L·h) PHBHV on 25%	[78]
´´	´´	200 g/L NaCl; T = 37 °C Starch and carbon-rich fibrous waste (cassava bagasse)	PHBHV (13.1% 3HV with starch, 19.7% 3HV with cassava waste)	Shaking flask cultivations in batch mode; Starch: 4.6 g/L PHA, 0.02 g/(L·h), 74.2% PHA in CDM, Cassava bagasse: 1.52 g/L, 0.006 g/(L·h), 44.7% PHA in CDM	[79]
Hbt. noricense	Bore core of an Austrian Permian salt deposit	200 g/L NaCl; T = 37 °C Glucose	PHBHV	Shaking flask scale; 0.11 wt.% PHA in CDM	[68]
Hcc. dombrowskii	Dry rock salt from Austrian alpine salt mine	Complex saline medium; T = 37 °C	PHBHV	Shaking flask scale; 0.16 wt.% PHA in CDM	[68]
Hcc. hamelinensis	Stromatolites from the Hamelin pool in the Australian Shark Bay	Complex saline medium; T = 37 °C	PHBHV	Shaking flask scale; Not quantified	[68]
Hcc. morrhuae	Dead Sea	Complex saline medium; T = 37 °C	PHBHV	Shaking flask scale; Not quantified	[68]
Hcc. qingdaonensis	Crude sea-salt sample collected near Qingdao, PR China	Complex saline medium; T = 37 °C	PHBHV	Shaking flask scale; Not quantified	[69]
Hcc. saccharolyticus	Salt; Cadiz, Spain	Complex saline medium; T = 37 °C	PHB	Shaking flask scale; 1.2 wt.% PHA in CDM	[68]
Hcc. salifodinae	Austrian alpine rock salt	Complex saline medium; T = 37 °C	PHBHV	Shaking flask scale; 0.06 wt.% PHA in CDM	[68]

Table 1. *Cont.*

Species	Strain Isolation	Salinity in Medium, Substrates, T	Product	Production Scale/Productivity	Ref.
´´ (strain BK6)	Solar salterns of Ribandar in Goa, India	200 g/L NaCl; T = 37 °C Sugarcane bagasse hydrolysate	n.d.	Shaking flask scale; Below detection limit	[78]
Hrr. chaviator	Sea salt in Baja California, Mexico, Western Australia and Greece	200 g/L NaCl; T = 37 °C Glucose	PHBHV	Shaking flask scale; Not quantified	[68]
Hrr. coriense	Dead Sea	200 g/L NaCl; T = 37 °C Glucose	PHBHV	Shaking flask scale; Not quantified	[68]
Hbf. Haloterrestris ("strain 135(T)")	Samples collected from surface of hypersaline soil collected in Aswan, Egypt	220 g/L NaCl; T = 42 °C (other T tested) Acetate + butyric acid or complex media	PHB	Shaking flask scale; 40 wt.% PHB in CDM on butyric acid, 15 wt.% PHB in CDM on complex medium	[83]
Nnm. ajinwuensis (=altunense)	Indian salt production pans	200 g/L NaCl (other salinities tested); T = 37 °C Glucose	PHBHV (13.9 mol.% 3HV)	Repeated batch cultivations in shaking flaks PHA content in CDM 61 wt.%; ca. 15 g/L PHA; 0.21 g/(L·h) PHA	[61]
Nnm. Palladium (strain JCM 8980, =isolate 1KYS1)	Kayacik saltern, Turkey	250 g/L NaCl; Starch	PHBHV (25 mol.% 3HV)	Shaking flak cultivations; PHA content in CDM 53 wt.%; 0.3 mg/(L·h) PHA	[84]
Nbt. gregoryi	Soda slat lake liquors from the East African Magadi soda lake	200 g/L NaCl; T = 37 °C alkaliphile; Carbohydrates	PHB	Shaking flask scale; 0.62 wt.% PHB	[68]
Ncc. occultus	Magadi Lake, Kenia	200 g/L NaCl; T = 37 °C alkaliphile; Glucose	PHBHV	Shaking flask scale; 3.1 wt.% PHB	[68]
Hrd. utahensis	Sediments of the Great Salt Lake in Utah	270 g/L NaCl (maximum described salinity optimum for living beings!); T = 50 °C Limited number of carbohydrates	Not specified ("PHB is produced")	Shaking flask scale; No quantitative data	[93]
Hrd. tiamatea	Hypersaline, anoxic deep-sea brine-sediment interface of the Red Sea	270 g/L NaCl (maximum described salinity optimum for living beings!); T = 45 °C Starch	Not specified ("PHB is produced")	Shaking flask scale; No quantitative data	[94]
Hrd. rudnickae	Borehole at Polish salt mine	200 g/L NaCl; T = 40 °C	Not specified ("PHB is produced")	Shaking flask scale; No quantitative data	[96]
Hqr. walsbyi	Sinai peninsula and saltern crystallizers in Australia and Spain	140–360 g/L NaCl for growth (optimum: >180 g/L); T = 25–45 °C	PHB	Shaking flaks scale; <1 wt.% PHA in CDM	[68,88,89]

Table 2. PHA production by haloarchaea on bioreactor scale—collected data from literature.

Species	Strain Isolation	Salinity in Medium, Substrates, T	Product	Production Scale/Productivity	Ref.
Hfx. mediterranei	Salt pond at the coast near Alicante, Spain	250 g/L marine salts Starch (20 g/L) Glucose (10 g/L) T = 38 °C (other T tested)	PHBHV (in publication: "PHB")	Stable (monoseptic) continuous cultivation over 3 months in 1.5 L bioreactor; 6.5 g/L PHA on starch 3.5 g/L on glucose	[32]
,,	,,	150 g/L NaCl; T = 37 °C Glucose plus yeast extract	PHBHV (10 mol.% 3HV)	10 L bioreactor; fed-batch feeding; 0.21 g/(L·h), 13 g/L PHA, 0.7 g PHA in CDM	[37]
,,	,,	200 g/L NaCl; T = 37 °C Hydrolyzed whey permeate Hydrolyzed whey permeate plus GBL	PHBHV (6 mol.% 3HV) P(3HB-*co*-3HV-*co*-4HB) (21.8 mol.% 3HV, 5.1 mol.% 4HB)	42 L bioreactor fed-batch process; 0.09 g/(L·h), 12.2 g/L PHBHV 0.14 g/(L·h), 14.7 g/L poly(3HB-*co*-3HV-*co*-4HB)	[47]
,,	,,	150 g/L NaCl; T = 37 °C Hydrolyzed whey permeate	PHBHV (10 mol.% 3HV)	200 L fed-batch **pilot process** (300 L bioreactor); **techno-economic assessment** 7.2 g/L PHA, 66 wt.% PHA in CDM, 0.11 g/(L·h)	[58,59]
,,	,,	200 g/L NaCl; T = 37 °C Hydrolyzed whey permeate, spent fermentation broth and saline cell debris from previous whey-based processes	PHBHV (10 mol.% 3HV)	10 L bioreactor batch process 0.04 g/(L·h), 2.28 g/L PHA	[58]
,,	,,	156 g/L NaCl; T = 37 °C Hydrolyzed whey permeate, elevated trace element concentration	PHBHV (<2 mol.% 3HV)	2 L bioreactor batch process 8 g/L PHBHV, 0.17 g/(L·h), 53 wt.% PHA in CDM	[48]
,,	,,	150 g/L NaCl; T = 37 °C CGP; CGP plus GBL	PHBHV (10 mol.% 3HV) P(3HB-*co*-3HV-*co*-4HB) (11 mol.% 3HV, 5 mol.% 4HB)	42 L/10 L bioreactor fed-batch process; 0.12 g/(L·h), 16.2 g/L PHA 0.10 g/(L·h), 11.1 g/L PHA	[33]
,,	,,	200–230 g/L NaCl; T = 37 °C Native cornstarch treated via enzymatic reactive extrusion	PHBHV (10.4 mol.% 3HV)	6 L bioreactor pH-stat fed-batch process; 0.28 g/(L·h), 0.508 g PHA in CDM; 20 g/L PHA	[49]

Table 2. *Cont.*

Species	Strain Isolation	Salinity in Medium, Substrates, T	Product	Production Scale/Productivity	Ref.
´´	´´	234 g/L NaCl; T = 37 °C Mixtures of extruded rice bran plus extruded cornstarch	PHBHV (about 11 mol.% 3HV)	5 L bioreactor; pH-stat feeding strategy; 77.8 g/L PHA	[50]
	´´	200 g/L NaCl; Rice-based stillage T: n.r,	PHBHV (17.9 mol.% 3HV)	Unsterile 50 L plug-flow PMMA bioreactor; **techno-economic assessment** 13 g/L PHA, 63 wt.% PHA in CDM, 0.14 g/(L·h)	[52]
´´	´´	156 g/L NaCl; Mixes of butyric & valeric acid; Tween80 T = 37 °C	PHBHV (43 mol.% 3HV at butyric/valeric acid = 56/44)	Fed-batch bioreactor cultivation 4.01 g/L PHA, 59 wt.% PHA in CDM; 0.01 g/(L·h)	[65]
´´ (EPS-negative mutant; strain "ES1")	´´	140 g/L total salts (110 g/L NaCl) Glucose and valerate T = 37 °C	*b*-PHBHV (up to 50 mol.% 3HV at end of fermentation)	7 L fed-batch bioreactor cultivation Results only reported for shaking flask experiments: max. ca. 5 g/L PHA, 50 wt.% PHA in CDM; 0.17 g/(L·h)	[64]
Hgr. amylolyticum	Tainan marine solar saltern near Lianyungang, PR China	200 g/L NaCl; T = 37 °C Glucose	PHBHV (>20 mol.% 3HV)	7.5 L bioreactor; fed-batch feeding strategy; 0.074 g/(L·h), 14 g/L PHBHV, 48 wt.% PHA in CDM	[89]
Hpg. Aswanensis ("strain 56")	Samples collected from surface of hypersaline soil collected in Aswan, Egypt	250 g/L NaCl; T = 40 °C Sodium acetate and butyric acid	PHB	Corrosion-resistant 8 L composite bioreactor; batch feeding; 0.0045 g/(L·h), 53 wt.% PHB in CDM, 4.6 g/L PHB, 0.018 g/(L·h)	[80]
Htg. hispanica	Saltern crystallizer pond at Fuente de Piedra saline lake, Malaga, Spain	200 g/L NaCl; T = 37 °C Complex medium Carrot waste	PHB (complex medium) P(3HB-*co*-3HV-*co*-4HB) (carrot waste)	Bioreactor; batch setups and bioreactor equipped with ultrafiltration unit 0.135 wt.% PHA in CDM (complex medium); 0.125 wt.% PHA in CDM (carrot waste)	[91]

Funding: This research received no external funding.

Conflicts of Interest: The author declares no conflict of interest.

References

1. Lemoigne, M. Produits de Deshydration et de Polymerisation de L'acide β = Oxybutyrique. *Bull. Soc. Chim. Biol.* **1926**, *8*, 770–782.
2. Jendrossek, D. Polyhydroxyalkanoate granules are complex subcellular organelles (carbonosomes). *J. Bacteriol.* **2009**, *191*, 3195–3202. [CrossRef]
3. Kourmentza, C.; Plácido, J.; Venetsaneas, N.; Burniol-Figols, A.; Varrone, C.; Gavala, H.N.; Reis, M.A. Recent advances and challenges towards sustainable polyhydroxyalkanoate (PHA) production. *Bioengineering* **2017**, *4*, 55. [CrossRef]
4. Koller, M.; Maršálek, L.; Miranda de Sousa Dias, M.; Braunegg, G. Producing microbial polyhydroxyalkanoate (PHA) biopolyesters in a sustainable manner. *New Biotechnol.* **2017**, *37*, 24–38. [CrossRef]
5. Koller, M. Chemical and biochemical engineering approaches in manufacturing Polyhydroxyalkanoate (PHA) biopolyesters of tailored structure with focus on the diversity of building blocks. *Chem. Biochem. Eng. Q.* **2018**, *32*, 413–438. [CrossRef]
6. Koller, M. A review on established and emerging fermentation schemes for microbial production of Polyhydroxyalkanoate (PHA) biopolyesters. *Fermentation* **2018**, *4*, 30. [CrossRef]
7. Oren, A.; Ventosa, A. International Committee on Systematics of Prokaryotes Subcommittee on the taxonomy of Halobacteriaceae and subcommittee on the taxonomy of Halomonadaceae. Minutes of the joint open meeting, 23 May 2016, San Juan, Puerto Rico. *Int. J. Syst. Evol. Microbiol.* **2016**, *66*, 4291. [CrossRef]
8. Gupta, R.S.; Naushad, S.; Baker, S. Phylogenomic analyses and molecular signatures for the class *Halobacteria* and its two major clades: A proposal for division of the class *Halobacteria* into an emended order *Halobacteriales* and two new orders, *Haloferacales* ord. nov. and *Natrialbales* ord. nov., containing the novel families *Haloferacaceae* fam. nov. and *Natrialbaceae* fam. nov. *Int. J. Syst. Evol. Microbiol.* **2015**, *65*, 1050–1069. [CrossRef] [PubMed]
9. Gupta, R.S.; Naushad, S.; Fabros, R.; Adeolu, M. A phylogenomic reappraisal of family-level divisions within the class *Halobacteria*: Proposal to divide the order *Halobacteriales* into the families *Halobacteriaceae*, *Haloarculaceae* fam. nov., and *Halococcaceae* fam. nov., and the order *Haloferacales* into the families, *Haloferacaceae* and *Halorubraceae* fam nov. *Antonie van Leeuwenhoek* **2016**, *109*, 565–587. [CrossRef] [PubMed]
10. Kirk, R.G.; Ginzburg, M. Ultrastructure of two species of halobacterium. *J. Ultrastruct. Res.* **1972**, *41*, 80–94. [CrossRef]
11. Nicolaus, B.; Lama, L.; Esposito, E.; Manca, M.C.; Improta, R.; Bellitti, M.R.; Duckworth, A.W.; Grant, W.D.; Gambacorta, A. *Haloarcula* spp able to biosynthesize exo-and endopolymers. *J. Ind. Microbiol. Biotechnol.* **1999**, *23*, 489–496. [CrossRef]
12. Quillaguamán, J.; Guzmán, H.; Van-Thuoc, D.; Hatti-Kaul, R. Synthesis and production of polyhydroxyalkanoates by halophiles: Current potential and future prospects. *Appl. Microbiol. Biotechnol.* **2010**, *85*, 1687–1696. [CrossRef] [PubMed]
13. Mezzolla, V.; D'Urso, O.; Poltronieri, P. Role of PhaC type I and Type II enzymes during PHA biosynthesis. *Polymers* **2018**, *10*, 910. [CrossRef]
14. Hezayen, F.F.; Steinbüchel, A.; Rehm, B.H. Biochemical and enzymological properties of the polyhydroxybutyrate synthase from the extremely halophilic archaeon strain 56. *Arch. Biochem. Biophys.* **2002**, *403*, 284–291. [CrossRef]
15. Baliga, N.S.; Bonneau, R.; Facciotti, M.T.; Pan, M.; Glusman, G.; Deutsch, E.W.; Shannon, P.; Chiu, Y.; Weng, R.S.; Gan, R.R.; et al. Genome sequence of *Haloarcula marismortui*: A halophilic archaeon from the Dead Sea. *Genome Res.* **2004**, *14*, 2221–2234. [CrossRef]
16. Bolhuis, H.; Palm, P.; Wende, A.; Falb, M.; Rampp, M.; Rodriguez-Valera, F.; Pfeiffer, F.; Oesterhelt, D. The genome of the square archaeon *Haloquadratum walsbyi*: Life at the limits of water activity. *BMC Genom.* **2006**, *7*, 169–180. [CrossRef] [PubMed]
17. Han, J.; Lu, Q.; Zhou, L.; Zhou, J.; Xiang, H. Molecular characterization of the $phaEC_{Hm}$ genes, required for biosynthesis of poly(3-hydroxybutyrate) in the extremely halophilic archaeon *Haloarcula marismortui*. *Appl. Environ. Microbiol.* **2007**, *73*, 6058–6065. [CrossRef] [PubMed]

18. Lu, Q.; Han, J.; Zhou, L.; Zhou, J.; Xiang, H. Genetic and biochemical characterization of the poly(3-hydroxybutyrate-*co*-3-hydroxyvalerate) synthase in *Haloferax mediterranei*. *J. Bacteriol.* **2008**, *190*, 4173–4180. [CrossRef]
19. Han, J.; Li, M.; Hou, J.; Wu, L.; Zhou, J.; Xiang, H. Comparison of four *phaC* genes from *Haloferax mediterranei* and their function in different PHBV copolymer biosyntheses in *Haloarcula hispanica*. *Saline Syst.* **2010**, *6*, 9. [CrossRef]
20. Han, J.; Zhang, F.; Hou, J.; Liu, X.; Li, M.; Liu, H.; Cai, L.; Zhang, B.; Chen, Y.; Zhou, J.; et al. Complete genome sequence of the metabolically versatile halophilic archaeon *Haloferax mediterranei*, a poly(3-hydroxybutyrate-*co*-3-hydroxyvalerate) producer. *J. Bacteriol.* **2012**, *194*, 4463–4464. [CrossRef]
21. Ding, J.Y.; Chiang, P.W.; Hong, M.J.; Dyall-Smith, M.; Tang, S.L. Complete genome sequence of the extremely halophilic archaeon *Haloarcula hispanica* strain N601. *Genome Announc.* **2014**, *2*, e00178-14. [CrossRef] [PubMed]
22. Hou, J.; Feng, B.; Han, J.; Liu, H.; Zhao, D.; Zhou, J.; Xiang, H. Haloarchaeal-type beta-ketothiolases involved in Poly(3-hydroxybutyrate-co-3-hydroxyvalerate) synthesis in *Haloferax mediterranei*. *Appl. Environ. Microbiol.* **2013**, *79*, 5104–5111. [CrossRef]
23. Han, J.; Hou, J.; Liu, H.; Cai, S.; Feng, B.; Zhou, J.; Xiang, H. Wide distribution among halophilic archaea of a novel polyhydroxyalkanoate synthase subtype with homology to bacterial type III synthases. *Appl. Environ. Microbiol.* **2010**, *76*, 7811–7819. [CrossRef] [PubMed]
24. Han, J.; Lu, Q.; Zhou, L.; Liu, H.; Xiang, H. Identification of the polyhydroxyalkanoate (PHA)-specific acetoacetyl coenzyme A reductase among multiple FabG paralogs in *Haloarcula hispanica* and reconstruction of the PHA biosynthetic pathway in *Haloferax volcanii*. *Appl. Environ. Microbiol.* **2009**, *75*, 6168–6175. [CrossRef] [PubMed]
25. Feng, B.; Cai, S.; Han, J.; Liu, H.; Zhou, J.; Xiang, H. Identification of the *phaB* genes and analysis of the PHBHV precursor supplying pathway in *Haloferax mediterranei*. *Acta Microbiol. Sin.* **2010**, *50*, 1305–1312.
26. Xiang, H. PHBHV Biosynthesis by *Haloferax mediterranei*: From Genetics, Metabolism, and Engineering to Economical Production. In *Microbial Biopolyester Production, Performance and Processing. Microbiology, Feedsstocks, and Metabolism*; Koller, M., Ed.; Book Series: Recent Advances in Biotechnology; Bentham Science Publishers: Sharjah, United Arab Emirates, 2016; Volume 1, pp. 348–379.
27. Rodríguez-Valera, F.; Ruiz-Berraquero, F.; Ramos-Cormenzana, A. Behaviour of mixed populations of halophilic bacteria in continuous cultures. *Can. J. Microbiol.* **1980**, *26*, 1259–1263. [CrossRef]
28. Rodriguez-Valera, F.; Juez, G.; Kushner, D.J. *Halobacterium mediterranei* spec, nov., a new carbohydrate-utilizing extreme halophile. *Syst. Appl. Microbiol.* **1983**, *4*, 369–381. [CrossRef]
29. Fernandez-Castillo, R.; Rodriguez-Valera, F.; Gonzalez-Ramos, J.; Ruiz-Berraquero, F. Accumulation of poly(β-hydroxybutyrate) by halobacteria. *Appl. Environ. Microbiol.* **1986**, *51*, 214–216.
30. Torreblanca, M.; Rodriguez-Valera, F.; Juez, G.; Ventosa, A.; Kamekura, M.; Kates, M. Classification of non-alkaliphilic halobacteria based on numerical taxonomy and polar lipid composition, and description of *Haloarcula* gen. nov. and *Haloferax* gen. nov. *Syst. Appl. Microbiol.* **1986**, *8*, 89–99. [CrossRef]
31. Rodriguez-Valera, F.; Lillo, J. Halobacteria as producers of polyhydroxyalkanoates. *FEMS Microbiol. Lett.* **1982**, *103*, 181–186. [CrossRef]
32. Lillo, J.G.; Rodriguez-Valera, F. Effects of culture conditions on poly(β-hydroxybutyric acid) production by *Haloferax mediterranei*. *Appl. Environ. Microbiol.* **1990**, *56*, 2517–2521.
33. Antón, J.; Meseguer, I.; Rodriguez-Valera, F. Production of an extracellular polysaccharide by *Haloferax mediterranei*. *Appl. Environ. Microbiol.* **1988**, *54*, 2381–2386.
34. Hermann-Krauss, C.; Koller, M.; Muhr, A.; Fasl, H.; Stelzer, F.; Braunegg, G. Archaeal production of polyhydroxyalkanoate (PHA) co-and terpolyesters from biodiesel industry-derived by-products. *Archaea* **2013**, *2013*, 129268. [CrossRef]
35. Oren, A. Microbial life at high salt concentrations: Phylogenetic and metabolic diversity. *Saline Syst.* **2008**, *4*, 1–13. [CrossRef]
36. Parolis, H.; Parolis, L.A.; Boán, I.F.; Rodríguez-Valera, F.; Widmalm, G.; Manca, M.C.; Jansson, P.-E.; Sutherland, I.W. The structure of the exopolysaccharide produced by the halophilic Archaeon *Haloferax mediterranei* strain R4 (ATCC 33500). *Carbohydr. Res.* **1996**, *295*, 147–156. [CrossRef]

37. Koller, M.; Chiellini, E.; Braunegg, G. Study on the production and re-use of poly(3-hydroxybutyrate-co-3-hydroxyvalerate) and extracellular polysaccharide by the archaeon *Haloferax mediterranei* strain DSM 1411. *Chem. Biochem. Eng. Q.* **2015**, *29*, 87–98. [CrossRef]
38. Cui, Y.W.; Gong, X.Y.; Shi, Y.P.; Wang, Z.D. Salinity effect on production of PHA and EPS by *Haloferax mediterranei*. *RSC Adv.* **2017**, *7*, 53587–53595. [CrossRef]
39. Han, J.; Hou, J.; Zhang, F.; Ai, G.; Li, M.; Cai, S.; Liu, H.; Wang, L.; Wang, Z.; Zhang, S.; Cai, L.; Zhao, D.; Zhou, J.; Xiang, H. Multiple propionyl coenzyme A-supplying pathways for production of the bioplastic poly(3-hydroxybutyrate-*co*-3-hydroxyvalerate) in *Haloferax mediterranei*. *Appl. Environ. Microbiol.* **2013**, *79*, 2922–2931. [CrossRef]
40. Koller, M. Switching from petro-plastics to microbial polyhydroxyalkanoates (PHA): The biotechnological escape route of choice out of the plastic predicament? *The EuroBiotech J.* **2019**, *3*, 32–44. [CrossRef]
41. Koller, M.; Hesse, P.; Bona, R.; Kutschera, C.; Atlić, A.; Braunegg, G. Potential of various archae-and eubacterial strains as industrial polyhydroxyalkanoate producers from whey. *Macromol. Biosci.* **2007**, *7*, 218–226. [CrossRef]
42. Cai, S.; Cai, L.; Liu, H.; Liu, X.; Han, J.; Zhou, J.; Xiang, H. Identification of the haloarchaeal phasin (PhaP) that functions in polyhydroxyalkanoate accumulation and granule formation in *Haloferax mediterranei*. *Appl. Environ. Microbiol.* **2012**, *78*, 1946–1952. [CrossRef]
43. Liu, G.; Hou, J.; Cai, S.; Zhao, D.; Cai, L.; Han, J.; Zhou, J.; Xiang, H. A patatin-like protein associated with the polyhydroxyalkanoate (PHA) granules of *Haloferax mediterranei* acts as an efficient depolymerase in the degradation of native PHA. *Appl. Environ. Microbiol.* **2015**, *81*, 3029–3038. [CrossRef]
44. Ferre-Güell, A.; Winterburn, J. Production of the copolymer poly(3-hydroxybutyrate-*co*-3-hydroxyvalerate) with varied composition using different nitrogen sources with *Haloferax mediterranei*. *Extremophiles* **2017**, *21*, 1037–1047. [CrossRef]
45. Melanie, S.; Winterburn, J.B.; Devianto, H. Production of biopolymer Polyhydroxyalkanoates (PHA) by extreme halophilic marine Archaea *Haloferax mediterranei* in medium with varying phosphorus concentration. *J. Eng. Technol. Sci.* **2018**, *50*, 255–271. [CrossRef]
46. Cui, Y.W.; Zhang, H.Y.; Ji, S.Y.; Wang, Z.W. Kinetic analysis of the temperature effect on polyhydroxyalkanoate production by *Haloferax mediterranei* in synthetic molasses wastewater. *J. Polym. Environ.* **2017**, *25*, 277–285. [CrossRef]
47. Koller, M.; Hesse, P.; Bona, R.; Kutschera, C.; Atlić, A.; Braunegg, G. Biosynthesis of high quality polyhydroxyalkanoate co-and terpolyesters for potential medical application by the archaeon *Haloferax mediterranei*. *Macromol. Symp.* **2007**, *253*, 33–39. [CrossRef]
48. Pais, J.; Serafim, L.S.; Freitas, F.; Reis, M.A. Conversion of cheese whey into poly(3-hydroxybutyrate-*co*-3-hydroxyvalerate) by *Haloferax mediterranei*. *New Biotechnol.* **2016**, *33*, 224–230. [CrossRef]
49. Chen, C.W.; Don, T.M.; Yen, H.F. Enzymatic extruded starch as a carbon source for the production of poly(3-hydroxybutyrate-*co*-3-hydroxyvalerate) by *Haloferax mediterranei*. *Process Biochem.* **2006**, *41*, 2289–2296. [CrossRef]
50. Huang, T.Y.; Duan, K.J.; Huang, S.Y.; Chen, C.W. Production of polyhydroxyalkanoates from inexpensive extruded rice bran and starch by *Haloferax mediterranei*. *J. Ind. Microbiol. Biotechnol.* **2006**, *33*, 701–706. [CrossRef]
51. Bhattacharyya, A.; Saha, J.; Haldar, S.; Bhowmic, A.; Mukhopadhyay, U.K.; Mukherjee, J. Production of poly-3-(hydroxybutyrate-*co*-hydroxyvalerate) by *Haloferax mediterranei* using rice-based ethanol stillage with simultaneous recovery and re-use of medium salts. *Extremophiles* **2014**, *18*, 463–470. [CrossRef]
52. Bhattacharyya, A.; Jana, K.; Haldar, S.; Bhowmic, A.; Mukhopadhyay, U.K.; De, S.; Mukherjee, J. Integration of poly-3-(hydroxybutyrate-*co*-hydroxyvalerate) production by *Haloferax mediterranei* through utilization of stillage from rice-based ethanol manufacture in India and its techno-economic analysis. *World J. Microbiol. Biotechnol.* **2015**, *31*, 717–727. [CrossRef]
53. Alsafadi, D.; Al-Mashaqbeh, O. A one-stage cultivation process for the production of poly-3-(hydroxybutyrate-*co*-hydroxyvalerate) from olive mill wastewater by *Haloferax mediterranei*. *New Biotechnol.* **2017**, *34*, 47–53. [CrossRef]
54. Bhattacharyya, A.; Pramanik, A.; Maji, S.K.; Haldar, S.; Mukhopadhyay, U.K.; Mukherjee, J. Utilization of vinasse for production of poly-3-(hydroxybutyrate-*co*-hydroxyvalerate) by *Haloferax mediterranei*. *AMB Express* **2012**, *2*, 34. [CrossRef]

55. Ghosh, S.; Gnaim, R.; Greiserman, S.; Fadeev, L.; Gozin, M.; Golberg, A. Macroalgal biomass subcritical hydrolysates for the production of polyhydroxyalkanoate (PHA) by *Haloferax mediterranei*. *Bioresour. Technol.* **2019**, *271*, 166–173. [CrossRef]
56. Koller, M.; Puppi, D.; Chiellini, F.; Braunegg, G. Comparing chemical and enzymatic Hydrolysis of whey lactose to generate feedstocks for haloarchaeal poly(3-hydroxybutyrate-*co*-3-hydroxyvalerate) biosynthesis. *Int. J. Pharm. Sci. Res.* **2016**, *3*, 112. [CrossRef]
57. Koller, M.; Atlić, A.; Gonzalez-Garcia, Y.; Kutschera, C.; Braunegg, G. Polyhydroxyalkanoate (PHA) biosynthesis from whey lactose. *Macromol. Symp.* **2008**, *27*, 287–292. [CrossRef]
58. Koller, M. Recycling of waste streams of the biotechnological poly(hydroxyalkanoate) production by *Haloferax mediterranei* on whey. *Int. J. Polym. Sci.* **2015**, *2015*, 370164. [CrossRef]
59. Koller, M.; Sandholzer, D.; Salerno, A.; Braunegg, G.; Narodoslawsky, M. Biopolymer from industrial residues: Life cycle assessment of poly(hydroxyalkanoates) from whey. *Resour. Conserv. Recycl.* **2013**, *73*, 64–71. [CrossRef]
60. Narodoslawsky, M.; Shazad, K.; Kollmann, R.; Schnitzer, H. LCA of PHA production–Identifying the ecological potential of bio-plastic. *Chem. Biochem. Eng. Q.* **2015**, *29*, 299–305. [CrossRef]
61. Mahansaria, R.; Dhara, A.; Saha, A.; Haldar, S.; Mukherjee, J. Production enhancement and characterization of the polyhydroxyalkanoate produced by *Natrinema ajinwuensis* (as synonym)≡ *Natrinema altunense* strain RM-G10. *Int. J. Biol. Macromol.* **2018**, *107*, 1480–1490. [CrossRef]
62. Don, T.M.; Chen, C.W.; Chan, T.H. Preparation and characterization of poly(hydroxyalkanoate) from the fermentation of *Haloferax mediterranei*. *J. Biomater. Sci. Polym. E* **2016**, *17*, 1425–1438. [CrossRef]
63. Koller, M.; Bona, R.; Chiellini, E.; Braunegg, G. Extraction of short-chain-length poly-[(*R*)-hydroxyalkanoates] (*scl*-PHA) by the "anti-solvent" acetone under elevated temperature and pressure. *Biotechnol. Lett.* **2013**, *35*, 1023–1028. [CrossRef]
64. Han, J.; Wu, L.P.; Hou, J.; Zhao, D.; Xiang, H. Biosynthesis, characterization, and hemostasis potential of tailor-made poly(3-hydroxybutyrate-*co*-3-hydroxyvalerate) produced by *Haloferax mediterranei*. *Biomacromolecules* **2015**, *16*, 578–588. [CrossRef]
65. Ferre-Güell, A.; Winterburn, J. Increased production of polyhydroxyalkanoates with controllable composition and consistent material properties by fed-batch fermentation. *Biochem. Eng. J.* **2019**, *141*, 35–42. [CrossRef]
66. Ferre-Güell, A.; Winterburn, J. Biosynthesis and characterization of Polyhydroxyalkanoates with controlled composition and microstructure. *Biomacromolecules* **2018**, *19*, 996–1005. [CrossRef] [PubMed]
67. Altekar, W.; Rajagopalan, R. Ribulose bisphosphate carboxylase activity in halophilic Archaebacteria. *Arch. Microbiol.* **1990**, *153*, 169–174. [CrossRef]
68. Legat, A.; Gruber, C.; Zangger, K.; Wanner, G.; Stan-Lotter, H. Identification of polyhydroxyalkanoates in *Halococcus* and other haloarchaeal species. *Appl. Microbiol. Biotechnol.* **2010**, *87*, 1119–1127. [CrossRef] [PubMed]
69. Taran, M.; Amirkhani, H. Strategies of poly (3-hydroxybutyrate) synthesis by *Haloarcula* sp. IRU1 utilizing glucose as carbon source: Optimization of culture conditions by Taguchi methodology. *Int. J. Biol. Macromol.* **2010**, *47*, 632–634. [CrossRef]
70. Taran, M. Synthesis of poly(3-hydroxybutyrate) from different carbon sources by *Haloarcula* sp. IRU1. *Polym.-Plast. Technol.* **2011**, *50*, 530–532. [CrossRef]
71. Taran, M. Utilization of petrochemical wastewater for the production of poly(3-hydroxybutyrate) by *Haloarcula* sp. IRU1. *J. Hazard. Mater.* **2011**, *188*, 26–28. [CrossRef]
72. Taran, M. Poly(3-hydroxybutyrate) production from crude oil by *Haloarcula* sp. IRU1: Optimization of culture conditions by Taguchi method. *Pet. Sci. Technol.* **2011**, *29*, 1264–1269. [CrossRef]
73. Taran, M.; Sharifi, M.; Bagheri, S. Utilization of textile wastewater as carbon source by newly isolated *Haloarcula* sp. IRU1: Optimization of conditions by Taguchi methodology. *Clean Technol. Environ.* **2011**, *13*, 535–538. [CrossRef]
74. Pramanik, A.; Mitra, A.; Arumugam, M.; Bhattacharyya, A.; Sadhukhan, S.; Ray, A.; Haldar, S.; Mukhopadhyay, U.K.; Mukherjee, J. Utilization of vinasse for the production of polyhydroxybutyrate by *Haloarcula marismortui*. *Folia Microbiol.* **2012**, *57*, 71–79. [CrossRef]
75. Oren, A.; Ventosa, A.; Gutiérrez, M.C.; Kamekura, M. *Haloarcula quadrata* sp. nov., a square, motile archaeon isolated from a brine pool in Sinai (Egypt). *Int. J. Syst. Evol. Microbiol.* **1999**, *49*, 1149–1155. [CrossRef] [PubMed]

76. Salgaonkar, B.B.; Mani, K.; Bragança, J.M. Accumulation of polyhydroxyalkanoates by halophilic archaea isolated from traditional solar salterns of India. *Extremophiles* **2013**, *17*, 787–795. [CrossRef]
77. Salgaonkar, B.B.; Bragança, J.M. Biosynthesis of poly(3-hydroxybutyrate-*co*-3-hydroxyvalerate) by *Halogeometricum borinquense* strain E3. *Int. J. Biol. Macromol.* **2015**, *78*, 339–346. [CrossRef]
78. Salgaonkar, B.B.; Bragança, J.M. Utilization of sugarcane bagasse by *Halogeometricum borinquense* strain E3 for biosynthesis of poly(3-hydroxybutyrate-*co*-3-hydroxyvalerate). *Bioengineering* **2017**, *4*, 50. [CrossRef] [PubMed]
79. Salgaonkar, B.B.; Mani, K.; Bragança, J.M. Sustainable bioconversion of cassava waste to Poly(3-hydroxybutyrate-*co*-3-hydroxyvalerate) by *Halogeometricum borinquense* strain E3. *J. Polym. Environ.* **2019**, *27*, 299–308. [CrossRef]
80. Hezayen, F.F.; Rehm, B.H.A.; Eberhardt, R.; Steinbüchel, A. Polymer production by two newly isolated extremely halophilic archaea: Application of a novel corrosion-resistant bioreactor. *Appl. Microbiol. Biotechnol.* **2000**, *54*, 319–325. [CrossRef] [PubMed]
81. Hezayen, F.F.; Gutiérrez, M.C.; Steinbüchel, A.; Tindall, B.J.; Rehm, B.H.A. *Halopiger aswanensis* sp. nov., a polymer-producing and extremely halophilic archaeon isolated from hypersaline soil. *Int. J. Syst. Evol. Microbiol.* **2010**, *60*, 633–637. [CrossRef]
82. Hezayen, F.F.; Tindall, B.J.; Steinbüchel, A.; Rehm, B.H.A. Characterization of a novel halophilic archaeon, *Halobiforma haloterrestris* gen. nov., sp. nov., and transfer of *Natronobacterium nitratireducens* to *Halobiforma nitratireducens* comb. nov. *Int. J. Syst. Evol. Microbiol.* **2002**, *52*, 2271–2280. [CrossRef]
83. Xu, X.W.; Wu, M.; Zhou, P.J.; Liu, S.J. *Halobiforma lacisalsi* sp. nov., isolated from a salt lake in China. *Int. J. Syst. Evol. Microbiol.* **2005**, *55*, 1949–1952. [CrossRef]
84. Danis, O.; Ogan, A.; Tatlican, P.; Attar, A.; Cakmakci, E.; Mertoglu, B.; Birbir, M. Preparation of poly(3-hydroxybutyrate-*co*-hydroxyvalerate) films from halophilic archaea and their potential use in drug delivery. *Extremophiles* **2015**, *19*, 515–524. [CrossRef]
85. Walsby, A.E. A square bacterium. *Nature* **1980**, *283*, 69. [CrossRef]
86. Walsby, A.E. Archaea with square cells. *Trends Microbiol.* **2005**, *13*, 193–195. [CrossRef] [PubMed]
87. Burns, D.G.; Janssen, P.H.; Itoh, T.; Kamekura, M.; Li, Z.; Jensen, G.; Rodríguez-Valera, F.; Bolhuis, H.; Dyall-Smith, M.L. *Haloquadratum walsbyi* gen. nov., sp. nov., the square haloarchaeon of Walsby, isolated from saltern crystallizers in Australia and Spain. *Int. J. Syst. Evol. Microbiol.* **2007**, *57*, 387–392. [CrossRef]
88. Saponetti, M.S.; Bobba, F.; Salerno, G.; Scarfato, A.; Corcelli, A.; Cucolo, A. Morphological and structural aspects of the extremely halophilic archaeon *Haloquadratum walsbyi*. *PLoS ONE* **2011**, *6*, e18653. [CrossRef]
89. Zhao, Y.X.; Rao, Z.M.; Xue, Y.F.; Gong, P.; Ji, Y.Z.; Ma, Y.H. Poly(3-hydroxybutyrate-*co*-3-hydroxyvalerate) production by Haloarchaeon *Halogranum amylolyticum*. *Appl. Microbiol. Biotechnol.* **2015**, *99*, 7639–7649. [CrossRef] [PubMed]
90. Romano, I.; Poli, A.; Finore, I.; Huertas, F.J.; Gambacorta, A.; Pelliccione, S.; Nicolaus, G.; Lama, L.; Nicolaus, B. *Haloterrigena hispanica* sp. nov., an extremely halophilic archaeon from Fuente de Piedra, southern Spain. *Int. J. Syst. Evol. Microbiol.* **2007**, *57*, 1499–1503. [CrossRef] [PubMed]
91. Di Donato, P.; Fiorentino, G.; Anzelmo, G.; Tommonaro, G.; Nicolaus, B.; Poli, A. Re-use of vegetable wastes as cheap substrates for extremophile biomass production. *Waste Biomass Valoriz.* **2011**, *2*, 103–111. [CrossRef]
92. Wainø, M.; Tindall, B.J.; Ingvorsen, K. *Halorhabdus utahensis* gen. nov., sp. nov., an aerobic, extremely halophilic member of the Archaea from Great Salt Lake, Utah. *Int. J. Syst. Evol. Microbiol.* **2000**, *50*, 183–190. [CrossRef] [PubMed]
93. Antunes, A.; Taborda, M.; Huber, R.; Moissl, C.; Nobre, M.F.; da Costa, M.S. *Halorhabdus tiamatea* sp. nov., a non-pigmented, extremely halophilic archaeon from a deep-sea, hypersaline anoxic basin of the Red Sea, and emended description of the genus *Halorhabdus*. *Int. J. Syst. Evol. Microbiol.* **2008**, *58*, 215–220. [CrossRef]
94. Antunes, A.; Alam, I.; Bajic, V.B.; Stingl, U. Genome sequence of *Halorhabdus tiamatea*, the first archaeon isolated from a deep-sea anoxic brine lake. *J. Bacteriol.* **2011**, *193*, 4553–4554. [CrossRef]
95. Albuquerque, L.; Kowalewicz-Kulbat, M.; Drzewiecka, D.; Stączek, P.; d'Auria, G.; Rosselló-Móra, R.; da Costa, M.S. *Halorhabdus rudnickae* sp. nov., a halophilic archaeon isolated from a salt mine borehole in Poland. *Syst. Appl. Microbiol.* **2016**, *39*, 100–105. [CrossRef] [PubMed]
96. Ye, J.; Huang, W.; Wang, D.; Chen, F.; Yin, J.; Li, T.; Zhang, H.; Chen, G.Q. Pilot Scale-up of Poly(3-hydroxybutyrate-*co*-4-hydroxybutyrate) Production by *Halomonas bluephagenesis* via Cell Growth Adapted Optimization Process. *Biotechnol. J.* **2018**, *13*, 1800074. [CrossRef] [PubMed]

97. Chen, X.; Yin, J.; Ye, J.; Zhang, H.; Che, X.; Ma, Y.; Li, M.; Wu, L.-P.; Chen, G.Q. Engineering *Halomonas bluephagenesis* TD01 for non-sterile production of poly(3-hydroxybutyrate-*co*-4-hydroxybutyrate). *Bioresour. Technol.* **2017**, *244*, 534–541. [CrossRef] [PubMed]
98. Ye, J.; Hu, D.; Che, X.; Jiang, X.; Li, T.; Chen, J.; Zhang, H.M.; Chen, G.Q. Engineering of *Halomonas bluephagenesis* for low cost production of poly (3-hydroxybutyrate-*co*-4-hydroxybutyrate) from glucose. *Metab. Eng.* **2018**, *47*, 143–152. [CrossRef] [PubMed]
99. Kucera, D.; Pernicová, I.; Kovalcik, A.; Koller, M.; Mullerova, L.; Sedlacek, P.; Mravec, F.; Nebesarova, J.; Kalina, M.; Marova, I.; et al. Characterization of the promising poly(3-hydroxybutyrate) producing halophilic bacterium *Halomonas halophila*. *Bioresour. Technol.* **2018**, *256*, 552–556. [CrossRef]
100. Yue, H.; Ling, C.; Yang, T.; Chen, X.; Chen, Y.; Deng, H.; Wu, Q.; Chen, J.; Chen, G.Q. A seawater-based open and continuous process for polyhydroxyalkanoates production by recombinant *Halomonas campaniensis* LS21 grown in mixed substrates. *Biotechnol. Biofuels* **2014**, *7*, 108. [CrossRef]

bioengineering

MDPI

Article

Tequila Agave Bagasse Hydrolysate for the Production of Polyhydroxybutyrate by *Burkholderia sacchari*

Yolanda González-García [1,*], Janessa Grieve [1], Juan Carlos Meza-Contreras [1], Berenice Clifton-García [2] and José Antonio Silva-Guzman [1]

[1] Department of Wood, Cellulose and Paper, University of Guadalajara, 45020 Zapopan, Mexico; janessagrieve@me.com (J.G.); jcmezac@gmail.com (J.C.M.-C.); jasilva@dmcyp.cucei.udg.mx (J.A.S.-G.)

[2] Department of Chemical Engineering, University of Guadalajara, 44430 Guadalajara, Mexico; bere_clifton@hotmail.com

* Correspondence: yolanda.ggarcia@academicos.udg.mx; Tel.: +52-33-3682-0110

Received: 25 October 2019; Accepted: 7 December 2019; Published: 17 December 2019

Abstract: Tequila agave bagasse (TAB) is the fibrous waste from the Tequila production process. It is generated in large amounts and its disposal is an environmental problem. Its use as a source of fermentable sugars for biotechnological processes is of interest; thus, it was investigated for the production of polyhydroxybutyrate (PHB) by the xylose-assimilating bacteria *Burkholderia sacchari*. First, it was chemically hydrolyzed, yielding 20.6 g·L^{-1} of reducing sugars, with xylose and glucose as the main components (7:3 ratio). Next, the effect of hydrolysis by-products on *B. sacchari* growth was evaluated. Phenolic compounds showed the highest toxicity (> 60% of growth inhibition). Then, detoxification methods (resins, activated charcoal, laccases) were tested to remove the growth inhibitory compounds from the TAB hydrolysate (TABH). The highest removal percentage (92%) was achieved using activated charcoal (50 g·L^{-1}, pH 2, 4 h). Finally, detoxified TABH was used as the carbon source for the production of PHB in a two-step batch culture, reaching a biomass production of 11.3 g·L^{-1} and a PHB accumulation of 24 g PHB g^{-1} dry cell (after 122 h of culture). The polymer structure resulted in a homopolymer of 3-hydroxybutyric acid. It is concluded that the TAB could be hydrolyzed and valorized as a carbon source for producing PHB.

Keywords: polyhydroxybutyrate; tequila bagasse; hydrolysate detoxification; activated charcoal; phenolic compounds

1. Introduction

Polyhydroxyalkanoate (PHA) is a family of biodegradable and biocompatible polymers produced by microorganisms. They have great potential as a substitute for petroleum-based plastics as packing material, disposable items, and biomedical devices [1]:

Polyhydroxybutyrate (PHB) is the main representative of these polymers. Nowadays, some manufacturers such as Metabolix (USA), Tianjin Green Bioscience Co., Ltd. (China), and Biocycle PHB Industrial S.A (Brazil) commercialize this biopolymer, which is produced from raw materials such as food crops and sugarcane [1]. Nevertheless, its production cost is 5 to 10 times higher than that of conventional plastics; in particular, the substrate cost for PHA production represents almost half of the production cost [2].

Thus, the use of low-cost substrates for producing PHAs is a matter of interest. Among various alternative substrates, lignocellulosic wastes have gained considerable attention since they could be hydrolyzed to yield sugars (i.e., glucose, xylose, and arabinose) for fermentation processes [3]. Examples of this type of waste, studied for PHA production include sugar cane bagasse, rice, wheat straw, and corn stover [4].

Tequila agave bagasse (TAB) is a residual fibrous material from the Tequila production process. In 2018, 346,700.00 tons of TAB were generated. This waste did not have any specific use, but since it contains large amounts of cellulose and hemicellulose [5], it might be used as a low-cost substrate for fermentation processes. It has been hydrolyzed and used as a carbon source in submerged fermentation for the production of bioethanol, organic acids, and lipids [6,7]. Nevertheless, the research about the use of TAB for the production of PHAs is scarce [8] as well as the effect of the hydrolysis byproducts generated from its chemical saccharification on the growth and PHB accumulation by any PHA-producing microorganism.

Lignocellulosic wastes conversion to PHAs generally requires a hydrolysis step to obtain fermentable sugars and then a detoxification process to remove inhibitory compounds produced during hydrolysis [9]. Different detoxification methodologies (activated charcoal, ionic resins, and enzymes) have been studied in bagasse hydrolysates, such as sugar cane bagasse hydrolysate, but there are not reports about their use for detoxification of TABH.

This research aimed to evaluate the effect of growth-inhibition compounds (present in the TABH) on the growth of the xylose-utilizing bacteria *B. sacchari*, their removal using activated charcoal, resins, and laccases, and the use of the detoxified TABH for the production of PHB.

2. Materials and Methods

2.1. Characterization TAB

TAB fibers were washed (Sprout-Waldron refiner, D2A509NH) and then centrifuged to remove water, sun-dried for 48 h, ground, and sieved (60 mesh). Cellulose, hemicellulose, lignin, ashes, extractable, and humidity content were determined by the Technical Association of the Pulp and Paper Industry (TAPPI) standards (T203, T222, and T257).

2.2. Chemical Hydrolysis of TAB and Hydrolysate Characterization

Acid hydrolysis of TAB fibers was performed in 250 mL capped flasks using the following conditions: H_2SO_4, 2.3% (*w*/*v*); TAB: acid solution, 1:10 (*w*/*v*); temperature, 130 °C (autoclave); time, 20 min. Sixty mesh sieved TAB (250 μm fiber size), and not sieved TAB (mixed fiber sizes, from 125–420 μm) were used. After hydrolysis, the remaining fibers were separated by filtration (filter paper Whatman 2). Next, pH was adjusted to 5.5 by the addition of $Ca(OH)_2$ (constant agitation), and the precipitated solids were removed by filtration (filter paper Whatman 2). The TABH was analyzed for determining: total sugars, reducing sugars, and total phenolic compounds (Phenol-sulfuric [10], DNS (dinitrosalicylic acid) [11], and Folin–Ciocalteu method [12], respectively). Monomeric sugars were analyzed by HPLC (Waters) with an IR detector and using an Aminex 87P column: mobile phase, water; flow 0.6 mL min^{-1}; temperature, 80 °C; sample volume, 20 μL).

2.3. Microorganism and Culture Media

The strain *B. sacchari* 17165 was purchased from DSMZ, reactivated according to DSMZ instructions in R2A medium (in $g{\cdot}L^{-1}$): yeast extract, 0.5; meat peptone 0.5; casein peptone, 0.5; glucose, 0.5; soluble starch, 0.5; sodium pyruvate, 0.3; K_2HPO_4, 0.3; and $MgSO_4{\cdot}7H_2O$, 0.05; pH 7. The strain was incubated at 30 °C and 150 rpm for 48 h and then frozen at −20 °C (2 mL microtubes with 0.8 mL of bacterial suspension and 0.2 mL of glycerol).

Two culture media were studied for *B. sacchari* growth and PHB production: control medium and Detoxified TABH medium. Control medium composition was (in $g{\cdot}L^{-1}$): xylose, 14; glucose, 6; KH_2PO_4, 2.5; Na_2HPO_4, 5.5; $(NH_4)_2SO_4$, 6; $MgSO_4{\cdot}7H_2O$, 0.5; $CaCl_2{\cdot}2H_2O$, 0.02; ammonium ferric citrate, 0.1; peptone, 1; and yeast extract, 1. Trace elements solution (1 $mL{\cdot}L^{-1}$) with the following composition ($g{\cdot}L^{-1}$) was also added: H_3BO_3, 0.30; $CoCl_2{\cdot}6H_2O$, 0.20; $ZnSO_4{\cdot}7H_2O$, 0.1; $MnCl_2{\cdot}4H_2O$, 0.03; $NaMoO_4{\cdot}2H_2O$, 0.03; $NiCl_2{\cdot}6H_2O$, 0.02; and $CuSO_4{\cdot}5H_2O$, 0.01.

The Detoxified TABH medium was based on the hydrolysate (20 $g \cdot L^{-1}$ of reducing sugars, xylose: glucose ratio of 7:3) with the addition of all the components above mentioned except for the sugars.

pH was adjusted to 6.5, and culture media were autoclaved (peptone and yeast extract were autoclaved separately) before inoculation with 10% (*v*/*v*) of *B. sacchari* pre-culture (OD_{600nm} = 0.5). The incubation conditions used were 30 °C and 150 rpm.

2.4. B. sacchari Growth Inhibition by TABH

TABH was used as a culture medium, without diluting and diluted with water (5 times), in order to determine the microorganism's tolerance to it. The sugars content of the diluted TABH were adjusted to the same concentration and proportion of the concentrated TABH, and the mineral salts, peptone, and yeast extract (as mentioned in Materials and Methods section) were added to both hydrolysates. After sterilization, 125 mL glass vials media (22 mL of TABH) were inoculated with 3 mL of *B. sacchari* pre-culture (control medium, OD_{600nm} = 0.5) and incubated under the conditions previously mentioned.

Microbial growth (Dry cell mass) at 0, 24, 48, and 72 h was estimated by measuring the optical density of the sample at 600 nm and by its correlation with the dry cell weight, obtained gravimetrically.

2.5. B. sacchari Growth Inhibition by Model Toxic Compounds

Acid hydrolysis by-products reported in other hydrolysates (inhibitory compounds) were added separately to the control medium (concentrated solutions previously sterilized), in order to evaluate their particular effect on *B. sacchari* growth. The following compounds (0.5–12 $g \cdot L^{-1}$) were studied: furfural, hydroxymethylfurfural, vanillin, coumaric acid, and ferulic acid. Glass vials of 125 mL containing 22 mL of control medium (added with each inhibitory compound) were inoculated with 3 mL of *B. sacchari* pre-culture (control medium, OD_{600nm} = 0.5), and the medium without inhibitory compounds was used as control.

Microbial growth was measured as previously mentioned at 0, 24, 48, and 72 h, and maximum biomass production was used for determining growth inhibition percentage I% as follows:

$$I = (X_{max}C - X_{max}I) \times 100 / X_{max}C$$

where,

$X_{max}C$ = maximum biomass produced in the control medium,

$X_{max}I$ = maximum biomass produced in the control medium with the inhibitory compound.

2.6. Detoxification of TABH by Different Methods

Elimination of growth inhibitory compounds, specifically total phenolic compounds, from the TABH (without diluting) was studied using activated charcoal (Golden bell) and resins (Sigma & Aldrich): DOWEX 1 × 8 (chloride form); DOWEX G26 (hydrogen form); Amberlite XAD7 (hydrophobic). Before use, resins were washed with distilled water (agitation, 5 min) and activated according to manufacturer indications (agitation, 1 h): DOWEX G26, HCl 0.4 N; DOWEX 1 × 8 NaOH 0.1 N; Amberlite XAD7, methanol. Finally, resins were washed three times with distilled water [13].

Each adsorbent (50 $mg \cdot mL^{-1}$) was added separately into 10 mL glass vials with 2 mL of TABH at pH 2 or 7 (previously adjusted with NaOH or H_2SO_4) and kept in agitation (150 rpm) in a shaker at 25 °C (1 and 4 h). Next, the adsorbent was separated by filtration, and the total phenolic compounds were quantified by the Folin–Ciocalteu method. The phenolic compound elimination percentage E% was calculated as follows:

$$E = (P_{t0} - P_{tf}) \times 100 / P_{t0}$$

where,

P_{t0} = Total phenolic compound before the detoxification process,

Ptf = Total phenolic compound after the detoxification process.

Detoxification of TABH using enzymes (*Trametes versicolor* laccase, Sigma & Aldrich 38429) was also studied. The pH was first adjusted to 5.5, and the effect of enzyme concentration (1 and 10 U) and contact time (1 and 5 h) on phenolic compounds elimination was investigated (2 mL microtubes, 50 °C, 150 rpm).

2.7. PHB Production from Detoxified TABH by B. sacchari

The detoxified TABH medium and the control medium were used for the production of PHB by *B. sacchari* in 500 mL Erlenmeyer flasks containing 90 mL of culture medium, and inoculated with 10 mL of bacterial pre-culture (DO_{600nm} = 0.5, at 30 °C, and 150 rpm).

A two-step batch culture was performed as follows: (1) Biomass production (72 h) in medium (TABH or control) with nitrogen sources ($(NH_4)_2SO_4$, peptone and yeast extract) as described in the Materials and Methods Section; (2) PHB accumulation (48 h) in nitrogen-limited medium (TABH or control with 0.6 $g{\cdot}L^{-1}$ of $(NH_4)_2SO_4$, without either peptone or yeast extract). For PHB accumulation, cells from the biomass production step were aseptically recovered by centrifugation and resuspended in nitrogen-limited culture media. Samples (5 mL) were withdrawn periodically and analyzed for quantifying biomass (dry cell weight), reducing sugars (DNS), pH, and PHB (dry weight) after solvent extraction. For polymer extraction, biomass was lyophilized, weighted, suspended in ethanol, and kept in constant agitation (24 h). Next, it was air-dried, suspended in chloroform, and kept in constant agitation (24 h). Cell debris was removed by filtration, and the organic phase was added to cold methanol (1:10 *v*/*v*) and kept in the freezer for 24 h for PHB precipitation. The polymer was recovered by centrifugation, air-dried, and weighed.

2.8. PHB Characterization

The polymer extracted from *B. sacchari* cells was analyzed by ATR-FTIR (Fourier Transform Infrared-Attenuated Total Reflectance) using a Perkin Elmer Spectrum Two FTIR spectrometer. For determining its monomeric composition, the polymer was subjected to acid methanolysis [14]. The resulting methyl esters were analyzed using a Perkin Elmer XL gas chromatograph, equipped with a CP-Wax 52 CB capillary column (25 m × 0.32 mm) and a flame ionization detector. The chromatographic conditions used were: sample injection volume, 1 μL; gas carrier, nitrogen; flow rate, 20 $cm{\cdot}s^{-1}$; injector and detector temperatures, 210 and 220 °C, respectively. A temperature ramp was used as follows: 50 °C for 1 min, incrementing by 8 °C min^{-1}, and 160 °C for 5 min. Methyl benzoate and polyhydroxybutyrate from Fluka (after methanolysis) were used as internal and external standards, respectively.

3. Results and Discussions

3.1. Characterization of TAB

To know the cellulose, hemicellulose, lignin, extractable, ashes, and humidity content of the TAB to be used, it was characterized by TAPPI standards. Table 1 presents the data obtained, as expected, cellulose was found as the primary polymer followed by hemicellulose and lignin. Compared to other TAB characterizations previously reported, there was no significant variation in respect to the proportions of the structural components of the bagasse used in this research: cellulose, 20–50%; hemicellulose, 19–27%; and lignin, 15–20% [5,15].

Table 1. TAB characterization.

Component	Content (%)
Cellulose	50.1 ± 2.1
Hemicellulose	21.1 ± 2.4
Lignin	13.1 ± 1.3
Extractable	8.0 ± 1.1
Ashes	0.8 ± 0.1
Humidity	7.0 ± 0.9

3.2. Chemical Hydrolysis of TAB

The effect of the TAB fiber size on the concentration of total and reducing sugars, xylose, glucose, and total phenolic compounds was investigated. The results are presented in Table 2. A slightly higher concentration of reducing sugars was obtained from the mixed TAB fiber sizes (20.6 vs. 19.14 $g{\cdot}L^{-1}$), but generally, the effect of the fiber size on the hydrolysates composition was not significant.

Table 2. Tequila agave bagasse hydrolysate (TABH) composition after acid hydrolysis of different Tequila agave bagasse (TAB) fiber size.

Compound	Fiber Size	
	Mixed (125–420 μm)	60 mesh (250 μm)
Total sugars ($g{\cdot}L^{-1}$)	25.5 ± 1.5	23.9 ± 1.9
Reducing sugars ($g{\cdot}L^{-1}$)	20.61 ± 0.92	19.14 ± 1.03
Xylose (%) [1]	72	71
Glucose (%)	28	29
Total phenolic compounds ($g{\cdot}L^{-1}$)	1.7 ± 0.12	1.6 ± 0.13

[1] Percentage concerning the total amount of reducing sugars.

The factors that usually influence the effectivity of the acid hydrolysis of lignocellulosic materials are the temperature and time of the process [16]. In some investigations, the influence of the fiber size had also been studied [17]. The benefit of grinding the fibers before performing the chemical hydrolysis is to increase the exposure area of the lignocellulosic material to the acid, as well as to reduce the crystallinity of cellulose, allowing it to hydrolyze with little generation of total phenolic compounds. Nevertheless, since sieving (60 mesh) the ground TAB to obtain a particular fiber size (250 μm) did not had a significant impact in the amount of reducing sugar or phenolic compounds obtained, this step could be avoided, representing a saving in time and energy.

TAB hydrolysis under similar conditions to those used in this investigation was reported previously [5], and a concentration of 24.9 $g{\cdot}L^{-1}$ of reducing sugars was achieved (Table 3). Similar results obtained in hydrolysis studies of different materials are presented in Table 3.

Table 3. Chemical composition of hydrolysates obtained from different lignocellulosic materials.

Lignocellulosic Material	Reducing Sugars ($g{\cdot}L^{-1}$)	Phenolic Compounds ($g{\cdot}L^{-1}$)	Reference
TAB	24.9	n.r.	[5]
Sugarcane bagasse	25.38	n.r.	[18]
Sugarcane bagasse	n.r.	2.86	[19]
Sago trunk cortex	29.46	2.15	[20]
Sugarcane bagasse	30.29	2.75	[13]
Saccharum spontaneum	32.15	2.01	[21]

n.r.—not reported.

The determination of monomeric sugars was performed using HPLC, finding that the xylose to glucose ratio was around 7:3. Xylose was expected to be found in higher concentrations than glucose

since xylose is the main product of the hydrolysis of hemicellulose. Hemicellulose, because of its branched chemical structure, results in being more easily hydrolyzed in comparison to cellulose, whose principal degradation product is glucose. The high crystallinity of cellulose makes it challenging to hydrolyze into monomers of glucose [22]. This tendency has been reported in other investigations using sugar cane bagasse [23,24] and wheat straw [25]. Generally, the high percentage of xylose present in the TABH would be a negative aspect, given that it is not an easily assimilated substrate for the majority of the PHA-producing microorganisms. However, *B. sacchari* is capable of metabolizing xylose [23] therefore, this should not be a limiting factor for the growth and synthesis of PHB by it.

3.3. B. sacchari Growth Inhibition by Toxic Compounds Present in the TABH

TABH was used as a culture medium, concentrated and diluted with water (5 times), in order to determine the microorganism's tolerance to it. It was found that only the diluted hydrolysate supported growth. On the other hand, the regular hydrolysate strongly inhibited the growth of *B. sacchari* (Figure 1), which evidences its toxic nature due to the presence of inhibitory compounds from the acid hydrolysis process.

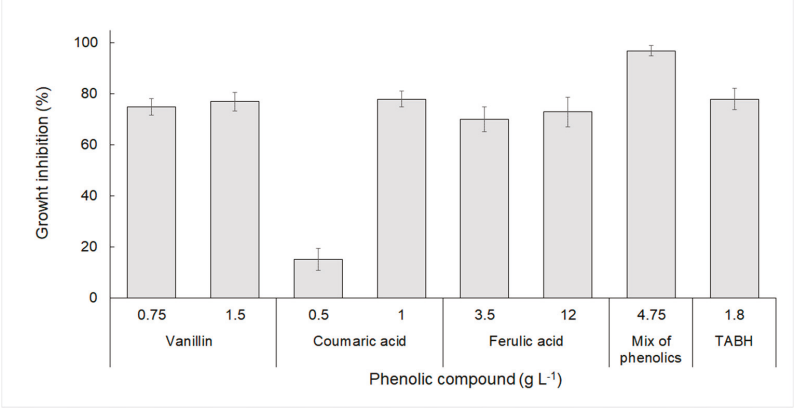

Figure 1. Inhibition of *B. sacchari* growth by model phenolic compounds associated with the acid hydrolysis of lignocellulosic materials.

The effect of pure inhibitory compounds such as furfural, hydroxymethylfurfural, acetic acid, levulinic acid, and phenolic compounds (vanillin, coumaric, and ferulic acids) on *B. sacchari* growth was investigated. It was found that the phenolic compounds caused the highest growth inhibition (above 60%), rather than the other inhibitory compounds investigated. The inhibitory effect of phenolic compounds (lowest and higher concentration used) are presented in Figure 1. Except for coumaric acid at 0.5 g·L^{-1}, all the phenolic compounds tested strongly inhibited *B. sacchari* growth, while their mixture was even highly inhibitory (97% inhibition). Such toxic synergistic behavior has been previously described for other bacteria [26].

As previously mentioned, various types of bagasse hydrolysates presented concentrations of total phenolic compounds ranging from 0.13 g·L^{-1} to 3 g·L^{-1} with different levels of toxicity to the microorganism used [27,28]. The amount of total phenolic compounds produced during acid hydrolysis of the TAB was significant (1.6–1.7 g·L^{-1}). Such compounds are known for decreasing the microbial growth rate associated with the loss of integrity of the cell membranes [26].

The evident growth inhibition of *B. sacchari* by the TABH confirmed the necessity of a detoxification treatment before using it as a cultivation media.

3.4. Elimination of Growth Inhibitory Compounds from TABH

Different detoxification methods were used in order to eliminate growth inhibitors (with emphasis on phenolic compounds) from the TABH, and the results are presented in Figure 2.

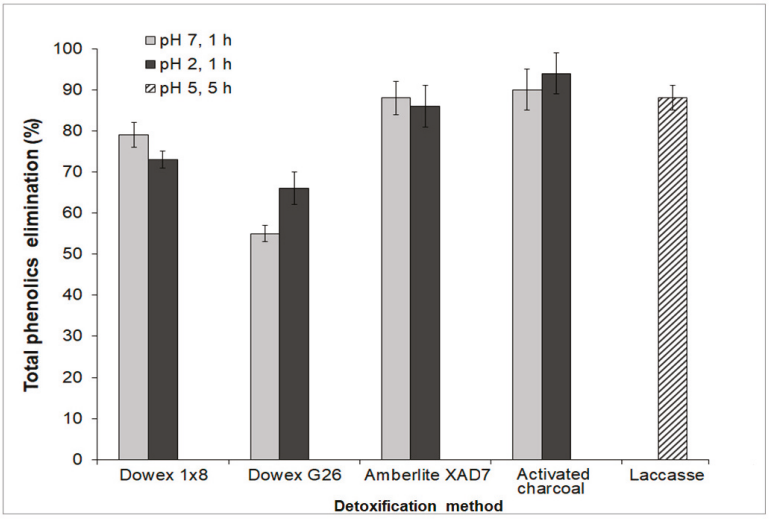

Figure 2. Total phenolic compounds removed from the TABH by different detoxification methods. For the treatment with resins and activated charcoal, 50 mg of adsorbent per mL of TABH were used. For laccase treatment, 1 U·mL^{-1} was used.

The detoxification with activated charcoal is a treatment frequently used to purify or to recover certain compounds from hydrolysates (lignin, tannin, furan derivatives, aromatic monomers, and phenolic acids) [29,30]. The pH of the hydrolysate, the concentration of activated carbon used, and the contact time are known factors that can influence the effectivity of the detoxification process with this adsorbent [31,32]. The phenolics elimination percentage using this method was around 90%, which is similar to values reported for other hydrolysates (sugarcane bagasse, 94%; olive tree pruning residue, 98%) [23,31]. The adsorptive behavior observed for the phenolic compounds on activated carbon could be explained by their polarity (electron distribution), hydrophobicity, and chemical structure [33]. The pH can affect its absorption capacity because it can influence the nature of functional groups for both adsorbent and adsorbate. Weak organic acids and phenolic compounds are better absorbed when they are in a non-ionized state (pH < 4) [34], this could be a possible explanation for the slight increase in the elimination of phenolic compounds at pH 2.

Regarding the elimination of phenolic compounds from TABH by the resins, it was from 55% to 88%; this result is similar to other values reported in the literature (64–94%) [35–38]. Using the Dowex 1 × 8 resin at acid pH, the amount of phenolic compounds adsorbed was lower than at pH 7; a comparable result was observed by Martos et al. [39]. However, the elimination of phenolic compounds using this adsorbent was higher (73–78%) than the achieved with the cation-exchange resin Dowex G26 (55–65%), which might be less efficient to adsorb phenolic compounds due to its overall negative charge. The same behavior was observed previously [36] using a similar resin (AG 50W-X8). Concerning the use of the Amberlite XAD7 resin, the elimination percentages of phenolic compounds were high (86–88%). This resin is an acrylic ester that is slightly polar and has been used for eliminating phenolic compounds from olive mill wastewater [40].

The last method assayed for detoxifying the TABH was the use of laccases. The elimination of total phenolic compounds by this method was 88%. The action mechanism of the laccase enzyme has

been previously elucidated. The enzyme oxidizes phenolic compounds that lead to the formation of phenoxy-type free radicals, which are unstable and polymerize into aromatic compounds that are less toxic [41]. Other compounds present in the hydrolysate (such as salts) might inhibit to a certain extent the enzyme activity. This is a probable reason why the elimination of phenolic compounds did not reach above 90% [42]. Similar results (70–75% of phenolic compounds elimination) were obtained using laccases for detoxifying wheat straw hydrolysate (0.5 U·mL^{-1} of laccase at pH 5 for 2 h) [42].

3.5. *B. sacchari* Growth in TABH Detoxified by Different Methods

B. sacchari growth was evaluated in the detoxified TAB hydrolysates, and it was found that some hydrolysates stimulated the growth, with respect to the control medium (Figure 3A), while others were still inhibitory (Figure 3B). The TABH treated with activated charcoal allowed the highest biomass production, 16% more biomass (Figure 3A) than the presented in the control medium, followed by the TABH detoxified with enzymes (10% more biomass than the produced in the control medium). Concerning the TABH treated with resins, the growth of *B. sacchari* with respect to the control medium varied: it was slightly inhibited in TABH detoxified with XAD7 or G26 resin (3 and 7% less biomass, respectively) (Figure 3B), but enhanced (8%) in TABH treated with 1 × 8 resin (Figure 3A).

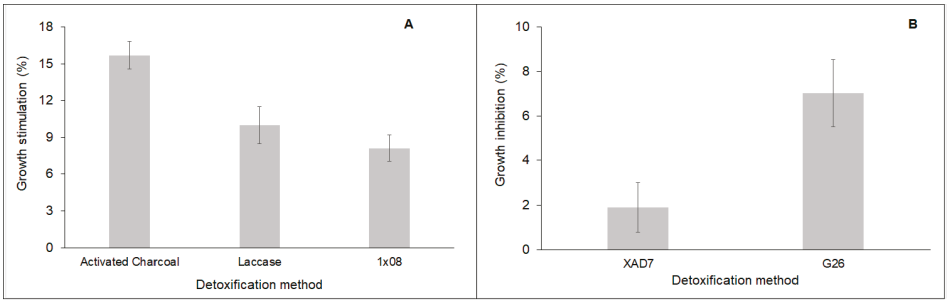

Figure 3. *B. sacchari* growth stimulation (**A**) or inhibition (**B**) by TABH detoxified using different methods.

Thus, the TABH treated with activated charcoal, resin 1 × 8, and enzymes not only supported the growth of *B. sacchari* but stimulated it. It is possible that such detoxification methods removed toxic compounds but left tolerable concentrations of some others that could act as growth factors, an effect that has been previously observed [26]. It has been mentioned that some organic acids and phenol-type compounds (including formic, acetic, levulinic, 4-hydroxybenzoic and gallic, and vanillic acid) at low concentration (below 10 mM) could stimulate the cell growth instead of suppressing it [43,44].

On the other hand, detoxification of TABH with XAD7 and G26 resins might not absorb other known toxic compounds such as furfural and HMF, which acted as growth inhibitors [35].

Activated charcoal eliminated more than 90% of total phenolic compounds from the TABH and the detoxified TABH not only supported but promoted the growth of *B. sacchari*, thus this treatment (50 g·L^{-1}, pH 2, and a contact time of 4 h) was selected for detoxifying the hydrolysate used in the PHB production experiment.

3.6. PHB Production from TABH Detoxified with Activated Charcoal

The production of PHB using *B. sacchari* from TABH detoxified with activated carbon, was investigated. After detoxification, TABH pH was adjusted to 7. Synthetic media with the same sugar concentration (20 g·L^{-1}) and xylose to glucose proportion (7:3) as the TABH was used as a control medium. Kinetics of *B. sacchari* growth, sugars consumption, and PHB production are depicted in Figure 4.

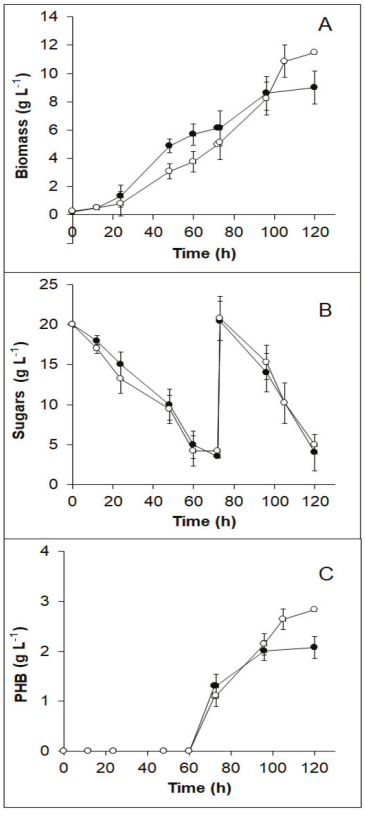

Figure 4. Kinetic profile of *B. sacchari* growing in TABH detoxified with activated charcoal (○) and control medium (●). (**A**) Biomass production. (**B**) Substrate consumption. (**C**) Polyhydroxybutyrate (PHB) production.

In both media, the lag phase was not evident, while exponential growth occurred from 12 to 72 h. Diauxic growth due to the presence of at least two carbon sources (xylose and glucose) was almost imperceptible, although a slight shift in the growth curve is observed at 40 h in both media used. At 72 h cells were harvested and resuspended in nitrogen-limited medium, cell growth continued until 96 h (control medium), and 105 h (TABH medium), although it represents both the PHB and non-PHB biomass (residual biomass). This is consistent with the PHB accumulation profile (Figure 4C) since the polymer production occurred from 72 to 96 h in the control medium, and from 72 to 105 h in TABH medium. The sugar consumption profile was similar in both culture media (Figure 4B).

The results of the kinetic parameters are presented in Table 4. Biomass and PHB production, as well as the maximum growth rate and PHB accumulation, were slightly higher in TABH medium (1.05–1.2 times) than in the control medium. Such results have been observed in other PHA producing bacteria growing in hydrolysates, and it has been hypothesized and researched that certain phenolic compounds and organic acids present in the hydrolysates in minimal concentrations, can stimulate growth and production of PHB [23].

Table 4. Biomass and PHB production by *B. sacchari* from activated charcoal detoxified TABH and mineral medium (120 h).

Parameter	Control Medium (CM)	TABH (Detoxified)
Total biomass ($g \cdot L^{-1}$)	8.78 ± 1.04	11.03 ± 1.14
Residual biomass ($g \cdot L^{-1}$) [a]	6.77 ± 1.09	8.36 ± 0.91
PHB ($g \cdot L^{-1}$)	2.01 ± 0.86	2.67 ± 0.96
PHB (%) [b]	22.91 ± 1.18	24.20 ± 1.26
μ_{max} (h^{-1})	0.08 ± 0.01	0.11 ± 0.02
$Y_{X/S}$ ($g \cdot g^{-1}$) [c]	0.23 ± 0.02	0.25 ± 0.02
$Y_{P/S}$ ($g \cdot g^{-1}$) [d]	0.10 ± 0.01	0.10 ± 0.01

[a] Total Biomass—PHB. [b] g of PHB g^{-1} total biomass × 100. [c] g of residual biomass g^{-1} reducing sugar consumed. [d] g of PHB g^{-1} reducing sugar consumed.

The PHB accumulation percentage achieved by *B. sacchari* from TABH, compares with values that have been reported from other hydrolysates (in shake flasks) by different strains: 34%, *Halomonas boliviensis* (wheat bran) [45]; 31.9% of PHB, *Ralstonia eutropha* (pulp fiber sludge); and 32% of PHB, *Sphingobium scionense* (softwood) [9].

B. sacchari has been previously used for PHB production from other lignocellulosic materials hydrolysates. The results of biomass production and PHB accumulation obtained from TABH are similar to those values reported from sugar cane bagasse hydrolysate (shaken flasks) by the same strain: 6.13 $g \cdot L^{-1}$, and 23.22%, respectively [23].

The biomass and PHB yields (on the substrate) obtained in the control medium and in the TABH medium were similar (0.23 and 0.10 $g \cdot g^{-1}$, respectively). Specifically, $Y_{P/S}$ value obtained for *B. sacchari* growing in the TABH medium is low compared to those reported for other hydrolysates (0.11 to 0.46 $g \cdot g^{-1}$) [23].

Although flask fermentations are very useful to study fermentation processes, they are restricted due to the incapacity to be controlling variables such as pH and dissolved oxygen. These are essential factors to optimize microbial growth and PHB accumulation. During the flask fermentation, the pH dropped from 7 to 5 and therefore affected the accumulation of the biopolymer [23]; thus, the production of PHB from TABH could be further optimized by using an automatized bioreactor and implementing a fed-batch system.

3.7. PHB Characterization

An FTIR analysis was performed on the polymer produced from detoxified TABH (Figure 5A), and it was compared against a Fluka ™ PHB standard. The peak around 2900 cm^{-1} is characteristic of carbon to hydrogen bonds, which are a part of the general structure of PHAs. The zone between 1700 and 1750 cm^{-1} relates to the stretching carbonyl C=O group, and the set of peaks from 1300 to 1000 cm^{-1} to the stretching of C–O bonds, both signals correspond to the ester bonds present in the PHAs structure. The peak around 1450 cm^{-1} originates from the asymmetric deformation and stretching of the bonds of methyl groups C–H, the same as the peak approximately at 1380 cm^{-1} [46].

The monomeric composition of the synthesized PHA was investigated by gas chromatography (GC). As depicted in Figure 5B, the biopolymer produced by *B. sacchari*, using the TABH as carbon source, is a homopolymer of 3-hydroxybutyric acid.

In previous experiments with *B. sacchari* using mixtures of glucose and xylose, as well as hydrolysates (wheat straw, sugar cane bagasse) as carbon sources, the polymer produced was also composed of repeating units of 3-hydroxybutyric acid [23,47].

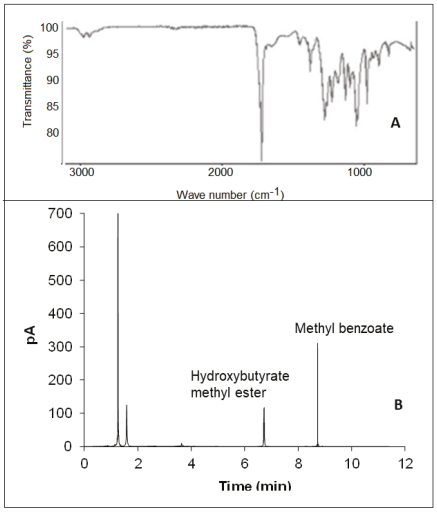

Figure 5. Characterization of the PHB produced by *B. sacchari* from TABH detoxified with activated charcoal. FTIR spectrum (**A**); GC chromatogram (**B**).

Author Contributions: Conceptualization, Y.G.-G.; formal analysis, Y.G.-G. and J.C.M.-C.; funding acquisition, J.A.S.-G.; investigation, Y.G.-G., J.G., J.C.M.-C., B.C.-G., and J.A.S.-G.; methodology, Y.G.-G., J.G., J.C.M.-C., and B.C.-G.; project administration, Y.G.-G.; supervision, Y.G.-G.; writing—original draft, Y.G.-G., J.G., J.C.M.-C., and B.C.-G..

Funding: CONACYT-Mexico (National Council of Science and Technology), grant 256506. COECYTJAL (Jalisco State Council for Scientific and Technological Research) project 8092-2019.

Conflicts of Interest: The authors declare no conflict of interest.

References

1. Tsang, Y.F.; Kumar, V.; Samadar, P.; Yang, Y.; Lee, J.; Ok, Y.S.; Song, H.; Kim, K.-H.; Kwon, E.E.; Jeon, Y.J. Production of bioplastic through food waste valorization. *Environ. Int.* **2019**, *127*, 625–644. [CrossRef]
2. Salgaonkar, B.B.; Bragança, J.M. Utilization of Sugarcane Bagasse by *Halogeometricum borinquense* Strain E3 for Biosynthesis of Poly(3-hydroxybutyrate-co-3-hydroxyvalerate). *Bioengineering* **2017**, *4*, 50. [CrossRef]
3. Sandhya, M.; Aravind, J.; Kanmani, P. Production of polyhydroxyalkanoates from *Ralstonia eutropha* using paddy straw as cheap substrate. *Int. J. Environ. Sci. Technol.* **2012**, *10*, 47–54. [CrossRef]
4. Nielsen, C.; Rahman, A.; Rehman, A.U.; Walsh, M.K.; Miller, C.D. Food waste conversion to microbial polyhydroxyalkanoates. *Microb. Biotechnol.* **2017**, *10*, 1338–1352. [CrossRef] [PubMed]
5. Saucedo-Luna, J.; Castro-Montoya, A.J.; Rico, J.L.; Campos-García, J. Optimization of acid hydrolysis of bagasse from *Agave tequilana* Weber. *Rev. Mex. Ing. Quim.* **2010**, *9*, 91–97.
6. Aguilar, D.L.; Rodríguez-Jasso, R.M.; Zanuso, E.; de Rodríguez, D.J.; Amaya-Delgado, L.; Sanchez, A.; Ruiz, H.A. Scale-up and evaluation of hydrothermal pretreatment in isothermal and non-isothermal regimen for bioethanol production using agave bagasse. *Bioresour. Technol.* **2018**, *263*, 112–119. [CrossRef] [PubMed]
7. Niehus, X.; Crutz-Le Coq, A.-M.; Sandoval, G.; Nicaud, J.-M.; Ledesma-Amaro, R. Engineering *Yarrowia lipolytica* to enhance lipid production from lignocellulosic materials. *Biotechnol. Biofuels* **2018**, *11*, 11. [CrossRef]
8. Alva Munoz, L.E.; Riley, M.R. Utilization of cellulosic waste from tequila bagasse and production of polyhydroxyalkanoate (PHA) bioplastics by *Saccharophagus degradans*. *Biotechnol. Bioeng.* **2008**, *100*, 882–888. [CrossRef]
9. Obruca, S.; Benesova, P.; Marsalek, L.; Marova, I. Use of lignocellulosic materials for PHA production. *Chem. Biochem. Eng. Q.* **2015**, *29*, 135–144. [CrossRef]

10. Dubois, M.; Gilles, K.; Hamilton, J.; Rebers, P.; Smith, F. Colorimetric method based on phenol sulfuric acid. *Anal. Chem.* **1956**, *28*, 356.
11. Miller, G.L. Use of dinitrosalicylic acid reagent for determination of reducing sugar. *Anal. Chem.* **1956**, *31*, 426–428. [CrossRef]
12. Singleton, V.L.; Orthofer, R.; Lamuela-Raventos, R.M. Analysis of total phenols and other oxidation substrates and antioxidants by means of Folin–Ciocalteau reagent. *Method. Enzymol.* **1999**, *299*, 152–178.
13. Chandel, A.K.; Kapoor, R.K.; Singh, A.; Kuhad, R.C. Detoxification of sugarcane bagasse hydrolysate improves ethanol production by *Candida shehatae* NCIM 3501. *Bioresour. Technol.* **2007**, *98*, 1947–1950. [CrossRef] [PubMed]
14. Linton, E.; Rahman, A.; Viamajala, S.; Sims, R.C.; Miller, C.D. Polyhydroxyalkanoate quantification in organic wastes and pure cultures using a single-step extraction and 1H NMR analysis. *Water Sci. Technol.* **2012**, *66*, 1000–1006. [CrossRef] [PubMed]
15. Núñez, H.M.; Rodríguez, L.F.; Khanna, M. Agave for tequila and biofuels: An economic assessment and potential opportunities. *GCB Bioenergy* **2011**, *3*, 43–57. [CrossRef]
16. Mussatto, S.I.; Roberto, I.C. Alternatives for detoxification of diluted-acid lignocellulosic hydrolyzates for use in fermentative processes: A review. *Bioresour. Technol.* **2004**, *93*, 1–10. [CrossRef] [PubMed]
17. Zamudio-Jaramillo, M.A.; Castro-Montoya, A.J.; Yescas, R.M.; Parga, M.D.C.C.; Hernández, J.C.G.; Luna, J.S. Optimization of particle size for hydrolysis of pine wood polysaccharides and its impact on milling energy. *IJRER* **2014**, *4*, 338–348.
18. Laopaiboon, P.; Thani, A.; Leelavatcharamas, V.; Laopaiboon, L. Acid hydrolysis of sugarcane bagasse for lactic acid production. *Bioresour. Technol.* **2010**, *101*, 1036–1043. [CrossRef]
19. Martinez, A.; Rodriguez, M.E.; Wells, M.L.; York, S.W.; Preston, J.F.; Ingram, L.O. Detoxification of dilute acid hydrolysates of lignocellulose with lime. *Biotechnol. Prog.* **2001**, *17*, 287–293. [CrossRef]
20. Kamal, S.M.M.; Mohamad, N.L.; Abdullah, A.G.L.; Abdullah, N. Detoxification of sago trunk hydrolysate using activated charcoal for xylitol production. *Procedia Food Sci.* **2011**, *1*, 908–913. [CrossRef]
21. Chandel, A.K.; Singh, O.V.; Rao, L.V.; Chandrasekhar, G.; Narasu, M.L. Bioconversion of novel substrate *Saccharum spontaneum*, a weedy material, into ethanol by *Pichia stipitis* NCIM3498. *Bioresour. Technol.* **2011**, *102*, 1709–1714. [CrossRef] [PubMed]
22. Palmqvist, E.; Hahn-Hägerdal, B. Fermentation of lignocellulosic hydrolysates. I: Inhibition and detoxification. *Bioresour. Technol.* **2000**, *74*, 17–24. [CrossRef]
23. Silva, L.; Taciro, M.; Ramos, M.; Carter, J.; Pradella, J.; Gomez, G. Poly-3-hydroxybutyrate (P3HB) production by bacteria from xylose, glucose, and sugarcane bagasse hydrolysate. *J. Ind. Microbiol. Biot.* **2004**, *31*, 245–254. [CrossRef] [PubMed]
24. Liu, R.; Liang, L.; Cao, W.; Mingke, W.; Chen, K.; Ma, J.; Jiang, M.; Wei, P.; Ouyang, P. Succinate production by metabolically engineered *Escherichia coli* using sugarcane bagasse hydrolysate as the carbon source. *Bioresour. Technol.* **2012**, *135*.
25. Nigam, J.N. Ethanol production from wheat straw hemicellulose hydrolysate by *Pichia stipitis*. *J. Biotechnol.* **2001**, *87*, 17–27. [CrossRef]
26. Palmqvist, E.; Hahn-Hägerdal, B. Fermentation of lignocellulosic hydrolysates. II: Inhibitors and mechanisms of inhibition. *Bioresour. Technol.* **2000**, *74*, 25–33. [CrossRef]
27. Millati, R.; Niklasson, C.; Taherzadeh, M.J. Effect of pH, time and temperature of overliming on detoxification of dilute-acid hydrolyzates for fermentation by *Saccharomyces cerevisiae*. *Proc. Biochem.* **2002**, *38*, 515–522. [CrossRef]
28. Monlau, F.; Sambusiti, C.; Barakat, A.; Quéméneur, M.; Trably, E.; Steyer, J.-P.; Carrere, H. Do furanic and phenolic compounds of lignocellulosic and algae biomass hydrolyzate inhibit anaerobic mixed cultures? A comprehensive review. *Biotechnol. Adv.* **2014**, *32*, 934–951. [CrossRef]
29. Liu, X.; Fatehi, P.; Ni, Y. Removal of inhibitors from pre-hydrolysis liquor of kraft-based dissolving pulp production process using adsorption and flocculation processes. *Bioresour. Technol.* **2012**, *116*, 492–496. [CrossRef]
30. Zhang, Y.; Xia, C.; Lu, M.; Tu, M. Effect of overliming and activated carbon detoxification on inhibitors removal and butanol fermentation of poplar prehydrolysates. *Biotechnol. Biofuels.* **2018**, *11*, 178. [CrossRef]
31. Mateo, S.; Roberto, I.C.; Sánchez, S.; Moya, A.J. Detoxification of hemicellulosic hydrolyzate from olive tree pruning residue. *Ind. Crop. Prod.* **2013**, *49*, 196–203. [CrossRef]

32. Sarawan, C.; Suinyuy, T.; Sewsynker-Sukai, Y.; Kana, E.B. Optimized activated charcoal detoxification of acid-pretreated lignocellulosic substrate and assessment for bioethanol production. *Bioresour. Technol.* **2019**, *286*, 121403. [CrossRef] [PubMed]
33. Michailof, C.; Stavropoulos, G.G.; Panayiotou, C. Enhanced adsorption of phenolic compounds, commonly encountered in olive mill wastewaters, on olive husk derived activated carbons. *Bioresour. Technol.* **2008**, *99*, 6400–6408. [CrossRef] [PubMed]
34. Costa, T.D.S.; Rogez, H.; Pena, R.D.S. Adsorption capacity of phenolic compounds onto cellulose and xylan. *Food Sci. Technol.* **2015**, *35*, 314–320. [CrossRef]
35. Carvalheiro, F.; Duarte, L.C.; Lopes, S.; Parajó, J.C.; Pereira, H.; Gírio, F.M. Evaluation of the detoxification of brewery's spent grain hydrolysate for xylitol production by *Debaryomyces hansenii* CCMI 941. *Proc. Biochem.* **2005**, *40*, 1215–1223. [CrossRef]
36. Nilvebrant, N.-O.; Reimann, A.; Larsson, S.; Jönsson, L.J. Detoxification of lignocellulose hydrolysates with ion-exchange resins. *Appl. Biochem. Biotechnol.* **2001**, *91*, 35–49. [CrossRef]
37. Mota, M.I.F.; Barbosa, S.; Pinto, P.C.R.; Ribeiro, A.M.; Ferreira, A.; Loureiro, J.M.; Rodrigues, A.E. Adsorption of vanillic and syringic acids onto a macroporous polymeric resin and recovery with ethanol:water (90:10 %V/V) solution. *Sep. Purif. Technol.* **2019**, *217*, 108–117. [CrossRef]
38. Nitzsche, R.; Gröngröft, A.; Kraume, M. Separation of lignin from beech wood hydrolysate using polymeric resins and zeolites—Determination and application of adsorption isotherms. *Sep. Purif. Technol.* **2019**, *209*, 491–502. [CrossRef]
39. Martos, N.; Sánchez, A.; Molina-Díaz, A. Comparative study of the retention of nine phenolic compounds on anionic exchanger resins. *Chem. Pap.* **2005**, *59*, 161.
40. Bertin, L.; Ferri, F.; Scoma, A.; Marchetti, L.; Fava, F. Recovery of high added value natural polyphenols from actual olive mill wastewater through solid phase extraction. *Chem. Eng. J.* **2011**, *171*, 1287–1293. [CrossRef]
41. Moreno, A.D.; Ibarra, D.; Fernández, J.L.; Ballesteros, M. Different laccase detoxification strategies for ethanol production from lignocellulosic biomass by the thermotolerant yeast *Kluyveromyces marxianus* CECT 10875. *Bioresour. Technol.* **2012**, *106*, 101–109. [CrossRef] [PubMed]
42. Jurado, M.; Prieto, A.; Martínez-Alcalá, A.; Martínez, A.T.; Martínez, M.J. Laccase detoxification of steam-exploded wheat straw for second generation bioethanol. *Bioresour. Technol.* **2009**, *100*, 6378–6384. [CrossRef] [PubMed]
43. Huang, C.; Wu, H.; Liu, Q.; Li, Y.; Zong, M. Effects of aldehydes on the growth and lipid accumulation of oleaginous yeast *Trichosporon fermentans*. *J. Agric. Food Chem.* **2011**, *59*, 4606–4613. [CrossRef] [PubMed]
44. Guo, Z.; Olsson, L. Physiological response of Saccharomyces cerevisiae to weak acids present in lignocellulosic hydrolysate. *FEMS Yeast Res.* **2014**, *14*, 1234–1248. [CrossRef] [PubMed]
45. Nikodinovic-Runic, J.; Guzik, M.; Kenny, S.T.; Babu, R.; Werker, A.; O Connor, K.E. Carbon-rich wastes as feedstocks for biodegradable polymer (Polyhydroxyalkanoate) production suing bacteria. In *Advances in Applied Microbiology*; Elsevier: Amsterdam, The Netherlands, 2013; Volume 84, pp. 139–200. ISBN 978-0-12-407673-0.
46. Arcos-Hernandez, M.V.; Gurieff, N.; Pratt, S.; Magnusson, P.; Werker, A.; Vargas, A.; Lant, P. Rapid quantification of intracellular PHA using infrared spectroscopy: An application in mixed cultures. *J. Biotechnol.* **2010**, *150*, 372–379. [CrossRef]
47. Lopes, M.S.G.; Gosset, G.; Rocha, R.C.S.; Gomez, J.G.C.; Ferreira da Silva, L. PHB biosynthesis in catabolite repression mutant of *Burkholderia sacchari*. *Curr. Microbiol.* **2011**, *63*, 319–326. [CrossRef] [PubMed]

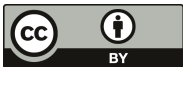

bioengineering

MDPI

Article

Biotechnological Production of Poly(3-Hydroxybutyrate-*co*-4-Hydroxybutyrate-*co*-3-Hydroxyvalerate) Terpolymer by *Cupriavidus* sp. DSM 19379

Dan Kucera [1,2], Ivana Novackova [1], Iva Pernicova [1,2], Petr Sedlacek [2] and Stanislav Obruca [1,2,*]

[1] Faculty of Chemistry, Brno University of Technology, Purkynova 118, 612 00 Brno, Czech Republic
[2] Material Research Centre, Faculty of Chemistry, Brno University of Technology, Purkynova 118, 612 00 Brno, Czech Republic
* Correspondence: obruca@fch.vut.cz; Tel.: +420-541-149-486

Received: 19 July 2019; Accepted: 20 August 2019; Published: 26 August 2019

Abstract: The terpolymer of 3-hydroxybutyrate (3HB), 3-hydroxyvalerate (3HV), and 4-hydroxybutyrate (4HB) was produced employing *Cupriavidus* sp. DSM 19379. Growth in the presence of γ-butyrolactone, ε-caprolactone, 1,4-butanediol, and 1,6-hexanediol resulted in the synthesis of a polymer consisting of 3HB and 4HB monomers. Single and two-stage terpolymer production strategies were utilized to incorporate the 3HV subunit into the polymer structure. At the single-stage cultivation mode, γ-butyrolactone or 1,4-butanediol served as the primary substrate and propionic and valeric acid as the precursor of 3HV. In the two-stage production, glycerol was used in the growth phase, and precursors for the formation of the terpolymer in combination with the nitrogen limitation in the medium were used in the second phase. The aim of this work was to maximize the Polyhydroxyalkanoates (PHA) yields with a high proportion of 3HV and 4HB using different culture strategies. The obtained polymers contained 0–29 mol% of 3HV and 16–32 mol% of 4HB. Selected polymers were subjected to a material properties analysis such as differential scanning calorimetry (DSC), thermogravimetry, and size exclusion chromatography coupled with multi angle light scattering (SEC-MALS) for determination of the molecular weight. The number of polymers in the biomass, as well as the monomer composition of the polymer were determined by gas chromatography.

Keywords: polyhydroxyalkanoates; terpolymer; P(3HB-*co*-3HV-*co*-4HB); *Cupriavidus malaysiensis*

1. Introduction

Polyhydroxyalkanoates (PHA) represent a very attractive family of materials which are considered as an alternative to petrochemical polymers in applications which may benefit from their fully biodegradable and biocompatible nature. PHA are produced via fermentation since they are biosynthesized by numerous prokaryotes in the form of intracellular granules primarily as storage of carbon and energy [1]. Nevertheless, according to recent findings, PHA also plays a crucial role in the stress robustness and resistance of bacterial cells against various stress factors [2,3].

PHA are disadvantaged in competition with petrochemical polymers by their high-production cost. Since a substantial amount of the final cost is attributed to the cost of the carbon substrate, there are many attempts to produce PHA from inexpensive or even waste products in the food industry [4] such as waste lipids [5,6], crude glycerol formed as a side product of biodiesel production [7,8], various lignocellulose materials [9], or even carbon dioxide [10,11].

In general, the material properties of PHA strongly depend upon monomer composition. The homopolymer of 3-hydroxybutyrate (3HB), poly(3-hydroxybutyrate) (P3HB) is the most studied member of the PHA family, as it possesses numerous desirable properties. It is very interesting that the material in the native intracellular granules is completely amorphous and demonstrates extraordinary properties resembling super-cooled liquid [12]; nevertheless, when extracted from bacterial biomass, it quickly crystalizes. Therefore, its application potential is limited mainly by its high crystallinity, which reduces flexibility and elongation of the material. Nevertheless, the properties of the materials could be tuned when other monomer structures are incorporated into the polymer chain by feeding microbial culture with a suitable precursor(s). Therefore, copolymers containing, aside from 3HB, 3-hydroxyvalarate (3HV) subunits could be gained when microbial culture is cultivated in the presence of a suitable precursor with an odd number of carbon atoms such as propanol, propionate, pentanol, valerate, etc. The resulting copolymer poly(3-hydroxybutyrate-*co*-3-hydroxyvalerate) (P[3HB-*co*-3HV]) reveals substantially improved material properties and decreased crystallinity [13]. Similarly, some bacterial strains exposed to 1,4-butanediol or γ-butyrolactone (GBL) are able to biosynthesize copolymers containing 3HB and 4-hydroxybutyrate (4HB) monomer units. The copolymer poly(3-hydroxybutyrate-*co*-4-hydroxybutyrate) (P[3HB-*co*-4HB]) reveals mechanical properties, which resemble thermoplastic elastomers [14]. Moreover, PHA possessing 4HB subunits demonstrate increased biodegradability because lipases, which with PHA depolymerases, also have the ability to degrade P(3HB-*co*-4HB) [15], show higher activity at a higher fraction of 4HB [16]. Therefore, they find numerous high-value applications in the medical field [17]. Of course, terpolymer P(3HB-*co*-3HV-*co*-4HB) containing all of the above-mentioned monomer subunits demonstrate even superior properties and could be used in numerous fields and applications [18].

There are several reports dealing with the production of P(3HB-*co*-3HV-*co*-4HB) terpolymers employing various microorganisms. *Cupriavidus necator* (formerly *Alcaligenes eutrophus*, *Ralstonia eutropha* and *Wautersia eutropha*) was capable of desirable terpolymer production when cultivated on GBL and propionate; it was observed that propionate served not only as a 3HV precursor but it also increased the efficiency of 4HB incorporation into the terpolymer chain [19]. Similarly, Cavalheiro et al. produced P(3HB-*co*-3HV-*co*-4HB) by *Cupriavidus necator* using crude glycerol as the main carbon source, GBL as the 4HB precursor, and the 3HV-related precursor compound propionic acid [20]. Also, *Haloferax mediterranei* could be employed for the production of the terpolyester poly(3HB-*co*-3HV-*co*-4HB) without the need for a specific 3HV precursor which is based on the extraordinary metabolism of this microorganism, since it is capable of 3HV production from structurally unrelated carbon sources such as sugars or glycerol [21]. Finally, Ramachandran et al. used *Cupriavidus* sp. USMAA2-4 (now designated as *Cupriavidus malaysiensis* DSM 19379) for the terpolymer production from oleic acid and various 4HB and 3HV precursors [22].

In this work, we attempted to develop an efficient process of P(3HB-*co*-3HV-*co*-4HB) production employing *Cupriavidus malaysiensis* DSM 19379. We aimed at the maximization of both PHA yields, as well as 3HV and 4HB monomer fractions in the polymer to achieve desired material properties of the produced materials. Various culture strategies were used for this purpose.

2. Materials and Methods

2.1. Microorganisms and Cultivation

Cupriavidus malaysiensis USMAA2-4 (DSM 19379) was purchased from Leibnitz Institute DSMZ-German Collection of Microorganism and Cell Cultures, Braunschweig, Germany. The nutrient broth (Himedi—10 g/L Peptone, 10 g/L Beef Extract, 5 g/L NaCl) (NB) medium was used for the inoculum development. The mineral salt medium (MSM) for cultivation was composed of 3 g/L $(NH_4)_2SO_4$, 1.02 g/L KH_2PO_4, 11.1 g/L $Na_2HPO_4 \cdot 12\ H_2O$, 0.2 g/L $MgSO_4 \cdot 7\ H_2O$, and 1 mL/L of microelement solution, the composition of which was as follows: 9.7 g/L $FeCl_3 \cdot 6\ H_2O$, 7.8 g/L $CaCl_2 \cdot 2\ H_2O$, 0.156 g/L $CuSO_4 \cdot 5\ H_2O$, 0.119 g/L $CoCl_2 \cdot 2\ H_2O$, 0.118 g/L $NiCl_2 \cdot 4\ H_2O$, and 1 L

0.1 M HCl. The following carbon sources were used to prepare the production media: GBL (8 g/L) (Sigma Aldrich, Steinheim, Germany); ε-caprolactone (8 g/L) (Sigma Aldrich, Steinheim, Germany); 1,4-butanediol (8 g/L) (Sigma Aldrich, Schnelldorf, Germany); 1,6-hexanediol (8 g/L) (Sigma Aldrich, Schnelldorf, Germany); fructose (20 g/L); glucose (20 g/L); sunflower oil (20 g/L); glycerol p.a. (20 g/L) (Lach-ner, Neratovice, Czechia). Carbon sources, salt solutions, and microelement solutions were autoclaved separately (121 °C, 20 min) and then aseptically reconstituted at room temperature prior to the inoculation (inoculum ratio was 10 vol%). The cultivations were performed in Erlenmeyer flasks (volume 250 mL) containing 100 mL of MSM. The temperature was set at 30 °C, the agitation at 180 rpm. The cells were harvested after 72 h of cultivation as described in Section 2.2. For a successful centrifugation process, the medium was heated to 70 °C for 15 min.

2.1.1. Single-Stage Cultivation Mode

GBL or 1,4-butanediol were used to prepare the production media in the same way as described in Section 2.1. Propionic acid (Sigma Aldrich, Schnelldorf, Germany) and valeric acid (Sigma Aldrich, Schnelldorf, Germany) as 3HV precursors were added at a concentration 1 g/L to media after 24 h of cultivation to minimize their toxic effect on growth of the microbial culture. After another 48 h of cultivation, the cells were harvested. The total length of the cultivation was 72 h. As a control, we chose to cultivate without adding any of the precursors of 3HV.

2.1.2. Two-Stage Cultivation Mode

Glycerol (20 g/L) or combination of glycerol and 1,4-butanediol (12 and 8 g/L, respectively) were used to prepare the production media based on MSM. After 48 h of cultivation (30 °C, 180 rpm), biomass was separated by centrifugation (6000 rpm, 4 °C) and aseptically transferred to fresh MSM with 0.1 g/L $(NH_4)_2SO_4$, 8 g/L 1,4-butanediol and 1 g/L valeric acid. Cultivation without valeric acid served as a control. The cells were harvested after another 48 h of cultivation (30 °C, 180 rpm).

2.2. Determination of the CDM and PHA Content

To determine the biomass concentration and PHA content in cells, samples (10 mL) were centrifuged (6000 rpm) and then the cells were washed with distilled water. The biomass concentration expressed as cell dry mass (CDM) was analyzed as reported previously [23]. The PHA content of dried cells was analyzed by gas chromatography (GC) (Trace GC Ultra, Thermo Scientific, Waltham, MA, USA) as reported by Brandl et al. [24]. Commercially available P(3HB-*co*-3HV) (Sigma Aldrich, Schnelldorf, Germany) composed of 88 mol% 3HB and 12 mol% 3HV were used as a standard and benzoic acid (LachNer, Neratovice, Czechia) was used as an internal standard. In addition to the quantification of total PHA in biomass, GC was also used to determine the monomeric composition and to determine the molar content of individual monomers in the obtained polymers.

2.3. Polymer Characterization

Following four polymers obtained by *Cupriavidus malaysiensis*, USMAA2-4 (DSM 19379) using different substrates and cultivation strategies were selected due to various 4HB content for polymer characterization: Sample 1—single-stage, fructose (20 g/L); Sample 2—single-stage, 1,4-butanediol + valeric acid; Sample 3—single-stage, 1,4-butanediol + propionic acid; Sample 4—two-stage, glycerol (20 g/L), and then 1,4-butanediol + valeric acid.

To determine the molecular weight of PHA, approximately 20 mg CDM was washed in 5 mL chloroform at 70 °C for 24 h under continuous stirring. Solid residues were separated by filtration and, finally, the solvent was removed by evaporation at 70 °C to a constant weight. The obtained polymer was also used for DSC analysis. After that, 5 mg of the polymer was solubilized in 1 mL of HPLC-grade chloroform and passed through syringe filters (nylon membrane, pore size 0.45 μm). Samples were analyzed by gel Size Exclusion Chromatography (Agilent, Infinity 1260 system containing PLgel MIXED-C column) coupled with Multiangle Light Scattering (Wyatt Technology, Dawn Heleos

II, Goleta, CA, USA) and Differential Refractive Index (Wyatt Technology, Optilab T-rEX, Goleta, CA, USA) detection [24]. The weight-average molecular weight (Mw) and polydispersity index (Đ) were determined using the ASTRA software (Wyatt Technology, Goleta, CA, USA) based on Zimm´s equations.

Melting behavior of the isolated PHA polymers was analyzed by means of a differential scanning calorimeter (DSC) Q2000 (TA Instruments, New Castle, DE, USA) equipped with an RCS90 cooling accessory as previously described by Kucera et al. [25]. Phase transitions of mercury and indium were used for the calibration in the applied temperature range. Approximately 5 mg of sample was placed in hermetically sealed Tzero aluminum pans, and the measurement was carried out under a dynamic nitrogen atmosphere. To ensure the same thermal history of all samples prior to the evaluation of their melting behavior, each sample was first heated at 10 °C/min to 190 °C and subsequently cooled down to −30 °C at the same cooling rate. Then the sample was heated again (10 °C/min to 200 °C) and the thermogram, recorded in this second heating step, was further evaluated.

Thermogravimetric analysis of the isolated polymers was performed on Q5000 TGA analyzer (TA Instruments, New Castle, DE, USA). During the analysis, a known weight of a sample (ca 5 um) was heated at 10 °C/min to 800 °C under oxidative atmosphere (air). The major decomposition step, characterized by a rapid fall in the sample weight in the temperature range 250 °C to 350 °C, was further processed using TGA data evaluation software Universal Analysis 2000 (TA Instruments, New Castle, DE, USA). The automated evaluation of the weight change provided two characteristic temperatures of the degradation step: onset temperature of the thermal decomposition (Td_{onset}) and temperature corresponding to the maximal rate of the weight change (Td_{max}).

3. Results and Discussion

3.1. Biosynthesis of P(3HB-co-4HB) Copolymer

Cupriavidus malaysiensis DSM 19379 was employed to produce polyhydroxyalkanoates (PHA) using different carbon sources. This bacterium was isolated from water samples collected from Sg. Pinang river, Penang, Malaysia based on its ability to produce various types of PHA, including copolymers containing 4HB [26]. According to our results shown in Table 1, P3HB or P(3HB-*co*-4HB) were produced according to the type of the substrate. The bacterial strain was capable to produce copolymer P(3HB-*co*-4HB) only in the presence of precursors structurally related to 4HB such as GBL, 1,4-butandiol, ε-caprolactone, or 1,6-hexanediol e.g., diols and carboxylic acids possessing hydroxy group at last carbon atom which is agreement with results of Rahayu et al. [27] The highest PHA titers were achieved when four-carbon precursors of 4HB such as 1,4-butanediol or GBL were used. When such a structural motif was lacking, the strain accumulated homopolymer consisting exclusively of 3HB subunits. In the results, the strain appears to be unable to utilize oil because the CDM yield was low, and GC did not reveal PHA in the cell structure. There is a significant difference between utilization of fructose and glucose. While the yield of CDM and PHA with fructose was 10.78 g/L and 7.54 g/L, respectively, the yield with glucose was only 2.29 g/L CDM and 0.23 g/L PHA. This is not a very surprising result, also the closely related wild-type strain *Cupriavidus necator* H16 is not able to efficiently utilize glucose because it does not possess the activity of 6-phosphofructokinase [28]. *Cupriavidus malaysiensis* USMAA2-4 was also able to utilize glycerol reaching relatively high biomass titers; nevertheless, PHA production was the lowest among the substrates used which enabled PHA biosynthesis.

Table 1. Substrates for P3HB and P(3HB-*co*-4HB) production by *Cupriavidus* sp. DSM 19379.

Substrate	CDM (g/L)	PHA (wt%)	PHA (g/L)	4HB (mol%)	3HB (mol%)
fructose	10.78 ± 0.06	69.95 ± 0.42	7.54 ± 0.10	0	100
glucose	2.29 ± 0.06	10.03 ± 0.06	0.23 ± 0.02	0	100
glycerol	4.60 ± 0.04	5.30 ± 0.05	0.24 ± 0.02	0	100
sunflower oil	1.33 ± 0.05	0	0	0	0
GBL	4.50 ± 0.02	35.84 ± 0.92	1.61 ± 0.12	22.18 ± 1.06	77.82 ± 1.06
1,4-butanediol	4.01 ± 0.02	11.67 ± 0.06	0.47 ± 0.03	23.12 ± 1.61	76.88 ± 1.61
ε-caprolactone	0.22 ± 0.04	42.80 ± 0.61	0.10 ± 0.04	68.89 ± 1.12	31.11 ± 1.12
1,6-hexanediol	2.64 ± 0.01	39.83 ± 0.95	1.05 ± 0.07	34.35 ± 0.96	65.65 ± 0.96

3.2. Biosynthesis of P(3HB-co-3HV-co-4HB) Terpolymer through Single-Stage Cultivation

The following experiments were focused on the production of the terpolymer P(3HB-*co*-3HV-*co*-4HB). To obtain the desired material, 1,4-butanediol and GBL have been selected as carbon sources since the bacteria can utilize these substances for growth but also incorporate them into the copolymer P(3HB-*co*-4HB). Sodium propionate and valeric acid were tested in this experiment as odd carbon atom precursors for the synthesis of 3HV monomer incorporated into the terpolymer chain. Results of the single-stage terpolymer production including yields of CDM and PHA are shown in Table 2.

Table 2. Single stage terpolymer production (72 h cultivation, application of 3HV precursor at the 24 h of cultivation 1 g/L).

Primary Substrate	3HV Precursor	CDM (g/L)	PHA (g/L)	PHA (wt%)	3HB (mol%)	4HB (mol%)	3HV (mol%)
GBL	none	3.64 ± 0.03	0.81 ± 0.05	22.14 ± 0.01	68.40 ± 0.23	31.60 ± 0.23	0
	propionic acid	5.06 ± 0.37	0.62 ± 0.06	12.16 ± 0.00	69.18 ± 0.22	23.41 ± 0.05	7.41 ± 0.16
	valeric acid	7.97 ± 1.85	0.82 ± 0.09	10.41 ± 0.01	56.22 ± 0.32	25.85 ± 0.40	17.92 ± 0.07
1,4-butanediol	none	7.41 ± 0.51	1.05 ± 0.19	14.44 ± 0.02	68.97 ± 2.26	31.03 ± 2.26	0
	propionic acid	8.19 ± 0.35	1.65 ± 0.43	20.01 ± 0.04	63.81 ± 1.71	27.87 ± 0.10	8.32 ± 1.80
	valeric acid	8.68 ± 0.14	1.79 ± 0.88	20.52 ± 0.10	60.63 ± 2.90	24.72 ± 7.42	14.65 ± 4.53

In the resulting Table 2, CDM column shows that it generally achieved better growth using 1,4-butanediol as carbon sources than with GBL. Surprisingly, with the addition of the precursors for terpolymer synthesis, the CDM gain was higher. Valeric acid appears to be superior in the production of the P(3HB-*co*-4HB-*co*-3HV) terpolymer. With the addition of this precursor, significant growth was achieved with both GBL and 1,4-butanediol. The highest biomass concentration was obtained using 1,4-butanediol in combination with valeric acid, with a biomass yield of 8.68 g/L.

The highest PHA production was achieved in combination with valeric acid. The PHA yields were 0.82 g/L and 1.79 g/L for GBL and 1,4-butanediol, respectively. Thus, the combination of 1,4-butanediol with valeric acid again appears to be the best for production terpolymer in the single-stage strategy. Regarding the composition of the polymers obtained in this experiment, the terpolymer was synthesized using both precursors of 3HV. However, a higher 3HV fraction was obtained using valeric acid. In the case of propionate, generation of 3HV requires activity of 3-ketothiolase coupling propionyl-CoA and acetyl-CoA such as BktB in *C. necator* H16 [29]. On the contrary, conversion of valerate into 3HV could be relatively simply performed within the first "turn" of β-oxidation. It is likely that *Cupriavidus* DSM 19379 reveals relatively lower 3-ketohiolase activity as compared to the activity of the β-oxidation pathway, and therefore, valerate seems to be superior to the 3HV precursor for terpolymer synthesis as compared with propionate. In the case of terpolymer composition, the highest 3HV content was achieved using GBL together with valeric acid. The monomeric composition of the P(3HB-*co*-3HV-*co*-4HB) terpolymer was 56.22, 17.92, and 25.85 mol%, respectively. The polymer produced by *Cupriavidus malaysiensis* DSM 19379 using 1,4-butanediol in combination with valeric acid had almost the same composition. Nevertheless, it should be pointed out that the overall PHA

productivity gained in the single-stage process was relatively low. The PHA content was about 20 weight percent of CDM and gained PHA titers were, therefore, also low. Hence, we attempted to improve the productivity of the culture by employing the two-stage cultivation.

3.3. Biosynthesis of the P(3HB-co-3HV-co-4HB)Tterpolymer through the Two-Stage Cultivation

To enhance PHA productivity, we performed an additional experiment in which cultivation was performed in two steps. In the first step, we aimed at a cultivation of maximal biomass using glycerol (20 g/L) as a cheap carbon source. According to our results, glycerol stimulates growth of the bacterium, but it is not converted into P(3HB) which could be taken as an advantage since the production of a desirable terpolymer with low 3HB fraction could be achieved in the second step. In addition, glycerol (12 g/L) was also mixed with 1,4-butanediol (8 g/L) in a parallel series of cultivations. The second stage was performed in the cultivation media with nitrogen limitation and 1,4-butanediol, and most importantly, 1,4-butanediol and valeric acids were used as 4HB and 3HV precursors, respectively. Valeric acid was chosen as the precursor of the 3HV since it was identified as the superior 3HV precursor for the investigated culture. The first phase of cultivation served to obtain a high amount of PHA-poor biomass. PHA production was then achieved by nitrogen limitation in the second phase. All results are shown in Table 3.

Table 3. Two-stage terpolymer production (48 h at glycerol or glycerol + 1,4-butanediol, after that transfer to nitrogen-limited medium with precursor of 3HV.

Primary Substrate	Secondary Precursor	CDM (g/L)	PHA (g/L)	PHA (wt%)	3HB (mol%)	4HB (mol%)	3HV (mol%)
Glycerol	1,4-butanediol	1.60 ± 0.03	0.84 ± 0.02	52.25 ± 0.12	80.85 ± 0.68	18.09 ± 0.26	1.06 ± 0.43
	1,4-butanediol + valeric acid	2.73 ± 0.58	1.42 ± 0.25	52.12 ± 1.76	53.78 ± 0.61	16.76 ± 0.87	29.46 ± 0.26
Glycerol + 1,4-butanediol	1,4-butanediol	3.26 ± 0.11	2.09 ± 0.01	64.14 ± 2.38	77.89 ± 0.53	21.60 ± 0.54	0.51 ± 0.01
	1,4-butanediol + valeric acid	5.94 ± 0.14	4.14 ± 0.05	69.64 ± 0.73	65.68 ± 1.02	16.46 ± 1.28	17.86 ± 0.26

From the results of this experiment shown above, it could be seen that the bacterial strain grew best when, in the first step, glycerol was used in combination with 1,4-butanediol and in the second one, 1,4-butanediol with valeric acid. The biomass gain was 5.94 g/L. Conversely, the smallest growth was achieved by cultivation using glycerol followed by 1,4-butanediol, where only 1.60 g/L CDM was obtained. CDM and PHA analysis was also performed on cultures after the first stage of the two-stage production. The assumption that at this stage a biomass with a low PHA content would be obtained, has been fulfilled. The glycerol-based medium reached 3.1 g/L CDM containing 5.3% PHB. Using a substrate containing 14-BD, we obtained 3.8 g/L CDM containing 24.0% P(3HB-*co*-4HB).

From the results, *Cupriavidus malaysiensis* DSM 19379 can efficiently synthesize the desired terpolymer P(3HB-*co*-3HV-*co*-4HB), PHA contents in bacterial cells are substantially higher when two-stage cultivation strategy was adopted. The highest weight fraction, 69.64 wt%, as well as the highest PHA gain, 4.14 g/L, was achieved when glycerol was used together with 1,4-butanediol in the first step and 1,4-butanediol with valeric acid in the second. Regarding polymer composition, good results were achieved when 1,4-butanediol was used in combination with valeric acid in the second step. When only glycerol was used in the first step, we obtained a terpolymer composed of 53.78 mol% 3HB, 16.76 mol% 4HB, and 29.46 mol% 3HV. Using glycerol together with 1,4-butanediol in the first step, a terpolymer composed of 3HB 65.68 mol%, 4HB 16.46 mol%, 3HV 17.86 mol% was subsequently obtained. It seems that a combination of glycerol and 1,4-butanediol in the first step of cultivation and 1,4-butanediol and valeric acid in the second stage of the cultivation is a very promising strategy which results in very high PHA titers and high PHA content in the cells and also high portions of 4HB and 3HV in the terpolymer structure.

3.4. Characteristics of Isolated Polymers

Differential scanning calorimetry and thermogravimetry were chosen to study the thermal properties of the polymers; size exclusion chromatography was used to determine molecular weight and polydispersity index of the polymers. The following samples of isolated polymers were selected for analysis. Sample No. 1 is a control polymer containing almost exclusively 3HB monomer units. Sample No. 2 was collected by cultivation using a combination of 1,4-butanediol and valeric acid; the proportion of 3-hydroxyvalerate in this sample is 14.65 mol%. Sample No. 3 was obtained from cultivation using 1,4-butanediol and sodium propionate, and the concentration of 3HV was 8.32 mol%. The last sample was isolated from a cell suspension-cultured to produce a terpolymer, using glycerol followed by 1,4-butanediol together with valeric acid. In this sample, the 3HV molar ratio was highest at all, namely 29.46 mol%. The results are placed in Table 4. From the thermograms recorded by differential scanning calorimetry, we determined glass transition temperature (Tg) and melting point (Tm). The total heat of fusion ΔH, was also determined via integration of the melting endotherm. Using thermogravimetry, the degradation onset temperature (Td_{onset}) and the temperature that corresponds to the maximal rate of sample decomposition (Td_{max}) were determined.

Table 4. Properties of the selected materials.

Sample	3HB (mol%)	4HB (mol%)	3HV (mol%)	Mw (kDa)	Đ (-)	Tg (°C)	Tm (°C)	ΔH (J/g)	Td_{onset} (°C)	Td_{max} (°C)
1	99.33	0.67	0	155.97	1.04	-	155.79 168.70	4.70 64.89	271.88	287.94
2	60.63	24.72	14.65	258.66	1.02	24.78	161.34	2.80	271.48	293.49
3	63.81	27.87	8.32	314.60	1.01	26.19	161.67	3.04	275.24	300.83
4	53.78	16.76	29.46	137.89	1.17	29.00	164.63	12.69	271.36	295.53

Comparison of DSC thermograms of the four isolated polymers is shown in Figure 1. In Sample No. 1, there is a sharp melting endotherm which appears at about 170 °C, which is typical of polyhydroxybutyrate. The peak area corresponds to the heat released in this process. The large area of the melting endotherm indicates a high tendency of the polymer to crystallize spontaneously which in turn causes no significant signs of glass transition and cold crystallization are found in its thermogram as compared to the other three analyzed samples. Further, the sample is characterized by a double peak at the melting point, indicating that the polymer crystallites are present in two forms with distinct thermal stability. On the other hand, for all the terpolymer samples (Samples 2–4), it can be seen at first sight that much less intensive melting peak is shown on the curves. Furthermore, apparent glass transition and cold crystallization of the polymer chains altogether indicates significantly reduced the tendency for spontaneous crystallization. In other words, involvement of and additional monomer to the copolymer structure resulted in a more amorphous structure. Incorporating 3HV into the polymer structure also caused a decrease in melting point to about 161 °C. Fahima Azira et al. [30] produced terpolymer P(3HB-co-3HV-co-4HB) and the melting points ranged from 160 to 164 °C.

The SEC-MALS technique was used to measure weight average molecular weight (Mw) of obtained polymers and values ranged from 137 to 314 kDa. The highest value was measured for the sample with the highest molar ratio of 4HB and the lowest for the sample with the highest molar ratio of 3HV. The Mw values measured are typical for the bacterial strain used and consistent with other studies [22].

Thermogravimetric analysis was performed in order to compare the thermal stability of the produced polymers. In a respective thermogram, decomposition of a polymer is represented by the onset temperature of the decomposition (the temperature at which the polymer starts to decompose, Td_{onset}) and by the temperature which corresponds to the maximal rate of the decomposition (Td_{max}). Among the isolated P(3HB-*co*-3HV-*co*-4HB) terpolymer samples, the highest degradation temperature (i.e., the highest thermal stability of the polymer) was measured for Sample No. 3 composed of

63.81 mol% 3HB, 27.87 mol% 4HB, and 8.32 mol% 3HV. This is the sample with the lowest 3HV but the highest 4HB. This suggests that a higher proportion of 4HB in the terpolymer leads to the higher thermal stability of the polymer. Thus, sample 3 has the most promising properties from a technological point of view because its melting point was set at near lowest, 161.67 °C, and the degradation temperature to highest 300.83 °C. The wide temperature window between melting temperature and degradation temperature is important for polymer processing. When working with the melt, it is important that it does not decompose.

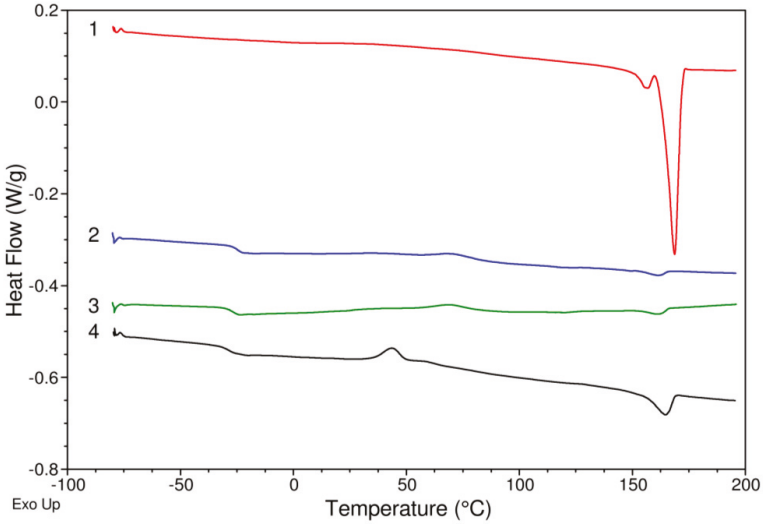

Figure 1. Results of DSC analysis of isolated polymers.

4. Conclusions

To sum-up, in flask experiments, we have developed a two-stage cultivation strategy which is based on the application of glycerol and 1,4-butanediol as the carbon substrates in the first stage of cultivation, after that the cells are transferred into nitrogen-limited cultivation media with 1,4-butanediol and valeric acids. This cultivation strategy provides high PHA yields and PHA content in bacterial cells. Moreover, the P(3HB-co-3HV-co-4HB) terpolymer with low 3HB fraction and high 3HV and 4HB contents is obtained. The material properties of obtained polymers were consistent with materials produced in previous studies aimed at the production of P(3HB-co-3HV-co-4HB) terpolymers. In our future experiments, we will transfer the process into laboratory bioreactors to evaluate its suitability for industrial production of PHA.

Author Contributions: Conceptualization—D.K. and S.O.; Data curation—D.K. and I.P.; Formal analysis—D.K. and P.S.; Funding acquisition—S.O.; Investigation—S.O.; Methodology—S.O.; Project administration—S.O.; Resources—S.O.; Supervision—S.O.; Validation—I.N. and I.P.; Visualization—D.K.; Writing—original draft—D.K.; Writing—review & editing—P.S. and S.O.

Funding: This study was funded by the project GA19-20697S of the Czech Science Foundation (GACR). Further, Ivana Novackova is Brno Ph.D. Talent Scholarship Holder—Funded by the Brno City Municipality.

Acknowledgments: Authors kindly thank to Leona Kubikova for all the help with TGA and DSC measurement and to Michal Kalina for determination of molecular weight analysis by SEC-MALS.

Conflicts of Interest: The authors declare no conflict of interest. The funders had no role in the design of the study; in the collection, analyses, or interpretation of data; in the writing of the manuscript, or in the decision to publish the results.

References

1. Kourmentza, C.; Plácido, J.; Venetsaneas, N.; Burniol-Figols, A.; Varrone, C.; Gavala, H.N.; Reis, M.A. Recent advances and challenges towards sustainable polyhydroxyalkanoate (PHA) production. *Bioengineering* **2017**, *4*, 55. [CrossRef]
2. Obruca, S.; Sedlacek, P.; Koller, M.; Kucera, D.; Pernicova, I. Involvement of polyhydroxyalkanoates in stress resistance of microbial cells: Biotechnological consequences and applications. *Biotechnol. Adv.* **2018**, *36*, 856–870. [CrossRef] [PubMed]
3. Slaninova, E.; Sedlacek, P.; Mravec, F.; Mullerova, L.; Samek, O.; Koller, M.; Hesko, O.; Kucera, D.; Marova, I.; Obruca, S. Light scattering on PHA granules protects bacterial cells against the harmful effects of UV radiation. *Appl. Microbiol. Biotechnol.* **2018**, *102*, 1923–1931. [CrossRef]
4. Haas, C.; Steinwandter, V.; De Apodaca, E.D.; Madurga, B.M.; Smerilli, M.; Dietrich, T.; Neureiter, M. Production of PHB from chicory roots - Comparison of three *Cupriavidus necator* strains. *Chem. Biochem. Eng. Q.* **2015**, *29*, 99–112. [CrossRef]
5. Verlinden, R.A.J.; Hill, D.J.; Kenward, M.A.; Williams, C.D.; Piotrowska-Seget, Z.; Radecka, I.K. Production of polyhydroxyalkanoates from waste frying oil by *Cupriavidus necator*. *Amb Express* **2011**, *1*, 1–8. [CrossRef] [PubMed]
6. Ciesielski, S.; Mozejko, J.; Pisutpaisal, N. Plant oils as promising substrates for polyhydroxyalkanoates production. *J. Clean. Prod.* **2015**, *106*, 408–421. [CrossRef]
7. Jiang, G.; Hill, D.J.; Kowalczuk, M.; Johnston, B.; Adamus, G.; Irorere, V.; Radecka, I. Carbon sources for polyhydroxyalkanoates and an integrated biorefinery. *Int. J. Mol. Sci.* **2016**, *17*, 1157. [CrossRef] [PubMed]
8. Moita, R.; Freches, A.; Lemos, P.C. Crude glycerol as feedstock for polyhydroxyalkanoates production by mixed microbial cultures. *Water Res.* **2014**, *58*, 9–20. [CrossRef]
9. Obruca, S.; Benesova, P.; Marsalek, L.; Marova, I. Use of lignocellulosic materials for PHA production. *Chem. Biochem. Eng. Q.* **2015**, *29*, 135–144. [CrossRef]
10. Meixner, K.; Kovalcik, A.; Sykacek, E.; Gruber-Brunhumer, M.; Zeilinger, W.; Markl, K.; Haas, C.; Fritz, I.; Mundigler, N.; Stelzer, F.; et al. Cyanobacteria Biorefinery—Production of poly(3-hydroxybutyrate) with *Synechocystis salina* and utilisation of residual biomass. *J. Biotechnol.* **2018**, *265*, 46–53. [CrossRef]
11. Troschl, C.; Meixner, K.; Drosg, B. Cyanobacterial PHA Production—Review of Recent Advances and a Summary of Three Years' Working Experience Running a Pilot Plant. *Bioengineering* **2017**, *4*, 26. [CrossRef]
12. Sedlacek, P.; Slaninova, E.; Enev, V.; Koller, M.; Nebesarova, J.; Marova, I.; Hrubanova, K.; Krzyzanek, V.; Samek, O.; Obruca, S. What keeps polyhydroxyalkanoates in bacterial cells amorphous? A derivation from stress exposure experiments. *Appl. Microbiol. Biotechnol.* **2019**, *103*, 1905–1917. [CrossRef]
13. Koller, M. Chemical and biochemical engineering approaches in manufacturing polyhydroxyalkanoate (PHA) biopolyesters of tailored structure with focus on the diversity of building blocks. *Chem. Biochem. Eng. Q.* **2018**, *32*, 413–438. [CrossRef]
14. Lee, W.H.; Azizan, M.N.M.; Sudesh, K. Effects of culture conditions on the composition of poly(3-hydroxybutyrate-*co*-4-hydroxybutyrate) synthesized by *Comamonas acidovorans*. *Polym Degrad Stab.* **2004**, *84*, 129–134. [CrossRef]
15. Rodríguez-Contreras, A.; Calafell-Monfort, M.; Marqués-Calvo, M.S. Enzymatic degradation of poly(3-hydroxybutyrate-*co*-4-hydroxybutyrate) by commercial lipases. *Polym. Degrad. Stabil.* **2012**, *97*, 597–604. [CrossRef]
16. Saito, Y.; Nakamura, S.; Hiramitsu, M.; Doi, Y. Microbial synthesis and properties of poly(3-hydroxybutyrate-*co*-4-hydroxybutyrate). *Polym. Int.* **1996**, *39*, 167–174. [CrossRef]
17. Singh, A.K.; Srivastava, J.K.; Chandel, A.K.; Sharma, L.; Mallick, N.; Singh, S.P. Biomedical applications of microbially engineered polyhydroxyalkanoates: an insight into recent advances, bottlenecks, and solutions. *Appl. Microbiol. Biotechnol.* **2019**, *103*, 2007–2032. [CrossRef]
18. Chanprateep, S.; Kulpreecha, S. Production and characterization of biodegradable terpolymer poly(3-hydroxybutyrate-*co*-3-hydroxyvalerate-*co*-4-hydroxybutyrate) by *Alcaligenes* sp. A-04. *J. Biosci. Bioeng.* **2006**, *101*, 51–56. [CrossRef]
19. Lee, Y.H.; Kang, M.S.; Jung, Y.M. Regulating the molar fraction of 4-hydroxybutyrate in poly(3-hydroxybutyrate-4-hydroxybutyrate) biosynthesis by *Ralstonia eutropha* using propionate as a stimulator. *J. Biosci. Bioeng.* **2000**, *89*, 380. [CrossRef]

20. Cavalheiro, J.M.; Raposo, R.S.; de Almeida, M.C.M.; Cesário, M.T.; Sevrin, C.; Grandfils, C.; Da Fonseca, M.M.R. Effect of cultivation parameters on the production of poly(3-hydroxybutyrate-*co*-4-hydroxybutyrate) and poly(3-hydroxybutyrate-4-hydroxybutyrate-3-hydroxyvalerate) by *Cupriavidus necator* using waste glycerol. *Biores. Technol.* **2012**, *111*, 391. [CrossRef]
21. Hermann-Krauss, C.; Koller, M.; Muhr, A.; Fasl, H.; Stelzer, F.; Braunegg, G. Archaeal production of polyhydroxyalkanoate (PHA) co-and terpolyesters from biodiesel industry-derived by-products. *Archaea* **2013**, *2013*, 129268. [CrossRef]
22. Ramachandran, H.; Iqbal, N.M.; Sipaut, C.S.; Abdullah, A.A.A. Biosynthesis and characterization of poly (3-hydroxybutyrate-*co*-3-hydroxyvalerate-*co*-4-hydroxybutyrate). Terpolymer with various monomer compositions by *Cupriavidus* sp. USMAA2-4. *Appl. Biochem. Biotechnol.* **2011**, *164*, 867–877. [CrossRef]
23. Obruca, S.; Marova, I.; Melusova, S.; Mravcova, L. Production of polyhydroxyalkanoates from cheese whey employing *Bacillus megaterium* CCM 2037. *Ann. Microbiol.* **2011**, *61*, 947–953. [CrossRef]
24. Brandl, H.; Gross, R.A.; Lenz, R.W.; Fuller, R.C. *Pseudomonas oleovorans* as a source of poly(beta-hydroxyalkanoates) for potential application as a biodegradable polyester. *Appl. Environ. Microb.* **1988**, *54*, 1977–1982.
25. Kucera, D.; Pernicová, I.; Kovalcik, A.; Koller, M.; Mullerova, L.; Sedlacek, P.; Mravec, F.; Nebesarova, J.; Kalina, M.; Marova, I.; et al. Characterization of the promising poly(3-hydroxybutyrate) producing halophilic bacterium *Halomonas halophila*. *Biores. Technol.* **2018**, *256*, 552–556. [CrossRef]
26. Amirul, A.A.; Yahya, A.R.M.; Sudesh, K.; Azizan, M.N.M.; Majid, M.I.A. Biosynthesis of poly(3-hydroxybutyrate-*co*-4-hydroxybutyrate) copolymer by *Cupriavidus* sp. USMAA1020 isolated from Lake Kulim, Malaysia. *Biores. Technol.* **2008**, *99*, 4903–4909.
27. Rahayu, A.; Zaleha, Z.; Yahya, A.R.M.; Majid, M.I.A.; Amirul, A. A Production of copolymer poly(3-hydroxybutyrate-co-4-hydroxybutyrate) through a one-step cultivation process. *World J. Microbiol. Biotechnol.* **2008**, *24*, 2403–2409. [CrossRef]
28. Lopar, M.; Špoljarić, I.V.; Cepanec, N.; Koller, M.; Braunegg, G.; Horvat, P. Study of metabolic network of *Cupriavidus necator* DSM 545 growing on glycerol by applying elementary flux modes and yield space analysis. *J. Ind. Microbiol. Biotechnol.* **2014**, *41*, 913–930. [CrossRef]
29. Lindenkamp, N.; Peplinski, K.; Volodina, E.; Ehrenreich, A.; Steinbuchel, A. Impact of multiple beta-ketothiolase deletion mutations in *Ralstonia eutropha* H16 on the composition of 3-mercaptopropionic acid-containing copolymers. *Appl. Environ. Microbiol.* **2010**, *76*, 5373–5382. [CrossRef]
30. Fahima Azira, T.M.; Nursolehah, A.A.; Norhayati, Y.; Majid, M.I.A.; Amirul, A.A. Biosynthesis of Poly(3-hydroxybutyrate-co-3-hydroxyvalerate-co-4-hydroxybutyrate) terpolymer by *Cupriavidus* sp. USMAA2-4 through two-step cultivation process. *World J. Microbiol. Biotechnol.* **2011**, *27*, 2287–2295. [CrossRef]

bioengineering

MDPI

Article

Rheological Behavior of High Cell Density *Pseudomonas putida* LS46 Cultures during Production of Medium Chain Length Polyhydroxyalkanoate (PHA) Polymers

Warren Blunt [1,*,†], Marc Gaugler [2], Christophe Collet [2], Richard Sparling [3], Daniel J. Gapes [2], David B. Levin [1] and Nazim Cicek [1]

[1] Department of Biosystems Engineering, University of Manitoba, Winnipeg, MB R3T 5V6, Canada; David.Levin@umanitoba.ca (D.B.L.); Nazim.Cicek@umanitoba.ca (N.C.)

[2] Scion Research, Te Papa Tipu Innovation Park, 49 Sala Street, Private Bag 3020, Rotorua 3046, New Zealand; Marc.Gaugler@scionresearch.com (M.G.); Christophe.Collet@scionresearch.com (C.C.); Daniel.Gapes@scionresearch.com (D.J.G.)

[3] Department of Microbiology, University of Manitoba, Winnipeg, MB R3T 2N2, Canada; Richard.Sparling@umanitoba.ca

* Correspondence: umbluntw@myumanitoba.ca or warren.blunt@nrc-cnrc.gc.ca; Tel.: +1-(514)-283-3399; Fax: +1-(514)-496-6265

† Present address of corresponding author: National Research Council of Canada, 6100 Royalmount Avenue Montreal, QC H4P 2R2, Canada.

Received: 30 August 2019; Accepted: 8 October 2019; Published: 9 October 2019

Abstract: The rheology of high-cell density (HCD) cultures is an important parameter for its impact on mixing and sparging, process scale-up, and downstream unit operations in bioprocess development. In this work, time-dependent rheological properties of HCD *Pseudomonas putida* LS46 cultures were monitored for microbial polyhydroxyalkanoate (PHA) production. As the cell density of the fed-batch cultivation increased (0 to 25 $g \cdot L^{-1}$ cell dry mass, CDM), the apparent viscosity increased nearly nine-fold throughout the fed-batch process. The medium behaved as a nearly Newtonian fluid at lower cell densities, and became increasingly shear-thinning as the cell density increased. However, shear-thickening behavior was observed at shearing rates of approximately 75 $rad \cdot s^{-1}$ or higher, and its onset increased with viscosity of the sample. The supernatant, which contained up to 9 $g \cdot L^{-1}$ soluble organic material, contributed more to the observed viscosity effect than did the presence of cells. Owing to this behavior, the oxygen transfer performance of the bioreactor, for otherwise constant operating conditions, was reduced by 50% over the cultivation time. This study has shown that the dynamic rheology of HCD cultures is an important engineering parameter that may impact the final outcome in PHA cultivations. Understanding and anticipating this behavior and its biochemical origins could be important for improving overall productivity, yield, process scalability, and the efficacy of downstream processing unit operations.

Keywords: PHA; viscosity; non-Newtonian fluid; fed-batch fermentation; oxygen transfer; *Pseudomonas putida*

1. Introduction

Recent concern over the accumulation of plastic waste in the natural environment (particularly micro-plastics) emphasizes the need to find alternative biodegradable polymers [1,2]. In this regard, PHA polymers are a promising replacement for petroleum-based plastic materials, being both renewable and completely biodegradable [3]. PHA polymers can have a variety of different monomer sub-unit

compositions. This enables, to a large extent, a wide-range of physical and thermal properties and numerous potential applications [4,5]. Indeed, certain PHAs (depending on the composition and arrangement of the monomer subunits) have properties comparable to conventional petroleum-based plastics, like polyethylene and polypropylene.

PHA polymers are synthesized as intracellular reserves of carbon, energy, and reducing power by a wide-range of bacteria, and some archaea. While the cost of production currently limits applications for PHA to niche markets [6,7], development of more efficient bioprocesses may help to increase the economic viability and lessen the environmental impact of PHA production [8,9]. Currently, HCD cultures are widely seen as the best cultivation strategy to achieve high volumetric productivities [10]. Some HCD cultures for PHA production have reached cell densities in excess of 200 $g \cdot L^{-1}$ CDM [11–13]. Further details on HCD cultivations in PHA production are available in several recent reviews [14,15]. However, a common problem with HCD cultures in general is increasing medium viscosity [16]. This can lead to dead zones in the bioreactor and reduced heat and mass transfer capabilities, especially in large-scale bioreactors with inherently poor mixing capability [17].

Rheology is the study of the deformation of matter (in this case, the flow of liquid fermentation medium) under an applied stress. Previous studies have examined the rheology of cultivation medium for a variety of bioprocessing applications using different microorganisms and fungi. These include: xanthan gum production using *Xanthomonas* spp. [18], viscous mycelial (fungal) cultures for variety of bio-products [19–24], polyglutamic acid (PGA) production using *Bacillus subtilis* [25], mixtures of primary and secondary sewage sludge [26], and fermentation of sewage sludge [27,28], amongst others. Multiple studies have looked at rheological properties of extracellular polymeric substances (EPS) produced by *Pseudomonas* spp. [29–33]. However, many of these assessments examined rheological properties of an extracted polymer of interest, but did not directly quantify its effect on culture medium. Most studies show that fermentation medium behaves as a non-Newtonian fluid, meaning the apparent viscosity is dependent on the shear rate [19,23,34,35].

Since lack of adequate dissolved oxygen (DO) is a significant factor that limits productivity in HCD cultivations for PHA production [36], the effect of medium viscosity on the oxygen transfer rate could be important. Several previous studies have demonstrated inversely proportional relationships between viscosity and oxygen transfer in both model Newtonian fluids (glycerol, glucose solutions) as well as non-Newtonian fluids (xanthan gum, carboxymethylcellulose solutions) [17,37–42]. Such model fluids are often preferred to actual biological cultures because they are cheaper and easier to work with [17]. A few studies, however, have evaluated oxygen transfer characteristics in a biological medium [19,25]. In all cases, there is a consensus that the volumetric oxygen mass transfer coefficient, $K_L a$, is inversely proportional to the medium viscosity.

Previous application of HCD cultivations in PHA production are numerous [15]. Yet, we can find no evidence that rheology of the culture medium has been studied to date; or at the very least, that information is not widely accessible. This includes both short-chain length (scl-) PHAs and medium chain length (mcl-) PHAs. Considering that PHAs are high molecular weight (M_w) polymers that can occupy up to 75–88% CDM [13,43] and be produced with relatively high titer [14,15], the examination of culture rheology and its effects on oxygen transfer could be an important contribution to process development, optimization, and scalability in PHA production. Furthermore, this could have significant impact on downstream processing, including pumping, filtration, centrifugation, or spray drying unit operations.

The objectives of this work were, therefore: 1) to examine time-dependent rheological behavior of HCD fed-batch cultures of *Pseudomonas putida* LS46 for production of medium chain length (mcl-) PHAs; 2) to gain understanding of the biochemical origins of these rheological changes; and 3) to further assess how viscosity impacts the oxygen mass transfer characteristics of the cultivation medium.

2. Materials and Methods

2.1. Micro-Organism, Medium, and Substrate

The strain used in this study was *Pseudomonas putida* LS46 [44], and strain maintenance procedures were as specified previously [45]. A slightly modified version of Ramsay's minimal medium used in all experimental studies [46]. However, the initial concentrations of $(NH_4)_2SO_4$, $MgSO_4$, $CaCl_2{\cdot}2H_2O$, and trace element solution were increased to 2 $g{\cdot}L^{-1}$, 0.2 $g{\cdot}L^{-1}$, 20 $mg{\cdot}L^{-1}$, and 2 $mL{\cdot}L^{-1}$, respectively. The $MgSO_4$, $CaCl_2{\cdot}2H_2O$, ferric ammonium citrate, and trace element solution were filter sterilized through a 0.2 μm filter after autoclaving. Octanoic acid was used as the substrate in these studies and was added through a sterile 0.2 μm filter after autoclaving to an initial concentration of 20 mM.

2.2. Reactor Setup and Operation

Most experiments for this work were conducted in a 7 L (total volume) bench-scale system with a 3 L working volume. This system was used to generate the meta-data supporting the rheological observations in the pilot-scale bioreactor, which is described below. The configuration and setup of the bench-scale bioreactor system has been described previously [45,47]. Aeration was maintained at a constant flow rate of 2 VVM (atmospheric air only), and a mixing cascade (350–1200 rpm) was used to control the DO signal at 40% (of saturation with atmospheric air at 30 °C) for as long as possible. A reactive pulse-feed strategy was applied in response to either a drop in the off-gas CO_2 signal or a rise in the DO signal, indicating carbon limitation. Sub-inhibitory pulses of octanoic acid (5–20 mM) and a 200 $g{\cdot}L^{-1}$ solution of $(NH_4)_2SO_4$ were added to the reactor via high-precision injector syringes automated by LabBoss software [48]. The bench-scale cultivation was performed three times.

Because of the larger sample volume (1 L) required for rheological analysis, the system used for generation of these samples was a pilot-scale stainless steel, sterilization in place (SIP) bioreactor with a 152 L total volume (Sartorius Stedim Biostat D-DCU, Göttingen, Germany). The bioreactor was equipped with three 160 mm diameter Rushton turbines, four baffles, pH and DO electrodes, and a ring-type sparger located underneath the impeller. The bioreactor was filled with an initial volume of 70 L medium, and sterilized at 121 °C for 20 min before cooling to 30 °C.

In the pilot-scale system, the DO was maintained at 40% (of air saturation at 30 °C) for as long as possible. The cascade for DO was maintained through: (1) incremental increases in pressure from 200 mbar to 1000 mbar; (2) incremental increases in stirring rate from 100 rpm to a maximum of 600 rpm; and (3) increasing aeration (atmospheric air only) from 10 litres per minute (LPM) up to 30 LPM (maximum of approx. 0.4 volumes of air per liquid volume per minute or VVM). At this scale, aeration was limited because of foaming and excessive gas holdup encountered at higher volumetric flow rates. The slight headspace overpressure was used to obtain similar growth rates and biomass production over time, as well as timing of the onset of oxygen-limited conditions, as compared to the bench-scale bioreactor. This implies less efficient mixing in the pilot-scale bioreactor. The pilot-scale experiment was also carried out using the above-described pulse-feed strategy, except feeding was done with calibrated peristaltic pumps. Due to time and resource constraints, the pilot scale cultivation was performed once.

In either bioreactor system, experiments were initiated with the addition of a 5% (vol/vol) inoculum, which was grown overnight in flask cultures. After 16–20 h, $(NH_4)_2SO_4$ was no longer fed because it was no longer being consumed rapidly due to DO limitation. The pH of the medium was generally maintained via the addition of NaOH with automated peristaltic pumps (4 M at bench-scale and 10 M at the pilot-scale).

2.3. Sample Treatment

Samples (20–40 mL) were periodically withdrawn from the bioreactor, generally in 1–3 h intervals. These were centrifuged for 10 min at 12,500× *g*. The pellet was washed once in PBS buffer, transferred into a pre-weighed 20 mL aluminum dish and dried at 60 °C until no further loss of mass was detected

to determine the total biomass concentration ($[X_t]$, g·L^{-1} CDM). The PHA content of the biomass ($\%_{PHA}$) was determined by gas chromatography with a flame ionization detector (GC-FID) using the sample preparation, instrument, and operating parameters described previously [45]. The supernatant was decanted and stored at −20 °C for analysis of residual octanoic acid by GC-FID and ammonium was determined spectrophotometrically by the indophenol blue method. Further details of these analyses are available elsewhere [45].

2.4. Viscosity Measurements (Pilot Scale)

Periodic 1 L samples were withdrawn from the bioreactor for rheological analysis. For certain samples, a portion of the medium was centrifuged at 12,500× *g* for 15 min (Sorvall RC-6 Plus with an F12-6 × 500 LEX rotor) to investigate the cell-free supernatants. The medium viscosity was assessed using a DHR-2 Rheometer (TA Instruments, New Castle, DE, USA) equipped with a cup-and-bob measurement system (30 mm cup diameter; 28 mm bob diameter). The cup and bob geometry was chosen to mitigate effects from sample drying, but plate-plate and cup/vane geometry were also assessed. Although good results for all three measurement geometries were obtained, the cup/bob system was chosen because of a more defined flow in the measurement gap, lower end-effects compared to the vane geometry [49] and fewer artefacts due to sample drying during the test compared to the parallel plate geometry.

The samples were conditioned at 30 °C for 20 min prior to measuring. During this conditioning step, a constant shear of 1 s^{-1} was applied to avoid settlement of the samples. All samples were measured using a flow sweep between 2 and 1000 s^{-1}. The samples in the cup/bob assembly were inspected after completion of the rheological testing to ensure that no significant evaporation occurred that would have affected the viscosity results. All samples were measured in triplicate. The data analysis was done using TRIOS v4.1.0.31739 (TA Instruments, New Castle, DE, USA).

The measured shear stress at different shear rates during rotational rheology can be described using a variety of established rheological models. In this work, the fit was best described using the power law. A power-law fluid is an idealized fluid, and its shear stress is a function of shear rate as described by

$$\tau = \varphi \times \dot{\gamma}^{n} \quad (1)$$

where τ is the shear stress (mPa); φ is the Power law viscosity constant (mPa·s); $\dot{\gamma}$ is the shear rate (s^{-1}), and n is the rate index (dimensionless).

2.5. Off-Line Measurement of the Volumetric Oxygen Mass Transfer Coefficient (Bench-Scale)

The global volumetric oxygen mass transfer coefficient, K_La, was measured using the dynamic out-gassing method [50]. To avoid the impracticality of K_La determinations at scale (which would require a 3 L sample volume), a small-scale reactor with a 200 mL working volume was constructed to allow at-line K_La determination while using minimal (150 mL) sample volume taken at various points throughout the bench scale fed-batch cultivations. The goal was to show that, for a given reactor environment (with constant mixing, geometry, gas flow rates, etc.) the oxygen transfer performance of that system is reduced as the chemical matrix of the supernatant becomes increasingly complex and viscous over time. An unfortunate consequence or limitation, however, is that the determined K_La values are not representative of the actual reactor environment from which the samples were derived. Because of this, the results were expressed as a percent of the value measured using the 0 h sample.

This 200 mL reactor used for K_La determination was constructed from plexi-glass with height 7.9 cm and 5.4 cm in diameter. The reactor was equipped with compression fitting ports for a DO probe, gas inlet, and gas outlet. The reactor was stirred magnetically with a 2.5 cm stir bar at 1000 rpm, and either air or N_2 was delivered to the reactor at flow rates of 200 or 500 mL·min^{-1}, respectively. This was done using thermal mass flow controllers (Bronkhorst Hi-Tech, Ruurlo, the Netherlands), which were part of an off-gas sensor system previously described [48]. A minimum of three determinations

was done for each sample, and this was replicated for three fed batch experiments. The unit was validated initially in trials using distilled water or Ramsay's medium, and K_La values of 34.3 ± 3.4 h^{-1} and 21.5 ± 2.1 h^{-1} were obtained, respectively. Not surprisingly, these were on the lower end of the values obtained previously in the bench-scale bioreactor system [45,47]. This is probably because: (1) lack of baffles in the miniature device; (2) a stir bar was used instead of a proper impeller in the miniature device; and (3) the point of release of the bubbles was above the stir bar in the miniaturized reactor (as opposed to underneath the impeller in the bioreactor).

2.6. Analysis of Organic Products in the Supernatant (Bench-Scale)

Soluble protein in the supernatant was determined spectrophotometrically at 595 nm using a modified Bradford Assay [51]. Briefly, 0.5 mL of supernatant was mixed with 0.5 mL of 0.4 M NaOH. The samples were boiled for 10 min, and centrifuged (12,500× *g* for 5 min). A 20 µL aliquot of each sample was then placed in triplicate wells of a 96-well plate with 200 µL of Bradford Reagent (obtained from Sigma-Aldrich, St Louis, MO, USA). Standards were prepared using bovine serum albumin (Sigma-Aldrich, St Louis, MO, USA) and diluted into 0.2 M NaOH at concentrations of 0–300 mg·L^{-1}. Samples outside this concentration range were diluted appropriately in distilled water and the analysis was redone.

Reducing sugars in the supernatant were determined by the Anthrone method adapted from a previous protocol [52]. Briefly, 0.5 mL of supernatant was added to glass reaction vials with sealed caps. Then 1 mL of 0.1% anthrone in concentrated H_2SO_4 was added to the vial (using filter tips) and sealed. Samples were placed in a water bath at 80 °C for 5 min, and then allowed to cool to room temperature. 200 µL of each sample was pipetted (again using filter tips) into triplicate wells in a 96-well plate and the color change (green-blue) was quantified spectrophotometrically at 620 nm. Standards were prepared using glucose at concentrations of 0–100 mg·L^{-1}.

DNA in the supernatant was quantified using the Qubit Fluorometer. A 5 to 20 µL volume of sample was diluted into a 200 µL total volume of the working solution and sample (working solution was the fluorescence dye diluted 1:200 in buffer). If further dilutions were required, the samples were diluted in distilled water. The broad range DNA standards were used, which had a concentration range of 0 to 5 ng·μL^{-1}.

Volatile solids in the supernatant were quantified using 50 mL crucibles. A known volume of supernatant was placed in pre-weighed crucibles that were kept in a desiccator. The crucibles were then oven-dried at 105 °C for 24 h and weighed again following an equilibration period in the desiccator, and then placed at 550 °C for at least 2 h. The final mass of the crucible was then measured following cooling and equilibration in a desiccator.

3. Results and Discussion

3.1. Growth and mcl-PHA Synthesis

The [X_t], $\%_{PHA}$, and resulting PHA biomass ([X_{PHA}], expressed in g·L^{-1}) are shown in Figure 1 for both bioreactor systems. The initially high mcl-PHA content at time zero is due to carry-over from the inoculum, which was grown in flasks for a sufficiently long period so as to induce oxygen limitation and mcl-PHA synthesis from octanoic acid [45]. At both scales, the onset of oxygen limitation occurred around 12–14 h post inoculation and caused carbon flux to shift from growth to mcl-PHA synthesis. Overall, growth and total biomass production were similar at both scales, although the final $\%_{PHA}$ in the pilot-scale bioreactor was slightly lower than at bench-scale.

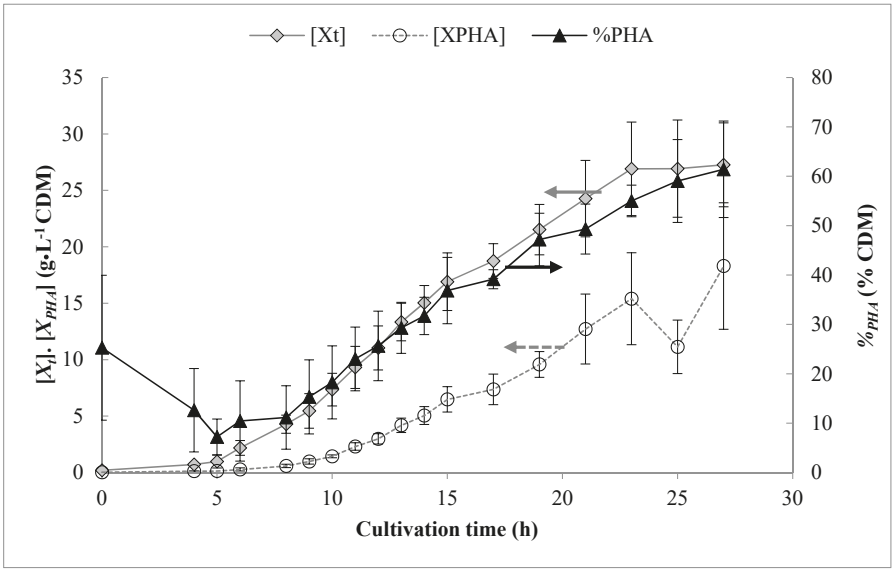

(**a**)

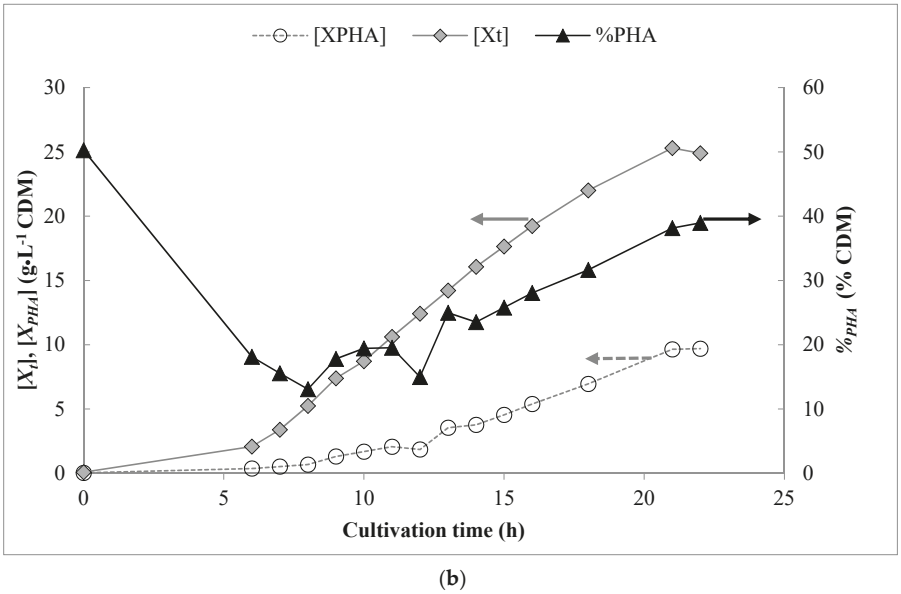

(**b**)

Figure 1. Results for biomass and PHA production obtained over the course of the pulse-feed fed-batch experiments (**a**) bench-scale bioreactor system (3 L initial working volume) and (**b**) pilot-scale bioreactor system (70 L initial working volume).

3.2. Rheological Characterization of the Cultivation Medium

Over the time course of the cultivation, the medium (even after centrifugation) became increasingly opaque and viscous. This appeared to significantly dampen the turbulence created for a given stirring input. The flow sweep curves for samples obtained from the pilot-scale system show viscosity as a function of shear rate for both cell suspensions (Figure 2a) and cell-free supernatants (Figure 2b) at

various points in time in the bioreactor. In both cases, the medium appeared to behave as a Newtonian fluid up until 12 h for shear rates of approximately 75 s^{-1} or less. By 14 h (which corresponded to the onset of O_2 limitation in the bioreactor), a significant increase in viscosity was observed and the samples also became increasingly shear-thinning.

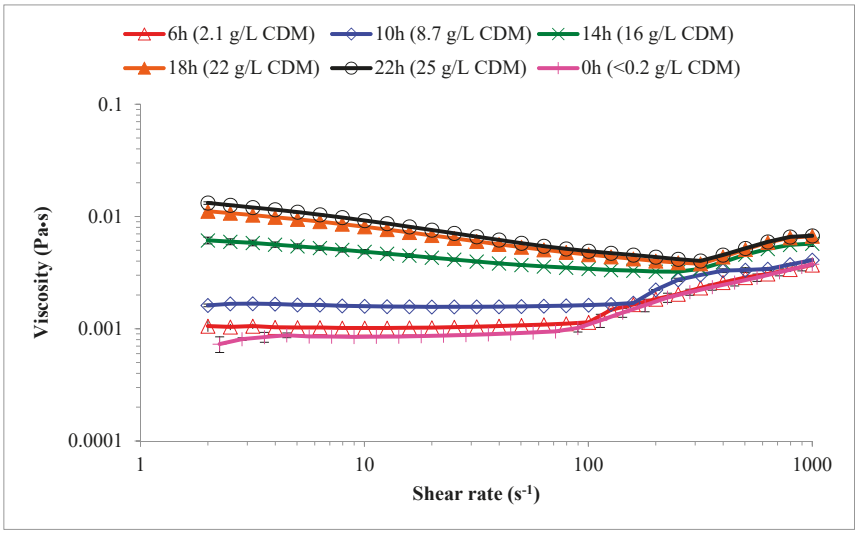

(**a**)

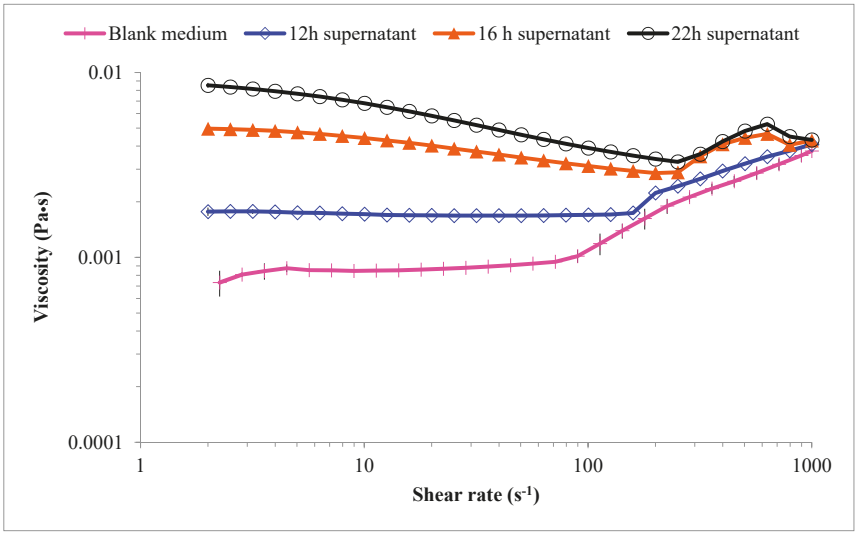

(**b**)

Figure 2. Flow sweep curves for samples of *P. putida* LS46 cultures obtained from the pilot-scale reactor. (**a**) Viscosity as a function of shear rate for 0–25 g·L^{-1} cell suspensions at various points in time and (**b**) viscosity as a function of shear rate for supernatant samples at various points in time. Error bars represent standard deviations of triplicate measurements for each sample.

This type of behavior has been described in previous studies of a variety of fermentation processes [34,35,53]. Similar rates were used in this study, but a unique attribute of this work is the viscosity of samples began to increase at a certain shear rate, which was consistent across the different measurements for the individual samples and increased with increasing sample viscosity (and hence cultivation time). This indicates a material property-related root cause rather than a measurement artefact.

In the initial (0 h) sample, this shear-thickening behavior was observed at shear rate of 76.5 s^{-1}, and increased with increasing sample viscosity up to nearly 300 s^{-1} in the final sample (25.3 $g{\cdot}L^{-1}$ CDM). This is an interesting observation because similar shear rates can easily be encountered in a bioreactor. This could suggest that increasing the shearing rate (bioreactor agitation rate) beyond this shear-thickening onset may actually cause a viscosity increase and reduce the oxygen transfer rate since viscosity is generally inversely proportional [41].

The relationship between shear-stress and shear rate was best described using the Power law ($R^2 > 0.99$ for all samples). A summary of model parameters for fitting the data from each sample with the power law is shown in Table 1, and in Figure 3 as a function of the corresponding total biomass of the sample. As shown, a strong linear relationship between the viscosity constant and the total biomass could be derived ($R^2 = 0.96$), and the slope was significantly different than zero ($p = 0.028$). However, the rate index did not seem to correlate with biomass in the culture ($R^2 = 0.63$), and the slope was not significantly different than zero ($p = 0.27$).

Table 1. Summary of model parameters ($n = 3$) for fitting the obtained data from each sample with the power law.

Sample	Power Law Constant: Viscosity (mPa·s)	Power Law Constant: Rate Index	Power Law: Regression
	Mean ± St. Dev.	Mean ± St. Dev.	Mean ± St. Dev.
0 h (<0.2 $g{\cdot}L^{-1}$)	0.16 ± 0.02	1.46 ± 0.02	1.00 ± 0.00
6 h (2.1 $g{\cdot}L^{-1}$)	0.22 ± 0.01	1.41 ± 0.01	1.00 ± 0.00
10 h (8.7 $g{\cdot}L^{-1}$)	0.45 ± 0.06	1.32 ± 0.02	1.00 ± 0.00
14 h (16.1 $g{\cdot}L^{-1}$)	0.55 ± 0.15	1.35 ± 0.04	1.00 ± 0.00
18 h (22 $g{\cdot}L^{-1}$)	0.62 ± 0.18	1.35 ± 0.05	1.00 ± 0.00
22 h (25.3 $g{\cdot}L^{-1}$)	0.80 ± 0.17	1.31 ± 0.03	0.99 ± 0.00
12 h supernatant	0.32 ± 0.02	1.37 ± 0.01	1.00 ± 0.00
16 h supernatant	1.91 ± 0.03	1.12 ± 0.00	0.99 ± 0.02
22 h supernatant	3.15 ± 0.13	1.05 ± 0.01	0.99 ± 0.00

The increase in viscosity of the culture as s function of $[X_t]$ is shown in Figure 3a. The viscosity at a shear rate of 10 s^{-1} was determined and compared from the flow sweep results to quantify the viscosity of the samples. Using a Tukey's range test, statistically significant (95%) differences in the rotational viscosities and shear-thickening onset across the different samples could be identified. These values are shown in Table 2, where it can be seen that over time, the apparent viscosity of the cell suspension (at a shear rate of 10 s^{-1}) increased from approximately 1.0 mPa·s to 9.2 mPa·s by 22 h. Interestingly, when the cells were removed by centrifugation, it was found that the viscosity of the 22 h supernatant was 6.8 mPa·s, which is nearly 75% of the value observed for the entire culture at 22 h (i.e., with $[X_t] = 25.3\ g{\cdot}L^{-1}$) suspended in that same matrix). From observations during the course of this work, when cells from 25.3 $g{\cdot}L^{-1}$ culture of *P. putida* LS46 (22 h) were re-suspended in fresh medium, the viscosity dropped to 1.7 mPa·s at shear rates of 10 s^{-1}, which was only slightly higher than the 0 h sample (1.01 mPa·s).

Table 2. Summary of average viscosity at a shearing rate of 10 rad·s^{-1} and onset of shear-thickening (n = 3).

Sample	Viscosity @ 10 s^{-1}, mPa·s	Shear Thickening Onset, s^{-1}
	Mean ± St.Dev	Mean ± St.Dev
0 h (<0.2 g·L^{-1})	1.01 ± 0.06	76.5 ± 13.0
6 h (2.1 g·L^{-1})	1.01 ± 0.02	94.8 ± 0.6
10 h (8.7 g·L^{-1})	1.59 ± 0.01	151.1 ± 0.6
14 h (16.1 g·L^{-1})	4.86 ± 0.21	258.9 ± 18.1
18 h (22 g·L^{-1})	8.10 ± 0.15	294.9 ± 9.1
22 h (25.3 g·L^{-1})	9.22 ± 0.11	293.3 ± 12.5
12 h supernatant	1.71 ± 0.01	156.3 ± 2.2
16 h supernatant	4.42 ± 0.07	218.9 ± 2.6
22 h supernatant	6.81 ± 0.09	256.6 ± 8.3

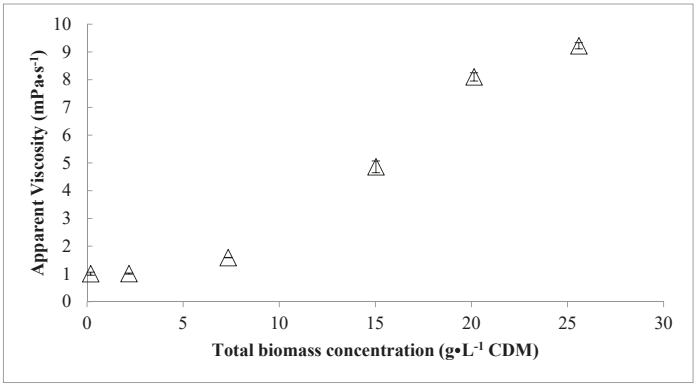

(**a**)

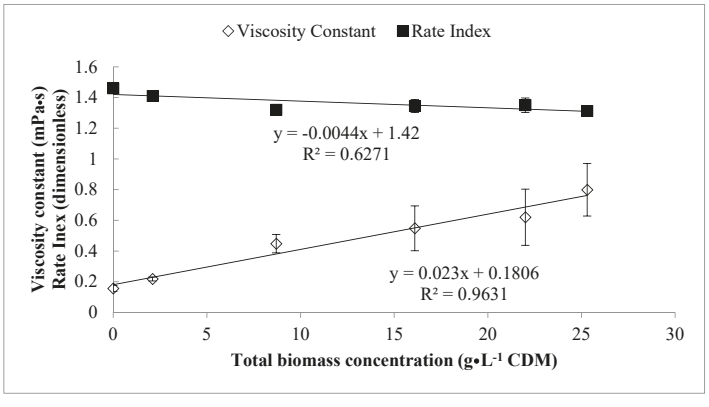

(**b**)

Figure 3. (**a**) Changes in apparent viscosity of the *P. putida* LS46 culture with increasing total biomass concentration over time and (**b**) changes in power-law constants describing culture rheology as a function of the total biomass in the (pilot-scale) fed batch cultivation at varying points over time. Error bars represent the standard deviations between technical replicate measurements (n = 3).

Typically, electrolyte solutions like microbial growth medium are slightly shear thinning [54]. In colloidal dispersions, shear-thinning is thought to be due to a more organized flow pattern of the molecules when subject to shear forces. This creates less stochastic (random) interactions, and results in reduced viscosity and decreased energy dissipation [55,56]. At higher shear rates, however, hydrodynamic forces can dominate over stochastic interactions, and the particle collisions are primarily due to shear forces rather than random thermal motions. This causes organization of the molecules into a more anisotropic state of so-called 'hydroclusters', and increases the difficulty by which molecules can flow around one another [55]. Although other theories exist (including order-disorder transition and dilatancy), this is perhaps the most commonly accepted mechanism for shear-thickening [56]. At the molecular level, the mechanism remains the subject of some debate, all theories essentially pertain to increased difficulty with particle-particle interactions in a flow path, and thus the volume fraction of particles is of importance [56,57]. The presence of high M_w polymers (particularly when suspended in a poor solvent), could further support the shear-thickening observations in this work [58]. In such situations, higher shear rates tend to cause high M_w macromolecules to extend in the flow path, breaking their intra-molecular associations and forming inter-molecular associations. This results in a gel network formation, which increases viscosity [59]. This is also a positive feedback mechanism in which the molecules of higher M_w extend first, and formation of gel networks causes the viscosity to increase. This, in turn, increases the shear stress, which then affects the molecules of lower M_w [59]. The intermolecular associations may include crosslinking, which is a known phenomenon with mcl-PHA [60–63].

3.3. Quantifying Components of the Extracellular Matrix

These data indicate that significant rheological changes to the culture medium occur over time, and much of this effect is not simply explained by the presence of cells. According to Newton et al. [53], in HCD *E. coli* cultures this behavior is the result of structural interactions between cells and cellular debris (high M_w nucleic acids, which can also from crosslinks) resulting from lysed cells. This could further contribute to a shear thickening effect. The following section describes the soluble organic material detected in the culture supernatant.

P. putida and other *Pseudomonas* spp. are known to produce significant quantities of extracellular polymeric substances (EPS) as precursors to biofilm formation. This is a particularly well-known phenomena with *P. aeruginosa.* Kachlany et al. [64] suggested that young *P. putida* G7 cells are encapsulated by an exopolysaccharide layer that is sloughed off as cells age. It is likely that high shear forces expedite the sloughing of this capsular material. That study also described the collapsed extracellular polymer from *P. putida* G7 as being a 'rope-like' material, which could certainly fit the proposed gel-formation theory for shear thickening behavior in polymer solutions.

Generally, the extracellular polymers associated with *Pseudomonas* spp. are composed predominantly of sugars, typically glucose, galactose, rhamnose and mannose [30,32,64–66]. Other extracellular secretions associated with *Pseudomonas* spp. include alginate [67], DNA [68–70], gellan [71], proteins [72], glycolipids and lipopolysaccharides [64,73,74], organic acids, [30,75], as well as acetylated sugars and uronic acids [65,66].

In this work, several of these putative EPS constituents and/or cell lysis products were monitored and quantified in the supernatants of cultivations performed at bench-scale to better understand the observed rheological behavior. These include proteins, reducing sugars, DNA, and extracellular PHA, as well as bulk measurement of carbonaceous products in the supernatant by volatile solids. These are shown over time in Figure 4.

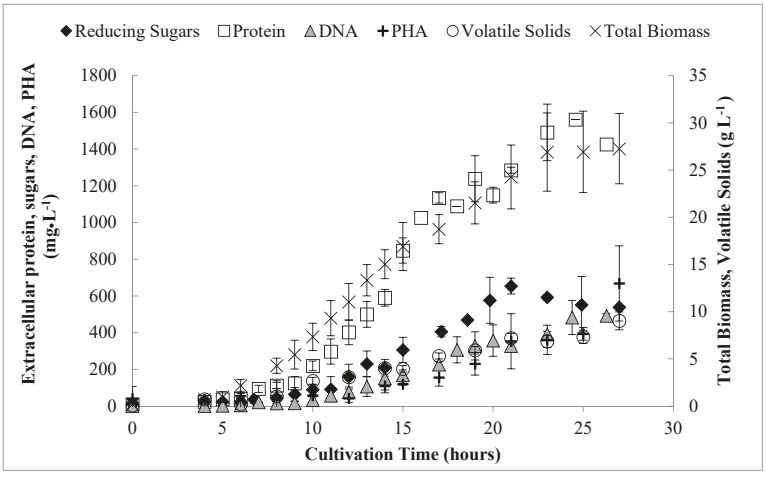

(**a**)

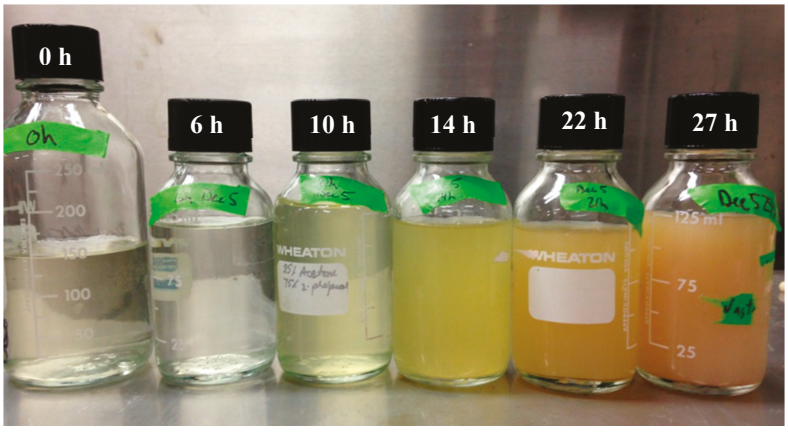

(**b**)

Figure 4. (**a**) Soluble (extracellular) organic material detected in the supernatant over the time course of the bench-scale cultivations, which is thought to contribute to the observed rheological behavior of the medium and (**b**) appearance of culture after centrifugation for fed-batch experiments at the cultivation time indicated. Error bars represent standard deviations between the mean values obtained from each of the biological replicate experiments.

In general, the concentrations of these components increased proportionally to $[X_t]$ with the exception of reducing sugars, which reached a maximum concentration of 0.65 g·L^{-1} at 21 h and then declined. The maximum concentrations (at 27 h) of proteins, PHA, and DNA in the medium were 1.56 g·L^{-1}, 0.67 g·L^{-1}, and 0.49 g·L^{-1}, respectively. Collectively, the components could account for at most 48% of the total VS detected in the supernatant, which reached a maximum of 9 g·L^{-1} by 27 h. Newton et al. [35] demonstrated that both protein (0–50 g·L^{-1}) and DNA (0–4 g·L^{-1}) contributed linearly to increased viscosity and the flow curves for solutions of protein and DNA exhibited shear thinning and Newtonian behavior, respectively. However, in that work a somewhat lesser increase in viscosity was noted (1.1 to 5.3 mPa·s) for a 48 g·L^{-1} *E. coli* culture, despite the presence of far more extracellular DNA (typically 3 g·L^{-1}) and protein (up to 40 g·L^{-1}).

In this work, we did not attempt to differentiate whether these components of the supernatant were due to the production of EPS or are simply cell lysis products from cultivation in a high-shear environment. We found evidence to make an argument in favor of either scenario, which likely implies the rheological behavior is due to a combination of physical and biochemical factors. Mg^{2+} is an intracellular metabolite that can leak from damaged cell membranes, which would precede cell lysis [76]. In this work, the Mg^{2+} concentration monitored in the supernatant began to increase after 14 h, which corresponds to the onset of O_2 limitation and maximum agitation rates. However, when the ratios of protein-to-DNA of the culture supernatant was compared to that of *P. putida* cell lysate, it was found that the cell lysate contained only about half the DNA fraction that was observed in the supernatant. This could suggest DNA release as a possible EPS component, and would be supported by previous studies using *Pseudomonas* spp. [68,72]. Furthermore, a similar experiment using lower shear rates using a maximum of 600 rpm mixing (compared to 1200 rpm) in the bench-scale bioreactor, but with pure O_2 to increase driving force for oxygen transfer. Although this method produced lower [X_t], statistically indifferent ($p < 0.05$) yields of extracellular organic content (protein, sugars, DNA per unit [X_t]) were observed in comparison with the normal mixing condition of 1200 rpm. While this does not disprove the occurrence of significant cell lysis, it does show that this behavior is difficult to avoid, even at comparatively low bioreactor mixing rates.

3.4. Engineering Significance: Effects on Oxygen Transfer Rate

Knowledge of viscosity in bioprocesses is important for process scale up. Many empirical relationships (or dimensionless parameters like the Reynold's number, *Re*) describing the K_La, are inversely proportional to viscosity [50]. The K_La measured using the 200 mL bioreactor system with different supernatant samples obtained from the bench-scale bioreactor over time were assessed. The reduction in K_La over time is shown in Figure 5 as a function of the increasing amount of soluble organic material in the culture supernatant. As shown, K_La is expressed as a percent of the value measured at 0 h. The final values (obtained at 27 h) showed a significant ($p < 0.05$) reduction of 45–52% from the values measured at 0 h or 6 h. It was intended to perform a similar test using the entire culture, but that was not possible due to the high oxygen demand of the culture preventing observable changes in DO as well as excessive foaming when air was bubbled through the cell suspensions in the miniature reactor.

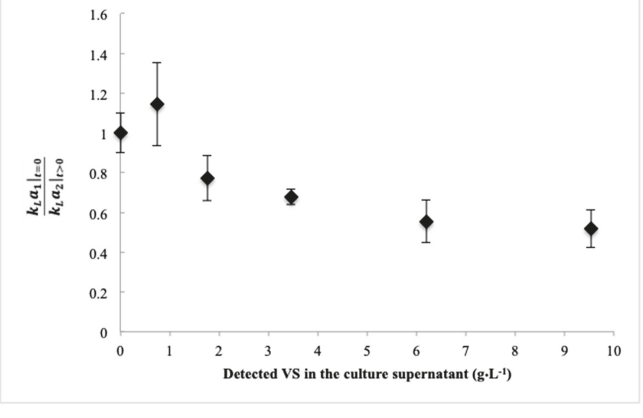

Figure 5. Shows the reduction in K_La over time (expressed as a fraction of the value measured at time zero) that might be anticipated from the increasing VS detected in the supernatant. The K_La values were measured in the described 200 mL reactor. Error bars represent standard deviation of the mean values determined for each biological replicate experiments.

According to Martin et al. [41], the reduction in oxygen transfer rates with increased fluid viscosity is due to: (1) reduced contact area between bubbles and a fluid because bubbles are more stable in viscous fluids; and (2) decreased liquid diffusivity due to reduced velocity profile in the liquid layer surrounding the bubble. Interestingly, the extracellular biosurfactants (glycolipids, lipopolysaccharides) known to be secreted by several *Pseudomonas* spp. can form a layer at the liquid–gas interface and decrease oxygen mass transfer [36].

Considering that other fed-batch strategies have achieved 100 g·L^{-1} CDM or more in PHA production [11,13,77,78], the reduction in K_La over time could be considerably more significant in those systems compared to that described in this work. This may often be neglected in bench-scale HCD PHA cultivations in which stirring and aeration are typically set as high as is realistically possible to maximize productivity. However, with increasing scale the required power consumption for mixing and aeration becomes significant [79], and so the bioreactor operation parameters must be carefully managed in order to save aeration costs. This aspect is emphasized in PHA production/waste treatment operations using enriched mixed cultures [80].

A characteristic of shear-thickening fluids is effective energy dissipation [56]. While this may be useful or interesting property for certain applications, for bioprocessing it is generally problematic, and would likely result in poor performance for the energy input to the bioreactor. The Reynold's number (*Re*) is often used as an dimensionless constant used to estimate power consumption required to mix the reactor contents, which can be a significant cost for aerobic processes like PHA production [79]. Using the obtained constants shown in Table 2, we estimated that for a given (un-gassed) power input to the stirrer, *Re* decreased by 44–55% as the cell density of the culture increased from approximately 0 to 25 g·L^{-1} following the approach of Gabelle et al. [17].

Shear thickening behaviour, although interesting, is problematic for the cultivation process as well as downstream operations, including pumping, centrifugation, filtration, or spray-drying [55,56]. In our production process using *P. putida* LS46, it certainly appears to be a difficult situation to avoid. Moving forward, efforts to alleviate such conditions might include: 1) investigation of lower-shear bioreactors such as air-lift configurations [81]; 2) modifying the medium with surface active molecules or flocculants to reduce or reverse shear-thickening [82]; 3) addition of extracellular enzymes to break up large macromolecules that may form gel networks and contribute to increased viscosity and shear-thickening; or 4) or engineering the bacterium to, or selection of strains that, avoid production of EPS. The latter could also help close the carbon balance and improve the overall PHA yield.

4. Conclusions

In moderately HCD fed-batch cultivations of *P. putida* LS46, significant changes in the rheological properties of the culture were observed. At lower shear rates the culture exhibited slight shear-thinning behavior, while the onset of shear-thickening was observed at shear rates that increased with sample viscosity (or increased [X_t]). A nearly nine-fold increase in viscosity (at 10 s^{-1}) was measured throughout the course of the cultivation process, approximately 75% of which was attributed to the supernatant rather than the presence of cells. Investigation of the culture supernatants revealed up to 9 g·L^{-1} VS being present in the supernatant, of which half was accounted for as extracellular proteins, sugars, DNA, and PHA. It was shown that this material could reduce the mass transfer coefficient associated with a given bioreactor system by up to 50% over the course of the cultivation process. Although difficulties in maintaining oxygen transfer are well known in HCD aerobic bioprocesses, this work has demonstrated that biochemically-induced changes in the medium composition played a significant role, rather than just the high oxygen demand associated with a HCD culture of strictly aerobic organisms.

Author Contributions: Individual contributions of authors are as follows: Design and conceptualization: W.B.; Methodology development: W.B. and C.C.; Acquisition of data: W.B. and M.G.; Formal analysis: W.B. and M.G.; Writing: W.B.; Review and editing: D.B.L., C.C., R.S., D.J.G., and N.C.; Supervision: C.C., R.S., D.J.G., D.B.L., and N.C.; Final approval: N.C.; Funding Acquisition: D.B.L. (GAPP and NSERC Discovery grants) and W.B. (NSERC CGS-D, NSERC-MSFSS, Sir Gordon Wu Scholarship, and Edward R. Toporeck fellowship).

Funding: Funding for this work was provided by: 1) Genome Canada, through the Genome Applications and Partnership Program (GAPP) grant titled "Fibre composite and biomatrix genomics (FiCoGen); 2) the Natural Sciences and Engineering Research Council (NSERC) of Canada through a Discovery grant (RGPIN-5961-2016), a Doctoral Alexander Graham Bell Canada Graduate Scholarship (CGS-D), and the Michael Smith Foreign Study Supplement (NSERC-MSFSS); and 3) the University of Manitoba through the Graduate Fellowship and Sir Gordon Wu Scholarship, and the University of Manitoba Faculty of Engineering through the Edward R. Toporeck Graduate Fellowship.

Acknowledgments: Special thanks my colleagues and friends on the Biotransformation and Clean Technologies teams at Scion—including Tracey Bowers, Mark West, Kim McGrouther, Wajid Waheed Bhat, and Martin Cooke-Willis—for their support in ensuring a safe and positive experience in learning and operating the pilot-scale SIP bioreactors. At the University of Manitoba, thanks to Tanner Devlin in the Civil Engineering Department for his help constructing the bioreactor for K_La determinations. Thanks also to Scott Wushke (Department of Microbiology) for being interested in this project and providing helpful insights and constructive feedback.

Conflicts of Interest: The authors declare no conflict of interest. The funding sponsors had no role in the design of the study; in the collection, analyses, or interpretation of data; in the writing of the manuscript, and in the decision to publish the results.

References

1. Gasperi, J.; Wright, S.L.; Dris, R.; Collard, F.; Mandin, C.; Guerrouache, M.; Langlois, V.; Kelly, F.J.; Tassin, B. Microplastics in air: Are we breathing it in? *Curr. Opin. Environ. Sci. Health* **2018**, *1*, 1–5. [CrossRef]
2. Hale, R.C. Are the Risks from Microplastics Truly Trivial? *Environ. Sci. Technol.* **2018**, *52*, 931. [CrossRef]
3. Harding, K.; Dennis, J.; Vonblottnitz, H.; Harrison, S. Environmental analysis of plastic production processes: Comparing petroleum-based polypropylene and polyethylene with biologically-based poly-β-hydroxybutyric acid using life cycle analysis. *J. Biotechnol.* **2007**, *130*, 57–66. [CrossRef]
4. Masood, F.; Yasin, T.; Hameed, A. Polyhydroxyalkanoates—What are the uses? Current challenges and perspectives. *Crit. Rev. Biotechnol.* **2015**, *35*, 514–521. [CrossRef]
5. Koller, M. Biodegradable and Biocompatible Polyhydroxyalkanoates (PHA): Auspicious Microbial Macromolecules for Pharmaceutical and Therapeutic Applications. *Molecules* **2018**, *23*, 362. [CrossRef]
6. Kourmentza, C.; Plácido, J.; Venetsaneas, N.; Burniol-Figols, A.; Varrone, C.; Gavala, H.N.; Reis, M.A.M. Recent advances and challenges towards sustainable polyhydroxyalkanoate (PHA) production. *Bioengineering* **2017**, *4*, 55. [CrossRef]
7. Możejko-Ciesielska, J.; Kiewisz, R. Bacterial polyhydroxyalkanoates: Still fabulous? *Microbiol. Res.* **2016**, *192*, 271–282. [CrossRef]
8. Kaur, G.; Roy, I. Strategies for large-scale production of polyhydroxyalkanoates. *Chem. Biochem. Eng. Q.* **2015**, *29*, 157–172. [CrossRef]
9. Koller, M.; Maršálek, L.; de Sousa Dias, M.M.; Braunegg, G. Producing microbial polyhydroxyalkanoate (PHA) biopolyesters in a sustainable manner. *New Biotechnol.* **2017**, *37*, 24–38. [CrossRef]
10. Ienczak, J.L.; Schmidell, W.; de Aragão, G.M.F. High-cell-density culture strategies for polyhydroxyalkanoate production: A review. *J. Ind. Microbiol. Biotechnol.* **2013**, *40*, 275–286. [CrossRef]
11. Ryu, H.W.; Hahn, S.K.; Chang, Y.K.; Chang, H.N. Production of poly(3-hydroxybutyrate) by high cell density fed-batch culture of *Alcaligenes eutrophus* with phospate limitation. *Biotechnol. Bioeng.* **1997**, *55*, 28–32. [CrossRef]
12. Shang, L.; Jiang, M.; Chang, H.N. Poly(3-hydroxybutyrate) synthesis in fed-batch culture of *Ralstonia eutropha* with phosphate limitation under different glucose concentrations. *Biotechnol. Lett.* **2003**, *25*, 1415–1419. [CrossRef]
13. Wang, F.; Lee, S.Y. Poly(3-hydroxybutyrate) production with high productivity and high polymer content by a fed-batch culture of *Alcaligenes latus* under nitrogen limitation. *Appl. Environ. Microbiol.* **1997**, *63*, 3703–3706.
14. Koller, M. A Review on Established and Emerging Fermentation Schemes for Microbial Production of Polyhydroxyalkanoate (PHA) Biopolyesters. *Fermentation* **2018**, *4*, 30. [CrossRef]

15. Blunt, W.; Levin, D.; Cicek, N. Bioreactor Operating Strategies for Improved Polyhydroxyalkanoate (PHA) Productivity. *Polymers* **2018**, *10*, 1197. [CrossRef]
16. Riesenberg, D.; Guthke, R. High-cell-density cultivation of microorganisms. *Appl. Microbiol. Biotechnol.* **1999**, *51*, 422–430. [CrossRef]
17. Gabelle, J.C.; Augier, F.; Carvalho, A.; Rousset, R.; Morchain, J. Effect of tank size on kLa and mixing time in aerated stirred reactors with non-newtonian fluids. *Can. J. Chem. Eng.* **2011**, *89*, 1139–1153. [CrossRef]
18. Rottava, I.; Batesini, G.; Silva, M.F.; Lerin, L.; de Oliveira, D.; Padilha, F.F.; Toniazzo, G.; Mossi, A.; Cansian, R.L.; Di Luccio, M.; et al. Xanthan gum production and rheological behavior using different strains of Xanthomonas sp. *Carbohydr. Polym.* **2009**, *77*, 65–71. [CrossRef]
19. Badino, A.C.; Facciotti, M.C.R.; Schmidell, W. Volumetric oxygen transfer coefficients (kLa) in batch cultivations involving non-Newtonian broths. *Biochem. Eng. J.* **2001**, *8*, 111–119. [CrossRef]
20. Sinha, J.; Tae Bae, J.; Pil Park, J.; Hyun Song, C.; Won Yun, J. Effect of substrate concentration on broth rheology and fungal morphology during exo-biopolymer production by *Paecilomyces japonica* in a batch bioreactor. *Enzym. Microb. Technol.* **2001**, *29*, 392–399. [CrossRef]
21. Pedersen, A.G.; Bundgaard-Nielsen, M.; Nielsen, J.; Villadsen, J.; Hassager, O. Rheological characterization of media containing *Penicillium chrysogenum*. *Biotechnol. Bioeng.* **1993**, *41*, 162–164. [CrossRef]
22. Riley, G.L.; Tucker, K.G.; Paul, G.C.; Thomas, C.R. Effect of biomass concentration and mycelial morphology on fermentation broth rheology. *Biotechnol. Bioeng.* **2000**, *68*, 160–172. [CrossRef]
23. Dhillon, G.S.; Brar, S.K.; Kaur, S.; Verma, M. Rheological studies during submerged citric acid fermentation by *Aspergillus niger* in stirred fermentor using apple pomace ultrafiltration sludge. *Food Bioprocess Technol.* **2013**, *6*, 1240–1250. [CrossRef]
24. Rodríguez Porcel, E.M.; Casas López, J.L.; Sánchez Pérez, J.A.; Fernández Sevilla, J.M.; García Sánchez, J.L.; Chisti, Y. *Aspergillus terreus* Broth Rheology, Oxygen Transfer, and Lovastatin Production in a Gas-Agitated Slurry Reactor. *Ind. Eng. Chem. Res.* **2006**, *45*, 4837–4843. [CrossRef]
25. Richard, A.; Margaritis, A. Rheology, oxygen transfer, and molecular weight characteristics of poly(glutamic acid) fermentation by *Bacillus subtilis*. *Biotechnol. Bioeng.* **2003**, *82*, 299–305. [CrossRef]
26. Baroutian, S.; Eshtiaghi, N.; Gapes, D.J. Rheology of a primary and secondary sewage sludge mixture: Dependency on temperature and solid concentration. *Bioresour. Technol.* **2013**, *140*, 227–233. [CrossRef]
27. Brar, S.K.; Verma, M.; Tyagi, R.D.; Valéro, J.R.; Surampalli, R.Y. *Bacillus thuringiensis* fermentation of hydrolyzed sludge – Rheology and formulation studies. *Chemosphere* **2007**, *67*, 674–683. [CrossRef]
28. Verma, M.; Brar, S.K.; Tyagi, R.D.; Sahai, V.; Prévost, D.; Valéro, J.R.; Surampalli, R.Y. Bench-scale fermentation of Trichoderma viride on wastewater sludge: Rheology, lytic enzymes and biocontrol activity. *Enzym. Microb. Technol.* **2007**, *41*, 764–771. [CrossRef]
29. Sun, F.; Huang, Q.; Wu, J. Rheological behaviors of an exopolysaccharide from fermentation medium of a *Cordyceps sinensis* fungus (Cs-HK1). *Carbohydr. Polym.* **2014**, *114*, 506–513. [CrossRef]
30. Freitas, F.; Alves, V.D.; Pais, J.; Costa, N.; Oliveira, C.; Mafra, L.; Hilliou, L.; Oliveira, R.; Reis, M.A.M. Characterization of an extracellular polysaccharide produced by a *Pseudomonas* strain grown on glycerol. *Bioresour. Technol.* **2009**, *100*, 859–865. [CrossRef]
31. Freitas, F.; Alves, V.D.; Carvalheira, M.; Costa, N.; Oliveira, R.; Reis, M.A.M. Emulsifying behaviour and rheological properties of the extracellular polysaccharide produced by Pseudomonas oleovorans grown on glycerol byproduct. *Carbohydr. Polym.* **2009**, *78*, 549–556. [CrossRef]
32. Maalej, H.; Hmidet, N.; Boisset, C.; Bayma, E.; Heyraud, A.; Nasri, M. Rheological and emulsifying properties of a gel-like exopolysaccharide produced by *Pseudomonas stutzeri* AS22. *Food Hydrocoll.* **2016**, *52*, 634–647. [CrossRef]
33. Maalej, H.; Moalla, D.; Boisset, C.; Bardaa, S.; Ayed, H.B.; Sahnoun, Z.; Rebai, T.; Nasri, M.; Hmidet, N. Rhelogical, dermal wound healing and in vitro antioxidant properties of exopolysaccharide hydrogel from Pseudomonas stutzeri AS22. *Colloids Surf. B Biointerfaces* **2014**, *123*, 814–824. [CrossRef]
34. Goudar, C.T.; Strevett, K.A.; Shah, S.N. Influence of microbial concentration on the rheology of non-Newtonian fermentation broths. *Appl. Microbiol. Biotechnol.* **1999**, *51*, 310–315. [CrossRef]
35. Newton, J.M.; Vlahopoulou, J.; Zhou, Y. Investigating and modelling the effects of cell lysis on the rheological properties of fermentation broths. *Biochem. Eng. J.* **2017**, *121*, 38–48. [CrossRef]

36. Papapostolou, A.; Karasavvas, E.; Chatzidoukas, C. Oxygen mass transfer limitations set the performance boundaries of microbial PHA production processes—A model-based problem investigation supporting scale-up studies. *Biochem. Eng. J.* **2019**, *148*, 224–238. [CrossRef]
37. Arjunwadkar, S.J.; Sarvanan, K.; Kulkarni, P.R.; Pandit, A.B. Gas-liquid mass transfer in dual impeller bioreactor. *Biochem. Eng. J.* **1998**, *1*, 99–106. [CrossRef]
38. Buchholz, H.; Buchholz, R.; Niebeschütz, H.; Schügerl, K. Absorption of oxygen in highly viscous newtonian and non-Newtonian fermentation model media in bubble column bioreactors. *Eur. J. Appl. Microbiol. Biotechnol.* **1978**, *6*, 115–126. [CrossRef]
39. García-Ochoa, F.; Gómez, E. Mass transfer coefficient in stirred tank reactors for xanthan gum solutions. *Biochem. Eng. J.* **1998**, *1*, 1–10. [CrossRef]
40. Herbst, H.; Schumpe, A.; Deckwer, W.D. Xanthan production in stirred tank fermenters: Oxygen transfer and scale-up. *Chem. Eng. Technol.* **1992**, *15*, 425–434. [CrossRef]
41. Martín, M.; Montes, F.J.; Galán, M.A. Mass transfer rates from bubbles in stirred tanks operating with viscous fluids. *Chem. Eng. Sci.* **2010**, *65*, 3814–3824. [CrossRef]
42. Puthli, M.S.; Rathod, V.K.; Pandit, A.B. Gas–liquid mass transfer studies with triple impeller system on a laboratory scale bioreactor. *Biochem. Eng. J.* **2005**, *23*, 25–30. [CrossRef]
43. Jiang, X.; Sun, Z.; Ramsay, J.A.; Ramsay, B.A. Fed-batch production of MCL-PHA with elevated 3-hydroxynonanoate content. *AMB Express* **2013**, *3*, 50. [CrossRef]
44. Sharma, P.K.; Fu, J.; Cicek, N.; Sparling, R.; Levin, D.B. Kinetics of medium-chain-length polyhydroxyalkanoate production by a novel isolate of *Pseudomonas putida* LS46. *Can. J. Microbiol.* **2012**, *58*, 982–989. [CrossRef]
45. Blunt, W.; Dartiailh, C.; Sparling, R.; Gapes, D.; Levin, D.B.; Cicek, N. Microaerophilic environments improve the productivity of medium chain length polyhydroxyalkanoate biosynthesis from fatty acids in *Pseudomonas putida* LS46. *Process Biochem.* **2017**, *59*, 18–25. [CrossRef]
46. Ramsay, B.A.; Lomaliza, K.; Chavarie, C.; Dubé, B.; Ramsay, J.A. Production of poly-(beta-hydroxybutyric-co-beta-hydroxyvaleric) acids. *Appl. Environ. Microbiol.* **1990**, *56*, 2093–2098.
47. Blunt, W.; Dartiailh, C.; Sparling, R.; Gapes, D.; Levin, D.B.; Cicek, N. Carbon flux to growth or polyhydroxyalkanoate synthesis under microaerophilic conditions is affected by fatty acid chain-length in *Pseudomonas putida* LS46. *Appl. Microbiol. Biotechnol.* **2018**, *102*, 6437–6449. [CrossRef]
48. Blunt, W.; Hossain, M.D.E.; Gapes, D.J.; Sparling, R.; Levin, D.B.; Cicek, N. Real-Time Monitoring of Microbial Fermentation End-Products in Biofuel Production with Titrimetric Off-Gas Analysis (TOGA). *Biol. Eng. Trans.* **2014**, *6*, 203–219.
49. Yang, H.; Wei, F.; Hu, K.; Zhou, G.; Lyu, J. Comparison of rheometric devices for measuring the rheological parameters of debris flow slurry. *J. Mt. Sci.* **2015**, *12*, 1125–1134. [CrossRef]
50. Garcia-Ochoa, F.; Gomez, E. Bioreactor scale-up and oxygen transfer rate in microbial processes: An overview. *Biotechnol. Adv.* **2009**, *27*, 153–176. [CrossRef]
51. Bradford, M.M. A rapid and sensitive method for the quantitation of microgram quantities of protein utilizing the principle of protein-dye binding. *Anal. Biochem.* **1976**, *72*, 248–254. [CrossRef]
52. Viles, F.J.; Silverman, L. Determination of Starch and Cellulose with Anthrone. *Anal. Chem.* **1949**, *21*, 950–953. [CrossRef]
53. Newton, J.M.; Schofield, D.; Vlahopoulou, J.; Zhou, Y. Detecting cell lysis using viscosity monitoring in *E. coli* fermentation to prevent product loss. *Biotechnol. Prog.* **2016**, *32*, 1069–1076. [CrossRef]
54. Doran, P.M. *Bioprocess Engineering Principles*, 2nd ed.; Elsevier/Academic Press: Amsterdam, The Netherlands; Boston, MA, USA, 2013; ISBN 978-0-12-220851-5.
55. Wagner, N.J.; Brady, J.F. Shear thickening in colloidal dispersions. *Phys. Today* **2009**, *62*, 27–32. [CrossRef]
56. Brown, E.; Jaeger, H.M. Shear thickening in concentrated suspensions: Phenomenology, mechanisms and relations to jamming. *Rep. Prog. Phys.* **2014**, *77*, 046602. [CrossRef]
57. Fernandez, N.; Mani, R.; Rinaldi, D.; Kadau, D.; Mosquet, M.; Lombois-Burger, H.; Cayer-Barrioz, J.; Herrmann, H.J.; Spencer, N.D.; Isa, L. Microscopic Mechanism for Shear Thickening of Non-Brownian Suspensions. *Phys. Rev. Lett.* **2013**, *111*, 108301. [CrossRef]
58. van Egmond, J.W. Shear-thickening in suspensions, associating polymers, worm-like micelles, and poor polymer solutions. *Curr. Opin. Colloid Interface Sci.* **1998**, *3*, 385–390. [CrossRef]

59. Ballard, M.J.; Buscall, R.; Waite, F.A. The theory of shear-thickening polymer solutions. *Polymer* **1988**, *29*, 1287–1293. [CrossRef]
60. Levine, A.C.; Sparano, A.; Twigg, F.F.; Numata, K.; Nomura, C.T. Influence of Cross-Linking on the Physical Properties and Cytotoxicity of Polyhydroxyalkanoate (PHA) Scaffolds for Tissue Engineering. *ACS Biomater. Sci. Eng.* **2015**, *1*, 567–576. [CrossRef]
61. Bassas, M.; Diaz, J.; Rodriguez, E.; Espuny, M.J.; Prieto, M.J.; Manresa, A. Microscopic examination in vivo and in vitro of natural and cross-linked polyunsaturated mclPHA. *Appl. Microbiol. Biotechnol.* **2008**, *78*, 587–596. [CrossRef]
62. Hazer, B.; Demirel, S.I.; Borcakli, M.; Eroglu, M.S.; Cakmak, M.; Erman, B. Free radical crosslinking of unsaturated bacterial polyesters obtained from soybean oily acids. *Polym. Bull.* **2001**, *46*, 389–394. [CrossRef]
63. Ashby, R.D.; Solaiman, D.K.Y.; Foglia, T.A.; Liu, C.K. Glucose/lipid mixed substrates as a means of controlling the properties of medium chain length poly(hydroxyalkanoates). *Biomacromolecules* **2001**, *2*, 211–216. [CrossRef]
64. Kachlany, S.C.; Levery, S.B.; Kim, J.S.; Reuhs, B.L.; Lion, L.W.; Ghiorse, W.C. Structure and carbohydrate analysis of the exopolysaccharide capsule of *Pseudomonas putida* G7. *Environ. Microbiol.* **2001**, *3*, 774–784. [CrossRef]
65. Celik, G.Y.; Aslim, B.; Beyatli, Y. Characterization and production of the exopolysaccharide (EPS) from *Pseudomonas aeruginosa* G1 and *Pseudomonas putida* G12 strains. *Carbohydr. Polym.* **2008**, *73*, 178–182. [CrossRef]
66. Wrangstadh, M.; Conway, P.L.; Kjelleberg, S. The production and release of an extracellular polysaccharide during starvation of a marine *Pseudomonas* sp. and the effect thereof on adhesion. *Arch. Microbiol.* **1986**, *145*, 220–227. [CrossRef]
67. Chang, W.S.; van de Mortel, M.; Nielsen, L.; Nino de Guzman, G.; Li, X.; Halverson, L.J. Alginate production by *Pseudomonas putida* creates a hydrated microenvironment and contributes to biofilm architecture and stress tolerance under water-limiting conditions. *J. Bacteriol.* **2007**, *189*, 8290–8299. [CrossRef]
68. Allesen-Holm, M.; Barken, K.B.; Yang, L.; Klausen, M.; Webb, J.S.; Kjelleberg, S.; Molin, S.; Givskov, M.; Tolker-Nielsen, T. A characterization of DNA release in *Pseudomonas aeruginosa* cultures and biofilms. *Mol. Microbiol.* **2006**, *59*, 1114–1128. [CrossRef]
69. Yang, L.; Hu, Y.; Liu, Y.; Zhang, J.; Ulstrup, J.; Molin, S. Distinct roles of extracellular polymeric substances in *Pseudomonas aeruginosa* biofilm development: EPS-mediated biofilm development. *Environ. Microbiol.* **2011**, *13*, 1705–1717. [CrossRef]
70. Steinberger, R.E.; Holden, P.A. Macromolecular composition of unsaturated *Pseudomonas aeruginosa* biofilms with time and carbon source. *Biofilms* **2004**, *1*, 37–47. [CrossRef]
71. Banik, R.M.; Kanari, B.; Upadhyay, S.N. Exopolysaccharide of the gellan family: Prospects and potential. *World J. Microbiol. Biotechnol.* **2000**, *16*, 407–414. [CrossRef]
72. Jahn, A.; Griebe, T.; Nielsen, P.H. Composition of *Pseudomonas putida* biofilms: Accumulation of protein in the biofilm matrix. *Biofouling* **1999**, *14*, 49–57. [CrossRef]
73. Wigneswaran, V.; Nielsen, K.F.; Sternberg, C.; Jensen, P.R.; Folkesson, A.; Jelsbak, L. Biofilm as a production platform for heterologous production of rhamnolipids by the non-pathogenic strain *Pseudomonas putida* KT2440. *Microb. Cell Factories* **2016**, *15*, 181. [CrossRef]
74. Gutiérrez-Gómez, U.; Servín-González, L.; Soberón-Chávez, G. Role of β-oxidation and de novo fatty acid synthesis in the production of rhamnolipids and polyhydroxyalkanoates by Pseudomonas aeruginosa. *Appl. Microbiol. Biotechnol.* **2019**, *103*, 3753–3760. [CrossRef]
75. Read, R.R.; Costerton, J.W. Purification and characterization of adhesive exopolysaccharides from *Pseudomonas putida* and *Pseudomonas fluorescens*. *Can. J. Microbiol.* **1987**, *33*, 1080–1090. [CrossRef]
76. Royce, L.A.; Liu, P.; Stebbins, M.J.; Hanson, B.C.; Jarboe, L.R. The damaging effects of short chain fatty acids on *Escherichia coli* membranes. *Appl. Microbiol. Biotechnol.* **2013**, *97*, 8317–8327. [CrossRef]
77. Cerrone, F.; Duane, G.; Casey, E.; Davis, R.; Belton, I.; Kenny, S.T.; Guzik, M.W.; Woods, T.; Babu, R.P.; O'Connor, K. Fed-batch strategies using butyrate for high cell density cultivation of *Pseudomonas putida* and its use as a biocatalyst. *Appl. Microbiol. Biotechnol.* **2014**, *98*, 9217–9228. [CrossRef]
78. Maclean, H.; Sun, Z.; Ramsay, J.A.; Ramsay, A.B. Decaying exponential feeding of nonanoic acid for the production of medium-chain-length poly(3-hydroxyalkanoates) by *Pseudomonas putida* KT2440. *Can. J. Chem.* **2008**, *86*, 564–569. [CrossRef]

79. Koller, M.; Sandholzer, D.; Salerno, A.; Braunegg, G.; Narodoslawsky, M. Biopolymer from industrial residues: Life cycle assessment of poly(hydroxyalkanoates) from whey. *Resour. Conserv. Recycl.* **2013**, *73*, 64–71. [CrossRef]
80. Coats, E.R.; Watson, B.S.; Brinkman, C.K. Polyhydroxyalkanoate synthesis by mixed microbial consortia cultured on fermented dairy manure: Effect of aeration on process rates/yields and the associated microbial ecology. *Water Res.* **2016**, *106*, 26–40. [CrossRef]
81. Da Cruz Pradella, J.G.; Taciro, M.K.; Mateus, A.Y.P. High-cell-density poly (3-hydroxybutyrate) production from sucrose using *Burkholderia sacchari* culture in airlift bioreactor. *Bioresour. Technol.* **2010**, *101*, 8355–8360. [CrossRef]
82. Brown, E.; Forman, N.A.; Orellana, C.S.; Zhang, H.; Maynor, B.W.; Betts, D.E.; DeSimone, J.M.; Jaeger, H.M. Generality of shear thickening in dense suspensions. *Nat. Mater.* **2010**, *9*, 220–224. [CrossRef]

bioengineering

MDPI

Article

Development of High Cell Density Cultivation Strategies for Improved Medium Chain Length Polyhydroxyalkanoate Productivity Using *Pseudomonas putida* LS46

Warren Blunt [1,*], Christopher Dartiailh [1], Richard Sparling [2], Daniel J. Gapes [3], David B. Levin [1] and Nazim Cicek [1]

[1] Department of Biosystems Engineering, University of Manitoba, Winnipeg, MB R3T 5V6, Canada; umdartia@myumanitoba.ca (C.D.); david.levin@umanitoba.ca (D.B.L.); Nazim.Cicek@umanitoba.ca (N.C.)
[2] Department of Microbiology, University of Manitoba, Winnipeg, MB R3T 2N2, Canada; Richard.Sparling@umanitoba.ca
[3] Scion Research, Te Papa Tipu Innovation Park, Sala Street, Private Bag 3020, Rotorua 3046, New Zealand; Daniel.Gapes@scionresearch.com
* Correspondence: warren.blunt@nrc-cnrc.gc.ca; Tel.: +1-(514)-283-3399

Received: 29 August 2019; Accepted: 24 September 2019; Published: 26 September 2019

Abstract: High cell density (HCD) fed-batch cultures are widely perceived as a requisite for high-productivity polyhydroxyalkanoate (PHA) cultivation processes. In this work, a reactive pulse feed strategy (based on real-time CO_2 or dissolved oxygen (DO) measurements as feedback variables) was used to control an oxygen-limited fed-batch process for improved productivity of medium chain length (mcl-) PHAs synthesized by *Pseudomonas putida* LS46. Despite the onset of oxygen limitation half-way through the process (14 h post inoculation), 28.8 ± 3.9 g L^{-1} total biomass (with PHA content up to 61 ± 8% cell dry mass) was reliably achieved within 27 h using octanoic acid as the carbon source in a bench-scale (7 L) bioreactor operated under atmospheric conditions. This resulted in a final volumetric productivity of 0.66 ± 0.14 g L^{-1} h^{-1}. Delivering carbon to the bioreactor as a continuous drip feed process (a proactive feeding strategy compared to pulse feeding) made little difference on the final volumetric productivity of 0.60 ± 0.04 g L^{-1} h^{-1}. However, the drip feed strategy favored production of non-PHA residual biomass during the growth phase, while pulse feeding favored a higher rate of mcl-PHA synthesis and yield during the storage phase. Overall, it was shown that the inherent O_2-limitation brought about by HCD cultures can be used as a simple and effective control strategy for mcl-PHA synthesis from fatty acids. Furthermore, the pulse feed strategy appears to be a relatively easy and reliable method for rapid optimization of fed-batch processes, particularly when using toxic substrates like octanoic acid.

Keywords: polyhydroxyalkanoates; fed-batch; productivity; *Pseudomonas*; bioreactor; microaerophilic

1. Introduction

The detrimental effects from accumulation of plastic waste in natural environments call for change at both the regulatory and behavioral levels [1]. Most (60–95%) ocean plastic has been classified as single-use in origin [2]; consequently, these single-use items are being increasingly banned by governments globally [3]. Alternative materials must be developed to offset the reduction in single-use items, and biodegradable polymers may be part of that solution.

Microbial polyhydroxyalkanoates (PHAs) are a promising class of biopolymers that are both renewable (bio-based) and biodegradable. PHAs are synthesized by a variety of microbial species, typically in environments not suitable for growth, but where excess carbon is present. There are two

main classes of PHAs defined by the carbon chain-length of the monomer subunits: (1) short chain length (scl-) PHAs, which consist of C3 to C5 monomer subunits; and (2) medium chain-length (mcl-) PHAs, which consist of C6 to C18 monomer subunits [4]. Some of these PHA polymers have properties comparable to conventional petrochemical plastics, including polyethylene and polypropylene [5], and may indeed be suitable alternatives.

Despite promise, the cost of production has limited commercial-scale production of PHAs, particularly for the mcl-PHAs [6,7]. There are a number of economic drivers for this, including the relatively recent drop in oil prices arising from increased exploitation of shale oil [8]. Production costs for PHA have been estimated to be as much as fifteen-fold higher than the petrochemical counterparts (polyethylene, polypropylene) they are intended to replace [9]. Development of productive and cost-effective bioreactor cultivation processes is an important aspect of improving the economic viability and lessening the environmental impacts of PHA production [10–12].

The overall volumetric productivity of any bioprocess is a crucial performance metric and is typically around 2 g L^{-1} h^{-1} for commercial production of bulk bio-products [13]. In PHA production, high cell density (HCD) cultures are widely seen as the best cultivation strategy to reduce costs by achieving high bioreactor productivities [14]. Several studies investigating HCD fed-batch cultivation strategies have obtained productivities of around 2 g L^{-1} h^{-1} in mcl-PHA research [15–18]. On the other hand, cell densities in excess of 200 g L^{-1} and productivities of 5.13 g L^{-1} h^{-1} have been reported for scl-PHA production operations [19–21]. While these results are indeed impressive, many of these studies were performed at bench-scale and used an aeration medium with enriched oxygen content, which can add significant costs in a large-scale setting. A recent survey of scale-up operations in PHA production pointed out that productivities reported for scaled-up operations have, for some time, been lagging behind those achieved in the lab [22]. This discrepancy is at least partly attributable to poor mass transfer characteristics within large-scale bioreactors, especially when it comes to maintaining dissolved oxygen (DO) in aerobic bioprocesses [23,24].

In this context, practical constraints prevent the solution from being as simple as dissipating more energy for mixing, aeration, and purifying oxygen for large-scale bioreactors. A life cycle analysis of scl-PHA synthesized from whey indicated that mechanical energy required for mixing during the fermentation process was one of the main factors contributing to the high environmental impact (and cost) of PHA production—even without mention of aeration supplementation with purified oxygen [25]. This highlights the need to develop processes at lab-scale that are representative of the environment that might be encountered in pilot- or industrial-scale bioreactors.

Previously, we have shown that in the production of mcl-PHAs from medium and long chain fatty acids, imposing O_2 limitation on the culture results in a significant redirection of carbon flux toward PHA synthesis [26,27]. However, the aforementioned studies used batch or simple fed-batch strategies as proof-of-concept, and overall productivities were relatively low. Improving the cell density of the cultivation using an appropriate feeding strategy under oxygen limited conditions could further improve overall productivity. Eventual scaled-up mcl-PHA cultivation processes may also benefit from an understanding of oxygen-limited metabolism brought on by a HCD environment as well as reduced energy consumption (for less rigorous mixing and aeration) resulting from oxygen-limited product synthesis.

In addition to maintaining an adequate supply of oxygen, there are several challenges that arise from HCD cultures. Monitoring and control of these processes is difficult because of the lack of real-time measurements of key process variables, such as substrate uptake [28,29]. This is particularly problematic when the substrate exhibits toxicity, and accumulation of substrate can have deleterious consequences [30]. Previously it was found that a fine threshold exists between carbon-limited growth and substrate-induced inhibition when feeding octanoic acid at a predetermined exponential rate (i.e., a proactive feeding approach) [26]. In those experiments, it was observed that carbon limitation was indicated by a rapid and sharp decrease in the off-gas CO_2 concentration, and subsequent rise in the DO signal, when feeding was briefly paused. Thus, a possible solution to the toxicity issue may be to

use a reactive feeding approach; that is, to feed sub-inhibitory amounts of carbon when needed, as indicated by real-time signals, rather than feeding at a predetermined rate.

Similar strategies have been used in the past. These have employed process indicators such as pH, dissolved oxygen (DO), and CO_2 production [17,29,31,32]. As pointed out by Riesenberg and Guthke [28], these strategies depend on carbon-limited growth, and thus may limit growth and product formation rates. While multiple studies have used predetermined feeding rates rather successfully [18,33,34], a reactive approach may be preferable during initial process optimization.

The objectives of this work, therefore, were: 1) to apply O_2-limited mcl-PHA synthesis from fatty acids to HCD cultures of *Pseudomonas putida* LS46; and 2) to evaluate the carbon flux for different feeding strategies used to obtain HCD cultures. This was done with the motivation of the development and evaluation of simple, effective, and readily scalable feeding strategies for improving mcl-PHA productivity, in addition to understanding the limits of oxygen limitation on mcl-PHA cultivations in a HCD environment.

2. Materials and Methods

2.1. Micro-Organism, Medium, and Substrates

The strain used in this study was *Pseudomonas putida* LS46 [35]. Strain culturing and maintenance procedures were as specified previously [27]. Ramsay's minimal medium [36] was used in all studies. However, the initial concentrations of $(NH_4)_2SO_4$, $MgSO_4$, $CaCl_2{\cdot}2H_2O$, and trace element solution were increased to 2 g L^{-1}, 0.2 g L^{-1}, 20 mg L^{-1}, and 2 mL L^{-1}, respectively. The $MgSO_4$, $CaCl_2{\cdot}2H_2O$, ferric ammonium citrate, and trace element solution were filter-sterilized through a 0.2 µm filter after autoclaving. Octanoic acid was used as the substrate with an initial concentration of 20 mM and was added through a sterile 0.2 µm filter after autoclaving.

2.2. Reactor Setup and Operation

A 7 L autoclavable glass reactor was used (Applikon, Foster City, CA, USA) with an initial working volume of 3 L. The reactor setup, sensor calibration, and sterilization procedures were identical to those previously described [27]. Experiments were initiated with the addition of a 5% (vol vol^{-1}) inoculum from an overnight culture of Ramsay's medium with 20 mM octanoic acid (9.5 mL into 3 L) as the carbon source. The medium pH was maintained at 6.5, which was controlled through the addition of 4 M NaOH via automated peristaltic pumps. The intended DO set point was 40% (of air saturation at 30 °C, implied hereafter), and this was controlled through constant aeration at 6 LPM (atmospheric air only) with a mixing cascade operating from 350–1200 rpm using a single six-blade Rushton turbine measuring six centimeters in diameter. After the mixing cascade could no longer maintain DO, the cultivation was continued for oxygen limitation-induced PHA accumulation with the DO probe reading 0% to 3% air saturation.

Feeding of octanoic acid and a 200 g L^{-1} solution of $(NH_4)_2SO_4$ was accomplished through two 10 mL precision injector syringes (Hamilton Company, Reno, NV, USA) coupled to three-way solenoid valves (Omnifit, Biochem Fluidics, Boonton, NJ, USA). The syringes were driven by pulse motors (SmartMotor™, Moog Animatics, Mountain View, CA, USA) and automated by LabBoss software (Scion, Rotorua, New Zealand).

2.3. Feeding Strategies

The above-described apparatus was used to feed pulses of octanoic acid in small amounts (2.5 to 9.5 mL at a time, total concentrations of approximately 5 to 20 mM) along with sufficient $(NH_4)_2SO_4$ for balanced growth until 20 hours (h), after which $(NH_4)_2SO_4$ was no longer fed. Pulse feeding was conducted in response to either a drop in the off-gas CO_2 concentration or a sudden rise in the DO, which indicated depletion of the carbon source. The volume of the pulse depended on the phase of growth, generally with smaller pulses (5 mM) in the early stages of growth or in late stationary

phase. Experiments were generally completed by 27 h post inoculation and were terminated when: (1) further addition of carbon had no effect on the (already declining) CO_2 production rates; (2) the measured OD_{600} decreased despite the presence of excess carbon; or (3) excessive and uncontrollable foaming, which usually occurred after the onset of the two previous symptoms. These experiments were replicated three times.

The pulse feed process was subsequently modeled and run as a continuous drip feed process (i.e., proactive feeding at predetermined rate) in order to compare with the pulse feed (i.e., a reactive feeding) approach. In the continuous approach, the motors driving the injector syringes were run continuously at very low speed, such that feeding was continual drop-wise addition as opposed to injecting a slug of octanoic acid at one time. From the pulse feed data, curves for the total uptake of carbon and NH_4 were plotted over time ($C(t)$ and $N(t)$, respectively). A satisfactory fit could be obtained with a piecewise function, in which the growth phase was fitted with an exponential function, whereas the PHA accumulation phase was fitted with a quadratic function. This trend is in agreement with what has been previously reported by MacLean et al. [18]. These equations were programmed into LabBoss software to automate a continuous drip feed process and compare the results to the pulse feed process. Within the 27 h cultivation, a total of 185 mL octanoic acid and 235 mL of the 200 g L^{-1} $(NH_4)_2SO_4$ solution were fed. These experiments were repeated three times.

$$C(t) = \begin{cases} 0.273e^{0.366t}, & t \leq 10 \text{ h} \\ -0.0293t^2 + 3.478t - 2.157, & t > 10 \text{ h} \end{cases}. \quad (1)$$

$$N(t) = \begin{cases} 0.034e^{0.418t}, & t \leq 9 \text{ h} \\ -0.0151t^2 + 0.628t - 3.0112, & t > 9 \text{ h} \\ 0, & t > 20 \text{ h} \end{cases}. \quad (2)$$

2.4. Measurement of CO_2 and Mass Balancing

The CO_2 signal was measured at a mass-to-charge (m/z) of 44 using a Hiden HPR-40 dissolved species membrane-inlet mass spectrometer (Hiden Analytical, Warrington, UK). Total CO_2 was quantified by integrating the measured off-gas concentration over the airflow rate to the bioreactor, while also accounting for dissolved carbonate species as described previously [37]. It was found that the off-gas CO_2 concentration was a more rapid indicator of carbon depletion during growth, while during PHA accumulation, changes in the off-gas CO_2 concentration were not as pronounced, making the DO signal a more reliable indicator. The carbon balance was performed assuming that all consumed carbon could be accounted for through measured CO_2, PHA biomass (X_{PHA}), and non-PHA residual cell mass (X_r). The mass balance followed the same approach described previously [26,27].

2.5. Yield Coefficients

The yield coefficient of X_r from NH_4 ($Y_{Xr/N}$) was determined to be 6.1 g g^{-1} from previous work [27]. This value is in reasonable agreement with the $Y_{Xr/N}$ of 5.44 g g^{-1} reported by Sun et al. [29]. Similarly, the yield coefficients of X_r and PHA from octanoic acid ($Y_{Xr/S}$ and $Y_{PHA/S}$, respectively) were derived from previous data as 0.72 g g^{-1} and 0.62 g g^{-1}. The $Y_{PHA/S}$ value was similar to the 0.63 g g^{-1} reported previously for nonanoic acid [34]. The $Y_{Xr/S}$ measured in this work is similar to the growth-phase $Y_{X/S}$ of 0.8 g g^{-1} reported previously for growth on nonanoic acid, although it is not clear if this value considered total biomass (X_t) or X_r only. Other medium components (PO_4^{3-}, Mg^{2+}, Fe^{3+}) were assumed to be in excess on the basis of the amount added to the medium and the yield coefficients reported previously [29,38]. The validity of this assumption was checked through measurement of residual trace metals in the culture supernatant (described below).

2.6. Sample Treatment

Samples (20 to 40 mL) were periodically withdrawn from the bioreactor, generally in 1 to 3 h intervals. These were centrifuged for 10 minutes at 12,500× *g*. The pellet was washed once in PBS buffer, transferred into a pre-weighed 20 mL aluminum tray and dried at 60 °C until no further loss of mass was detected to determine [X_t] (g L^{-1} cell dry mass, CDM). The PHA was extracted in chloroform using the acid-catalyzed methanolysis procedure [39]. The PHA content ($\%_{PHA}$) of the biomass was quantified using a gas chromatograph equipped with a flame ionization detector (GC-FID) identical to that described previously [40]. The supernatant was decanted and stored at −20 °C until further analyses could be performed. These are described below.

2.7. Measurement of Residual Carbon, NH_4-N PO_4^{3-}-P, and Trace Medium Components

Residual octanoic acid in the culture supernatants was measured by GC-FID as previously described [26]. Residual free NH_4 was measured spectrophotometrically at 630 nm via the indophenol blue method (Lachat QuikChem® Method 10–107-06-1-J) as previously described [27]. Residual PO_4^{3-} was also measured spectrophotometrically in a flow injection system using the Quikchem® method 10-115-01-1-A. Briefly, PO_4^{3-} reacts with ammonium molybdate and antimony tartarate to form a complex that produced a blue color when reduced with ascorbic acid, which is measured at 880 nm. Samples were diluted 250X prior to measurement.

The concentration of trace elements was measured via inductively coupled plasma optical emission spectrophotometer (ICP-OES) at intervals over time. Samples were prepared without dilution, although the samples were acidified by adding nitric acid to a final concentration of 2% (vol vol^{-1}) prior to filtering through a 0.2 µm filter. The eluent used for the ICP-OES was also 2% nitric acid.

3. Results

3.1. Pulse Feed Strategy

Figure 1A shows the results for biomass and PHA production obtained from three independent pulse fed-batch experiments. Despite constant aeration set at 6 LPM and a cascading stirrer reaching its maximal value, the DO could not be maintained at the intended set point of 40% beyond 11 h (Figure 1B). By 14 h, the DO was consistently below 5% while excess carbon was present. From previous results, these conditions are normally expected to cause a shift in carbon flux from growth to PHA synthesis [27]. However, the PHA content of the biomass started increasing significantly from about 8 h onward, while DO was still maintained at relatively high levels. The low residual levels of carbon and/or NH_4 detected in the culture medium at this time (discussed below) may have slowed the growth rate and caused storage of carbon as PHA [34]. This is supported by the observation that X_r production continued until 14 h and then declined to nearly negligible values due to DO limitation, which is consistent with previous work using octanoic acid [26].

3.2. Residual Concentrations of Octanoic Acid, NH_4^+-N, and PO_4^{3-}-P

Figure 1C shows the profiles of residual carbon NH_4, and PO_4^{3-} detected in the culture medium. As shown, the initial 20 mM of carbon added to the reactor was depleted within 6 h. Subsequently, octanoic acid was fed in small, frequent pulses (~5 to 20 mM) in response to either a drop in off-gas CO_2 concentration or a rise in DO signal, and the residual concentration remained low until after 20 h, at which point slight excess was observed at the indicated sampling points. NH_4 appeared to have been briefly limited around 9–10 h, but began to accumulate after 10 h, likely due to cessation of growth from the onset of O_2-limitation. By 20 h, the residual NH_4 concentration reached 700 mg L^{-1} and feeding of $(NH_4)_2SO_4$ was stopped (to prevent accumulation to toxic levels). The excess was consumed to a final concentration of 49 mg L^{-1} by 27 h, resulting in an uptake rate of 5.90 ± 0.25 mg

NH_4 g X_r^{-1} h^{-1}. By comparison, the measured uptake rate of NH_4 during the growth phase (0–14 h) was 286.5 ± 25.9 mg NH_4 g X_r^{-1} h^{-1}.

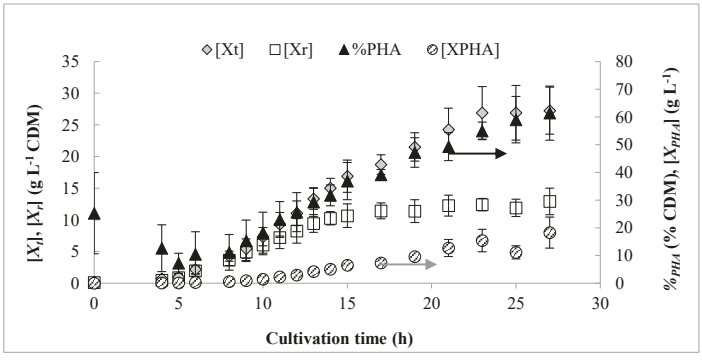

(**A**)

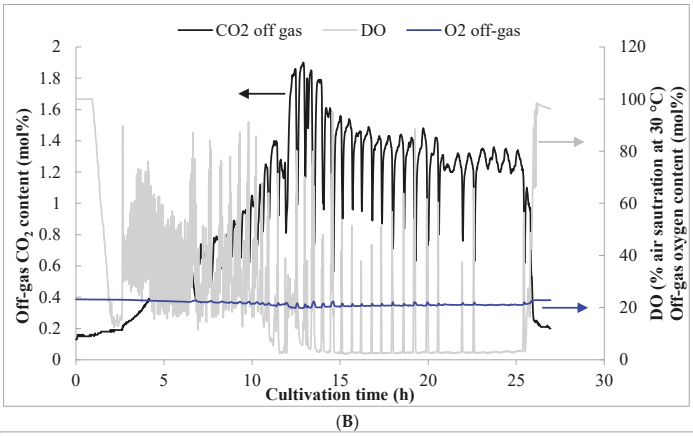

(**B**)

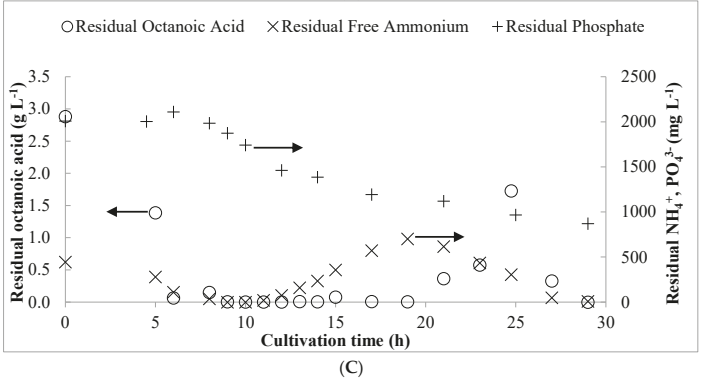

(**C**)

Figure 1. (**A**) Results for biomass and polyhydroxyalkanoate (PHA) production obtained over the course of the pulse feed experiments. (**B**) Representative profile for dissolved oxygen (DO) content over time as well as off-gas CO_2 and O_2 content. (**C**) Residual concentrations of octanoic acid, free ammonium, and phosphate observed during the bench scale pulse feed experiments. Results shown are for a representative pulse feed experiment. Error bars represent standard deviations between three biological replicates.

Phosphate was consumed most rapidly during the growth phase from 6 to 12 h and the slope of a plot between PO_4^{3-} consumption and X_r production (R^2 = 0.91) produced a yield coefficient of 13.48 g X_r g PO_4^{3-} $^{-1}$ (Table 1). This is similar to the value of 13.7 g g^{-1} reported by Sun et al. [29] for *P. putida* KT2440. Consumption of PO_4^{3-} was also observed during the PHA accumulation phase (14 h and onward) at the rate of 3.08 ± 0.96 mg PO_4^{3-} g X_r^{-1} h^{-1}. Prior to 14 h, the obtained growth-phase PO_4 uptake rate was 52.7 ± 11.1 mg PO_4 g X_r^{-1} h^{-1}.

Table 1. Yield coefficients for C, N, P, and certain (detectable) trace elements.

Medium Component	Yield Coefficient
Octanoic Acid (g g^{-1})	0.62 [a]
NH_4^+ (g g^{-1})	6.1 [a]
PO_4^{3-} (g g^{-1})	13.5
Ca^{2+} (g mg^{-1})	2.6
Cu^{2+} (g mg^{-1})	15.5
Fe^{3+} (g mg^{-1})	2.2
Mg^{2+} (g mg^{-1})	0.5

[a] results obtained from previous batch tests, Blunt et al. [27].

3.3. Residual Trace Elements

For measurement of trace residual metals with ICP-OES, satisfactory resolution was found for Fe^{3+}, Ca^{2+}, and Mg^{2+} (Figure 2). The concentrations of Mg^{2+} decreased until 14 h, and then the concentration began to slowly increase. The concentration of Fe^{3+} decreased rapidly until 6 h, and then remained relatively constant at a low concentration for the remainder of the cultivation. The concentration of Ca^{2+} decreased until 10 h and showed little change subsequently. Poor resolution was obtained for Cu^{2+}, Mn^{2+}, and Zn^{2+}. Even initially, these were present in extremely low concentrations, but did not appear to be depleted at any point during the cultivation. Growth-phase yield coefficients (obtained prior to 12 h) for all detectable medium components are shown in Table 1. None of these trace metals reported zero concentration values at any time and, therefore, were likely not limiting. However, for cultivations targeting even higher cell densities, increasing the concentration of these metals would be advisable, particularly for Fe^{3+} and Mg^{2+}.

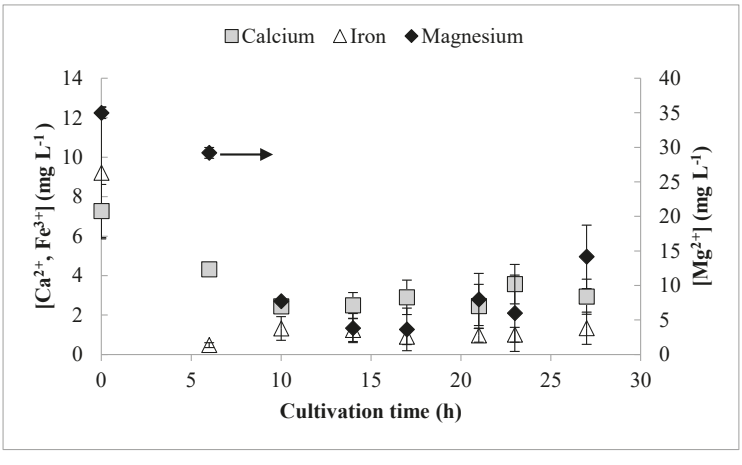

Figure 2. Analysis of residual concentrations of trace elements (calcium, iron, magnesium) in the culture supernatant by inductively coupled plasma optical emission spectrophotometer (ICP-OES). Error bars represent standard deviations between three biological replicates.

3.4. Modeling of Feeding Rates—Continuous Drip Feed Strategy

Curves for carbon and ammonium uptake rates over time in the pulse feed process were modeled as piecewise functions, shown in Figure 3. The results from three replicates of these experiments are shown in Figure 4 and summarized in Table 2 with comparison to previous work. The process was very consistent between replicates, and the concentration profiles for DO, carbon, and NH_4 behaved similarly to the pulse feed experiments described above. As shown in Table 2, the drip feed strategy appeared to favor production of X_r over X_{PHA}, as indicated by the slightly higher [X_t], lower $\%_{PHA}$, lower $Y_{PHA/S}$, and a lower rate of PHA synthesis (indicated by specific productivity, Q_s) during the accumulation phase.

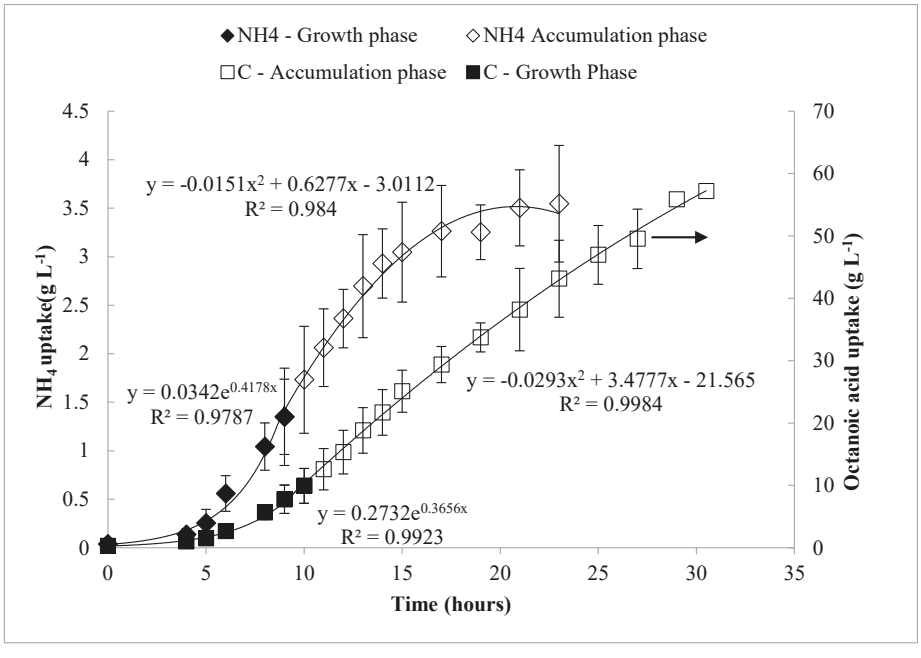

Figure 3. Modeled cumulative feeding of carbon and ammonium over the time course of the pulse feed experiments. Error bars represent standard deviations between three biological replicates.

3.5. PHA Composition

The detected monomer composition for both fed-batch cultivation processes is shown in Table 3. The monomeric composition was similar in both cases, but the dominant monomer was C8 (90–93 mol%), followed by C6 (6–7 mol%), with traces of C10 and C12.

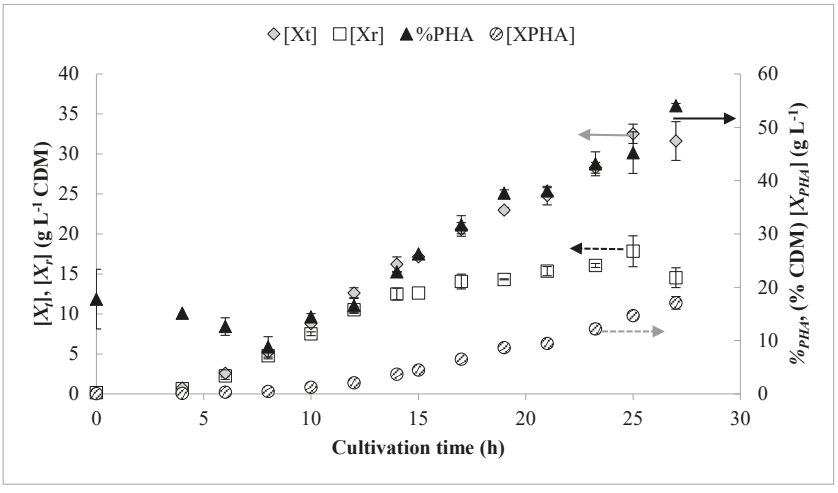

Figure 4. Growth curves shown for continuous drip strategy derived from modeled feeding rates. Error bars represent standard deviations between three biological replicates.

Table 2. Comparison of key process performance indicators of previous batch cultivations with the current fed-batch process.

Process Performance Indicator	Previous Batch Results [a]	Pulse Feed Strategy (at 27 h Unless Otherwise Stated)	Continuous, Drip Feed Strategy (at 27 h Unless Otherwise Stated)
$[X_t]$ (g L^{-1})	2.37 ± 0.1	28.9 ± 4.0	32.4 ± 0.9
$\%_{PHA}$ (g g^{-1})	44.4 ± 1.3	60.6 ± 8.2	52.9 ± 2.5
$[X_r]$ (g L^{-1})	2.37 ± 0.5	11.2 ± 1.5	17.4 ± 2.1 [b]
$[X_{PHA}]$ (g L^{-1})	1.01 ± 0.12	17.7 ± 4.8	15.4 ± 1.2
$\mu_{avg/Xr}$, growth phase (h^{-1})	0.29 ± 0.03	0.35 ± 0.11 (0–14 h)	0.31 ± 0.03 (0–14 h)
$\mu_{avg/Xr}$, storage phase (h^{-1})	0.11 ± 0.01	0.03 ± 0.01 (14–27 h)	0.03 ± 0.01 (14–27 h)
$Q_{v,\,final}$ (g L^{-1} h^{-1})	0.08 ± 0.00	0.61 ± 0.12	0.60 ± 0.04
$Q_{v,\,max}$ (g L^{-1} h^{-1})	0.08 ± 0.01	0.66 ± 0.14 (23–27 h)	0.60 ± 0.04 (27 h)
$Q_{s,\,max}$ (g PHA g X_r^{-1} h^{-1})	0.18 ± 0.03	0.18 ± 0.03 (15–19 h)	0.10 ± 0.03 (23–25 h) [b]
$Q_{s,\,avg}$ (g PHA g X_r^{-1} h^{-1})	0.11 ± 0.00	0.09 ± 0.01 (14–27 h)	0.06 ± 0.01 (14–27 h) [b]
$Y_{PHA/S}$, overall (C-mol C-mol^{-1})	0.35 ± 0.04	0.33 ± 0.05	0.26 ± 0.04
$Y_{PHA/S}$, storage phase (C-mol C-mol^{-1})	0.57 ± 0.05	0.52 ± 0.13 (14–27 h)	0.31 ± 0.06 (14–27 h) [b]
Carbon Recovery	1.04 ± 0.00	0.90 ± 0.15	0.89 ± 0.04

[a] results chosen for O_2-limited conditions with 6 LPM aeration and 250 rpm mixing (k_La = 78 h^{-1}), obtained from Blunt et al. [27]; [b] results that are compared for the two fed-batch strategies that are statistically different using a two-tailed homoscedastic comparison of sample means ($p < 0.05$). Tolerances indicate standard deviations between three biological replicates.

Table 3. Monomer composition of polymer synthesized from octanoic acid using *P. putida* LS46 under different fed-batch strategies. Tolerances indicate standard deviations between three biological replicates.

Feeding Strategy	C6	C8	C10	C12
		(Mol %)		
Pulse	5.8 ± 0.6	92.9 ± 0.6	1.1 ± 0.2	0.6 ± 0.2
Continuous drip	7.4 ± 0.2	89.7± 0.3	2.2 ± 0.1	0.6 ± 0.2

3.6. Carbon Flux and Yield Analysis

An overall yield analysis (on a C-mol basis) is shown in Figure 5, for both pulse-fed and continuous drip feed experiments. In either case, there was little change in the CO_2 production (which accounted

for approximately 50% of the consumed carbon on a molar basis) throughout the cultivation, which is consistent with previous results [26,27]. However, the carbon flux to X_r was higher during the O_2-limited phase in comparison with previous work, which caused lower PHA yield. This comparison is also shown in Table 2, along with several other key indicators of process performance. The maximum observed Q_s and overall $Y_{PHA/S}$ yield from octanoic acid were similar in both cases, while the maximum $Y_{PHA/S}$ during the O_2-limited PHA storage phase was somewhat lower than in previous batch experiments. The carbon recovery approached one (0.9 ± 0.15, Table 2) for the fed-batch experiments, but was generally more variable than in previous batch experiments. Worth noting is that, as shown in Table 2, if only carbon consumed during the PHA storage phase is considered, a significantly higher proportion was allocated to PHA synthesis in the pulse feed experiments compared to the drip feed experiments.

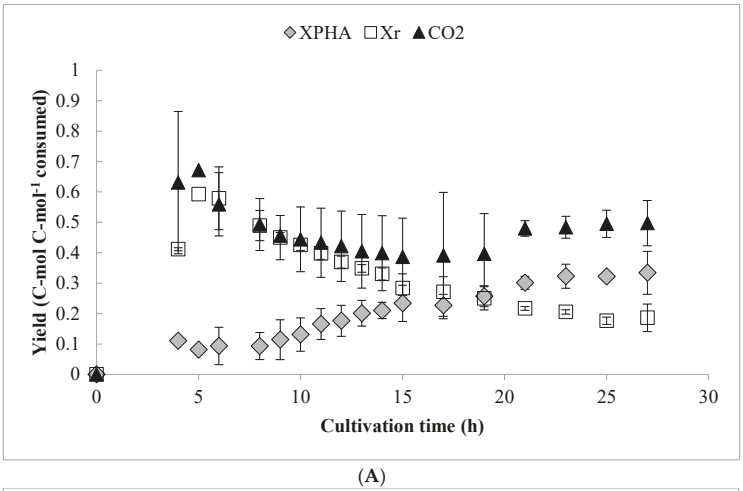

Figure 5. Overall (cumulative) yield analysis for X_{PHA}, X_r, and CO_2 over the duration of: (**A**) the pulse fed-batch cultivations and (**B**) the continuous drip feed experiments. Values expressed on a C-mol basis. Error bars represent standard deviations between three biological replicates.

4. Discussion

This work has shown that: (1) oxygen limitation can be a viable strategy for inducing mcl-PHA accumulation from fatty acids using *P. putida* in HCD fed-batch cultivations; and (2) this process can be rapidly optimized through simple pulse feeding in response to DO and/or off-gas CO_2 signals as real-time feedback variables. One advantage of this approach is that it eliminates the need to predict growth rates or feeding rates over time, which can lead to complicated automation and programming [29]. Previously, a similar strategy proved to be a significant challenge to optimize when using toxic substrates like octanoic acid [26]. Furthermore, this approach can be implemented with standard bioreactor equipment (i.e., the setup could be as simple as a DO probe and a feed pump), and should be independent of the bioreactor type, configuration, and to some extent also the scale and mass transfer capability. Although O_2-limitation has been reported to cause excessive foaming and termination of fed-batch processes [17,34,41], in this work we found that foam was manageable throughout the O_2-limited phase (except for at the very end of the process). In fact, foaming was observed upon carbon limitation in the pulse feed process, and was alleviated by further addition of octanoic acid.

During the storage phase, consumption of both NH_4 and PO_4 was observed, albeit at a considerably slower rate than during growth. This may be due to residual growth and/or maintenance functions during the O_2-limited PHA storage phase, which could be advantageous compared to strict N or P limitation. Andin et al. [42] examined the effect of maintaining a low residual growth rate on metabolic flux during synthesis of mcl-PHA from fatty acids in fed-batch culture using *P. putida* KT2440. Their analysis showed that when residual growth was present, the reduced co-factors from mcl-PHA synthesis (NADH, $FADH_2$) could be coupled to anabolic demand, and this improved the overall mcl-PHA yield from approximately 0.6 to 0.7 C-mol C-mol^{-1}. Another study reported a similar finding for PHB synthesized from butyrate using *C. necator* [43]. In this work, the yield coefficient during the storage phase was lower at 0.52 ± 0.13 C-mol C-mol^{-1} and the average residual growth rate during the storage phase was 0.03 ± 0.01 h^{-1} (Table 2). As suggested previously, co-feeding LCFAs may help improve residual growth during the PHA storage phase, and perhaps even further improve overall $Y_{PHA/S}$ [26].

Differences in the carbon feeding methods were also evaluated via a continuous drip feed process developed using an empirical model of the pulse feed data. Although the processes were largely similar, more favorable PHA storage characteristics (higher $Q_{s,\,max}$ and $Y_{PHA/S}$) were observed under pulse feeding conditions, whereas the drip feed process resulted in significantly higher [X_r], but lower $Y_{PHA/S}$ and $Q_{s,\,max}$.

A previous study indicated a significant improvement in $\%_{PHA}$ (from 25% to 44% of CDM) when *Pseudomonas* sp. G101 was pulse-fed waste canola oil, in comparison to a continuous drip feed [44]. The results of the present study do not suggest such a drastic difference between drip feed and pulse feed methodologies. However, the findings do imply that pulse feeding may help to maximize the yield and synthesis rate of mcl-PHA during the accumulation phase, whereas a continuous drip feed process may help boost biomass production during the growth phase. This may be due to the constant cycling between carbon excess and carbon-limited conditions imposed by the pulse feed strategy. However, it should be noted that during the course of these drip feed experiments, periodic carbon limitation was still imposed when the injector syringe was briefly paused to refill, which may have dampened the observed effect. Perhaps a more optimized strategy could result from coupling a continuous, drip feed strategy for growth with a pulse feed strategy in the PHA accumulation phase.

The effects of the feeding strategy on molecular weight of the polymer is an issue that needs to be addressed in mcl-PHA production when considering different feeding strategies, and should be the subject of future studies. Indeed, it has been previously shown that molecular mass of the polymer can be affected by cultivation conditions, even for PHB homopolymers [45,46]. Further, understanding the effects of the feeding strategy on polymer synthesis (constant carbon limitation compared to

periodic carbon limitation) at a more mechanistic level (polymer chain termination, preferential back consumption of lower molecular weight polymers) would be a valuable contribution [4].

Interestingly, mcl-PHA synthesis characteristics were not improved over previous batch [27] and/or simple fed-batch experiments [26]. This difference might reveal that the kinetics of mcl-PHA synthesis and storage are perhaps more well suited to the simpler, more gradually changing chemical environment of a batch system. This implies that the main mode of advancing HCD fed-batch productivities, at least in this work, was solely through boosting [X_t] rather than improving mcl-PHA synthesis characteristics. The overall carbon recovery was also somewhat lower in the HCD fed-batch cultivations, which could indicate that carbon was used for end products other than X_{PHA}, X_r, and CO_2. These were not accounted for in this work.

Compared to other HCD fed-batch processes, several previous bench-scale studies have demonstrated improved results over the fed-batch process described in this work [17,18,33,34]. Many of these studies have used an aeration medium with enriched oxygen content, which increases the driving force for oxygen transfer nearly fivefold, and has been shown to improve PHA productivity nearly fourfold in bench-scale reactors [47]. Thus, using a technique to increase the driving force for oxygen transfer (enriched O_2, bioreactor pressurization) would help make this fed-batch process more competitive with previous studies documented in the literature, but that was not within the objectives of this work. It is important to point out that the main contribution of this work was to show the effects of low-DO environments in HCD fed-batch cultivations under different feeding strategies, and not necessarily to maximize overall Q_v using techniques to keep DO in excess. Although those are worthwhile pursuits, they have been extensively explored in the literature, but have not necessarily been replicated in larger scale bioreactors [22]. Regardless of how much the oxygen transfer rate might be improved, at some point microaerophilic conditions will persist beyond a certain cell density.

5. Conclusions

A fed-batch method was developed using a CO_2 and/or DO-based pulse feed strategy using atmospheric air as the aeration medium and O_2-limitation as the main driving force for mcl-PHA production. The process consistently produced 25–30 g L^{-1} total biomass and resulted in an overall Q_v of 0.66 ± 0.14 g L^{-1} h^{-1}. Interestingly, no improvement to mcl-PHA synthesis characteristics (Q_s, $Y_{PHA/S}$) was observed when compared to previous oxygen-limited batch cultivations, meaning that the productivity advances were solely due to increased total biomass. Furthermore, the overall carbon recovery was lower, suggesting that carbon may be utilized less efficiently in HCD cultures. Finally, while a continuous drip feed strategy favored growth and production of X_r, a pulse feed strategy favored the production of mcl-PHA during the storage phase.

Author Contributions: Individual contributions of authors are as follows: (1) design and conceptualization, W.B.; (2) methodology development, W.B. and C.D.; (3) acquisition of data, W.B. and C.D.; (4) formal analysis and writing, W.B.; (5) review and editing, D.B.L., R.S., D.J.G., and N.C.; (6) supervision and final approval, N.C.; (7) funding acquisition: D.B.L. (GAPP and NSERC Discovery grants) and W.B. (NSERC CGS-D, Sir Gordon Wu Scholarship and Edward R. Toporeck fellowship).

Funding: Funding for this work was provided by: (1) Genome Canada, through the Genome Applications and Partnership Program (GAPP) grant titled "Fibre composite and biomatrix genomics (FiCoGen)"; (2) the Natural Sciences and Engineering Research Council (NSERC) of Canada through a Discovery grant (RGPIN-5961-2016) and a Doctoral Alexander Graham Bell Canada Graduate Scholarship (CGS-D), the University of Manitoba through the Graduate Fellowship and Sir Gordon Wu Scholarship, and the University of Manitoba Faculty of Engineering through the Edward R. Toporeck Graduate Fellowship.

Acknowledgments: Special thanks to Elsie Jordaan, Joe Ackerman, and Tom Ward in the Department of Chemistry at the University of Manitoba for their help with the ICP-OES analysis. Thanks also to Jacob Harvey for his help with medium preparation, bioreactor setup, collecting samples, and measuring OD_{600}.

Conflicts of Interest: The authors declare no conflict of interest. The funding sponsors had no role in the design of the study; in the collection, analyses, or interpretation of data; in the writing of the manuscript, and in the decision to publish the results.

Abbreviations

CDM	cell dry mass (g L^{-1})
C(t)	cumulative octanoic acid uptake as a function of time (g L^{-1})
N(t)	cumulative $(NH_4)_2SO_4$ uptake as a function of time (g L^{-1})
Qv	overall volumetric productivity of PHA (g L^{-1} h^{-1})
Qs	specific productivity or PHA synthesis rate (g g X_r^{-1} h^{-1})
X_{PHA}	PHA biomass (g)
X_r	non-PHA (residual) cell mass (g)
X_t	total biomass (g)
$Y_{PHA/S}$	yield coefficient of PHA per unit carbon substrate consumed (g g^{-1} or C-mol C-mol^{-1})
$Y_{Xr/N}$	yield coefficient of non-PHA cell mass per unit ammonium consumed (g g^{-1} or mol mol^{-1})
$Y_{Xr/S}$	yield coefficient of non-PHA cell mass per unit carbon substrate consumed (g g^{-1} or C-mol C-mol^{-1})
$Y_{X/S}$	yield coefficient of total biomass per unit carbon substrate consumed (g g^{-1} or mol mol^{-1})
$\mu_{avg/Xr}$	average specific growth rate over a defined period (h^{-1}, calculated using increases in X_r)
$\%_{PHA}$	intracellular PHA content (% of CDM)
[ ]	concentration braces (g L^{-1} or mg L^{-1})

References

1. Dauvergne, P. The power of environmental norms: Marine plastic pollution and the politics of microbeads. *Environ. Polit.* **2018**, *27*, 579–597. [CrossRef]
2. Schnurr, R.E.J.; Alboiu, V.; Chaudhary, M.; Corbett, R.A.; Quanz, M.E.; Sankar, K.; Srain, H.S.; Thavarajah, V.; Xanthos, D.; Walker, T.R. Reducing marine pollution from single-use plastics (SUPs): A review. *Mar. Pollut. Bull.* **2018**, *137*, 157–171. [CrossRef] [PubMed]
3. Walker, T.R.; Xanthos, D. A call for Canada to move toward zero plastic waste by reducing and recycling single-use plastics. *Resour. Conserv. Recycl.* **2018**, *133*, 99–100. [CrossRef]
4. Laycock, B.; Halley, P.; Pratt, S.; Werker, A.; Lant, P. The chemomechanical properties of microbial polyhydroxyalkanoates. *Prog. Polym. Sci.* **2013**, *38*, 536–583. [CrossRef]
5. Noda, I.; Lindsey, S.B.; Caraway, D. Nodax™ Class PHA Copolymers: Their Properties and Applications. In *Plastics from Bacteria*; Chen, G.G.-Q., Ed.; Springer: Berlin/Heidelberg, Germany, 2010; Volume 14, pp. 237–255.
6. Kourmentza, C.; Plácido, J.; Venetsaneas, N.; Burniol-Figols, A.; Varrone, C.; Gavala, H.N.; Reis, M.A.M. Recent advances and challenges towards sustainable polyhydroxyalkanoate (PHA) production. *Bioengineering* **2017**, *4*, 55. [CrossRef] [PubMed]
7. Wang, Y.; Yin, J.; Chen, G.-Q. Polyhydroxyalkanoates, challenges and opportunities. *Curr. Opin. Biotechnol.* **2014**, *30*, 59–65. [CrossRef] [PubMed]
8. Chen, G.Q. New challenges and opportunities for industrial biotechnology. *Microb. Cell Factories* **2012**, *11*, 111. [CrossRef] [PubMed]
9. Możejko-Ciesielska, J.; Kiewisz, R. Bacterial polyhydroxyalkanoates: Still fabulous? *Microbiol. Res.* **2016**, *192*, 271–282. [CrossRef] [PubMed]
10. Kaur, G.; Roy, I. Strategies for large-scale production of polyhydroxyalkanoates. *Chem. Biochem. Eng. Q.* **2015**, *29*, 157–172. [CrossRef]
11. Koller, M.; Maršálek, L.; de Sousa Dias, M.M.; Braunegg, G. Producing microbial polyhydroxyalkanoate (PHA) biopolyesters in a sustainable manner. *New Biotechnol.* **2017**, *37*, 24–38. [CrossRef]
12. Koller, M.; Braunegg, G. Advanced approaches to produce polyhydroxyalkanoate (PHA) biopolyesters in a sustainable and economic fashion. *EuroBiotech J.* **2018**, *2*, 89–103. [CrossRef]
13. Heijnen, J.J.; Terwisscha van Scheltinga, A.H.; Straathof, A.J. Fundamental bottlenecks in the application of continuous bioprocesses. *J. Biotechnol.* **1992**, *22*, 3–20. [CrossRef]
14. Ienczak, J.L.; Schmidell, W.; de Aragão, G.M.F. High-cell-density culture strategies for polyhydroxyalkanoate production: A review. *J. Ind. Microbiol. Biotechnol.* **2013**, *40*, 275–286. [CrossRef] [PubMed]
15. Cerrone, F.; Duane, G.; Casey, E.; Davis, R.; Belton, I.; Kenny, S.T.; Guzik, M.W.; Woods, T.; Babu, R.P.; O'Connor, K. Fed-batch strategies using butyrate for high cell density cultivation of *Pseudomonas putida* and its use as a biocatalyst. *Appl. Microbiol. Biotechnol.* **2014**, *98*, 9217–9228. [CrossRef] [PubMed]

16. Jiang, X.; Sun, Z.; Ramsay, J.A.; Ramsay, B.A. Fed-batch production of MCL-PHA with elevated 3-hydroxynonanoate content. *AMB Express* **2013**, *3*, 50. [CrossRef] [PubMed]
17. Lee, S.Y.; Wong, H.H.; Choi, J.; Lee, S.H.; Lee, S.C.; Han, C.S. Production of medium-chain-length polyhydroxyalkanoates by high-cell-density cultivation of *Pseudomonas putida* under phosphorus limitation. *Biotechnol. Bioeng.* **2000**, *68*, 466–470. [CrossRef]
18. Maclean, H.; Sun, Z.; Ramsay, J.A.; Ramsay A., B. Decaying exponential feeding of nonanoic acid for the production of medium-chain-length poly(3-hydroxyalkanoates) by *Pseudomonas putida* KT2440. *Can. J. Chem.* **2008**, *86*, 564–569. [CrossRef]
19. Ryu, H.W.; Hahn, S.K.; Chang, Y.K.; Chang, H.N. Production of poly (3-hydroxybutyrate) by high cell density fed-batch culture of *Alcaligenes eutrophus* with phospate limitation. *Biotechnol. Bioeng.* **1997**, *55*, 28–32. [CrossRef]
20. Shang, L.; Jiang, M.; Chang, H.N. Poly (3-hydroxybutyrate) synthesis in fed-batch culture of *Ralstonia eutropha* with phosphate limitation under different glucose concentrations. *Biotechnol. Lett.* **2003**, *25*, 1415–1419. [CrossRef]
21. Wang, F.; Lee, S.Y. Poly (3-hydroxybutyrate) production with high productivity and high polymer content by a fed-batch culture of *Alcaligenes latus* under nitrogen limitation. *Appl. Environ. Microbiol.* **1997**, *63*, 3703–3706.
22. Blunt, W.; Levin, D.; Cicek, N. Bioreactor Operating Strategies for Improved Polyhydroxyalkanoate (PHA) Productivity. *Polymers* **2018**, *10*, 1197. [CrossRef] [PubMed]
23. Bylund, F.; Collet, E.; Enfors, S.-O.; Larsson, G. Substrate gradient formation in the large-scale bioreactor lowers cell yield and increases by-product formation. *Bioprocess Eng.* **1998**, *18*, 171. [CrossRef]
24. Lara, A.R.; Galindo, E.; Ramírez, O.T.; Palomares, L.A. Living with heterogeneities in bioreactors. *Mol. Biotechnol.* **2006**, *34*, 355–381. [CrossRef]
25. Koller, M.; Sandholzer, D.; Salerno, A.; Braunegg, G.; Narodoslawsky, M. Biopolymer from industrial residues: Life cycle assessment of poly (hydroxyalkanoates) from whey. *Resour. Conserv. Recycl.* **2013**, *73*, 64–71. [CrossRef]
26. Blunt, W.; Dartiailh, C.; Sparling, R.; Gapes, D.; Levin, D.B.; Cicek, N. Carbon flux to growth or polyhydroxyalkanoate synthesis under microaerophilic conditions is affected by fatty acid chain-length in *Pseudomonas putida* LS46. *Appl. Microbiol. Biotechnol.* **2018**, *102*, 6437–6449. [CrossRef] [PubMed]
27. Blunt, W.; Dartiailh, C.; Sparling, R.; Gapes, D.; Levin, D.B.; Cicek, N. Microaerophilic environments improve the productivity of medium chain length polyhydroxyalkanoate biosynthesis from fatty acids in *Pseudomonas putida* LS46. *Process Biochem.* **2017**, *59*, 18–25. [CrossRef]
28. Riesenberg, D.; Guthke, R. High-cell-density cultivation of microorganisms. *Appl. Microbiol. Biotechnol.* **1999**, *51*, 422–430. [CrossRef] [PubMed]
29. Sun, Z.; Ramsay, J.A.; Guay, M.; Ramsay, B.A. Automated feeding strategies for high-cell-density fed-batch cultivation of *Pseudomonas putida* KT2440. *Appl. Microbiol. Biotechnol.* **2006**, *71*, 423–431. [CrossRef] [PubMed]
30. Kellerhals, M.B.; Kessler, B.; Witholt, B. Closed-loop control of bacterial high-cell-density fed-batch cultures: Production of mcl-PHAs by *Pseudomonas putida* KT2442 under single-substrate and cofeeding conditions. *Biotechnol. Bioeng.* **1999**, *65*, 306–315. [CrossRef]
31. Kim, B.S. Production of medium chain length polyhydroxyalkanoates by fed-batch culture of *Pseudomonas oleovorans*. *Biotechnol. Lett.* **2002**, *24*, 125–130. [CrossRef]
32. Kim, G.J.; Lee, I.Y.; Yoon, S.C.; Shin, Y.C.; Park, Y.H. Enhanced yield and a high production of medium-chain-length poly (3-hydroxyalkanoates) in a two-step fed-batch cultivation of *Pseudomonas putida* by combined use of glucose and octanoate. *Enzyme Microb. Technol.* **1997**, *20*, 500–505. [CrossRef]
33. Gao, J.; Ramsay, J.A.; Ramsay, B.A. Fed-batch production of poly-3-hydroxydecanoate from decanoic acid. *J. Biotechnol.* **2016**, *218*, 102–107. [CrossRef] [PubMed]
34. Sun, Z.; Ramsay, J.A.; Guay, M.; Ramsay, B.A. Carbon-limited fed-batch production of medium-chain-length polyhydroxyalkanoates from nonanoic acid by *Pseudomonas putida* KT2440. *Appl. Microbiol. Biotechnol.* **2007**, *74*, 69–77. [CrossRef] [PubMed]
35. Sharma, P.K.; Fu, J.; Cicek, N.; Sparling, R.; Levin, D.B. Kinetics of medium-chain-length polyhydroxyalkanoate production by a novel isolate of *Pseudomonas putida* LS46. *Can. J. Microbiol.* **2012**, *58*, 982–989. [CrossRef] [PubMed]

36. Ramsay, B.A.; Lomaliza, K.; Chavarie, C.; Dubé, B.; Ramsay, J.A. Production of poly-(beta-hydroxybutyric-co-beta-hydroxyvaleric) acids. *Appl. Environ. Microbiol.* **1990**, *56*, 2093–2098. [PubMed]
37. Blunt, W.; Hossain, M.E.; Gapes, D.J.; Sparling, R.; Levin, D.B.; Cicek, N. Real-time monitoring of microbial fermentation end-products in biofuel production with Titrimetric Off-Gas Analysis (TOGA). *Biol. Eng. Trans.* **2014**, *6*, 203–219.
38. Preusting, H.; Hazenberg, W.; Witholt, B. Continuous production of poly (3-hydroxyalkanoates) by *Pseudomonas oleovorans* in a high-cell-density, two-liquid-phase chemostat. *Enzyme Microb. Technol.* **1993**, *15*, 311–316. [CrossRef]
39. Brandl, H.; Gross, R.A.; Lenz, R.W.; Fuller, R.C. *Pseudomonas oleovorans* as a source of poly (β-hydroxyalkanoates) for potential applications as biodegradable polyesters. *Appl. Environ. Microbiol.* **1988**, *54*, 1977–1982.
40. Fu, J.; Sharma, U.; Sparling, R.; Cicek, N.; Levin, D.B. Evaluation of medium-chain-length polyhydroxyalkanoate production by *Pseudomonas putida* LS46 using biodiesel by-product streams. *Can. J. Microbiol.* **2014**, *60*, 461–468. [CrossRef]
41. Sun, Z.; Ramsay, J.A.; Guay, M.; Ramsay, B.A. Enhanced yield of medium-chain-length polyhydroxyalkanoates from nonanoic acid by co-feeding glucose in carbon-limited, fed-batch culture. *J. Biotechnol.* **2009**, *143*, 262–267. [CrossRef]
42. Andin, N.; Longieras, A.; Veronese, T.; Marcato, F.; Molina-Jouve, C.; Uribelarrea, J.-L. Improving carbon and energy distribution by coupling growth and medium chain length polyhydroxyalkanoate production from fatty acids by *Pseudomonas putida* KT2440. *Biotechnol. Bioprocess Eng.* **2017**, *22*, 308–318. [CrossRef]
43. Grousseau, E.; Blanchet, E.; Déléris, S.; Albuquerque, M.G.E.; Paul, E.; Uribelarrea, J.-L. Impact of sustaining a controlled residual growth on polyhydroxybutyrate yield and production kinetics in *Cupriavidus necator*. *Bioresour. Technol.* **2013**, *148*, 30–38. [CrossRef] [PubMed]
44. Możejko, J.; Ciesielski, S. Pulsed feeding strategy is more favorable to medium-chain-length polyhydroxyalkanoates production from waste rapeseed oil. *Biotechnol. Prog.* **2014**, *30*, 1243–1246. [CrossRef] [PubMed]
45. Peña, C.; López, S.; García, A.; Espín, G.; Romo-Uribe, A.; Segura, D. Biosynthesis of poly-β-hydroxybutyrate (PHB) with a high molecular mass by a mutant strain of *Azotobacter vinelandii* (OPN). *Ann. Microbiol.* **2014**, *64*, 39–47. [CrossRef]
46. Myshkina, V.L.; Nikolaeva, D.A.; Makhina, T.K.; Bonartsev, A.P.; Bonartseva, G.A. Effect of growth conditions on the molecular weight of poly-3-hydroxybutyrate produced by *Azotobacter chroococcum* 7B. *Appl. Biochem. Microbiol.* **2008**, *44*, 482–486. [CrossRef]
47. Shang, L.; Jiang, M.; Ryu, C.H.; Chang, H.N.; Cho, S.H.; Lee, J.W. Inhibitory effect of carbon dioxide on the fed-batch culture of *Ralstonia eutropha*: Evaluation by CO_2 pulse injection and autogenous CO_2 methods. *Biotechnol. Bioeng.* **2003**, *83*, 312–320. [CrossRef] [PubMed]

bioengineering

MDPI

Review

Production of Polyhydroxyalkanoates and Extracellular Products Using *Pseudomonas Corrugata* and *P. Mediterranea*: A Review

Grazia Licciardello [1,*], Antonino F. Catara [2] and Vittoria Catara [3]

[1] Consiglio per la Ricerca in agricoltura e l'analisi dell'Economia Agraria-Centro di ricerca Olivicoltura, Frutticoltura e Agrumicoltura (CREA), Corso Savoia 190, 95024 Acireale, Italy
[2] Formerly, Science and Technologies Park of Sicily, ZI Blocco Palma I, Via V. Lancia 57, 95121 Catania, Italy; antoninocatara@virgilio.it
[3] Dipartimento di Agricoltura, Alimentazione e Ambiente, Università degli studi di Catania, Via Santa Sofia 100, 95130 Catania, Italy; vcatara@unict.it
* Correspondence: grazia.licciardello@crea.gov.it

Received: 24 October 2019; Accepted: 12 November 2019; Published: 14 November 2019

Abstract: Some strains of *Pseudomonas corrugata* (*Pco*) and *P. mediterranea* (*Pme*) efficiently synthesize medium-chain-length polyhydroxyalkanoates elastomers (mcl-PHA) and extracellular products on related and unrelated carbon sources. Yield and composition are dependent on the strain, carbon source, fermentation process, and any additives. Selected *Pco* strains produce amorphous and sticky mcl-PHA, whereas strains of *Pme* produce, on high grade and partially refined biodiesel glycerol, a distinctive filmable PHA, very different from the conventional microbial mcl-PHA, suitable for making blends with polylactide acid. However, the yields still need to be improved and production costs lowered. An integrated process has been developed to recover intracellular mcl-PHA and extracellular bioactive molecules. Transcriptional regulation studies during PHA production contribute to understanding the metabolic potential of *Pco* and *Pme* strains. Data available suggest that *pha* biosynthesis genes and their regulations will be helpful to develop new, integrated strategies for cost-effective production.

Keywords: medium-chain-length polyhydroxyalkanoate (mcl-PHA); alginate; biosurfactants; biopolymer; *Pseudomonas*; blends; film

1. Introduction

Polyhydroxyalkanoates (PHAs) are microbial polyesters synthesized by both Gram-negative and Gram-positive eubacteria, and an increasing number of archaea isolated from environmentally extreme habitats, to increase their survival and competition in environments where carbon and energy sources are limited, such as soil and rhizosphere [1–3].

Based on their repeat unit composition, the up to 150 different PHA structures identified so far [4] are classified mainly in two distinct groups: (i) short chain length (scl) PHAs where the repeat units are hydroxy fatty acids (HFAs) of 3–5 carbon chain length (C3–C5); and (ii) medium chain length (mcl) PHAs with repeat units of C6–14. In general, scl-PHAs are crystalline polymers with a fragile, rigid structure, whereas mcl-PHAs are amorphous thermoplastics, which have various degrees of crystallinity as well as elastomeric and adhesive properties [5]. Less common and least studied are long chain length (lcl) PHAs, constituted of monomers with more than 14 carbon atoms.

Thanks to two metabolic pathways based on the degradation of aliphatic carbon sources or *de novo* synthesis of fatty acids from unrelated carbon sources, *Pseudomonas* species included in the rRNA homology group I are among the most important producers of PHA [6–9]. Historically, fatty acids

have been the preferred substrate for the microbial synthesis of mcl-PHA. Glucose, gluconate or ethanol, as well soy molasses [10], biodiesel co-product stream [11] and glycerol [12,13], have been successfully used. The fatty acyl composition of the substrate reflects the repeat unit composition of biopolymers [14]. Biodiesel glycerol has been recognized as a suitable and cost attractive substrate for PHA production, and therefore constitutes the main focus of this review [15,16].

Medium chain length-PHAs in *Pseudomonas* bacteria were first detected in *P. oleovorans* [17] and later in a variety of *Pseudomonas* [10]. *Pseudomonas*-PHAs are biodegradable, non-toxic and biocompatible and can be produced using a wide range of carbon sources. In fact, there has been considerable research exploring their potential in medical devices, foods, agriculture and consumer products [18,19]. Their elastic and flexibility properties improve the processability and mechanical properties of blends with other biodegradable polymers [20–22]. Of the various species tested worldwide, *P. aeruginosa*, *P. putida*, *P. resinovorans*, *P. mendocina*, and *P. chlororaphis* are the most extensively studied to clarify the metabolic processes of the production of PHA and to enhance the bioconversion efficiency [3,23].

This review focuses on the two taxonomically related Gram-negative rod ubiquitous bacteria, *P. corrugata* and the strictly related *P. mediterranea*, which cause disease on several crop species [24] and can produce an arsenal of secondary metabolites [25]. Among them, are biosurfactants (BSs) [26] as well as poly-mannuronic acid alginate [27], bioactive cyclic lipopeptides (CLPs), such as cormycin A and corpeptins [28–30], and a lipopeptide siderophore, corrugatin [31].

These bacteria produce different cellular mcl-PHAs and extracellular products, on waste fried edible oils, biodiesel glycerol and high-grade glycerol [13,32,33]. Selected *P. corrugata* strains produce intracellular mcl-PHA with a molecular weight of 120–150 kDa on waste edible oils, whereas strains of *P. mediterranea* generate a distinctive filmable PHA around 55–65 kDa on high-grade and partially refined biodiesel glycerol. Extracellular products, such as biosurfactants, exopolysaccharides (EPS, mostly alginate) and bioactive molecules, accumulate in the supernatant during the bioconversion process. Genome analysis of nine *P. corrugata* and *P. mediterranea* strains has helped to develop molecular and genetic investigations to enhance productivity [25].

2. Production of mcl-PHA and Extracellular Products

The first strain of *P. corrugata* investigated for its capacity to convert triacylglycerols to produce mcl-PHA was strain 388 [7,14,34]. The positive results led to the screening of different carbon sources of 56 strains of *P. corrugata* and 21 strains of its closely related *P. mediterranea* [9]. Flask-scale tests, carried out on related and unrelated carbon sources, have been reported [9,13,32–34].

Subsequently, some strains of *P. corrugata* producing lipase have been reported as being able to bioconvert waste exhausted fried edible oils, from a licensed collector, in mcl-PHAs [9,32]. One of these strains, namely *P. corrugata A1* (DSM 18227) (hereafter *Pco A1*), obtained through culturing *P. corrugata* CFBP5454 in E* medium with triolein, helped to patent a fermentation process validated on a 5000 L fermenter [35]. This increased the productivity of the process from 2.90 g/L up to 26 g/L of dry cell weight with 38% of PHA [32,35].

To overcome the variable composition of licensed exhausted edible oils and the difficulty in collecting adequate stocks for industrial production, several sources of glycerol have been extensively tested to screen many strains of *P. corrugata* and *P. mediterranea*. Three of them, *Pco 388*, *Pco A1* and *P. mediterranea 9.1* (deposited as CFBP5447, hereafter *Pme 9.1*), have been selected to study the bioconversion processes exploiting commercial high-grade glycerol (≥99%, pH 7) and biodiesel glycerol obtained from the transesterification of rapeseed oils (*Brassica carenata* and *B. napus*). Crude biodiesel (15% glycerol), oil free (40%) and partially refined glycerol (87.5%) performed differently from commercial high grade glycerol in terms of yield, composition and properties of the mcl-PHA and extracellular products. It has also been highlighted that some apparently small differences in the carbon sources may have a large impact, and that the genetic and metabolic system of the strain are key to the bioconversion process [11–13,33].

P. mediterranea 9.1 reached a production of 2.93 g/L of mcl-PHA on 2% crude biodiesel glycerol with a PHA/cell dry weight ratio >60%, whereas on high-grade glycerol it yielded 0.81 g/L (Table 1) [33]. In parallel tests, *P. corrugata* A.1 produced 1.8 g/L of PHA with 51.5% in cultivation for 72 h [33]. The productivity of batch fermentations on E* medium with the addition of 1% or 2% of glycerol showed only minor differences, but decreased yields and mass molecular weight (Mw) were observed when 5% of glycerol was added. The same results were reported by Ashby et al. [11], in the case of Mw of PHB produced by *P. oleovorans* and mcl-PHAs accumulated by *P. corrugata 388*.

Another flask-scale experiment, carried out with *Pme 9.1* growing on a medium containing 2% refined glycerol, yielded 3.3 g/L in cell dry weight (CDW) after cultivation for 48 h, with a PHA/CDW ratio close to 18% (Table 1) [13]. No significant changes were observed after 60 and 72 h of cultivation. Soxhlet extraction of biomass with acetone produced 0.75 g/L of a thin opalescent film of crude mcl-PHA. Parallel fermentation carried out with partially refined glycerol (87.5%) obtained from the esterification of *B. napus* oil produced 3.1 g/L of biomass and 0.5 g/L of raw PHA (PHA/CDW = 16.5%) [13].

Besides the different conversion efficiencies, other chemical and technological properties of the PHA were even more relevant. Regardless of the carbon source, both strains of *P. corrugata* (*388* and *A1*) produced very similar mcl-PHA elastomers, whereas PHA obtained from *P. mediterranea* 9.1 grown on refined biodiesel glycerol, generated a transparent filmable polymer with a low molecular weight (56,000 Da) and very distinctive characteristics (Figure 1) [13].

Figure 1. Crude PHA film (**A**) and transparent PHA film obtained after floating a toluene solution on a water surface (**B**) achieved from *Pseudomonas mediterranea* 9.1 using refined glycerol as carbon source (Figure 1B courtesy of Copyright Elsevier from [13]).

The extracellular biosurfactants released by these strains during the bioconversion process showed their dependence on the carbon sources, and the highest yields were reached much later than the PHA. *Pme 9.1* grown on crude glycerol (15%) obtained from *Brassica* spp. seed oil, was able to recover up to 14 g/L of surfactants with E24 (emulsification index) 54%, via chloroform:methanol (2:1) [36]. The highest accumulation occurred after 96–144 h. At the early stationary phase (48 h) *P. mediterranea 9.1* yielded 6.9 g/L of partially purified EPS, 17-fold higher than in *Pco A1* (0.39 g/L). PHA production was slightly higher in *Pco A1* than in *Pme 9.1* (respectively 0.92 g/L and 0.52 g/L) [37].

Table 1. Cell dry weight and raw PHA percentage obtained through bioconversion of different carbon sources by selected strains of *Pseudomonas mediterranea* and *P. corrugata*.

Carbon Source	Grade	% V:V	Time (h) [1]	*P. mediterranea* 9.1		*P. corrugata* A1		*P. corrugata* 388		References
				CDW (g/L)	Raw PHA (%)	CDW (g/L)	Raw PHA (%)	CDW (g/L)	Raw PHA (%)	
Glycerol	15% ≥99%	1	72	3.4 3	50.2 25.3	4.7 3.5	50 29.4	4 4.2	28.5 18.7	[33]
	15% ≥99%	2	72	4.8 3.2	61.6 26.1	3.5 3.4	51.5 30.2	3.8 3.6	33.6 15.7	
	15% ≥99%	5	72	4.2 3.3	38 21.5	4.1 4.1	48.5 22.1	3.2 2.8	32.1 14.3	
Glycerol	87.5% ≥99%	2	48	3.1 3.3	16.5 18					[13]
Glycerol	≥99%	2	66	2.9	17.9	3.1	29.4			[37]
Glycerol	≥99%	2	66	3.6 [2]	38.8 [2]					[38]
Glucose Oleic acid	≥99% ≥99%	0.5	72					1.5 1.6	31.3 61.8	[34]
Oleic acid Glucose	≥99% ≥99%	2	72 48					3.1 1.3	24 2	[39]

[1] time of cultivation; [2] this specific test was carried out with a modified strain of *P.mediterranea 9.1 VVC1GI.*

3. Conversion Process and Recovery

In order to establish standard and suitable protocols to scale up the production of PHAs, many strategies have been investigated using batch and fed-batch processes in flasks and low-medium volume fermenters (3–30 L). Fed-batch fermentation has always been shown to be more productive than the batch mode, as reported for *Cupriavidus* sp. [40].

A fed-batch cultivation has also been used in a process of glycerol conversion by growing *P. mediterranea 9.1* in a substrate with 2% glycerol. The cultivation was conducted in a 30 L bioreactor, 30 °C, pH 7.0, and dissolved oxygen maintained at 20% saturation, using E* medium (pH 7.0) containing 5.8 g/L K_2HPO_4, 3.7 g/L KH_2PO_4, 10 mL/L $MgSO_4$ 0.1 M, supplemented with 1 mL/L of a microelement solution, with the addition of 2% glycerol (1% at the start, and 1% after 24 h) [13,33].

The biomass obtained has been routinely harvested by centrifugation, washed with saline solution and lyophilized. The extraction of the PHA using acetone [41] in an automatic Soxhlet was found to be more effective than chloroform extraction and less impactful for the environment. Treatments with mild alkaline solution [42] or maceration, attempted considering the potential use of mcl-PHA in the biomedical field, have yielded a lower recovery of products.

The analysis of PHA composition was carried out by gas chromatography/mass spectrometry (GC/MS) of the 3-hydroxymethylesters, after the removal of all the residual free glycerol [13]. Overall, different approaches have been evaluated to reduce the very high production costs by increasing the yield or by recovering both the PHA and extracellular products simultaneously from the fermentation process. The addition of either meat or yeast extracts at 0.1% to crude glycerol or glucose eliminated the prolonged lag-phase (5–12 h) [43].

Rizzo et al. [44] showed that adding 5 mM glutamine as a co-feeder significantly increased the biomass and PHA production, inducing the early expression of *phaC1* and *phaC2* genes. This was due to the improvement in the specific growth rate and cell metabolic activity, and to the enhanced uptake of the unrelated (glycerol and glucose) and related (sodium octanoate) carbon sources.

An integrated process for the bioconversion of crude biodiesel glycerol to simultaneously produce biosurfactants and PHAs by *Pme 9.1*, has also been established by applying a mathematical mechanistic model to define nutritional requirements, as well as pH and temperature, which mutually influenced PHA and BSs production within a narrow range of variation [43]. Surface response methodology analysis showed that, after 72 h, up to 1.1 g/L of crude PHA and 0.72 g/L of biosurfactants were recovered. On the other hand, the respective best single yields were obtained after 48 h for PHA (60% of CDW) and 96 h for BSs (0.8 g/L) [43].

4. Composition and Technological Properties of mcl-PHA

GC/MS profiles of mcl-PHA were largely affected by the carbon source and bacteria species. PHAs obtained on waste food oils have been found to be very different from those obtained on glycerol, and different types of glycerol produced different mcl-PHAs [13,32].

GC/MS chromatograms of mcl-PHAs obtained by *Pco A1* and *Pme 9.1* on crude glycerol revealed similar profiles and technological properties, whereas substantial differences were observed with respect to those obtained on partially refined biodiesel glycerol and high-grade glycerol. They showed monomeric units of side chains from C12 to C19 in length on crude glycerol (15% glycerol), and from C5 to C16 on refined glycerol (≥99%) (Table 2) [33,45]. Interestingly, mcl-PHA produced by *Pme 9.1* on high-grade glycerol was less sticky and produced a thin film (Figure 1A) [33]. These properties have been shown to be associated with differences at transcriptomic level [37], and in the genetic organization of *pha* gene locus which affects *pha* polymerase gene expression, PHA composition, and granule morphology [39].

Other experiments on *Pme 9.1* have been conducted in Erlenmeyer flasks containing 500 mL volumes of E* medium (pH 7.0) with 2% high grade glycerol or a partially refined glycerol (87.5%) obtained from a biodiesel process of *Brassica napus* [13]. The polyesters obtained on high grade commercial glycerol highlighted a structure composed of six monomers, indicative of elastic and flexibility properties: 3-hydroxyhexanoate (C6), 3-hydroxyoctanoate (C8), 3-hydroxydeca-noate (C10), 3-hydroxydodecanoate (C12), cis 3-hydroxydodec-5-enoate (C12:1Δ^5), and cis 3-hydroxydodec-6-enoate (C12:1Δ^6). The molecular weight (Mw) was 55,480 Da and polydispersity index (PDI = Mw/Mn) was 1.34 (Table 2). On the other hand, PHA obtained from glycerol 87.5% had a small variation in monomeric composition, a Mw of 63,200 Da, and a PDI of 1.38. Tsuge et al. [46] also observed that a higher glycerol concentration induced a considerable reduction in the molecular mass of PHA, caused by a termination of the PhaC polymerization activity. The NMR spectra and MALDI-TOF data were almost identical regardless of the glycerol grade, but different in intensity. The degradation temperature started at 230 °C, higher than the melting temperatures, with a volatilization rate of about −40%/min.

Table 2. Molecular weight and monomer composition of PHAs obtained in different bioconversion processes of different carbon sources by *Pseudomonas corrugata* and *P. mediterranea*.

Strain	Carbon Source	Grade	% V:V	Time (h) [1]	Mw (kDa)	PDI	Molar Composition (mol %)								Reference
							C6	C8	C10	C12:0	C12:1	C12:0	C14	C14:1	
Pme 9.1	Waste fried oil						2	34	44	14			5		Pappalardo et al., unpublished
	Glycerol	80%	2				1	7	71	8	13		1		
	Glycerol	40%	2				1	15	43	11	7		24		
	Glycerol	≥99%	2	48	55.5	1.34	4.2	17.0	60.8	1.1	11.2	5.7	-	-	[13]
		87.5%			63.2	1.38	0.1	9.3	66.6	1.5	14.8	7.7	-	-	
	Glycerol	≥99%	2	66			4	17	60	7	12		0.4		[37]
Pme 9.1 VVC1GI	Glycerol	≥99%						0.9	13.5	57.5	12.8	11.8		3.7	[38]
Pco A1	Glucose		0.5	72	125.8	2.4	2	14	52	11	17		0.4	3.6	[47]
	Oleic acid				159.0	1.5	10	48	28	8				6	
	Na octanoate				183.2	2.1	11	82	7						
	Glycerol	≥99%	2	66			2	12	53	14	17		5		[37]
Pco 388	Oleic acid		0.5	72	735	4.1		47	24.5					16.5	[8]
	Glucose		0.5	72	nd		2	19	56	11			2	9	[34]
	Oleic acid				nd		5	37	33	12			2	12	
	Na octanoate		0.5	168	114	1.8	7	82	11						[47]
	Oleic acid		2	-			5	54	20	5			15		[39]
	Glucose			-			2	28	35	9	14		9		

[1] time of cultivation.

Drop casting a toluene solution of polymers in Petri dishes resulted in quite different films, depending on the carbon source used to produce the PHA (Figure 1B). The PHA obtained on

high-grade glycerol produced an optically transparent film with a UV–vis absorption spectrum that was above the 800–350 nm range, comparable to the polyester film used for laser printer transparency.

The mechanical proprieties (tensile strength, Young's modulus and elongation at break of both PHAs) were not substantially affected by the different purities of the glycerol grade (87.5% and ≥99%). All these characteristics make the PHA obtained from *P. mediterranea 9.1* on glycerol quite different to most mcl-PHAs produced from bacteria of the same phylogenetic group.

5. Evaluation of Mixed Blends and Coatings

The distinctive characteristics of a mcl-PHA obtained from *Pme 9.1* grown on glycerol led to the investigation of the processability of blends with polylactide acid (PLA) to improve the mechanical and gas/vapors barrier properties of PLA [48]. Rheological tests indicated a significant increase in the elongation at break, while the elastic modulus was significantly lower only at higher contents of PHA. This suggests that the PHA macromolecules exert both a plasticization and lubricant action, which enable the PLA macromolecules subjected to solid deformation to slide more efficiently [48].

Preliminary investigation of blends of polyhydroxybutyrate (PHB) and a glycerol mcl-PHA obtained from *B. napus* oil showed an increase in crystallization temperature and a small increase in elongation at break, but at low concentrations of PHA (5%) the blend revealed some spaces between the two polymers.

Blends of mcl-PHA obtained from *Pco A1* on exhausted edible oils with Mater-Bi ZI01U/C polymers have poorly improved the processability of blends prepared by compression [22]. Soil mulching tests of paper sheets coated with blends based on PHA suggested some positive effects of coating. However, the expensive costs, as well the difficulty to obtain standardized exhausted edible oils as a carbon source, have discouraged further research [49,50].

6. *P. corrugata* and *P. mediterranea* PHA Locus

Genomic studies which investigated potential correlations between the phenotype and genotype of *Pco 388*, *Pco A1* and *Pme 9.1* have shown that, similarly to other *Pseudomonas*, the three strains have a class II PHA genetic system consisting of two synthase genes (*phaC1*, *phaC2*), separated by a gene coding for the depolymerization of PHA (*phaZ*) [8,9,23]. This genetic system allows *Pseudomonas* strains to utilize medium-chain-length (mcl) monomers (C6–C14), whereas class I, III and IV systems polymerize short-chain-length (scl) monomers (C3–C5) [6].

Sequence analysis of the *pha* locus revealed that the strains *Pco A1* (AY910767), *Pmed 9.1* (AY910768) and *Pco 388* (EF067339) share a high homology at nucleotide (93–95%) and amino acid levels (96–98%) [39, 51,52]. An additional 121 bp in the *phaC1–phaZ* intergenic region containing a predicted strong hairpin structure were present in both strains *388* and *A1* of *P. corrugata*, but not in *P. mediterranea* [39]. According to the authors, in *Pco A1* and *388* strains this additional sequence likely acts as a rho-independent terminator for the transcriptional terminator of *phaC1*, which would appear to be responsible for the slight variation in the PHA composition and granule organization [39].

Subsequently, genome analysis of strains *Pco A1* (ATKI01000000) and *Pme 9.1* (AUPB01000000) enabled the six genes of the entire *pha* locus to be studied (*phaC1*, *phaZ*, *phaC2*, *phaD*, *PhaF*, *PhaI*) [53,54]. Genome mining also identified gene coding for enzymes involved in β-oxidation (*fad*), fatty acid *de novo* synthesis (*fab*), and mcl-PHA precursor availability (*phaG* and *phaJ*) [53,54]. Pfam search domain and Blastp analysis on the *glp* operon, responsible for glycerol catabolism, revealed that both *P. corrugata* and *P. mediterranea* lack the *glpF* gene, coding for the glycerol uptake facilitator protein [53]. This condition had already been verified in all the *Pco* and *Pme* strains sequenced, which explains the prolonged lag growth phase observed during *P. mediterranea 9.1* growth with glycerol as the sole carbon source [25,55].

7. Transcriptional Regulation during PHA Production

To improve the knowledge about PHA biosynthesis genes and their regulations, helpful to increase mcl-PHAs production and also to obtain new, tailor-made polymers [6], regulatory mechanisms during

PHA accumulation have been investigated in *Pco A1*, *Pco 388* and *Pme 9.1* through different gene expression studies and full transcriptome analysis.

7.1. Expression of phaC1 and phaC2 under Different Carbon Sources

Preliminary studies on the transcriptional levels of *phaC1* and *phaC2* genes in *Pco 388* and *Pco A1* showed an up-regulation of *phaC1* in cultures with oleic acid as the sole carbon source (Table 3) [47]. On the other hand, both *phaC1* and *phaC2* were induced in cultures with glucose or sodium octanoate [47]. The significant correlation between PHA production and *phaC1*/*phaC2* expression suggested at least two distinct networks for the regulation of the two PHA polymerases genes, and that a putative promoter(s) is likely present upstream of *phaC2*. In addition, the lack of polycistronic transcripts under any culture conditions indicated that *phaC1* and *phaC2* were not co-transcribed (Table 3) [47].

Table 3. Gene expression detected in *P. corrugata* and *P. mediterranea* strains during mcl-PHA biosynthesis on different carbon sources.

Bacterial Strain	Carbon Source	% V/V	Time (h)	Detection Method	*PhaC1*	*PhaC2*	*PhaI*	*Alg* Genes	Operon	Reference
Pco 388	Oleic acid	2	48	Real-time PCR [1]	1.2	1.4	nt	nt	nt	[39]
Pco 388 clone XI 32-1					6.6	4.7	nt	nt	nt	
Pco 388 clone XI 32-4					7.0	5.4	nt	nt	nt	
Pco 388	Glucose	2			5.6	No change	nt	nt	nt	
Pco 388 clone XI 32-1					6.3	No change	nt	nt	nt	
Pco 388 clone XI 32-4					8.2	No change	nt	nt	nt	
Pco A1	Oleic acid	0.5	48 72	Real-time PCR [1]	6.8 10.5	No change	nt	nt	NO	[47]
Pco 388			48 72		2.7 2	No change	nt	nt	NO	
Pco A1	Glucose	2	72		6.2	3.5	nt	nt	NO	
Pco 388			72		3.8	3	nt	nt	NO	
Pme 9.1	Glycerol	2	24 48	β-gal [2]	420 U 300 U	340 U 400 U	2200 U 7000 U	nt	*PhaC1ZC2D* *PhaIF*	[56]
Pme 9.1 VVD (*phaD*-)			24 48	β-gal	140 U 300 U	350 U 400 U	45 U 45 U	nt	*PhaC1ZC2D* *PhaIF*	
Pme 9.1	Glycerol	2	48	RNA-Seq [3]	No change	No change	No change	5.53–2.32	nt	[37]
Pco A1			48	RNA-Seq	No change	No change	No change		nt	

[1] The relative quantification was performed by comparing ΔCt (i.e., Ct of the 16S rRNA housekeeping gene subtracted to the Ct of the target gene). The ΔCt value of the control sample (time 0) was used as the calibrator and fold-activation was calculated by the expression: $2^{-\Delta\Delta Ct}$. [2] β–galactosidase activities detected by transcriptional fusion plasmids for *phaC1*, *phaC2*, and *phaI* promoter regions based on the pMP220 promoter probe vector and expressed as Miller units. [3] Pairwise comparison of mRNA levels analysis, using the *Pme 9.1* sample as a reference (log2 fold change ≥ 2 and *p*-value ≤ 0.05).

Parallel studies showed that, in *Pco 388*, the *phaC1–phaZ* intergenic region plays an important but unclear role in the regulation of the carbon source-dependent expression of *phaC1* and *phaC2* genes [39]. Derivative mutants XI 32-1 and XI 32-4 of this strain (obtained by replacing the *phaC1–phaZ* intergenic region with a kanamycin resistance gene), showed a significant increase in *phaC1* and *phaC2* expression when grown for 48 h with oleic acid, but not with glucose. In addition, the wild type strain produced only a few large PHA inclusion bodies when grown with oleic acid, whereas the mutants showed numerous smaller PHA granules that line the periphery of the cells, as result of phasin activities [3,39]. A high content of the monounsaturated 3-hydroxydodecanoate as a repeat unit monomer was observed in the PHA of the mutant strains [39].

Diversely, the study of the promoter activity of *pha* genes in *Pme 9.1* grown on high-grade glycerol, revealed that the upstream regions of *phaC1* (PC1) and *phaI* genes (PI) are the most active [56]. PC1 is responsible for the *phaC1ZC2D* polycistronic unit transcription (Table 3). On the other hand, PI regulates the *phaIF* operons, as confirmed by the presence of three and two putative rho independent terminators, respectively located downstream of *phaD* and *phaF* [56]. In turn, PI and PC1 are controlled

by PhaD, which acts as a transcriptional activator, as shown by the reduced promoter activities in the *phaD*- mutant [55]. Similar results were observed in *P. putida* KT2442 [23,57].

7.2. Transcriptome Analysis on Glycerol-Grown Strains

The transcriptional profiles of *Pco A1* and *Pme 9.1* growing on a substrate with 2% of high-grade glycerol under inorganic nutrient-limited conditions were investigated at the early stationary phase of the bioconversion into mcl-PHAs [37]. RNA-seq analysis revealed that in *P. mediterranea*, 175 genes were significantly upregulated and 217 downregulated, compared to *P. corrugata.* The genes responsible for stress response, central and peripheral metabolic routes and transcription factors involved in mcl-PHA biosynthesis, made up 39% of the genes differently transcribed by the two bacteria. Nonetheless, among the genes directly involved in PHA biosynthesis, slight differences were observed only in *phaZ* depolymerase and *phaG* transacylase genes (Table 3). Weak differences occurred in the expression levels of genes that are crucial for glycerol catabolism and pyruvate metabolism, transcriptionally downregulated, and fatty acid *de novo* biosynthesis pathways.

Interestingly, a significantly increased expression of 21 genes involved in alginate exopolysaccharide production was observed in *Pme 9.1* compared to *Pco A1* (Table 3), related to a 17-fold higher production of EPS (6.9 g/L compared to 0.39 g/L). A simultaneous production of PHA and alginate has been reported in some *P. mendocina* strains [58,59]. The increased EPS production, associated with the different transcriptome profiling between the two bacteria, suggests competition for the acetyl-CoA precursor amongst PHA and alginate metabolic pathways. Further studies on *P. corrugata A1* showed that regulation of alginate production is controlled by quorum sensing and the RfiA regulator [60].

8. Genetically Modified Bacteria to Improve the Production of mcl-PHAs

Two different approaches have been made to evaluate the feasibility of improving the efficiency of the conversion by using genetically modified-*Escherichia coli* and *P. mediterranea*.

Cloning of *pha* synthases genes of *Pco A.1* and *Pme 9.1* in *Escherichia coli,* a well-known organism in the research on PHA biosynthesis, yielded 2%–4% of PHA/CDW on sodium decanoate [61].

In a second approach, additional copies of *phaC1*, *phaG* and *phaI* genes, cloned in two plasmids under the control of strong promoters, were transferred into *Pme 9.1* [38]. When grown on high-grade glycerol, the modified *Pme VVC1GI* showed a higher cell fluorescence than WT, due to the presence of larger granules (Figure 2). It also showed a 40% increase in the cellular accumulation of crude PHA and a better PHA/CDW ratio (1.4 g/L, 38.8%), whereas the WT strain produced 1 g/L of PHA (23%) (Table 1). Biomass yield was 3.6 g/L in *VVC1GI* and 4.2 g/L in WT [38]. GC/MS analysis showed that the PHA structure was composed of six monomers, like PHA produced by the WT, although there were some differences in the ratio between C12 and C12:1 (12.8:11.8 in strain *VVC1GI* and 6:12 in Wt) (Table 2).

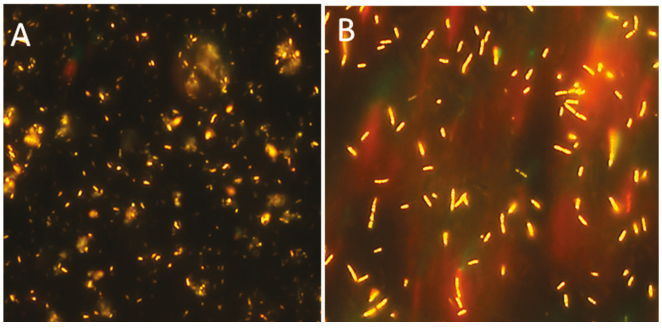

Figure 2. Fluorescent granules of PHA after Nile red-staining of *Pseudomonas mediterranea 9.1* wild-type strain (**A**) and *VVC1GI* recombinant strain (**B**) grown on high-grade glycerol (≥99%) as carbon source and limited nitrogen condition after 66 h of incubation.

9. Conclusions

Despite the fact that the PHAs market is still very small, the worldwide focus on the development of bio-polymers highlights that one day polyhydroxyalkanoates will replace some petroleum-based plastics. *Pseudomonas* species are a potential cell factory for their production [3]. Some strains of *P. corrugata* and its related *P. mediterranea* are able to convert different carbon sources and provide interesting mcl-PHA and co-products. They are naturally present in the soil and produce valuable extracellular co-products [37,43].

A manageable mcl-PHA film, unlike other mcl-PHAs reported to date, can be obtained by *P. mediterranea 9.1*. Although the yields are currently not particularly viable, their distinctive characteristics suggest a potential application as a softener in (bio) polymeric blends, for food packaging or medical devices. The unsaturated double bonds in the side chains could be used to enhance its properties and/or to help extend its applications to other biomaterials for food packaging or biomedicine [13].

P. mediterranea 9.1 also produces high-quality extracellular products (above all alginate) on a proper medium, which is very promising for high-level applications and which may orient further investigation towards an efficient co-production of cellular mcl-PHA and extracellular biosurfactants, EPS and other bioactive molecules [43]. These results and those available for other systems highlight the potential of such integrated microbial conversion processes [62]. Further top strategies are required to find solutions for the industrial production of such compounds and new ones.

Pioneering work on other PHA producers *Pseudomonas*, such as on expanding the number of inexpensive carbon sources [63], increasing the productivity [64,65] or making the PHA deposition extracellular [66], highlight the potential for successful future investments in this sector. In the meantime, given that robust strains are needed to reduce the high production costs, using genetic engineering and metabolic studies on these two bacteria should focus on developing over-producer strains of mcl-PHA, as well as the co-production of other valuable products, such as EPS and biosurfactants.

Author Contributions: The authors have several years of research experience on *Pseudomonas corrugata* and *P. mediterranea* and their bioconversion of waste oils and biodiesel co-products stream, mostly based on the long term projects "Biopolimeri" and "Polybioplast" (acknowledged below). All authors have contributed the writing and editing of the manuscript and approved the manuscript.

Funding: This paper has been prepared without any funding.

Acknowledgments: The results presented were partly generated by the projects MIUR PON 2000–2006 N.12842 "Biopolimeri" and MIUR PON 2007-2013N. 01 01377 "Polybioplast", both co-funded by EU.

Conflicts of Interest: The authors declare no conflict of interest.

References

1. Wu, Q.; Sun, S.Q.; Yu, P.H.F.; Chen, A.X.Z.; Chen, G.Q. Environmental dependence of microbial synthesis of polyhydroxyalkanoates. *Acta Polym. Sin.* **2000**, *6*, 751–756.
2. Kadouri, D.; Jurkevitch, E.; Okon, Y.; Castro-Sowinski, S. Ecological and agricultural significance of bacterial polyhydroxyalkanoates. *Crit. Rev. Microbiol.* **2005**, *31*, 55–56. [CrossRef]
3. Mozejko-Ciesielska, J.; Szacherska, K.; Marciniak, P. *Pseudomonas* species as producers of eco-friendly polyhydroxyalkanoates. *J. Polym. Environ.* **2019**, *27*, 1151–1166. [CrossRef]
4. Chen, G.Q. A microbial polyhydroxyalkanoates (PHA) based bio- and materials industry. *Chem. Soc. Rev.* **2009**, *38*, 2434–2446. [CrossRef]
5. Zinn, M.; Witholt, B.; Egli, T. Occurrence, synthesis and medical application of bacterial polyhydroxyalkanoate. *Adv. Drug Del. Rev.* **2001**, *53*, 5–21. [CrossRef]
6. Możejko-Ciesielska, J.; Kiewisz, R. Bacterial polyhydroxyalkanoates: Still fabulous? *Microbiol. Res.* **2016**, *192*, 271–282. [CrossRef] [PubMed]
7. Kessler, B.; Palleroni, N. Taxonomic implications of synthesis of poly-beta-hydroxybutyrate and other poly-beta-hydroxyalkanoates by aerobic pseudomonads. *Int. J. Syst. Evol. Microbiol.* **2000**, *50*, 711–713. [CrossRef]

8. Solaiman, D.K.Y.; Ashby, R.D.; Foglia, T.A. Rapid and specific identification of medium-chain-length polyhydroxyalkanoate synthase gene by polymerase chain reaction. *Appl. Microbiol. Biotechnol.* **2000**, *53*, 690–694. [CrossRef]
9. Solaiman, D.K.Y.; Catara, V.; Greco, S. Poly(hydroxyalkanoate) synthase genotype and PHA production of *Pseudomonas corrugata* and *P. mediterranea*. *J. Ind. Microbiol. Biotechnol.* **2005**, *32*, 75–82. [CrossRef]
10. Solaiman, D.K.Y.; Ashby, R.D.; Foglia, T.A.; Marmer, W.N. Conversion of agricultural feedstockand coproducts into poly(hydroxyalkanoates). *Appl. Microbiol. Biotechnol.* **2006**, *71*, 783–789. [CrossRef]
11. Ashby, R.D.; Solaiman, D.K.Y.; Foglia, T.A. Bacterial poly(hydroxyalcanoate) polymer production from the biodiesel co-product stream. *J. Polym. Environ.* **2004**, *12*, 105–112. [CrossRef]
12. Ashby, R.D.; Solaiman, D.K.Y.; Foglia, T.A. Synthesis of short-/medium-chain-length poly(hydroxyalkanoate) blends by mixed culture fermentation of glycerol. *Biomacromolecules* **2005**, *6*, 2106–2112. [CrossRef] [PubMed]
13. Pappalardo, F.; Fragalà, M.; Mineo, P.G.; Damigella, A.; Catara, A.F.; Palmeri, R.; Rescifina, A. Production of filmable medium-chain-length polyhydroxyalkanoates produced from glycerol by *P. mediterranea*. *Int. J. Biol. Macromol.* **2014**, *65*, 89–96. [CrossRef] [PubMed]
14. Ashby, R.D.; Foglia, T.A. Poly(hydroxyalkanoates) biosynthesis from triglyceride substrates. *Appl. Microbiol. Biotechnol.* **1998**, *49*, 431–437. [CrossRef]
15. Da Silva, G.P.; Mack, M.; Contiero, J. Glycerol: A promising and abundant carbon source for industrial microbiology. *Biotechnol. Adv.* **2009**, *27*, 30–39. [CrossRef]
16. Koller, M.; Marsalek, L. Principles of Glycerol-Based Polyhydroxyalkanoate Production. *Appl. Food Biotechnol.* **2015**, *2*, 3–10.
17. De Smet, M.J.; Eggink, G.; Witholt, B.; Kingma, J.; Wynberg, H. Characterization of intracellular inclusions formed by *Pseudomonas oleovorans* during growth on octane. *J. Bacteriol.* **1983**, *154*, 870–878.
18. Panith, N.; Assavanig, A.; Lertsiri, S.; Bergkvist, M.; Surarit, R.; Niamsiri, N. Development of tunable biodegradable polyhydroxyalkanoates microspheres for controlled delivery of tetracycline for treating periodontal disease. *J. Appl. Polym. Sci.* **2016**, *133*, 44128–44140. [CrossRef]
19. Zhang, J.; Shishatskaya, E.I.; Volova, T.G.; da Silva, L.F.; Chen, G.Q. Polyhydroxyalkanoates (PHA) for therapeutic applications. *Mater. Sci. Eng. C* **2018**, *86*, 144–150. [CrossRef]
20. Basnett, P.; Ching, K.Y.; Stolz, M.; Knowles, J.C.; Boccaccini, A.R.; Smith, C.; Locke, I.C.; Keshavarz, T.; Roy, I. Novel poly(3-hydroxyoctanoate)/poly(3-hydroxybutyrate) blends for medical applications. *React. Funct. Polym.* **2013**, *73*, 1340–1348. [CrossRef]
21. Takagi, Y.; Yasuda, R.; Yamaoka, M.; Yamane, T. Morphologies and mechanical properties of polylactide blends with medium chain length poly(3-hydroxyalkanoate) and chemically modified poly(3-hydroxyalkanoate). *J. Appl. Polym. Sci.* **2004**, *93*, 2363–2369. [CrossRef]
22. Scaffaro, R.; Dintcheva, N.T.; Marino, R.; La Mantia, F.P. Processing and properties of biopolymer/polyhydroxyalkanoates blends. *J. Polym. Environ.* **2012**, *20*, 267–272. [CrossRef]
23. Prieto, A.; Escapa, I.F.; Martínez, V.; Dinjaski, N.; Herencias, C.; de la Peña, F.; Tarazona, N.; Revelles, O. A holistic view of polyhydroxyalkanoate metabolism in *Pseudomonas putida*. *Environ. Microbiol.* **2016**, *18*, 341–357. [CrossRef] [PubMed]
24. Catara, V. *Pseudomonas corrugata*: Plant pathogen and/or biological resource? *Mol. Plant. Pathol.* **2007**, *8*, 233–244. [CrossRef]
25. Trantas, E.A.; Licciardello, G.; Almeida, N.F.; Witek, K.; Strano, C.P.; Duxbury, Z.; Ververidis, F.; Goumas, D.E.; Jones, J.D.G.; Guttman, D.S.; et al. Comparative genomic analysis of multiple strains of two unusual plant pathogens: *Pseudomonas corrugata* and *Pseudomonas mediterranea*. *Front. Microbiol.* **2015**, *6*, 811. [CrossRef] [PubMed]
26. Corsaro, N.M.; Piaz, F.D.; Lanzetta, R.; Naldi, T.; Parrilli, M. Structure of Lipid A from *Pseudomonas corrugata* by electrospray ionisation quadrupole time-of-flight tandem mass spectrometry. *Rapid Commun. Mass Spectrom.* **2004**, *18*, 853–858. [CrossRef]
27. Fett, W.F.; Cescutti, P.; Wijey, C. Exopolysaccharides of the plant pathogens *Pseudomonas corrugata* and *Ps. flavescens* and the saprophyte *Ps. chlororaphis*. *J. Appl. Bacteriol.* **1996**, *81*, 181–187. [CrossRef]
28. Scaloni, A.; Dalla Serra, M.; Amodeo, P.; Mannina, L.; Vitale, R.M.; Segre, A.L.; Cruciani, O.; Lodovichetti, F.; Greco, M.L.; Fiore, A.; et al. Structure, conformation and biological activity of a novel lipodepsipeptide from *Pseudomonas corrugata*: Cormycin A. *Biochem. J.* **2004**, *384*, 25–36. [CrossRef]

29. Emanuele, M.C.; Scaloni, A.; Lavermicocca, P.; Jacobellis, N.S.; Camoni, L.; Di Giorgio, D.; Pucci, P.; Paci, M.; Segre, A.; Ballio, A. Corpeptins, new bioactive lipodepsipeptides from cultures of *Pseudomonas corrugata*. *FEBS Lett.* **1998**, *433*, 317–320. [CrossRef]
30. Strano, C.P.; Bella, P.; Licciardello, G.; Fiore, A.; Lo Piero, A.R.; Fogliano, V.; Venturi, V.; Catara, V. *Pseudomonas corrugata crpCDE* is part of the cyclic lipopeptide corpeptin biosynthetic gene cluster and is involved in bacterial virulence in tomato and in hypersensitive response in *Nicotiana benthamiana*. *Mol. Plant Pathol.* **2014**, *9*. [CrossRef]
31. Risse, D.; Beiderbeck, H.; Taraz, K.; Budzikiewicz, H.; Gustine, D. Bacterial constituents part LXXVII. Corrugatin, a lipopeptide siderophore from *Pseudomonas corrugata*. *Z. Naturforsch. C* **1998**, *53*, 295–304.
32. Alicata, R.; Ballistreri, A.; Catara, V.; Conte, E.; Di Silvestro, S.; Ferreri, A.; Greco, S.; Guglielmino, S.; Impallomeni, G.; La Porta, S.; et al. Used cooking oils as renewable source for polyhydroxyalkanoates production. In Proceedings of the 3th European Symposium on Biopolymers CIB-CSIC, Madrid, Spain, 24–25 November 2005; p. 35.
33. Palmeri, R.; Pappalardo, F.; Fragalà, M.; Tomasello, M.; Damigella, A.; Catara, A.F. Polyhydroxyalkanoates (PHAs) production through conversion of glycerol by selected strains of *Pseudomonas mediterranea* and *Pseudomonas corrugata*. *Chem. Eng. Trans.* **2012**, *27*, 121–126.
34. Solaiman, D.K.Y.; Ashby, R.D.; Foglia, T.A. Physiological characterization and genetic engineering of *Pseudomonas corrugata* for medium-chain-length polyhydroxyalkanoates synthesis from triacylglycerols. *Curr. Microbiol.* **2002**, *44*, 189–195. [CrossRef]
35. Bella, P.; Catara, A.; Catara, V.; Conte, E.; Di Silvestro, S.; Ferreri, A.; Greco, S.; Guglielmino, S.; Immirzi, B.; Licciardello, G.; et al. Fermentation Process for the Production of Polyhydroxyalkanoates and the Digestion of Cooked Oils by Strains of *Pseudomonas* Producing Lipase. Italian Industrial Patent No. RM2005A000190, 20 April 2005.
36. Samadi, N.; Abadian, N.; Akhavan, A.; Fazeli, M.R.; Tahzibi, A.; Jamalifar, H. Biosurfactant production by the strain isolated from contaminated soil. *J. Biol. Sci.* **2007**, *7*, 1266–1269.
37. Licciardello, G.; Ferraro, R.; Russo, M.; Strozzi, F.; Catara, A.F.; Bella, P.; Catara, V. Transcriptome analysis of *Pseudomonas mediterranea* and *P. corrugata* plant pathogens during accumulation of medium-chain-length PHAs by glycerol bioconversion. *New Biotechnol.* **2017**, *37*, 39–47. [CrossRef] [PubMed]
38. Licciardello, G.; Russo, M.; Pappalardo, F.; Fragalà, M.; Catara, A. Genetically Modified Bacteria Producing Mcl-PHAs. Italian Industrial Patent No.15MG37I, 12 May 2015.
39. Solaiman, D.K.Y.; Ashby, R.D.; Licciardello, G.; Catara, V. Genetic organization of pha gene locus affects phaC expression, poly(hydroxyalkanoate) composition and granule morphology in *Pseudomonas corrugata*. *J. Ind. Microb. Biotech.* **2008**, *35*, 111–120. [CrossRef] [PubMed]
40. Shantini, K.; Yahya, A.R.; Amirul, A.A. Influence of feeding and controlled dissolved oxygen level on the production of poly(3-hydroxybutyrate-co-3-hydroxyvalerate) copolymer by *Cupriavidus* sp. USMAA2-4 and its characterization. *Appl. Biochem. Biotechnol.* **2015**, *176*, 1315–1334. [CrossRef]
41. Jiang, X.; Ramsay, J.A.; Ramsay, B.A. Acetone extraction of mcl-PHA from *Pseudomonas putida* KT2440. *J. Microb. Methods* **2006**, *67*, 212–219. [CrossRef]
42. Koller, M.; Niebelschütz, H.; Braunegg, G. Strategies for recovery and purification of poly[(R)-3-hydroxyalkanoates] (PHA) biopolyesters from surrounding biomass. *Eng. Life Sci.* **2013**, *13*, 549–562. [CrossRef]
43. Nicolò, M.S.; Franco, D.; Camarda, V.; Gullace, R.; Rizzo, M.G.; Fragalà, M.; Licciardello, G.; Catara, A.F.; Guglielmino, S.P.P. Integrated microbial process for bioconversion of crude glycerol from biodiesel into biosurfactants and PHAs. *Chem. Eng. Trans.* **2014**, *38*, 187–192.
44. Rizzo, M.G.; Chines, V.; Franco, D.; Nicolò, M.S.; Guglielmino, S.P.P. The role of glutamine in *Pseudomonas mediterranea* in biotechnological processes. *New Biotechnol.* **2017**, *37*, 144–151. [CrossRef] [PubMed]
45. Fragalà, M.; Palmeri, R.; Ferro, G.; Damigella, A.; Pappalardo, F.; Catara, A.F. Production of mcl-PHAs by *Pseudomonas mediterranea* conversion of biodiesel-glycerol. In Proceedings of the European Symposium on Biopolymers, Lisbon, Portugal, 7–9 October 2013.
46. Tsuge, T. Fundamental factors determining the molecular weight of polyhydroxyalkanoate during biosynthesis. *Polym. J.* **2016**, *48*, 1051–1057. [CrossRef]

47. Conte, E.; Catara, V.; Greco, S.; Russo, M.; Alicata, R.; Strano, L.; Lombardo, A.; Di Silvestro, S.; Catara, A. Regulation of polyhydroxyalcanoate synthases (*phaC1* and *phaC2*) gene expression in *Pseudomonas corrugata*. *Appl. Microbiol. Biotechnol.* **2005**, *72*, 1054–1062. [CrossRef] [PubMed]
48. Botta, L.; Mistretta, M.C.; Palermo, S.; Fragalà, M.; Pappalardo, F. Characterization and processability of blends of polylactide acid with a new biodegradable medium-chain-length polyhydroxyalkanoate. *J. Polym. Environ.* **2015**, *23*, 478–486. [CrossRef]
49. Cascone, G.; D'Emilio, A.; Buccellato, E.; Mazzarella, R. New biodegradable materials for greenhouse soil mulching. *Acta Hortic.* **2008**, *801*, 283–290. [CrossRef]
50. Salemi, F.; Lamagna, G.; Coco, V.; Barone, L.G. Preparation and characterization of biodegradable paper coated with blends based on PHA. *Acta Hortic.* **2008**, *801*, 203–210. [CrossRef]
51. Catara, V.; Bella, P.; Greco, S.; Licciardello, G.; Pitman, A.; Arnold, D.L. Cloning and sequencing of *Pseudomonas corrugata* polyhydroxyalkanoates biosynthesis genes. In Proceedings of the National Biotechnology Congress (CNB7), Catania, Italy, 8–10 September 2004; p. 199.
52. Bella, P.; Licciardello, G.; Lombardo, A.; Pitman, A.; Arnold, D.L.; Solaiman, D.K.Y.; Catara, V. Cloning and sequencing of *Pseudomonas mediterranea* PHA locus. In Proceedings of the 4th European Symposium on Biopolymers, Kuşadası, Turkey, 2–4 October 2007; p. 131.
53. Licciardello, G.; Bella, P.; Devescovi, G.; Strano, C.P.; Catara, V. Draft genome sequence of *Pseudomonas mediterranea* strain CFBP 5447T, a producer of filmable medium-chain-length polyhydroxyalkanoates. *Genome Announc.* **2014**, *2*, e01260-14. [CrossRef]
54. Licciardello, G.; Jackson, R.W.; Bella, P.; Strano, C.P.; Catara, A.F.; Arnold, D.L.; Venturi, V.; Silby, M.W.; Catara, V. Draft genome sequence of *Pseudomonas corrugata*, a phytopathogenic bacterium with potential industrial applications. *J. Biotechnol.* **2014**, *17*, 65–66. [CrossRef]
55. Zachow, C.; Müller, H.; Laireiter, C.M.; Tilcher, R.; Berg, G. Complete genome sequence of *Pseudomonas corrugata* strain RM1-1-4, a stress protecting agent from the rhizosphere of an oilseed rape bait plant. *Stand. Genomic Sci.* **2017**, *12*, 66. [CrossRef]
56. Licciardello, G.; Devescovi, G.; Bella, P.; De Gregorio, C.; Catara, A.F.; Gugliemino, S.P.P.; Venturi, V.; Catara, V. Transcriptional analysis of pha genes in *Pseudomonas mediterranea* CFBP 5447 grown on glycerol. *Chem. Eng. Trans.* **2014**, *38*, 289–294.
57. De Eugenio, L.I.; Escapa, I.F.; Morales, V.; Dinjaski, N.; Galán, B.; García, J.L.; Prieto, M.A. The turnover of medium-chain-length polyhydroxyalkanoates in *Pseudomonas putida* KT2442 and the fundamental role of PhaZ depolymerase for the metabolic balance. *Environ. Microbiol.* **2010**, *12*, 207–221. [CrossRef] [PubMed]
58. Guo, W.; Song, C.; Kong, M.; Geng, W.; Wang, Y.; Wang, S. Simultaneous production and characterization of medium-chain-length polyhydroxyalkanoates and alginate oligosaccharides by *Pseudomonas mendocina* NK-01. *Appl. Microbiol. Biotechnol.* **2011**, *92*, 791–801. [CrossRef] [PubMed]
59. Chanasit, W.; Hodgson, B.; Sudesh, K.; Umsakul, K. Efficient production of polyhydroxyalkanoates (PHAs) from *Pseudomonas mendocina* PSU using a biodiesel liquid waste (BLW) as the sole carbon source. *Biosci. Biotechnol. Biochem.* **2016**, *80*, 1440–1450. [CrossRef] [PubMed]
60. Licciardello, G.; Caruso, A.; Bella, P.; Gheleri, R.; Strano, C.P.; Anzalone, A.; Trantas, E.A.; Sarris, P.F.; Almeida, N.F.; Catara, V. The LuxR regulators PcoR and RfiA co-regulate antimicrobial peptide and alginate production in Pseudomonas corrugata. *Front. Microbiol.* **2018**, *9*, 521. [CrossRef]
61. Lombardo, A.; Bella, P.; Licciardello, G.; Palmeri, R.; Catara, V.; Catara, A. Poly(hydroxyalkanoate) synthase genes in *Pseudomonads* strains, isolation and heterologous expression. *J. Biotechnol.* **2010**, *150*, 420–421. [CrossRef]
62. Hori, K.; Marsudi, S.; Unno, H. Simultaneous production of polyhydroxyalkanoates and rhamnolipids by *Pseudomonas aeruginosa*. *Biotechnol. Bioeng.* **2002**, *78*, 699–707. [CrossRef]
63. Wang, Q.; Tappei, R.C.; Zhu, C.; Nomura, T.C. Development of a new strategy for production of medium-chain-length polyhydroxyalkanoates by recombinant *Escherichia coli* via inexpensive non fatty acid feedstocks. *Appl. Environ. Microbiol.* **2012**, *78*, 519–527. [CrossRef]
64. Lopez-Cortes, A.; Lanz-Landazuri, A.; Garcia-Maldonado, J.Q. Screening and isolation of PHB-producing bacteria in a polluted marine microbial mat. *Microb. Ecol.* **2008**, *56*, 112–120. [CrossRef]

65. Luengo, J.M.; García, B.; Sandoval, A.; Naharro, G.; Olivera, E.R. Bioplastics from microorganisms. *Curr. Opin. Microbiol.* **2003**, *6*, 251–260. [CrossRef]
66. Sabirova, J.S.; Ferrer, M.; Lünsdorf, H.; Wray, V.; Kalscheuer, R.; Steinbüchel, A.; Timmis, K.N.; Golyshin, P.N. Mutation in a tesB-Like hydroxyacyl-Coenzyme a-specific thioesterase gene causes hyperproduction of extracellular polyhydroxyalkanoates by *Alcanivorax borkumensis* SK2. *J. Bacteriol.* **2006**, *188*, 8452–8459. [CrossRef]

bioengineering

MDPI

Article

In-Line Monitoring of Polyhydroxyalkanoate (PHA) Production during High-Cell-Density Plant Oil Cultivations Using Photon Density Wave Spectroscopy

Björn Gutschmann [1], Thomas Schiewe [2], Manon T.H. Weiske [1], Peter Neubauer [1], Roland Hass [2] and Sebastian L. Riedel [1,*]

[1] Bioprocess Engineering, Department of Biotechnology, Technische Universität Berlin, 13355 Berlin, Germany; bjoern.gutschmann@tu-berlin.de (B.G.); manon.th.weiske@campus.tu-berlin.de (M.T.H.W.); peter.neubauer@tu-berlin.de (P.N.)

[2] innoFSPEC, University of Potsdam, 14476 Potsdam, Germany; tschiewe@uni-potsdam.de (T.S.); rh@pdw-analytics.de (R.H.)

* Correspondence: riedel@tu-berlin.de

Received: 29 August 2019; Accepted: 17 September 2019; Published: 19 September 2019

Abstract: Polyhydroxyalkanoates (PHAs) are biodegradable plastic-like materials with versatile properties. Plant oils are excellent carbon sources for a cost-effective PHA production, due to their high carbon content, large availability, and comparatively low prices. Additionally, efficient process development and control is required for competitive PHA production, which can be facilitated by *on-line* or *in-line* monitoring devices. To this end, we have evaluated photon density wave (PDW) spectroscopy as a new process analytical technology for *Ralstonia eutropha* (*Cupriavidus necator*) H16 plant oil cultivations producing polyhydroxybutyrate (PHB) as an intracellular polymer. PDW spectroscopy was used for *in-line* recording of the reduced scattering coefficient μ_s' and the absorption coefficient μ_a at 638 nm. A correlation of μ_s' with the cell dry weight (CDW) and μ_a with the residual cell dry weight (RCDW) was observed during growth, PHB accumulation, and PHB degradation phases in batch and pulse feed cultivations. The correlation was used to predict CDW, RCDW, and PHB formation in a high-cell-density fed-batch cultivation with a productivity of 1.65 $g_{PHB} \cdot L^{-1} \cdot h^{-1}$ and a final biomass of 106 $g \cdot L^{-1}$ containing 73 wt% PHB. The new method applied in this study allows *in-line* monitoring of CDW, RCDW, and PHA formation.

Keywords: polyhydroxyalkanoate; PHA; process analytical technologies; PAT; plant oil; high-cell-density fed-batch; photon density wave spectroscopy; PDW; *Ralstonia eutropha*; *Cupriavidus necator*; *on-line*; *in-line*

1. Introduction

When the US Food and Drug Administration (FDA) announced their process analytical technology (PAT) directives, the investigation of PAT became a key research area in bioprocess development. The main objectives are designing, developing, and operating bioprocesses to guarantee a targeted final product quality [1,2]. The focus of this initiative was predominantly on biopharmaceutical processes, while novel PAT tools could be integrated into any bioprocess. Especially, the implementation of PAT for polyhydroxyalkanoate (PHA) production can provide significant benefits to facilitate a consistent and highly efficient production. Techniques such as FTIR, Raman spectroscopy, fluorescence staining associated with flow cytometry, and enzymatic approaches were reported as novel methods for a rapid characterization of PHA production [3–7]. A comprehensive overview of qualitative and quantitative

methods for PHA analysis was published by Koller et al. [8]. However, the reported methods have not been applied for *in-line* or *at-line* measurements of the PHA production process so far.

Photon density wave (PDW) spectroscopy is an *in-line* technique, which has been used as an analytical tool for measurements of various highly turbid chemical processes [9–12]. The method is based on the theory of photon migration in multiple light scattering material. If intensity-modulated light is introduced into a strongly light scattering but weakly light absorbing material, a PDW is generated. Absorption and scattering properties of the material influence the amplitude and phase of the PDW. By quantifying these shifts as a function of the emitter fiber and detector fiber distance and of the modulation frequency, the absorption coefficient μ_a and the reduced scattering coefficient μ_s' can be determined independently [9,13,14]. The mentioned features make PDW spectroscopy very attractive for the monitoring of high-cell-density bioprocesses.

Currently, PHA production costs are not compatible with the low-priced production of conventional plastics. The main cost driving factors are the feedstocks for PHA accumulation and the recovery process. Thus, alternative low-cost substrates, e.g., biogenic waste streams, are of high interest to reduce the final production price. Other attempts concentrate on finding more sustainable and price efficient purification strategies [15–21]. *Ralstonia eutropha* (also known as *Cupriavidus necator*) is one of the main species studied for polyhydroxybutyrate (PHB) accumulation and the model organism for PHA accumulation [22]. Growth of *R. eutropha* on oleaginous feedstocks is particularly attractive due to their high carbon contents, high conversion rates to PHA, and low culture dilution in fed-batch processes. Efficient growth on these feedstocks is facilitated by the expression of extracellular lipases, which emulsify the lipids [23–27]. A large biomass accumulation prior to PHA accumulation is very important for a high final product titer. In this context, it has been shown that urea is an inexpensive nitrogen source, which allows excellent growth [24,28]. Despite alternative substrates and downstream approaches, highly efficient bioprocesses are required for an economic feasible PHA production. Recently, high-cell-density cultivations with *R. eutropha* on various renewable feedstocks have been published presenting the production of over 100 $g \cdot L^{-1}$ PHA and space time yields from 1 to 2.5 $g_{PHA} \cdot L^{-1} \cdot h^{-1}$ [21,24,29–31]. However, none of the presented studies describe *in-line* PAT-based monitoring or control strategies for the enhancement of process results.

This work aims to integrate PDW spectroscopy into high-cell-density bioprocesses, for the monitoring of the highly turbid and complex PHB production with *R. eutropha* in plant oil cultivations. As a result, total cell dry weight (CDW) and residual cell dry weight (RCDW, the difference of CDW and the PHB concentration) accumulation could be distinguished with the PDW spectroscopy probe as a new *in-line* tool for bioprocesses.

2. Materials and Methods

2.1. Bacterial Strain

All cultivations were performed with the wild type strain *R. eutropha* H16 (DSM-428, Leibniz Institute DSMZ-German Collection of Microorganisms and Cell Cultures, Germany).

2.2. Growth Media and Preculture Cultivation Conditions

Tryptic soy broth (TSB) media (17 $g \cdot L^{-1}$ tryptone, 5 $g \cdot L^{-1}$ NaCl, 3 $g \cdot L^{-1}$ peptone) was used for the first precultures and with an additional supply of 2% ($w \cdot v^{-1}$) agar for culture plates. The second precultures and bioreactor cultivations were conducted in mineral salt media (MSM) containing 4.62 $g \cdot L^{-1}$ $NaH_2PO_4 \cdot H_2O$, 5.74 $g \cdot L^{-1}$ $Na_2HPO_4 \cdot 2H_2O$, 0.45 $g \cdot L^{-1}$ K_2SO_4, 0.04 $g \cdot L^{-1}$ NaOH, 0.80 $g \cdot L^{-1}$ $MgSO_4 \cdot 7H_2O$, 0.06 $g \cdot L^{-1}$ $CaCl_2 \cdot 2H_2O$ and 1 $mL \cdot L^{-1}$ trace element solution consisting of 0.48 $g \cdot L^{-1}$ $CuSO_4 \cdot 5H_2O$, 2.4 $g \cdot L^{-1}$ $ZnSO_4 \cdot 7H_2O$, 2.4 $g \cdot L^{-1}$ $MnSO_4 \cdot H_2O$, 15 $g \cdot L^{-1}$ $FeSO_4 \cdot 7H_2O$. All cultivation media and plates contained 10 $mg \cdot L^{-1}$ sterile filtered gentamycin sulfate. Rapeseed oil (Edeka Zentrale AG & Co. KG, Germany) was used as the sole carbon source and urea as the sole nitrogen source in the

MSM. The explicit amounts are described in the text. All chemicals were purchased from Carl Roth GmbH & Co. KG (Germany) unless stated otherwise.

R. eutropha H16 was streaked from a cryoculture on a TSB agar plate and incubated for 3–4 days at 30 °C. A single colony from the plate was used to inoculate the first preculture in 10 mL TSB media in a 125-mL Ultra Yield™ Flask (Thomson Instrument Company, USA) sealed with an AirOtop™ enhanced flask seal (Thomson Instrument Company, USA). After incubating for 16 h, 2.5 mL were used to inoculate the second preculture (250 mL MSM with 3% ($w \cdot v^{-1}$) rapeseed oil and 4.5 $g \cdot L^{-1}$ urea) in a 1-L DURAN® baffled glass flask with a GL45 thread (DWK Life Sciences GmbH, Germany) sealed with an AirOtop membrane. After 24 h of incubation, the complete second preculture was used to inoculate the main bioreactor culture. The precultures were incubated at 30 °C and shaken at 200 rpm (first preculture) or 180 rpm (second preculture) in an orbital shaker (Kühner LT-X incubator, Adolf Kühner AG, Switzerland, 50 mm amplitude).

2.3. Bioreactor Cultivation Conditions

Mineral salts dissolved in deionized (DI) water and rapeseed oil were added prior autoclavation in a 6.6-L stirred tank bioreactor with two six-blade Rushton impellers (BIOSTAT® Aplus, Sartorius AG, Germany). $MgSO_4$, $CaCl_2$, trace elements, gentamycin, and urea were added into the medium after autoclavation from sterile stock solutions. The temperature was maintained at 30 °C and the pH was kept constant at 6.8 ± 0.2 using 2 M NaOH and 1 M H_3PO_4 for pH control. The dissolved oxygen concentration (DO) was kept above 40% using a stirrer cascade ranging from 400 to 1350 rpm. The cultures were aerated with a constant aeration rate of 0.5 vvm throughout the cultivations. Five pairs of cable ties were mounted on the upper part of the stirrer shaft in order to break the foam mechanically and thus preventing overfoaming of the reactor.

2.3.1. Batch Cultivations

For a first evaluation of the PDW spectroscopy signal, three batch cultivations were performed in which the carbon and nitrogen content was varied. The concentrations of rapeseed oil were 3, 4, and 4% ($w \cdot v^{-1}$), and 2.25 (corresponding to 75 mM nitrogen), 4.5, and 2.25 $g \cdot L^{-1}$ for urea, respectively.

2.3.2. Pulse-Based Fed-Batch Cultivation

A cultivation strategy with a pulse feeding was performed in biological duplicates. The cultures initially contained 0.5% ($w \cdot v^{-1}$) rapeseed oil and 4.5 $g \cdot L^{-1}$ urea. Pulses were given whenever the PDW spectroscopy *in-line* signal (μ_s' at 638 nm) indicated a decreased cell activity. After 8.2 h, the first pulse (15 g rapeseed oil) was added, followed by two more rapeseed oil pulses at 14.3 h (30 g) and at 21.1 h (60 g). At 31.7 h a pulse consisting of 110 mL urea solution (122 $g \cdot L^{-1}$), 15.6 mL 0.5 M K_2SO_4, 30 mL 0.042 M $CaCl_2$, 30 mL 0.32 M $MgSO_4$, and 3 mL trace element solution was added to restore the initial media concentrations of the components. The last pulse (120 g rapeseed oil) was added after 48.4 h.

2.3.3. Fed-Batch High-Cell-Density Cultivation

The culture initially contained 4% ($w \cdot v^{-1}$) rapeseed oil and 4.5 $g \cdot L^{-1}$ urea (150 mM nitrogen). Continuous feeding of pure rapeseed oil and a 30% ($w \cdot v^{-1}$) urea solution was started 7 h after inoculation with initial feeding rates of 3.5 $g \cdot h^{-1}$ and 0.39 $mL \cdot h^{-1}$, respectively. Both feeding rates were linearly increased up to 6.58 $mL \cdot h^{-1}$ (urea) at 16 h, after which the urea feed was stopped to cause nitrogen starvation, and 23 $g \cdot h^{-1}$ (rapeseed oil) at 35 h to final concentrations of 480 mM nitrogen and 170 $g \cdot L^{-1}$ rapeseed oil. A single injection of $MgSO_4$, $CaCl_2$, K_2SO_4, and trace elements was performed after 20 h with the amounts as described above (see Section 2.3.2.) to restore the initial concentrations and prevent nutrient depletion. An additional pulse of $CaCl_2$ with the same concentration was added after 32 h.

2.4. Photon Density Wave Spectroscopy

A PDW spectrometer built by the University of Potsdam was used for the measurement of the absorption coefficient μ_a and the reduced scattering coefficient μ_s'. Identical devices are commercially available at PDW Analytics GmbH (Potsdam, Germany). The general set-up of the PDW spectrometer was described by Bressel et al., as follows: "A schematic set-up of the spectrometer is shown in Figure 1. Light from a laser diode with wavelength λ [m] (typ. 400–1000 nm) is sinusoidally intensity modulated by a vector network analyzer (typ. $f = \omega/(2\pi)$ = 10–1300 MHz). The light is then coupled into the material via an optical fiber, acting as a point-like light source. A second optical fiber, positioned at a distance r to the emission fiber (typ. r = 5–30 mm), collects light of the PDW and guides it onto an avalanche photodiode (APD) as detector." [13].

To integrate the multifiber PDW spectroscopy *in-line* probe into the system, a DN25 safety Ingold socket (elpotech GmbH & Co. KG, Germany) was welded onto the lid of the bioreactor. The probe was mounted before autoclaving and sterilized with the bioreactor inside the autoclave. The optical fibers of the probe were connected to the PDW spectrometer after autoclaving. μ_s' and μ_a were analyzed at 638 nm with a temporal resolution of 0.8 min^{-1}. A 10-point moving average was used to reduce the signal noise.

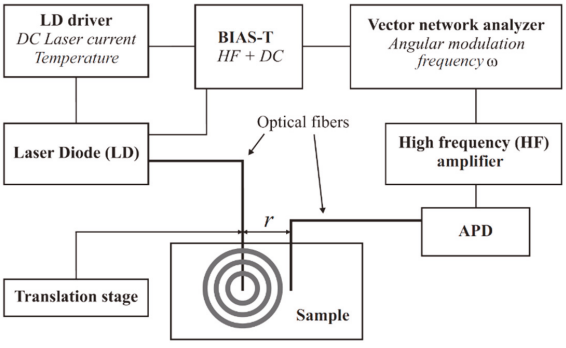

Figure 1. Schematic experimental set-up of a photon density wave (PDW) spectrometer [13].

2.5. Analytical Methods

For each *off-line* reference analysis time point, two aliquots of 10 mL were sampled in preweighed 15-mL polypropylene test tubes. The samples were centrifuged for 15 min at 6000× *g* and pellets were washed either with a mixture of 5 mL cold deionized (DI) water and 2 mL cold hexane or with 7 mL cold DI water to remove residual lipids. The washed pellets were resuspended in 2–4 mL ice cold DI water, frozen at −80 °C, and dried for 24 h by lyophilization (Gamma 1–20, Martin Christ Gefriertrocknungsanlagen GmbH, Germany). Then the CDW was determined by weighing the test tubes.

The PHB content was determined *off-line* by high-performance liquid chromatography with a diode array detector (HPLC-DAD 1200 series, Agilent Technologies, USA). The method was adapted from Karr et al. [32]. Pure PHB (Sigma-Aldrich Corporation, USA) or 8–15 mg freeze-dried cells were depolymerized by boiling samples with 1 mL concentrated H_2SO_4 to yield crotonic acid. Dilution series of the depolymerized PHB were prepared to yield standards in the range of 0.1–10 mg·mL^{-1}. Samples were diluted with 4 mL 5 mM H_2SO_4, filtered through a 0.2 µm cellulose acetate syringe filter, and subsequently 100 µL were transferred to a HPLC vial containing 900 µL of 5 mM H_2SO_4. HPLC analysis was performed with an injection volume of 20 µL using 5 mM H_2SO_4 as an eluent with an isocratic flow rate of 0.4 mL·min^{-1} for 60 min on a NUCLEOGEL® ION 300 OA column

(Macherey-Nagel, Germany). Crotonic acid was detected at 210 nm. RCDW was determined by subtracting the PHB from the CDW concentration.

The nitrogen content was indirectly determined *off-line* by measuring ammonia, resulting from urea cleavage, in the supernatant using a pipetting robot (Cedex Bio HT Analyzer, Roche Diagnostics International AG, Switzerland) with the NH3 Bio HT test kit (Roche Diagnostics International AG, Switzerland).

During the fed-batch cultivation the *in-line* PDW spectroscopy signals were used for an *on-line* determination of the CDW, RCDW, and PHB content (see Section 3.4).

3. Results

A reduction of the PHA production price is crucial for commercialization [33], which can be facilitated by maximization of the biotechnological process performance using PAT. In this context, our group is interested in developing biotechnological processes for PHA production from renewable resources [24] and biogenic waste streams [17,18].

In this study, PDW spectroscopy was evaluated as a novel *in-line* tool to monitor the PHA production process with *R. eutropha* from plant oil.

3.1. Batch Cultivations

For an initial evaluation of the PDW spectroscopy signals, batch cultivations with different C/N ratios were performed to trigger different PHB and CDW accumulation. The results of the three batch cultivations are shown in Figure 2. Detailed graphs of the cultivations can be found in the in Supplementary Materials in Figures S1–S3. The first batch cultivation was performed as a reference batch containing 3% ($w \cdot v^{-1}$) rapeseed oil and 75 mM nitrogen (2.25 $g \cdot L^{-1}$ urea). Nitrogen limitation was indirectly detected by ammonia quantification, which is released from urea cleavage prior nitrogen uptake [24,28]. Nitrogen was depleted between 9.2 and 14.2 h, which triggered PHB accumulation. Within this period, the CDW increased from 6 to 15 $g \cdot L^{-1}$ and the PHB content increased from 7 to 35 wt% (0.4 to 5.3 $g_{PHB} \cdot L^{-1}$). The PDW spectroscopy signals μ_a and μ_s' did not show any analyzable signals until 6.5 h. Subsequently, both signals exponentially increased until 10.5 h. After this time point, μ_a linearly increased until 16 h and did not further rise afterwards. An increase of the μ_s' signal was detected from 10.5 to 20 h and remained constant afterwards. The maximum CDW (25.5 $g \cdot L^{-1}$) was achieved after 33.2 h containing 65 wt% PHB (16.8 $g_{PHB} \cdot L^{-1}$), which represents an overall yield of 0.56 $g_{PHB} \cdot g_{Oil}{}^{-1}$. Over the entire cultivation, the urea consumption for biomass accumulation was 0.26 $g_{Urea} \cdot g_{RCDW}{}^{-1}$.

The purpose of Batch 2 was to decrease the C/N ratio compared to the reference batch for an increased accumulation of active biomass (RCDW) and decreased PHB content. Nitrogen was depleted between 11.6 and 19.8 h. Within this period, the CDW and PHB content increased from 12.3 to 38.3 $g \cdot L^{-1}$ and 7 to 62 wt% (0.8 to 23.7 $g_{PHB} \cdot L^{-1}$), respectively. The PDW spectroscopy signals μ_a and μ_s' simultaneously increased from the beginning of the cultivation until 12 h in an exponential manner. No significant changes of μ_a were detected after that time point, whereas μ_s' increased until 18 h and subsequently remained constant. After 23.8 h the maximum CDW of 40 $g \cdot L^{-1}$ containing 63 wt% (26.2 $g_{PHB} \cdot L^{-1}$) was achieved. Overall, a PHB yield of 0.66 $g_{PHB} \cdot g_{Oil}{}^{-1}$ and urea consumption of 0.29 $g_{Urea} \cdot g_{RCDW}{}^{-1}$ was achieved.

The C/N ratio in the third batch was increased compared to the reference batch by keeping the initial nitrogen concentration constant (75 mM) but increasing the rapeseed oil content to 4% ($w \cdot v^{-1}$). Depletion of nitrogen occurred between 10.3 and 11.3 h. Within this period the CDW increased from 7.7 $g \cdot L^{-1}$ with 8 wt% PHB (0.6 $g_{PHB} \cdot L^{-1}$) to 9.6 $g \cdot L^{-1}$ with 20 wt% PHB (1.9 $g_{PHB} \cdot L^{-1}$). PDW signals were detectable after 2 h. A comparable increase of μ_a and μ_s' was detected until 10 h. An attenuated increase of μ_a until 17.5 h was detected, whereas a diminished increase of μ_s' was detected from 10 to 22.5 h. The CDW further increased to 33.7 $g \cdot L^{-1}$ containing 73 wt% PHB (24.5 $g_{PHB} \cdot L^{-1}$). Overall, a PHB yield of 0.61 $g_{PHB} \cdot g_{Oil}{}^{-1}$ and urea consumption of 0.25 $g_{Urea} \cdot g_{RCDW}{}^{-1}$ was achieved.

To summarize, the C/N ratio influenced the yield coefficients for PHB accumulation and urea usage within these three batch cultivations. During the batch cultivations, μ_s' and μ_a simultaneously increased until nitrogen depletion. Subsequently, μ_a leveled off and μ_s' increased further until maximum PHB accumulation.

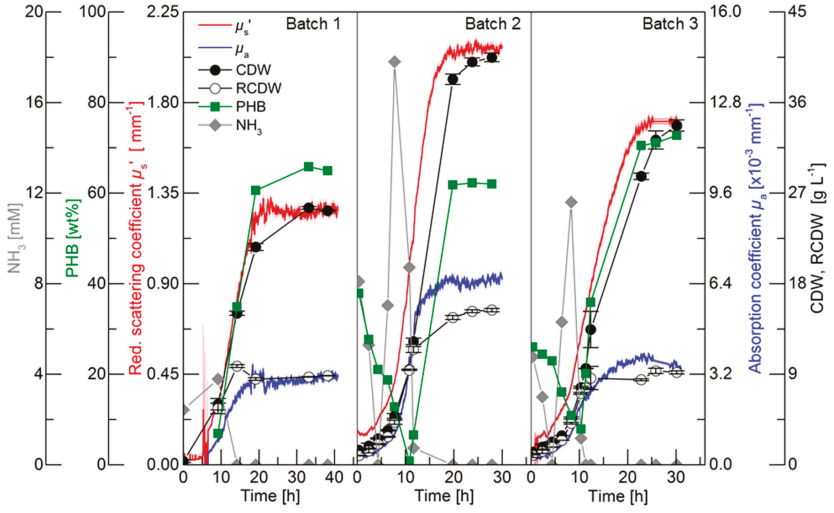

Figure 2. Batch cultivations for polyhydroxybutyrate (PHB) production by *R. eutropha* H16. Batch 1 contained 3% (w·v^{-1}) rapeseed oil and 2.25 g·L^{-1} urea (75 mM nitrogen), Batch 2 contained 4% (w·v^{-1}) rapeseed oil and 4.5 g·L^{-1} urea, and Batch 3 contained 4% (w·v^{-1}) rapeseed oil and 2.25 g·L^{-1} urea. Ammonia content (grey diamonds, mM), PHB content (green squares, wt%), cell dry weight (CDW) (filled circles, g·L^{-1}), residual cell dry weight (RCDW) (empty circles, g·L^{-1}), reduced scattering coefficient μ_s' (red line, mm^{-1}), and absorption coefficient μ_a (blue line, ×10^{-3} mm^{-1}) at 638 nm are shown. Error bars indicate minimum and maximum values of technical duplicates.

3.2. Pulse-Based Fed-Batch Cultivation

While the batch cultivations aimed to initially evaluate the relationship of the PDW spectroscopy signals with process relevant characteristics, a pulse-based fed-batch cultivation was conducted to: (i) show the feasibility to control the process by monitoring the process with PDW spectroscopy; (ii) confirm signal relationships; and (iii) validate the reproducibility during biological duplicate cultivations with independent seed trains. The process intention was implemented without difficulty: a pulse of either rapeseed oil or a nutrient bolus (see dashed lines in Figure 3 and details in the legend), respectively, was added to the culture when the μ_s' signal showed no further changes and indicated either carbon or nitrogen limitation. It is worth mentioning, that no signal deflections were observed whenever oil pulses were added to the bioreactor, which would account for an effect of the added oil on μ_s' or μ_a.

Within the first 8 h, the intracellular PHB content decreased from 36 to 14 wt% (Figure 3). An increase of the CDW, RCDW, μ_s' and μ_a was observed in the first 6 h of the cultivation. Subsequently, only minor increases of the CDW and RCDW of about 0.7 g·L^{-1} were detected until 8 h, whereas the PDW spectroscopy signals did not further increase during this period. After addition of the first pulse (0.5% (w·v^{-1}) rapeseed oil), μ_s' and μ_a resumed to increase until reaching constant levels at 11.5 h until the next pulse addition (1% (w·v^{-1}) rapeseed oil). The increase of μ_a stopped at 16.5 h, whereas μ_s' increased further until 18 h. Nitrogen depletion was detected at 17.5 h (Figure S4, Supplementary Materials). The PHB content had already increased to 30 wt% at this time point and further increased to 38 wt% before addition of the next pulse. The CDW increased up to 23 g·L^{-1}, whereas the RCDW

stopped at a value of 14 g·L^{-1} at 20.5 h. Addition of the next rapeseed oil pulse (2% (w·v^{-1})) at 21 h did not trigger a significant change of the μ_s' signal and of the RCDW. In contrast, a sharp increase of μ_s' resulted from the rapeseed oil addition and the CDW increased up to 43 g·L^{-1} at 31 h containing 66 wt% PHB. At 31.6 h, a bolus containing urea as a nitrogen source was supplemented to the culture. The addition resulted in a dilution of the culture, which was seen in a step decrease of both PDW spectroscopy signals at this time point. Subsequently, μ_s' decreased until 42 h and stayed constant until the next pulse addition. In contrast, μ_a resumed to increase until 45 h. The CDW decreased during this period to 24 g·L^{-1}, resulting from intracellular PHB degradation. The PHB content decreased to 30 wt%. At the same time, the RCDW increased to 17 g·L^{-1}. The addition of the next pulse (4% (w·v^{-1}) rapeseed oil) resulted in resumed growth on rapeseed oil as the primary carbon source instead of degrading the intracellular carbon storage. The PDW spectroscopy signals increased after the rapeseed oil supplementation. The scattering signal μ_s' increased until 70 h, whereas the absorption coefficient μ_a only slightly increased after 52 h. At 52 h, nitrogen was depleted again. The cells accumulated 66 wt% PHB until the end of the cultivation and the CDW increased to 53 g·L^{-1}. When the whole cultivation was repeated, the PDW spectroscopy signals showed an equivalent course and a final CDW of 52 g·L^{-1} CDW containing 64 wt% PHB, indicating a high robustness, i.e., repeatability, of the process.

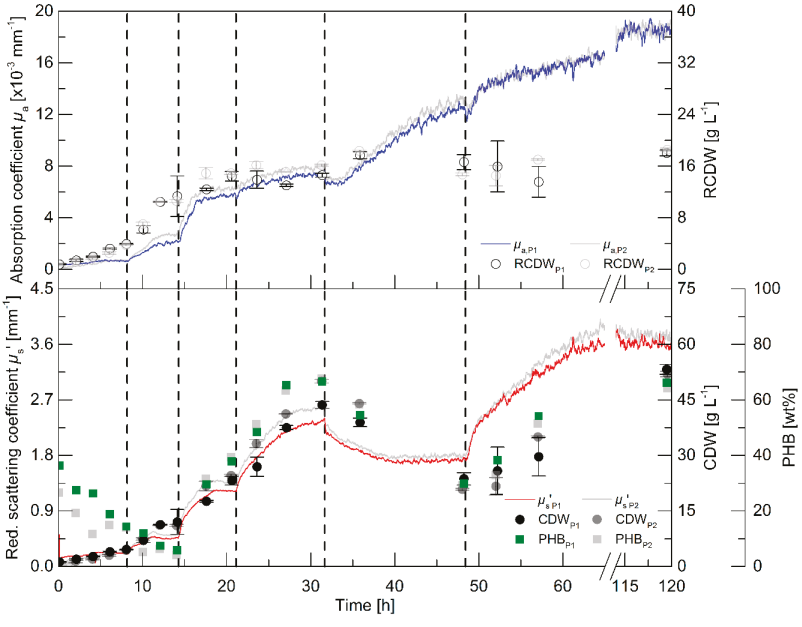

Figure 3. Pulse feeding cultivations for PHB production by *R. eutropha* H16. The cultures were initially started with 0.5% (w·v^{-1}) rapeseed oil and 4.5 g·L^{-1} urea (150 mM nitrogen). The dashed vertical lines represent time points of pulse additions: 0.5% (w·v^{-1}) rapeseed oil at 8.2 h, 1% (w·v^{-1}) rapeseed oil at 14.3 h, and 2% (w·v^{-1}) rapeseed oil at 21.1 h. At 31.7 h a bolus consisting of 110 mL urea solution (122 g·L^{-1}), 15.6 mL 0.5 M K_2SO_4, 30 mL 0.32 M $MgSO_4$, 30 mL 0.042 mM $CaCl_2$, and 3 mL trace element solution was added to the bioreactor. A final bolus of 4% (w·v^{-1}) rapeseed oil was added at 48.4 h. Data from the reference experiment is shown in color (indexed P1) and the biological duplicate (with an independent seed train) in transparent grey (indexed P2). Absorption coefficient μ_a (upper graph, solid line, ×10^{-3} mm^{-1}), RCDW (upper graph, empty circles, g·L^{-1}), PHB content (bottom graph, squares, wt%), CDW (bottom graph, filled circles, g·L^{-1}), and reduced scattering coefficient μ_s' (bottom graph, solid line, mm^{-1}) are shown. Error bars indicate minimum and maximum values of technical duplicates.

The pulse-based fed-batch experiment showed the possibility to control the rapeseed oil-based cultivation for PHB production using the *in-line* PDW spectroscopy probe. The highly reproducible course of the PDW spectroscopy signals strongly imply the connection of biological events with this measurement technique. The coefficients μ_s' and μ_a show the same trend as the CDW and RCDW, respectively. Nevertheless, a more significant change was observed for the μ_a signal after addition of the nitrogen pulse than the *off-line* determined RCDW. Regardless of this discrepancy, the hypothesis was that the μ_s' and μ_a correspond and can be correlated with the CDW and RCDW, respectively.

3.3. PDW Spectroscopy Signal Correlation

For an analysis of the correlation between the PDW spectroscopy signals μ_s' and μ_a at 638 nm, respectively, with process relevant characteristics, the experiments described above were analyzed. The reduced scattering coefficient μ_s' followed the course of the CDW, while the absorption coefficient μ_a increased with the rise of RCDW. The correlation of the respective values from all five cultivations (i.e., batch and pulse-based fed-batch cultures) are shown in Figure 4. A root mean squared error of 0.96 for the linear correlation of μ_s' and the CDW was obtained, whereas the linear correlation of μ_a and the RCDW resulted in a R^2 of 0.90. Equations (A1)–(A3) in Appendix A show the obtained formulas for calculating the CDW, RCDW, and subsequently the PHB concentration using the linear relationships of the *in-line* PDW spectroscopy signals with the corresponding *off-line* values. Due to disproportionally large PDW spectroscopy signal intensification after 48 h of the pulse feeding experiments (Figure 3), the last four data points of each replicate were not included in the correlation analysis.

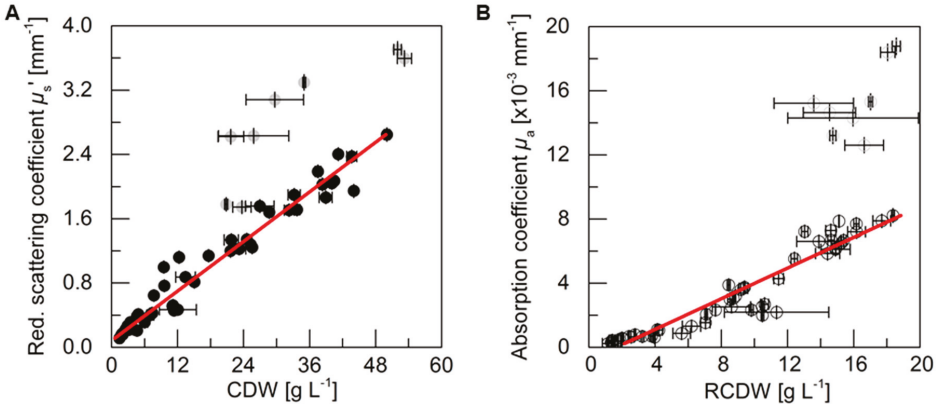

Figure 4. Correlation analysis of PDW spectroscopy signals with *off-line* values. (**A**) Reduced scattering coefficient μ_s' at 638 nm is correlated with CDW. (**B**) Absorption coefficient μ_a at 638 nm is correlated with RCDW. Data points are from five cultivations with different rapeseed oil and urea contents (cf. Figures 2 and 3). The gray data points comprise the last four samples of the two pulse-based fed-batch experiments (cf. Figure 3), which differ significantly from the other samples and were therefore not considered for the linear fit with the experimental data. A squared correlation coefficient R^2 of 0.96 was obtained for μ_s' and CDW and R^2 of 0.90 for μ_a and RCDW. Error bars indicate minimum and maximum values of technical duplicates (CDW, RCDW). STDEV of the 10-point average is shown for μ_s' and μ_a.

3.4. High-Cell-Density Fed-Batch Cultivation

High-cell-density cultivations are essential for a competitive production of PHA biopolymers. Therefore, it was aimed to perform such a cultivation to evaluate the PDW spectroscopy probe performance at industrial relevant biomass concentrations. The correlation factors obtained from the

first five cultivations (Equations (A1)–(A3) in Appendix A) were used to calculate the CDW, RCDW, and PHB content from the *in-line* PDW spectroscopy signals (Figure 5).

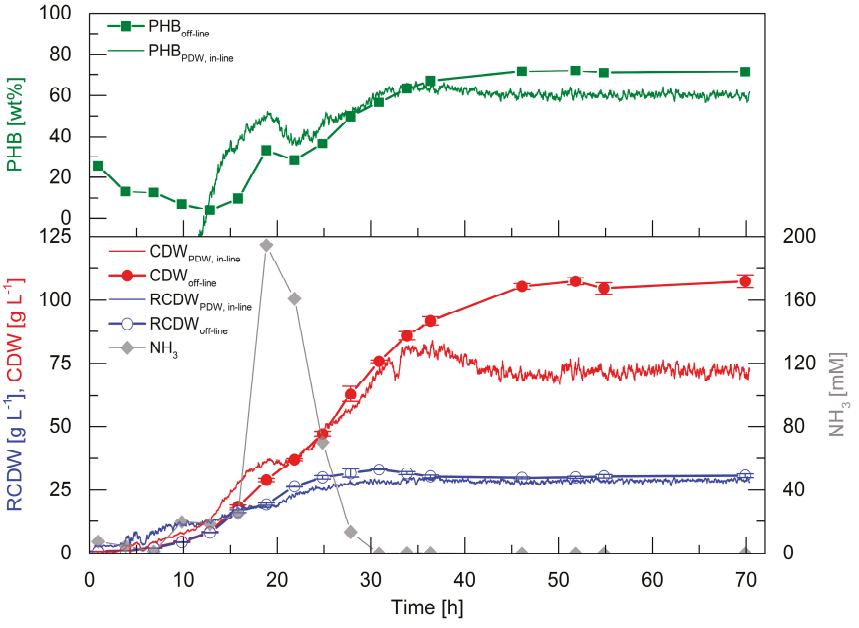

Figure 5. Fed-batch cultivation of *R. eutropha* H16 for PHB production. The culture was started with 4% (w·v^{-1}) rapeseed oil and 4.5 g·L^{-1} urea (150 mM nitrogen). Rapeseed oil feeding linearly increased from 7 h with an initial feeding rate of 3.5 g·h^{-1} to 35 h with a final feeding rate of 23 g·h^{-1} up to a total concentration of 17% (w·v^{-1}). Urea (30% (w·v^{-1})) feeding was linearly increased from 7 h with an initial feeding rate of 0.39 mL·h^{-1} up to a final feeding rate of 6.58 mL·h^{-1} at 16 h to a total concentration of 14.4 g·L^{-1}. *In-line* PHB content (upper graph, green line, wt%) by PDW spectroscopy and *off-line* PHB content (upper graph, green squares, wt%), estimated *in-line* CDW by PDW spectroscopy (bottom graph, red line, g·L^{-1}), *off-line* CDW (bottom graph, red filled circles, g·L^{-1}), estimated *in-line* RCDW by PDW spectroscopy (bottom graph, blue line, g·L^{-1}), *off-line* RCDW (bottom graph, blue empty circles, g·L^{-1}), and ammonia content (bottom graph, grey diamonds, mM) are shown. Error bars indicate minimum and maximum values of technical duplicates.

In the first 13 h, the *off-line* CDW increased to 8.5 g·L^{-1} and the RCDW to 8.2 g·L^{-1}. In the same period, the PHB content decreased to 4 wt%. Within this time frame, the *in-line* signals overestimated CDW and RCDW to 13.9 and 12.3 g·L^{-1} at 13 h, respectively. The estimated RCDW was higher than the estimated CDW until 12 h, which yielded a negative calculated PHB content. An accumulation of ammonia up to 195 mM at 19 h was detected, which subsequently decreased and was depleted after 28 h. The CDW and RCDW increased up to 63 and 32 g·L^{-1}, respectively, during this period. Contrary to expectation, PHB accumulation was detected from 13 to 19 h up to 33 wt%. Subsequently, the PHB content decreased again to 28 wt% during ammonia consumption and further accumulation started after 25 h. Subsequently, the PHB content increased to 72 wt% at 46 h. The preliminary accumulation and degradation of PHB until 25 h was also detected by the calculated *in-line* PHB signal. Subsequently, the *in-line* PHB content increased to 61 wt% at 46 h and ceased afterwards. At 46 h, the *off-line* CDW and RCDW had increased to 106 and 30 g·L^{-1}, respectively. In total, 76 g·L^{-1} PHB accumulated in 46 h, which represents a space time yield of 1.65 g_{PHB}·L^{-1}·h^{-1} and a yield coefficient of 0.43 g_{PHB}·g_{Oil}^{-1}. The overall urea usage was 0.48 g_{Urea}·g_{RCDW}^{-1}. The *in-line* RCDW signal indicated an accumulation

until 29 h to a final RCDW of 29 g·L^{-1}. The *in-line* CDW signal increased simultaneously with the *off-line* CDW until 36 h to 82 g·L^{-1}. Unexpectedly, the *in-line* CDW signal decreased afterwards until 46 h and stayed constant at a value of 71 g·L^{-1}.

The high-cell-density cultivation showed that PDW spectroscopy is capable of a qualitative tracking of the CDW, RCDW, and PHB content. Nevertheless, the quantitative accuracy was not precise during the first 12 h of the cultivation at low cell densities. However, the estimated *in-line* CDW showed a good representation until 36 h. Also, the *in-line* RCDW was estimated from the μ_a with a very good accuracy for the rest of the cultivation. In contrast, a drop of the μ_s' signal after 36 h did not correlate with CDW during PHB production.

4. Discussion

The purpose of this study was to evaluate the potential of PDW spectroscopy for monitoring plant oil-based *R. eutropha* cultivations. The batch (Figure 2) and pulse-based fed-batch (Figure 3) cultivations showed that the reduced scattering coefficient μ_s' correlates strongly with the CDW and the absorption coefficient μ_a with the RCDW (Figure 4). These results demonstrate that PDW spectroscopy is a valuable tool for *in-line* monitoring of the CDW, RCDW, and PHB accumulation. To the best of our knowledge, the results of this study are the first data showing *in-line* quantification of PHB. The lack of such *in-line* or *on-line* monitoring devices for an adaptive control of the production process was recently emphasized by Koller et al. [3]. Previously, Cruz et al. reported the possibility to use a NIR transflectance probe for an *in-line* quantification of PHB. However, the authors showed only *at-line* data quantifying the PHB and CDW concentration (up to 9.3 g·L^{-1} and 13.7 g·L^{-1}, respectively) during batch cultivations [34].

During the initial batch cultivations, PHB yields of 0.56–0.66 g_{PHB}·$g_{Oil}{}^{-1}$ were obtained (Figure 2), which are similar to previously reported yields for *R. eutropha* H16 growth on palm oil [35]. During the high-cell-density fed-batch cultivation 106 g·L^{-1} CDW (72 wt% PHB) with a space time yield of 1.65 g_{PHB}·L^{-1}·h^{-1} were reached, which is comparable to other published high-cell-density plant oil cultivations [21,24,25,29,36,37].

In the pulse experiment, a nitrogen bolus was added (32 h) after the PHB production phase to trigger PHB degradation, as described previously [38]. The PDW spectroscopy signal μ_s' decreased with the declining CDW while μ_a increased with an increasing RCDW (Figure 3). Currently, we do not understand why the strength of the signal was not proportional with the determined *off-line* value changes after that time point (32 h). For this reason, these measurement points were not used for the linear correlation. A potential hypothesis could be an unequal distribution of PHA granules during PHA mobilization, as it was reported for *Pseudomonas putida* [39], which might have an effect on scattering and absorption coefficients during PHA degradation.

Atypical PHB formation before nitrogen depletion was detected during the high-cell-density cultivation (Figure 5). This preliminary formation of PHB could explain the low yield coefficient of 0.43 g_{PHB}·$g_{Oil}{}^{-1}$, which is significant lower than the typical yield of PHB in *R. eutropha* plant oil cultivations [37]. The formation of PHB without nutrient starvation could indicate a stress response triggered by the high urea levels. Stress responses typically involve the formation of the alarmone (p)ppGpp. For *R. eutropha* it is known that formation of this alarmone triggers PHB formation [38,40], but (p)ppGpp formation due to excess urea or ammonia availability was not studied so far. Additionally, it was reported that controlled induction of stress could also been used for an enhanced PHB formation [41]. Such stress responses should be thoroughly considered during the scale-up of a *R. eutropha* PHA production process, as zones of high or low substrate availability occur in large scale bioreactors. The high impact of such substrate gradients on a reduction of biomass and product yields were intensively studied for *Escherichia coli* [42]. Adapting the feeding strategy during the PHA production process by using *in-line* monitoring devices could be a potential scenario for avoiding such negative impacts on the process.

A reduction of the μ_s' signal after 35 h was observed during the high-cell-density fed-batch cultivation, whereas μ_a stayed constant during that period (Figure 5). The decrease of μ_s' instead of a leveling off of the signal contradicts that a signal saturation effect was observed. Additionally, scattering coefficients in suspensions with particle contents of up to 40% ($v \cdot v^{-1}$) were measured successfully with this technology [9,10]. Heavy foaming, which occurred after 35 h, could be the reason for the observed signal reductions. The surplus of foam was constantly forced into the liquid phase, which increased the overall gas hold-up and total reaction volume in the system. This additional gas volume results in a dilution of the system, which could explain the μ_s' decrease (35–45 h) even though the culture continued to accumulate PHB (Figure 5). The foaming occurred after the end of the continuous rapeseed oil feed at 35 h. Before 35 h, the added oil functioned as a natural antifoam agent by decreasing the surface tension of the culture broth. During plant oil cultivations foaming occurs through the emulsification process. *R. eutropha* emulsifies plant oils before uptake, which is catalyzed by extracellular lipases. The lipases cleave the triacylglycerols in diacylglycerols, monoacylglycerols, glycerol, and free fatty acids (FFAs) [23,43,44], which causes heavy foaming during aerated bioreactor cultivations. Nevertheless, μ_s' stayed constant after the CDW did not further increase at 45 h, which could indicate the perfect time point for harvesting in an industrial process. A reliable *in-line* quantification of CDW, RCDW, and subsequently PHA concentration was reached until a CDW of 84 $g \cdot L^{-1}$. To increase the robustness of the method further at higher cell densities, the calculated gas-hold up in the bioreactor [45] could be integrated in the correlation of the PDW spectroscopy signals. In order to quantify the direct impact of the PHA concentration on the optical coefficients, further studies referencing cell counts and sizes by flow cytometry and microscopy need to be conducted.

A wavelength of 638 nm was used to evaluate the PDW spectroscopy signals during this study, which did not show any correlations with the oil addition or emulsification (Figure 3). The emulsification process is very important for an efficient growth. It was previously shown that an overexpression of lipases results in a reduced lag phase and subsequently a more efficient process [43]. In previous studies, it was shown that PDW spectroscopy was used to measure emulsions [46,47]. An *in-line* determination of the oil content or the emulsion formation would be a very valuable additional information for bioprocess development and process control. This information might result from integration of additional wavelengths into the PDW spectroscopy set-up.

To summarize, PDW spectroscopy allows *in-line* estimation of the CDW, RCDW, and PHB content in real-time. In contrast, *off-line* analysis is typically carried out to determine the PHB content, which includes drying the cells and polymer derivatization before time-consuming HPLC or GC analysis. By using PDW spectroscopy, process development and scale-up could be accelerated. In addition, this technology could be used at a large scale for process monitoring and control of *R. eutropha* cultivations. Specifically, the real-time adjustment of feeding strategies according to the PHA production rates—determined by PDW spectroscopy signals—holds great potential.

5. Conclusions

Here, we show that *in-line* PDW spectroscopy is a powerful PAT tool for monitoring *R. eutropha*-based PHB production. The reduced scattering coefficient μ_s' and absorption coefficient μ_a showed very reproducible signals during different biological cultivations. The new method described in this study allows *in-line* monitoring of CDW, RCDW, and PHB concentrations in *R. eutropha* cultivations up to a CDW of 84 $g \cdot L^{-1}$. PDW spectroscopy could contribute to improving the scaling-up process and thus to performing PHA production processes in an economical efficient way with the ultimate goal to commercialize a green sustainable plastic.

Supplementary Materials: The following are available online at http://www.mdpi.com/2306-5354/6/3/85/s1, Figure S1: Detailed figure of Batch 1, Figure S2: Detailed figure of Batch 2, Figure S3: Detailed figure of Batch 3, Figure S4: Ammonia contents from the pulse feed cultivations.

Author Contributions: Conceptualization, B.G., T.S., R.H., S.L.R.; Methodology, B.G., T.S., R.H., S.L.R.; Validation, B.G., T.S.; Formal analysis, B.G., T.S.; Investigation, B.G., T.S., M.T.H.W.; Resources, P.N., R.H., S.L.R.; Data curation, B.G., T.S.; Writing—original draft preparation, B.G., S.L.R.; Writing—review and editing, B.G., T.S., M.T.H.W., P.N., R.H., S.L.R.; Visualization, B.G.; Supervision, R.H., S.L.R.; Project administration, S.L.R.; Funding acquisition, R.H., S.L.R., P.N.

Funding: This research was funded by the German Federal Ministry of Education and Research, grant number 03Z22AN12.

Acknowledgments: We thank Roche CustomBiotech (Mannheim, Germany) for the supply of the Cedex Bio HT Analyzer. We thank Thomas Högl for helping with the installation of the PDW spectroscopy probe. We acknowledge support by the Open Access Publication Funds of TU Berlin.

Conflicts of Interest: The authors declare no conflict of interest.

Appendix A

$$\text{CDW } [\text{g}\cdot\text{L}^{-1}] = 19.012\ [\text{mm}\cdot\text{g}\cdot\text{L}^{-1}]\ \mu_s'\ [\text{mm}^{-1}] - 1.2404\ [\text{g}\cdot\text{L}^{-1}]\ R^2 = 0.96 \quad \text{(A1)}$$

$$\text{RCDW } [\text{g}\cdot\text{L}^{-1}] = 1872\ [\text{mm}\cdot\text{g}\cdot\text{L}^{-1}]\ \mu_a\ [\text{mm}^{-1}] + 2.5722\ [\text{g}\cdot\text{L}^{-1}]\ R^2 = 0.90 \quad \text{(A2)}$$

$$\text{PHB } [\text{wt\%}] = 100\ [\text{wt\%}]\ (\text{CDW } [\text{g}\cdot\text{L}^{-1}] - \text{RCDW } [\text{g}\cdot\text{L}^{-1}])/\text{CDW } [\text{g}\cdot\text{L}^{-1}] \quad \text{(A3)}$$

References

1. FDA Guidance for Industry PAT: A Framework for Innovative Pharmaceutical Development, Manufacuring, and Quality Assurance. FDA Off. Doc. 2004. Available online: https://www.fda.gov/regulatory-information/search-fda-guidance-documents/pat-framework-innovative-pharmaceutical-development-manufacturing-and-quality-assurance (accessed on 18 September 2019).
2. Gomes, J.; Chopda, V.R.; Rathore, A.S. Integrating systems analysis and control for implementing process analytical technology in bioprocess development. *J. Chem. Technol. Biotechnol.* **2015**, *90*, 583–589. [CrossRef]
3. Karmann, S.; Follonier, S.; Bassas-Galia, M.; Panke, S.; Zinn, M. Robust *at-line* quantification of poly(3-hydroxyalkanoate) biosynthesis by flow cytometry using a BODIPY 493/503-SYTO 62 double-staining. *J. Microbiol. Methods* **2016**, *131*, 166–171. [CrossRef] [PubMed]
4. Lee, J.H.; Lee, S.H.; Yim, S.S.; Kang, K.; Lee, S.Y.; Park, S.J.; Jeong, K.J. Quantified High-Throughput Screening of *Escherichia coli* Producing Poly (3-hydroxybutyrate) Based on FACS. *Appl. Biochem. Biotechnol.* **2013**, *170*, 1767–1779. [CrossRef] [PubMed]
5. Samek, O.; Obruča, S.; Šiler, M.; Sedláček, P.; Benešová, P.; Kučera, D.; Márova, I.; Ježek, J.; Bernatová, S.; Zemánek, P. Quantitative Raman Spectroscopy Analysis of Polyhydroxyalkanoates Produced by *Cupriavidus necator* H16. *Sensors* **2016**, *16*, 1808. [CrossRef] [PubMed]
6. Porras, M.A.; Cubitto, M.A.; Villar, M.A. A new way of quantifying the production of poly(hydroxyalkanoate)s using FTIR. *J. Chem. Technol. Biotechnol.* **2016**, *91*, 1240–1249. [CrossRef]
7. Hesselmann, R.P.X.; Fleischmann, T.; Hany, R.; Zehnder, A.J.B. Determination of polyhydroxyalkanoates in activated sludge by ion chromatographic and enzymatic methods. *J. Microbiol. Methods* **1999**, *35*, 111–119. [CrossRef]
8. Koller, M.; Rodríguez-Contreras, A. Techniques for tracing PHA-producing organisms and for qualitative and quantitative analysis of intra- and extracellular PHA. *Eng. Life Sci.* **2015**, *15*, 558–581. [CrossRef]
9. Hass, R.; Munzke, D.; Vargas Ruiz, S.; Tippmann, J.; Reich, O. Optical monitoring of chemical processes in turbid biogenic liquid dispersions by Photon Density Wave spectroscopy. *Anal. Bioanal. Chem.* **2015**, *407*, 2791–2802. [CrossRef]
10. Münzberg, M.; Hass, R.; Dinh Duc Khanh, N.; Reich, O. Limitations of turbidity process probes and formazine as their calibration standard. *Anal. Bioanal. Chem.* **2017**, *409*, 719–728. [CrossRef]
11. Häne, J.; Brühwiler, D.; Ecker, A.; Hass, R. Real-time inline monitoring of zeolite synthesis by Photon Density Wave spectroscopy. *Microporous Mesoporous Mater.* **2019**, *288*, 109580. [CrossRef]
12. Hass, R.; Münzberg, M.; Bressel, L.; Reich, O. Industrial applications of photon density wave spectroscopy for *in-line* particle sizing. *Appl. Opt.* **2013**, *52*, 1429–1431. [CrossRef] [PubMed]

13. Bressel, L.; Hass, R.; Reich, O. Particle sizing in highly turbid dispersions by Photon Density Wave spectroscopy. *J. Quant. Spectrosc. Radiat. Transf.* **2013**, *126*, 122–129. [CrossRef]
14. Hass, R.; Reich, O. Photon density wave spectroscopy for dilution-free sizing of highly concentrated nanoparticles during starved-feed polymerization. *ChemPhysChem* **2011**, *12*, 2572–2575. [CrossRef] [PubMed]
15. Koller, M.; Shahzad, K.; Braunegg, G. Waste streams of the animal-processing industry as feedstocks to produce polyhydroxyalkanoate biopolyesters. *Appl. Food Biotechnol.* **2018**, *5*, 193–203.
16. Kourmentza, C.; Plácido, J.; Venetsaneas, N.; Burniol-Figols, A.; Varrone, C.; Gavala, H.N.; Reis, M.A.M. Recent Advances and Challenges towards Sustainable Polyhydroxyalkanoate (PHA) Production. *Bioengineering* **2017**, *4*, 55. [CrossRef] [PubMed]
17. Riedel, S.L.; Jahns, S.; Koenig, S.; Bock, M.C.E.; Brigham, C.J.; Bader, J.; Stahl, U. Polyhydroxyalkanoates production with *Ralstonia eutropha* from low quality waste animal fats. *J. Biotechnol.* **2015**, *214*, 119–127. [CrossRef] [PubMed]
18. Brigham, C.J.; Riedel, S.L. The Potential of Polyhydroxyalkanoate Production from Food Wastes. *Appl. Food Biotechnol.* **2018**, *6*, 7–18.
19. Ong, S.Y.; Kho, H.P.; Riedel, S.L.; Kim, S.W.; Gan, C.Y.; Taylor, T.D.; Sudesh, K. An integrative study on biologically recovered polyhydroxyalkanoates (PHAs) and simultaneous assessment of gut microbiome in yellow mealworm. *J. Biotechnol.* **2018**, *265*, 31–39. [CrossRef]
20. Riedel, S.L.; Brigham, C.J.; Budde, C.F.; Bader, J.; Rha, C.; Stahl, U.; Sinskey, A.J. Recovery of poly(3-hydroxybutyrate-*co*-3-hydroxyhexanoate) from *Ralstonia eutropha* cultures with non-halogenated solvents. *Biotechnol. Bioeng.* **2013**, *110*, 461–470. [CrossRef]
21. Obruca, S.; Marova, I.; Snajdar, O.; Mravcova, L.; Svoboda, Z. Production of poly(3-hydroxybutyrate-*co*-3-hydroxyvalerate) by *Cupriavidus necator* from waste rapeseed oil using propanol as a precursor of 3-hydroxyvalerate. *Biotechnol. Lett.* **2010**, *32*, 1925–1932. [CrossRef]
22. Reinecke, F.; Steinbüchel, A. *Ralstonia eutropha* strain H16 as model organism for PHA metabolism and for biotechnological production of technically interesting biopolymers. *J. Mol. Microbiol. Biotechnol.* **2008**, *16*, 91–108. [CrossRef] [PubMed]
23. Brigham, C.J.; Budde, C.F.; Holder, J.W.; Zeng, Q.; Mahan, A.E.; Rha, C.K.; Sinskey, A.J. Elucidation of β-oxidation pathways in *Ralstonia eutropha* H16 by examination of global gene expression. *J. Bacteriol.* **2010**, *192*, 5454–5464. [CrossRef] [PubMed]
24. Riedel, S.L.; Bader, J.; Brigham, C.J.; Budde, C.F.; Yusof, Z.A.M.; Rha, C.; Sinskey, A.J. Production of poly(3-hydroxybutyrate-*co*-3-hydroxyhexanoate) by *Ralstonia eutropha* in high cell density palm oil fermentations. *Biotechnol. Bioeng.* **2012**, *109*, 74–83. [CrossRef]
25. Kahar, P.; Tsuge, T.; Taguchi, K.; Doi, Y. High yield production of polyhydroxyalkanoates from soybean oil by *Ralstonia eutropha* and its recombinant strain. *Polym. Degrad. Stab.* **2004**, *83*, 79–86. [CrossRef]
26. Rehm, B.H.A. Polyester synthases: Natural catalysts for plastics. *Biochem. J.* **2003**, *376*, 15–33. [CrossRef] [PubMed]
27. Pohlmann, A.; Fricke, W.F.; Reinecke, F.; Kusian, B.; Liesegang, H.; Cramm, R.; Eitinger, T.; Ewering, C.; Pötter, M.; Schwartz, E.; et al. Genome sequence of the bioplastic-producing "Knallgas" bacterium *Ralstonia eutropha* H16. *Nat. Biotechnol.* **2006**, *24*, 1257–1262. [CrossRef] [PubMed]
28. Ng, K.S.; Ooi, W.Y.; Goh, L.K.; Shenbagarathai, R.; Sudesh, K. Evaluation of jatropha oil to produce poly(3-hydroxybutyrate) by *Cupriavidus necator* H16. *Polym. Degrad. Stab.* **2010**, *95*, 1365–1369. [CrossRef]
29. Arikawa, H.; Matsumoto, K. Evaluation of gene expression cassettes and production of poly(3-hydroxybutyrate-*co*-3-hydroxyhexanoate) with a fine modulated monomer composition by using it in *Cupriavidus necator*. *Microb. Cell Fact.* **2016**, *15*, 1–11. [CrossRef]
30. Arikawa, H.; Matsumoto, K.; Fujiki, T. Polyhydroxyalkanoate production from sucrose by *Cupriavidus necator* strains harboring csc genes from *Escherichia coli* W. *Appl. Microbiol. Biotechnol.* **2017**, *101*, 7497–7507. [CrossRef]
31. Sato, S.; Maruyama, H.; Fujiki, T.; Matsumoto, K. Regulation of 3-hydroxyhexanoate composition in PHBH synthesized by recombinant *Cupriavidus necator* H16 from plant oil by using butyrate as a co-substrate. *J. Biosci. Bioeng.* **2015**, *120*, 246–251. [CrossRef]
32. Karr, D.B.; Waters, J.K.; Emerich, D.W. Analysis of poly-β-hydroxybutyrate in *Rhizobium japonicum* bacteroids by ion-exclusion high-pressure liquid chromatography and UV detection. *Appl. Environ. Microbiol.* **1983**, *46*, 1339–1344. [PubMed]

33. Koller, M. Advances in Polyhydroxyalkanoate (PHA) Production. *Bioengineering* **2017**, *4*, 88. [CrossRef] [PubMed]
34. Cruz, M.V.; Sarraguça, M.C.; Freitas, F.; Lopes, J.A.; Reis, M.A.M. Online monitoring of P(3HB) produced from used cooking oil with near-infrared spectroscopy. *J. Biotechnol.* **2015**, *194*, 1–9. [CrossRef] [PubMed]
35. Budde, C.F.; Riedel, S.L.; Hübner, F.; Risch, S.; Popović, M.K.; Rha, C.; Sinskey, A.J. Growth and polyhydroxybutyrate production by *Ralstonia eutropha* in emulsified plant oil medium. *Appl. Microbiol. Biotechnol.* **2011**, *89*, 1611–1619. [CrossRef] [PubMed]
36. Sato, S.; Fujiki, T.; Matsumoto, K. Construction of a stable plasmid vector for industrial production of poly(3-hydroxybutyrate-*co*-3-hydroxyhexanoate) by a recombinant *Cupriavidus necator* H16 strain. *J. Biosci. Bioeng.* **2013**, *116*, 677–681. [CrossRef] [PubMed]
37. Fadzil, F.I.B.M.; Tsuge, T. Bioproduction of polyhydroxyalkanoate from plant oils. In *Microbial Applications*; Springer: Berlin, Germany, 2017; Volume 2, pp. 231–260. ISBN 9783319526690.
38. Juengert, J.R.; Borisova, M.; Mayer, C.; Wolz, C.; Brigham, C.J.; Sinskey, A.J.; Jendrossek, D. Absence of ppGpp leads to increased mobilization of intermediately accumulated poly(3-hydroxybutyrate) in *Ralstonia eutropha* H16. *Appl. Environ. Microbiol.* **2017**, *83*, 1–16. [CrossRef] [PubMed]
39. Karmann, S.; Panke, S.; Zinn, M. The Bistable Behaviour of *Pseudomonas putida* KT2440 during PHA Depolymerization under Carbon Limitation. *Bioengineering* **2017**, *4*, 58. [CrossRef] [PubMed]
40. Brigham, C.J.; Speth, D.R.; Rha, C.K.; Sinskey, A.J. Whole-genome microarray and gene deletion studies reveal regulation of the polyhydroxyalkanoate production cycle by the stringent response in *Ralstonia eutropha* H16. *Appl. Environ. Microbiol.* **2012**, *78*, 8033–8044. [CrossRef] [PubMed]
41. Obruca, S.; Marova, I.; Svoboda, Z.; Mikulikova, R. Use of controlled exogenous stress for improvement of poly(3-hydroxybutyrate) production in *Cupriavidus necator*. *Folia Microbiol.* **2010**, *55*, 17–22. [CrossRef]
42. Enfors, S.O.; Jahic, M.; Rozkov, A.; Xu, B.; Hecker, M.; Jürgen, B.; Krüger, E.; Schweder, T.; Hamer, G.; O'Beirne, D.; et al. Physiological responses to mixing in large scale bioreactors. *J. Biotechnol.* **2001**, *85*, 175–185. [CrossRef]
43. Lu, J.; Brigham, C.J.; Rha, C.; Sinskey, A.J. Characterization of an extracellular lipase and its chaperone from *Ralstonia eutropha* H16. *Appl. Microbiol. Biotechnol.* **2013**, *97*, 2443–2454. [CrossRef] [PubMed]
44. Riedel, S.L.; Lu, J.; Stahl, U.; Brigham, C.J. Lipid and fatty acid metabolism in *Ralstonia eutropha*: Relevance for the biotechnological production of value-added products. *Appl. Microbiol. Biotechnol.* **2014**, *98*, 1469–1483. [CrossRef] [PubMed]
45. Sieblist, C.; Lübbert, A. Gas Holdup in Bioreactors. In *Encyclopedia of Industrial Biotechnology*; John Wiley & Sons: New York, NY, USA, 2010; pp. 1–8.
46. Reich, O.; Bressel, L.; Hass, R. Sensing emulsification processes by Photon Density Wave spectroscopy. In *the 21st International Conference on Optical Fiber Sensors*; The Institute of Electrical and Electronics Engineers: New York, NY, USA, 2011; Volume 7753, p. 77532J.
47. Münzberg, M.; Hass, R.; Reich, O. *In-line* characterization of phase inversion temperature emulsification by photon density wave spectroscopy. *SOFW J.* **2013**, *4*, 38–46.

bioengineering

MDPI

Article

Polyhydroxybutyrate Production from Natural Gas in A Bubble Column Bioreactor: Simulation Using COMSOL

Mohsen Moradi [1], Hamid Rashedi [2], Soheil Rezazadeh Mofradnia [1], Kianoush Khosravi-Darani [3,*], Reihaneh Ashouri [4] and Fatemeh Yazdian [5,*]

[1] Department of Chemical Engineering, Faculty of Engineering, Islamic Azad University North Tehran Branch, Tehran 1651153311, Iran; khakeraheyar110@yahoo.com (M.M.); srezazadeh69@gmail.com (S.R.M.)
[2] Biotechnology Group, School of Chemical Engineering, College of Engineering, University of Tehran, Tehran 11155-4563, Iran; hrashedi@ut.ac.ir
[3] Department of Food Technology Research, Faculty of Nutrition Sciences and Food Technology/National Nutrition and Food Technology Research Institute, Shahid Beheshti University of Medical Sciences, Tehran 19395–4741, Iran
[4] Department of Environment, Faculty of Environment and Energy, Science and Research Branch, Islamic Azad University, Tehran 1477893855, Iran; reihaneh.ashouri@yahoo.com
[5] Department of Life Science Engineering, Faculty of New Science & Technology, University of Tehran, Tehran 1417466191, Iran
* Correspondence: k.khosravi@sbmu.ac.ir (K.K.-D.); yazdian@ut.ac.ir (F.Y.); Tel.: +98-21-22376473 (K.K.-D.); +98-21-22086348 (F.Y.); Fax: +98-21-22376473 (K.K.-D.)

Received: 1 June 2019; Accepted: 9 September 2019; Published: 16 September 2019

Abstract: In this study, the simulation of microorganism ability for the production of poly-β-hydroxybutyrate (PHB) from natural gas (as a carbon source) was carried out. Based on the Taguchi algorithm, the optimum situations for PHB production from natural gas in the columnar bubble reactor with 30 cm length and 1.5 cm diameter at a temperature of 32 °C was evaluated. So, the volume ratio of air to methane of 50:50 was calculated. The simulation was carried out by COMSOL software with two-dimensional symmetric mode. Mass transfer, momentum, density-time, and density-place were investigated. The maximum production of biomass concentration reached was 1.63 g/L, which shows a 10% difference in contrast to the number of experimental results. Furthermore, the consequence of inlet gas rate on concentration and gas hold up was investigated Andres the simulation results were confirmed to experimental results with less than 20% error.

Keywords: bubble column bioreactor; COMSOL; microorganism; PHB; simulation

1. Introduction

The facility of use and desirability of plastic materials properties led to their growing utilization in packaging and food industries [1]. At present, 30% of urban waste includes plastic waste. The extremely long durability of plastic (about three hundred years) has led to many environmental problems and destroyed the attractiveness of cities and nature. Burning polymeric lesions causes air pollution and according to the type of material used in their preparation, gases, such as hydrogen cyanide and other hazardous gases are released into the environment [1,2]. On the other hand, recycling has a lot of economic problems and costs. Since 1970, with the decline of the landfill problem worldwide, the issue of the use of biodegradable polymers was raised [3]. Polymers can be generally classified into two major biodegradable and non-degradable groups [4]. Non-degradable polymers, such as polyethylene, polypropylene, and polystyrene are produced from monomeric sources of oil and are resistant to environmental issues. Biodegradable polymers are separated according to their constituent

components, their preparation process or their application. Biodegradable plastics or bioplastics with properties, such as biodegradability, environmental compatibility, the ability to produce renewable sources, less energy consumption in production, the production of water and carbon dioxide when degrading, compete with conventional plastics obtained from oil, especially with declining demand in the global market [4–7].

Amongst the biodegradable plastics, polyhydroxyalkanoates (PHAs) were considered due to the similarity of these materials with conventional plastics. The flexibility and expandable strength of PHA are similar to that of polypropylene and polystyrene polymers [2,8]. The agglomeration of PHAs in the cell can be enhanced by creating inhomogeneous growth conditions by limiting some nutrients like the source of nitrogen, phosphorus or sulfate, by reducing the concentration of oxygen, or by increasing the fraction of carbon to nitrogen in the feed [9,10].

One of the most important PHAs is polyhydroxy butyrate (PHB), which forms in the form of intracellular granules in different microorganisms. The high price of these biopolymers has led to limitations in their use of petrochemical polymers [11]. The main factor influencing the final cost of these polymers is the carbon origin, the carbon substrate yield, the method of fermentation, and its extraction method [12,13].

PHB can be synthesized by microorganisms with a special application in food packing [14]. However, their use is presently limited owing to the high production cost. PHB production cost is related to several key factors including the substrate, chosen strain, cultivation strategy, and downstream processing. The utilization of smart and cheap [14–22] modeling [23], proper bioreactors, experimental design [24,25], and the development of a new recovery method [24–26], as well as chances for their competition in the global market have recently been addressed. Efforts were made to optimize the growth of *Ralstonia eutropha* NRRL B14690 in the existence of nutrients, which would not only decrease the production cost of PHB but also help in increasing productivity [9].

Methane is the most suitable substrate for the production of PHB, both natural gas and biogas, between the most widely used carbon sources. Natural gas includes 85–90% of methane and is also produced by methane-producing bacteria in biological degradation of organic matter [27–30]. In many European countries, methane produced in low-cost biotechnology is accessible while in the United States, methane production units of urban waste are increasing rapidly; therefore, switching from PHB to natural gas to replace biodegradable plastics is necessary [7,31,32].

One way to enhance the production of PHB from natural gas is to use new bacterial types in a hydrodynamic biosystem. In a study, the PHB from natural gas was studied. After selecting the appropriate method, the effect of two key parameters of methane to air ratio and nitrogen on the production of PHB in a bubble pillar reactor revealed that both factors had a significant effect on the PHB density. The production of PHB by *Methylocystis* (*M.*) *hirsuta* was obtained in contrast to other methanotrophic bacteria to increase metabolism. After sampling from southern oilfields, suitable microorganisms were isolated for the production of PHB from natural gas (as a carbon source). Then, according to the Taguchi model, optimal conditions for the production of PHB from natural gas were appraised in the bubble column reactor [33]. The results showed the growth of microorganisms and the production of PHB in the existence of methane in the liquid phase. The variables affecting the production of PHB include temperature, air volume to methane gas, nitrogen source pH, phosphate source, age of inoculation, and culture medium [7,34].

In this study, first, the studies conducted in line with PHB production are conducted for familiarity and knowledge of the operation of the bioreactor activity. Then, the process is simulated using COMSOL software to find optimal circumstances and to reach a precise view for the production of PHB in a bubbler bioreactor. After this stage, the process of production of PHB in the bioreactor is investigated. Since no study was published in, the field of simulating the performance of the Methylocystis bacteria in the production of PHB in a bubble column bioreactor, the function of microorganisms in the production of PHB is simulated, which precipitates the production process and reduces costs using the results of the experiment.

2. Materials and Methods

In order to examine the simulation of the process by using COMSOL software (Version 5.2: downloady.ir) and the production review in the bioreactor, first, a number of effective simplifying assumptions were selected:

- The temperature of the system is always constant at 32 °C.
- The physical properties of the solute with time are discarded.
- The velocity of all compounds in the same phase is equal.
- The culture medium and the microorganism mixture are considered as a single phase.

2.1. Reaction Kinetics

The production of PHB involves a type of methanotrophic bacterium, such as *M. hirsuta*, which is an aerobic and gram-negative bacteria that can produce PHB from the serum pathway. This methylotrophic bacterium of type II is used to investigate the production of PHB in the bioreactor, and the mathematical model equations provided by Equation (1) [35]:

$$r_{PHB} = \frac{dC_{PHB}}{dt} = \mu C_{PHB} - K_d C_{PHB} \quad (1)$$

while C_{PHB} is the dry weight of cell (g/L), K_d is the cell death rate (s/1), and μ is specific growth rates for cell mass (1/s) (Appendix A). The modular kinetic model for producing PHB by Equation (2):

$$\mu = \mu_{max}\left(\frac{s}{K_s + s}\right), \quad (2)$$

In Equation (2), μ_{max} is the maximum specific growth rate of microorganisms (1/s), S is the concentration of limited substrate for growth (g/L), and K_S is the Monod constant (g/L). The kinetic of the Monod causes the substrate outlet concentration to be low in the CSTR because the K_S is usually small. In order to create a delay phase, it is suggested that K_d changes with time in Equation (3):

$$K_d = K_d(\infty)(1 - \exp(\alpha t)) \quad (3)$$

α is the reversal of fixed cell death time (s^{-1}), K_d (∞) is the infinite cell death rate (s^{-1}), and t is the time in seconds. It should be noted that for the implementation of the simulation reaction, the following simple reaction to the metabolic reactions is used for simulation:

$$6(CH_4) + NH_3 + 7(O_2) \rightarrow C_5H_7NO_2 + CO_2 + 10\,(H_2O)$$

2.2. The Equation of the Governing Model

The bubble flow model with two phases (diffused air in the liquid phase) was used in this study. In this model, the equations of continuity, momentum, and energy are solved for each step. The equation of motion is calculated by Equation (4) [34,35]:

$$\phi_l \rho_l \partial u_l / \partial t + \phi_l \rho_l (u_l \cdot \nabla) u_l = \nabla \cdot [-p_l + \phi_l \mu_l (\nabla u_l + (\nabla u_l)^T - {}^2/_3 (\nabla \cdot u_l) I)] + \phi_l \rho_l g + F \quad (4)$$

In this equation, u_l indicates the velocity value in (m/s), p is the pressure in (Pa), and ϕ is the volume fraction indicated with m^3/m^3. ρ is density value with kg/m^3, g is the gravity unit with m/s^2, F is (N/m^3), μl is the dynamic velocity of the liquid replaced Pa.s in the equation. The values I and g, respectively, show the values of the liquid phase and the gas phase. The right-hand side of Equation (4) shows all forces that involve gradient, pressure, stress, adhesion, gravity, and force between the two

phases, such as pulling, lifting, and virtual collective forces. In this study, a tension force is involved in the model. Based on the explanation, the continuity equation is written as Equation (5):

$$\frac{\partial}{\partial t}\left(\phi_l\rho_l + \phi_g\rho_g\right) + \nabla.\left(\phi_l\rho_l\mu_l + \phi_g\rho_g\mu_g\right) \quad (5)$$

and the gas phase transfer equation is calculated as in Equation (6):

$$\frac{\partial\phi_g\rho_g}{\partial t} + +\nabla.\left(\phi_g\rho_g\mu_g\right) = -m_{gl} \quad (6)$$

m_{gl} is the mass transfer rate from gas to liquid (kg/m^3). The gas velocity ug is equal to the sum of the velocity of Equation (7):

$$U_g = U_l + U_{slip} + U_{drift} \quad (7)$$

U_{slip} is the relative velocity among phases and U_{drift} is the drift velocity. The physics relation calculates the density of gas from the ideal gas law by Equation (8):

$$\rho_g = \frac{\left(p + p_{ref}\right)M}{RT} \quad (8)$$

M is the molecular weight of the gas (kg/mol), R is the ideal gas constant (J/(mol·K) 3/3141472), and T is the temperature (K). p_{ref} is a scalar variable being 1 at (1 at or 101.325 Pa) as a default. While a drift velocity is calculated by Equation (9)

$$U_{drif} = \frac{\mu\nabla\phi_g}{\rho\phi_g} \quad (9)$$

μ is the effective viscosity, which causes it to fall. By putting Equations (9) and (7) in (6), we will have Equation (10):

$$\frac{\partial\phi_g\rho_g}{\partial t} = \nabla\cdot\left(\phi_g\rho_g\left(U_l + U_{slip}\right)\right) = \nabla\cdot\left(\frac{\mu\nabla\phi_g}{\rho\phi_g}\right) - m_{gl} \quad (10)$$

The drift velocity of the transfer equation is introduced in the gas transfer equation. This means that the gas transport equation is actually implemented in the physics interface. The equation of the bubble flow equation is relatively simple but it can indicate non-physical behavior. An artificial accumulation of bubbles, for example, is at the base of the walls in which the pressure gradients raise the bubbles while the bubbles have no place to go and there is no model for modifying the amount of gas fraction to grow. In order to prevent this, μ is set to μl for laminar. The only clear effect in most cases when the bubble flow equations are applicable is that the non-physical accumulation of bubbles reduces. The small effective viscosity in the transfer equation for φ_g has beneficial effects on the numerical properties of the equation system.

2.3. Simulation Operations

In order to define the system, the properties and repercussions contained in COMSOL software were given to the simulation system. COMSOL simulation software has a complete set of information, properties, and constancy of materials, and if there is no specific information for a system, it can be found with the help Perry's handbook and enter into the physics of the problem. The geometry of the system was cylindrical with a radius of 0.015 m and a stanchion at the end of the cylinder with a radius of 0.1 mm. In order to prevent computing and convergence, and in view of the symmetry in the given geometry, the problem was solved in the symmetric two-dimensional mode, which did not have an effect on the overall solution due to the application of boundary conditions. All three components of water, methane, and ammonium were regarded as a phase. In this way, the liquid environment

indicates the environment of the wastewater in which the ammonium and methane are soluble, and the properties of the bacteria are applied to the environment. The reaction occurred to produce biomass of an irreversible first-degree reaction with a reaction constant $k_1 = 10^{-5}$ in form of Va → W with the reaction rate, $r = k_1 C_{va}$. The system temperature was set to 305.15 K. Since the environment is water, the incompressible flow with density and dynamic viscosity, respectively, were regarded as 1000 kg/m^3 and 10^{-3} Pa.s. The initial pressure level (P_0) was considered zero and the permeation coefficient of the environment 10^{-9} m^2/s applied. The system under the boundary conditions of sleep with the equation u = 0 means that the system boundary was fixed and the simulation conducted in the symmetric two-dimensional mode. Figure 1 shows a schematic view of system geometry in the two-dimensional mode.

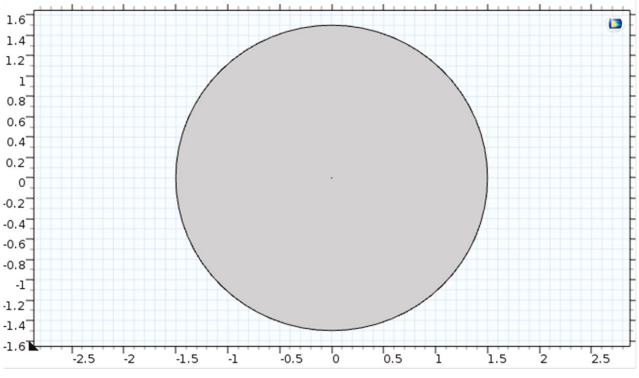

Figure 1. A schematic view of the system geometry.

2.4. Resolution Independence Analysis of Numerical Grid

The number of model components is designed to meet the conditions of numerical resolution independence from the computational grid size and gradually increases the number of components. The resolution independence test of the computational grid to a point in which the difference in response is less than 5%. The number of components in resolution independence tests of the numerical grid is given in Table 1.

Table 1. Constants and values of the parameters inputted.

Constants	Value
Temperature	32 °C
Physical properties of the solute	discard
Velocity	Equal in all part
Situation of flow	Single-phase
Columnar bubble reactor	30 cm and 1.5 cm

2.5. Meshing

At this stage, the geometry of the system was considered under meshing. In a two-dimensional model, the symmetrical mesh arrangement was selected based on the free triangular model and fine mesh size. The geometry of this system was split into 34,279 components. In Figure 2, a schematic view of the system meshing is presented in a two-dimensional mode.

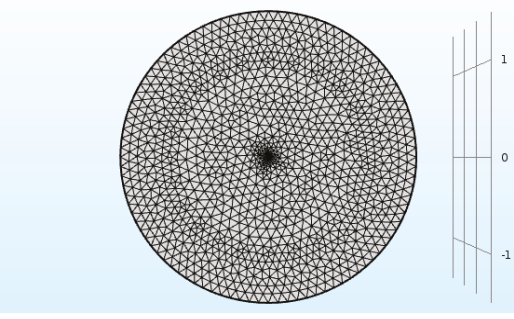

Figure 2. A schematic view of the geometry meshing with 34,269 components.

3. Results

In the production of PHB from natural gas, the objective of optimizing the composition of the culture medium is to provide important and sensitive food, increase the yield of the product, prevent product degradation, and decrease the formation of harmful side effects.

3.1. The Results of Resolution Independence Analysis of Numerical Grid

As indicated in Table 2, three large, medium, and fine grid sizes were applied separately in the model and the final concentration of the biomass in each mesh size was studied to examine the sensitivity of the computational grid. Table 3 indicates the final concentration of biomass in the last step of solving equations in three computational grids.

Table 2. The number of elements in different groups to check the resolution independence of the numerical grid.

Mesh Size	Fine	Medium	Coarse
Number of elements	70,563	34,269	16,396

Table 3. Final concentration of biomass in the last step of solving equations in three computational grids.

Mesh Size	Fine	Medium	Coarse
Concentration (g/L)	1.63474	1.63338	1.63233

3.2. Concentration of Biomass

3.2.1. Concentration Contour

Biomass ($C_5H_7NO_2$) is generated under the applied conditions according to the reaction from Va → W. After the simulation, the concentration contour was determined at 14 min. Figure 3 displays the concentration contour of biomass. Figure 3 shows the concentration gradient is from the center toward the wall. As indicated in Figure 4, the concentration contour at time t = 2 min and t =10 min can be seen for the circulation and mixing of PHB [36].

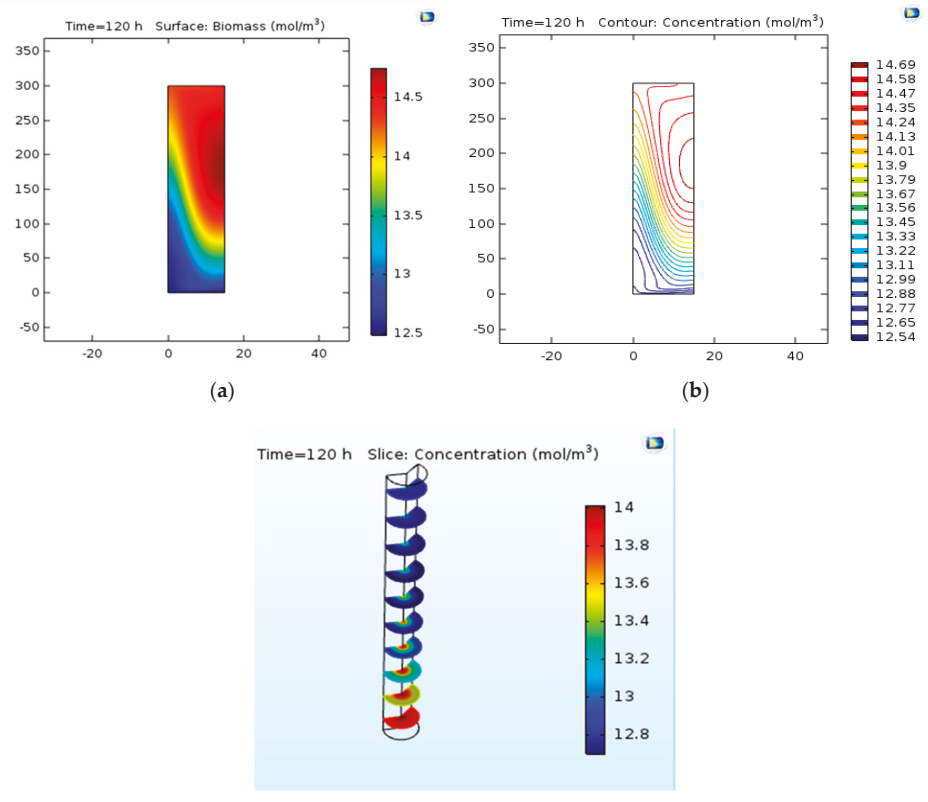

Figure 3. (**a**) The concentration surface contour of biomass. (**b**) The concentration contour of biomass. (**c**) The slice concentration contour of biomass.

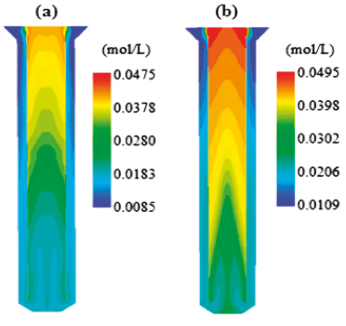

Figure 4. The concentration contour of polyhydroxy butyrate (PHB) at time (**a**) t = 2min and (**b**) t = 10 min [36].

3.2.2. Concentration Variations versus Time

The changes in the concentration of biomass were studied with time and the results are shown in Figure 5. As can be seen in this curve, the final concentration of biomass is almost 14 mol/m^3, which is less than 5% in comparison to laboratory values (14.5-mol/m^3). Figure 6 indicates concentration-location

changes in the two-dimensional model. As can be observed, the concentration at the beginning of the reactor is maximized because of the rapid reaction.

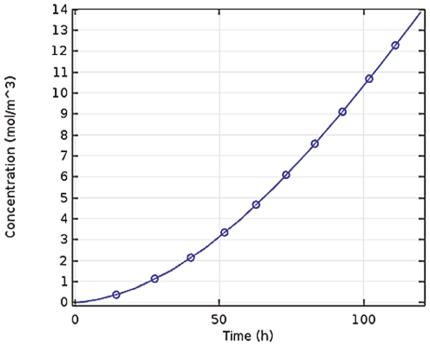

Figure 5. Changes in the concentration of biomass with time.

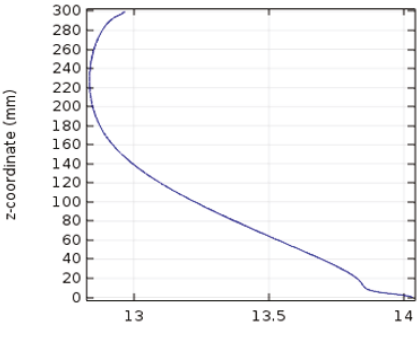

Figure 6. Linear changes of the reactor location concentration.

3.3. Velocity Contour

Figure 7a,b indicate the results of spatial changes of fluid velocity in the bioreactor. On the right side of Figure 7, the velocity assigned to each color is represented.

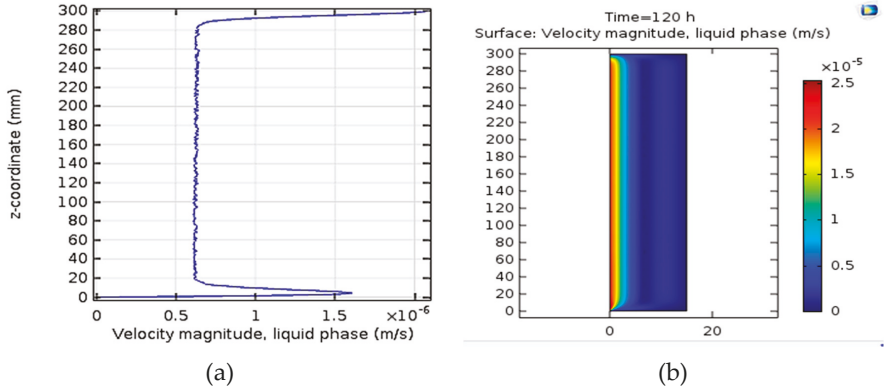

Figure 7. (**a**) Spatial changes of velocity in the liquid phase along the reactor. (**b**) Surface spatial changes of velocity in the liquid phase along the reactor.

3.4. Analysis of Variations in the Input Gas Velocity

The gas flow rate inside the reactor will influence the number of bubbles and the mass transfer rate. Thus, the simulation was studied at four different velocities of 0.0015, 0.065, and 0.15 m/s. The results are displayed in Figure 8a–c.

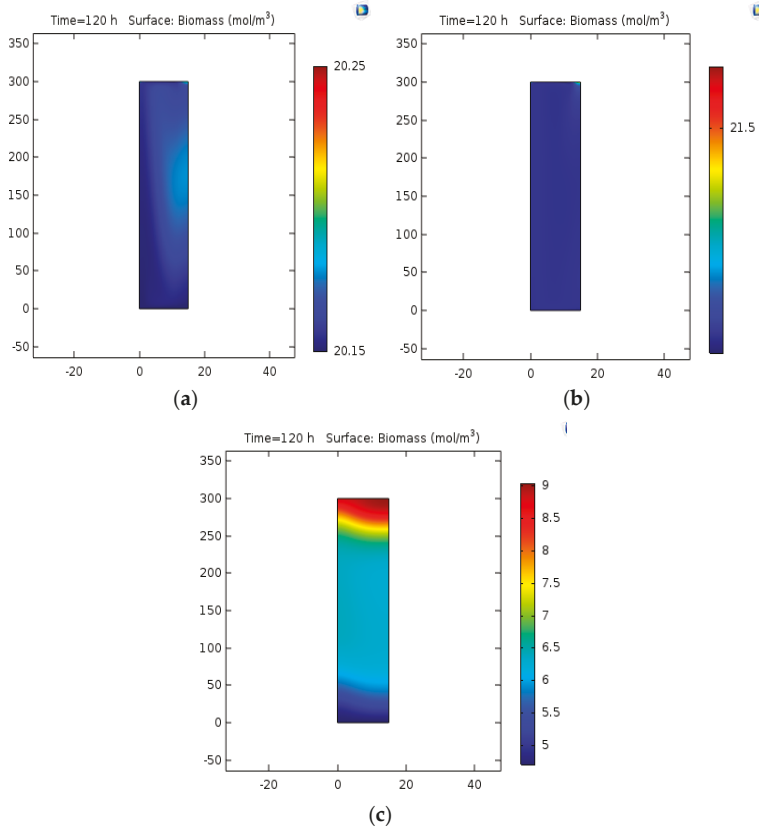

Figure 8. (**a**) Biomass concentration at the gas velocity of 0.0015 m/s, (**b**) biomass concentration at the gas velocity of 0.065 m/s, (**c**) biomass concentration at the gas velocity of 0.15 m/s.

3.5. Effect of Changing the Bubble Diameter on the Concentration

In Figure 9a,b, the change of concentration of the biomass can be observed with a bubble diameter of 3.5 and 1.5 mm.

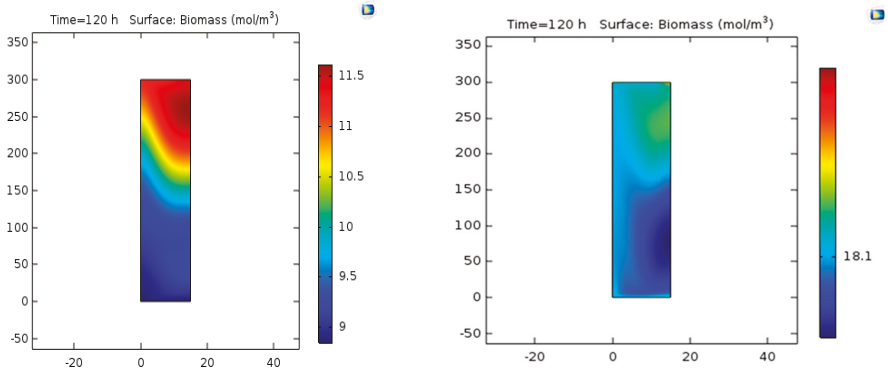

Figure 9. (**a**) Biomass concentration with a bubble diameter of 3.5 mm. (**b**) Biomass concentration with a bubble diameter of 1.5 mm.

3.6. Pressure Analysis

The relation between the amount of gravity and the bubbles are directed which are effected on pressure changes as presented in Figure 10.

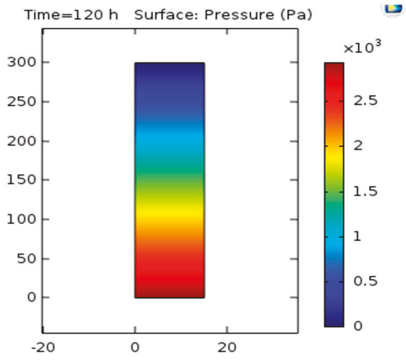

Figure 10. Pressure contour in two-dimensional mode.

3.7. Gas Accumulation

Gas accumulation is a dimensionless key dimensional parameter for design purposes identifying the phenomenon of transition in bubble column systems (Equation (11)). It is basically defined as the volume fraction of gas-phase occupied by gas bubbles. Similarly, liquid and solid phases can be determined as a liquid and solid phase coefficient. All studies examined gas accumulation because it plays an essential role in the design and analysis of bubble columns. The volume of gas accumulation with the mathematical relation was studied. In similar, the results achieved in the simulation show the very low gas accumulation in the lower part of the reactor and around the central axis, which can be observed in Figure 11a,b. Along the reaction, gas accumulation increases throughout the reactor but it is false since the accumulated gas is eliminated from the upper end of the reactor and ultimately the amount of accumulated gas at the bottom of the reactor is computed. The graph of gas volume coefficient throughout the reactor can be seen in Figure 11c, such as the value of gas volume coefficient and their increase and decrease tendency with time and position.

$$\varepsilon\_g=u\_g/(0.3+2u\_g) \quad (11)$$

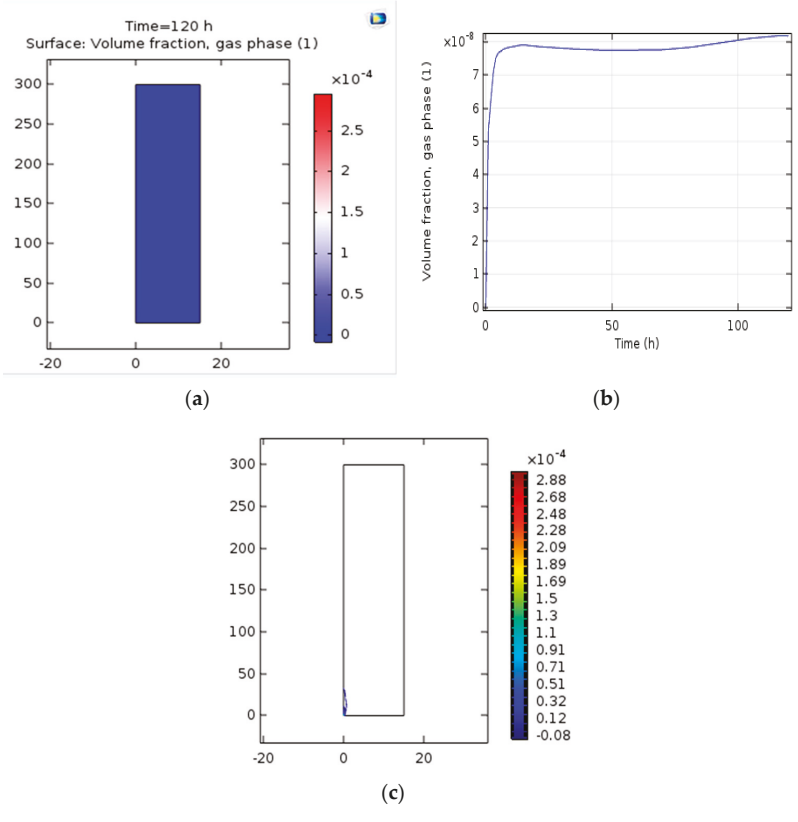

Figure 11. (**a**) The surface rate of gas accumulation along the reactor. (**b**) The rate of gas accumulation along the reactor. (**c**) Gas volume coefficient versus time.

3.8. Shear Stress

In the present project, the shear stress in different input flows was studied indicating (20) and (21) the stress rate, which is based on the scale available on the right of these shapes, the results achieved in line with the expectation of the sign, which contributes to an increase in the stress rate at the vicinity of the oven in line with the increase in the rate of intake gas and discharge. Figure 12 indicates the stress rate over time.

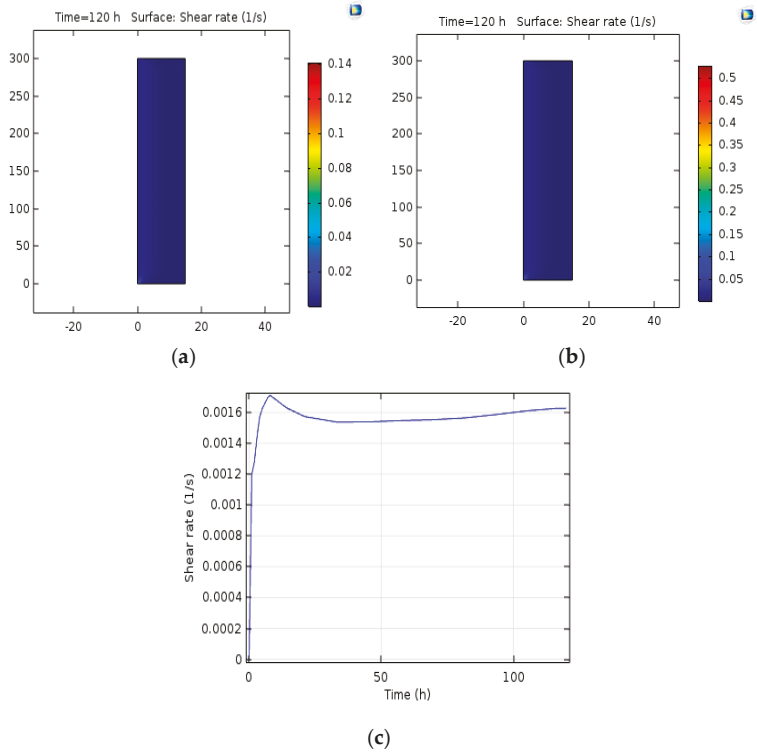

Figure 12. (**a**) The stress rate at the gas input velocity of 0.015 m/s. (**b**) The stress rate at the gas input velocity of 0.055 m/s. (**c**) The stress rate over time.

4. Discussion

4.1. The Results of Resolution Independence Analysis of Numerical Grid

As Table 2 shows, the variance in the three large, medium, and fine grid sizes is less than 1% indicating the independence of the obtained responses on the type and size of the grid.

4.2. Concentration of Biomass

4.2.1. Concentration Contour

Figure 3 shows that from the center toward the wall, concentrations are reducing being observed in Figure 3b. Thus, the largest value of production is located near the central axis. By enhancing the velocity of the areas around the center of the bioreactor, the maximum concentration, and with a distance less than the center of the percentage of production means that the increase in velocity would lead to a shorter spatial dimension to the final production.

Mousavi et al. examined the simulation of PHB production in an aircraft bioreactor with Fluent software. The average molecular concentration of PHB in the bioreactor was almost 0.331 and 0.3337 mol/L [36].

4.2.2. Concentration Variations versus Time

Figure 5 shows the changes in the concentration of biomass were investigated vs. time. The final concentration of biomass is 14 mol/m^3. The researchers showed the production of PHB was 8 g/L in

a bubble column bioreactor at optimized conditions [17]. In addition, Shah Hosseini et al. applied a dynamic optimization program written in MATLAB software to specify the optimal amount of carbon and nitrogen sources on PHB production. The proposed model presented was confirmed on the experimental data. Using the preferred feed strategy, PHB was enhanced by 100% [37].

4.3. Velocity Contour

Figure 7 shows the results of spatial changes in fluid velocity in the bioreactor. Dean et al. (2013) evaluated the use of large-spin simulations (LES) in mathematical simulations of microwave in bubble column reactors. The Euler–Euler approach is used to clarify two-phase motion equations that correspond slightly to the experimental data for both mid-velocity and motor velocities. LES provides better matching with simulation data through the k-ε model [38].

Mousavi et al. studied the fluid velocity fluctuations of the aircraft bioreactor in which the maximum fluid velocity can be seen in the input aperture at the bottom of the reactor. Similarly, the velocity of the fluid in the Down Comer is much lower than the Riser section [36].

Liquid velocity can directly effect production and methane gas enhances the growth structure of the biomass because these two parameters change in parallel. The flow rate can also change the behavior of the bioreactor and can change the production speed according to the size of the meshes designed [39,40].

4.4. Analysis of Variations in the Input Gas Velocity

The result of change of the gas flow rate inside the reactor vs. the number of bubbles and mass transfer rate (at four different velocities of 0.055, 0.015, 0.065, and 0.15 m/s) are displayed in Figure 8. As can be observed, as the gas flow rate increases, the content of biomass increases because of the increase in the number of bubbles and the number of encounters, which finally leads to an increase in the mass transfer rate and biomass production. The effects of gas and liquid velocity in a bubble pillar biomass with COMSOL software varying in the gas-liquid bubble column system, the velocity of gas and liquid with time and space in the column. Weather velocity vectors were achieved after a semi-stable mode at an input velocity of 0.001 m/s [41]. Such vectors indicated the velocity of the path along the path, which is useful in specifying the patterns of flow in the bubble column system. That contour indicated a gas concentration of 0.001 m/s.

4.5. Effect of Changing the Bubble Diameter on the Concentration

Figure 9 shows that the concentration of the biomass is reduced by increasing the diameter of the bubble to reduce the flow rate. In addition, it enhances the final concentration of biomass by decreasing the diameter of the bubble.

4.6. Pressure Analysis

As it can be observed in Figure 10, the pressure across the reactor from bottom to top reduces because of the presence of gravity on the bubbles.

4.7. Gas Accumulation

The graph of changes in gas volume throughout the reactor can be seen in Figure 11. In 2010, Mousavi et al. studied gas cumulating in aircraft bioreactors at numerous aeration rates [36]. The results obtained from the simulation were compared to the results of different mathematical relations related to the bubble columns and aircraft reactors. The simulation results are relatively suitable in comparison to the relationships and it approves the reliability of the simulation. For the aeration rate of 30 L/g. min, the mean diameter of the bubble was 5.1 mm [36].

Gas accumulation occurs during the five different phases of aeration. As expected, the amount of gas accumulation increased with aeration. The highest volume is always increased initially and then

gas accumulation decreases because of the gas outflow from the bioreactor. However, in cases with higher aeration rates (40 and 50 L/min), the final amount of gas accumulation is higher than the peak value. In higher aeration conditions (40 and 50 L/min), the amount of gas accumulation is higher than the initial rate of gas accumulation in comparison to the lower aeration rate due to the accumulation of gas in the liquid phase.

4.8. Shear Stress

Wall shear stress is a critical parameter for determining energy transfer and movement in a two-phase flow system. The shear stress properties play an essential role in understanding the internal state of the two-phase flow because the liquid velocity and the highest grade of turbulence fluctuations are specified with the highest gradient. In order to clarify the mechanism of the two-phase bubble flow, it is significant to know the performance of the bubbles in the fluid flow. The movement of isolated bubbles seems to be related to the bubble distortion, the location of the injection point, and the average fluid flow rate. They found the only bubbles with diameters less than 5 mm along the wall while all the spherical bubbles and elliptical bubbles with a diameter greater than 5 milligram meters in the core of the stream [42,43]. Mousavi et al. in a study on shear stress in aircraft bioreactors specified the average shear stress in the bioreactor by applying the equations in FLUENT software for five different conditions. As expected, aeration enhances the shear stress in the bioreactor. Since airborne bioreactors and bubble columns fail at having a propellant, their tensions are lower than those of cohesive bioreactors, and the shear stress in the bioreactor is not likely to be significant, while the ability of the software to calculate shear stress is critical. The greatest shear stress relates to areas where gas is flowing from the opening. Vortices are located at the vicinity of upstream and downstream sections as well as the walls with higher shear stresses compared to other points [36].

5. Conclusions

In this study, a simulation of microorganisms capability for the production of PHB from natural gas (source of carbon) was carried out. The error interval is normally up to 20% for the difference between laboratory data and simulation because the resulting error can be because of simple simulation assumptions; thus, the simulation results were in good accordance with empirical results. Regarding the concentration contour, concentration is the lowest in the center of maximum concentration near the wall. The concentration gradient from the center is toward the wall and produces the highest percentage of production near the central axis of the bioreactor. Substrates and microorganisms with the environment were considered homogeneous, thus we would not have much difference in production compared to the place. Enhancing the gas flow rate has a direct relation to the production rate. Based on the three-velocity concentration-time graph, enhancing the intake rate of the agitator stirring increases and the percent of production enhances. The flow pattern in a bioreactor is dependent on the diameter of the bioreactor and the flow rate of the inlet gas. In this study, the bubble flow studied it placed due to the low velocity of the inlet gas (0.015 m/s) and the low diameter of the bioreactor (1.5 cm). Because of the concentration contour with enhancing the flux, the number of bubbles increases and results in more mass transfer and an increase in the value of biomass production. With increasing fluid velocity, a decrease can be seen in the amount of gas accumulation because liquid bubbles are rapidly displaced by liquid at higher velocities. Moreover, increasing fluid velocity decreases the duration of bubble stays.

Furthermore, based on the results in volume concentration, 50/50 from air and methane, the highest rate of microorganism growth and PHB production was achieved. According to presented graphs, such as time concentration and location concentration, the final amount of biomass production extracted was 1.6338 g/L under optimal conditions. The reason for selecting the volume of 50/50 was the coordination with the Taguchi algorithm that is based on research in the same conditions is the ideal conditions for evaluation of chosen sizes of the system. In addition, the amount of mesh size in the system was not significantly affected by the final concentration of production, so the ideal condition

was regularly 1.6338 g/L. Thus, in different conditions of meshes, less than 1% difference was observed. In addition, the amount of gas accumulation decreases with increasing gas velocity.

Author Contributions: Conceptualization, M.M., F.Y., and S.R.M.; methodology, F.Y.; software, M.M.; validation, R.A. and F.Y.; formal analysis, R.A. and K.K.-D.; investigation, M.M.; resources, F.Y.; data curation, K.K.-D.; guidance and validation: H.R.; writing—original draft preparation, F.Y. and K.K.-D.; writing—review and editing, F.Y. and K.K.-D.; supervision, F.Y.

Funding: This research received no external funding.

Acknowledgments: Authors wish to acknowledge all administrative and technical support supports given by Tehran University.

Conflicts of Interest: The authors declare no conflict of interest. The funders had no role in the design of the study; in the collection, analyses, or interpretation of data; in the writing of the manuscript, or in the decision to publish the results.

Appendix A

List of symbols in equations:

Parameters	Description
C_{PHB}	Dry weight of cell (g/L)
K_d	Cell death rate (s/1)
μ	Growth rates for cell mass (1/s)
μ_{max}	The maximum specific growth rate of microorganisms (1/s)
S	The concentration of limited substrate for growth (g/L)
Ks	Monod constant (g/L)
α	Fixed cell death time (s^{-1})
K_d (∞)	Infinite cell death rate (s^{-1})
u_l	Velocity value in (m/s)
p	Pressure in (Pa)
ϕ	Volume fraction indicated with m^3/m^3
ρ	Density value with kg/m^3
g	Gravity unit with m/s^2
F	N/m^3
μL	Dynamic velocity Pa.s
m_{gl}	The mass transfer rate from gas to liquid (kg/m^3)
U_{slip}	Relative velocity
U_{drift}	Drift velocity
M	The molecular weight of the gas (kg/mol)
R	Ideal gas constant (J/(mol·K) 3/3141472)
T	Temperature (K)
P_{ref}	Scalar variable at (1 at or 101.325 Pa)
μ	Effective viscosity

References

1. Brandl, H.; Gross, R.A.; Lenz, R.W.; Fuller, R.C. Plastics from bacteria and for bacteria: Poly (β-hydroxyalkanoates) as natural, biocompatible, and biodegradable polyesters. In *Microbial Bioproducts*; Springer: Berlin, Germany, 1990; pp. 77–93.
2. Reddy, C.S.K.; Ghai, R.; Kalia, V. Polyhydroxyalkanoates: An overview. *Bioresour. Technol.* **2003**, *87*, 137–146. [CrossRef]
3. Shimao, M. Biodegradation of plastics. *Curr. Opin. Biotechnol.* **2001**, *12*, 242–247. [CrossRef]
4. Chen, C.S.; Liu, T.G.; Lin, L.W.; Xie, X.D.; Chen, X.H.; Liu, Q.C.; Liang, B.; Yu, W.W.; Qiu, C.Y. Multi-walled carbon nanotube-supported metal-doped ZnO nanoparticles and their photocatalytic property. *J. Nanopart. Res.* **2013**, *15*, 1295. [CrossRef] [PubMed]

5. Braunegg, G.; Lefebvre, G.; Genser, K.F. Polyhydroxyalkanoates, biopolyesters from renewable resources: Physiological and engineering aspects. *J. Biotechnol.* **1998**, *65*, 127–161. [CrossRef]
6. Mofradnia, S.R.; Tavakoli, Z.; Yazdian, F.; Rashedi, H.; Rasekh, B. Fe/starch nanoparticle-Pseudomonas aeruginosa: Bio-physiochemical and MD studies. *Int. J. Biol. Macromol.* **2018**, *117*, 51–61. [CrossRef] [PubMed]
7. Mofradnia, S.R.; Ashouri, R.; Tavakoli, Z.; Shahmoradi, F.; Rashedi, H.; Yazdian, F. Effect of zero-valent iron/starch nanoparticle on nitrate removal using MD simulation. *Int. J. Biol. Macromol.* **2018**, *121*, 727–733. [CrossRef] [PubMed]
8. Ashouri, R.; Ghasemipoor, P.; Rasekh, B.; Yazdian, F.; Mofradnia, S.R.M.; Ghasemipoor, R.A.P.; Yazdian, B.R.F.; Mofradnia, S.R.M. The effect of ZnO-based carbonaceous materials for degradation of benzoic pollutants: A review. *Int. J. Environ. Sci. Technol.* **2018**, *16*, 1–12. [CrossRef]
9. Khanna, S.; Srivastava, A.K. Statistical media optimization studies for growth and PHB production by Ralstonia eutropha. *Process Biochem.* **2005**, *40*, 2173–2182. [CrossRef]
10. Young, F.K.; Kastner, J.R.; May, S.W. Microbial production of poly-β-hydroxybutyric acid from D-xylose and lactose by Pseudomonas cepacia. *Appl. Environ. Microbiol.* **1994**, *60*, 4195–4198. [PubMed]
11. Lee, S.Y. Bacterial polyhydroxyalkanoates. *Biotechnol. Bioeng.* **1996**, *49*, 1–14. [CrossRef]
12. Yamane, T. Yield of poly-D (−)-3-hydroxybutyrate from various carbon sources: A theoretical study. *Biotechnol. Bioeng.* **1993**, *41*, 165–170. [CrossRef] [PubMed]
13. Saratale, R.G.; Saratale, G.D.; Cho, S.K.; Kim, D.S.; Ghodake, G.S.; Kadam, A.; Kumar, G.; Bharagava, R.N.; Banu, R.; Shin, H.S. Pretreatment of kenaf (*Hibiscus cannabinus* L.) biomass feedstock for polyhydroxybutyrate (PHB) production and characterization. *Bioresour. Technol.* **2019**, *282*, 75–80. [CrossRef] [PubMed]
14. Khosravi-Darani, K.; Bucci, D.Z. Application of poly (hydroxyalkanoate) in food packaging: Improvements by nanotechnology. *Chem. Biochem. Eng. Q.* **2015**, *29*, 275–285. [CrossRef]
15. Darani, K.K.; Vasheghani-Farahani, E.; Tanaka, K. Hydrogen oxidizing bacteria as poly (hydroxybutyrate) producers. *Iran. J. Biotechnol.* **2006**, *4*, 193–196.
16. Khosravi-Darani, K.; Yazdian, F.; Babapour, F.; Amirsadeghi, A.R. Poly (3-hydroxybutyrate) Production from Natural Gas by a Methanotroph Native Bacterium in a Bubble Column Bioreactor. *Chem. Biochem. Eng. Q.* **2019**, *33*, 69–77. [CrossRef]
17. Ghoddosi, F.; Golzar, H.; Yazdian, F.; Khosravi-Darani, K.; Vasheghani-Farahani, E. Effect of carbon sources for PHB production in bubble column bioreactor: Emphasis on improvement of methane uptake. *J. Environ. Chem. Eng.* **2019**, *7*, 102978. [CrossRef]
18. Mokhtari-Hosseini, Z.B.; Vasheghani-Farahani, E.; Heidarzadeh-Vazifekhoran, A.; Shojaosadati, S.A.; Karimzadeh, R.; Darani, K.K. Statistical media optimization for growth and PHB production from methanol by a methylotrophic bacterium. *Bioresour. Technol.* **2009**, *100*, 2436–2443. [CrossRef] [PubMed]
19. Mokhtari-Hosseini, Z.B.; Vasheghani-Farahani, E.; Shojaosadati, S.A.; Karimzadeh, R.; Heidarzadeh-Vazifekhoran, A. Effect of feed composition on PHB production from methanol by HCDC of Methylobacterium extorquens (DSMZ 1340). *J. Chem. Technol. Biotechnol. Int. Res. Process. Environ. Clean Technol.* **2009**, *84*, 1136–1139.
20. Bozorg, A.; Vossoughi, M.; Kazemi, A.; Alemzadeh, I. Optimal medium composition to enhance poly-β-hydroxybutyrate production by Ralstonia eutropha using cane molasses as sole carbon source. *Appl. Food Biotechnol.* **2015**, *2*, 39–47.
21. Koller, M.; Hesse, P.; Fasl, H.; Stelzer, F.; Braunegg, G. Study on the Effect of Levulinic Acid on Whey-Based Biosynthesis of Poly (3-hydroxybutyrate-co-3-hydroxyvalerate) by Hydrogenophaga pseudoflava. *Appl. Food Biotechnol.* **2017**, *4*, 65–78.
22. Khosravi-Darani, K.; Mokhtari, Z.B.; Amai, T.; Tanaka, K. Microbial production of poly (hydroxybutyrate) from C 1 carbon sources. *Appl. Microbiol. Biotechnol.* **2013**, *97*, 1407–1424. [CrossRef] [PubMed]
23. Shahhosseini, S.; Sadeghi, M.T.; Khosravi Darani, K. Simulation and Model Validation of Batch PHB production process using Ralstonia eutropha. *Iran. J. Chem. Chem. Eng.* **2003**, *22*, 35–42.
24. Khosravi Darani, K.; Vasheghani Farahani, E.; Shojaosadati, S.A. Application of the Plackett-Burman Statistical Design to Optimize Poly (Î²-hydroxybutyrate) Production by Ralstonia eutropha in Batch Culture. *Iran. J. Biotechnol.* **2003**, *1*, 155–161.
25. Vasheghani Farahani, E.; Khosravi Darani, K.; Shojaosadati, S.A. Application of the Taguchi Design for Production of Poly (β-hydroxybutyrate) by Ralstonia eutropha. *Iran. J. Chem. Chem. Eng.* **2004**, *23*, 131–136.

26. Khosravi-Darani, K.; Vasheghani-Farahani, E. Application of supercritical fluid extraction in biotechnology. *Crit. Rev. Biotechnol.* **2005**, *25*, 231–242. [CrossRef] [PubMed]
27. Asenjo, J.A.; Suk, J.S. Microbial conversion of methane into poly-β-hydroxybutyrate (PHB): Growth and intracellular product accumulation in a type II methanotroph. *J. Ferment. Technol.* **1986**, *64*, 271–278. [CrossRef]
28. Yazdian, F.; Shojaosadati, S.A.; Nosrati, M.; Pesaran Hajiabbas, M.; Vasheghani-Farahani, E. Investigation of gas properties, design, and operational parameters on hydrodynamic characteristics, mass transfer, and biomass production from natural gas in an external airlift loop bioreactor. *Chem. Eng. Sci.* **2009**, *64*, 2455–2465. [CrossRef]
29. Bozorg, M.; Mofradnia, R. Simulation of Bioreactors for Poly (3-hydroxybutyrate) Production from Natural Gas. *IJCCE* **2018**. (In press)
30. Pérez, R.; Casal, J.; Muñoz, R.; Lebrero, R. Polyhydroxyalkanoates production from methane emissions in Sphagnum mosses: Assessing the effect of temperature and phosphorus limitation. *Sci. Total Environ.* **2019**, *688*, 684–690. [CrossRef]
31. Zinn, M.; Witholt, B.; Egli, T. Occurrence, synthesis and medical application of bacterial polyhydroxyalkanoate. *Adv. Drug Deliv. Rev.* **2001**, *53*, 5–21. [CrossRef]
32. Rezapour, N.; Rasekh, B.; Mofradnia, S.R.; Yazdian, F.; Rashedi, H.; Tavakoli, Z. Molecular dynamics studies of polysaccharide carrier based on starch in dental cavities. *Int. J. Biol. Macromol.* **2018**, *121*, 616–624. [CrossRef] [PubMed]
33. Bordel, S.; Rodríguez, E.; Muñoz, R. Genome sequence of Methylocystis hirsuta CSC1, a polyhydroxyalkanoate producing methanotroph. *Microbiologyopen* **2019**, *8*, e00771. [CrossRef] [PubMed]
34. Rahnama, F.; Vasheghani-Farahani, E.; Yazdian, F.; Shojaosadati, S.A. PHB production by Methylocystis hirsuta from natural gas in a bubble column and a vertical loop bioreactor. *Biochem. Eng. J.* **2012**, *65*, 51–56. [CrossRef]
35. Yang, H.; Ye, H.; Zhai, S.; Wang, G.; Mavaddat, P.; Mousavi, S.M.; Amini, E.; Azargoshasb, H.; Shojaosadati, S.A. Modeling and CFD-PBE simulation of an airlift bioreactor for PHB production. *Asia Pac. J. Chem. Eng.* **2014**, *9*, 562–573.
36. Mousavi, S.M.; Shojaosadati, S.A.; Golestani, J.; Yazdian, F. CFD simulation and optimization of effective parameters for biomass production in a horizontal tubular loop bioreactor. *Chem. Eng. Process. Process Intensif.* **2010**, *49*, 1249–1258. [CrossRef]
37. Shah, A.A.; Hasan, F.; Hameed, A.; Ahmed, S. Biological degradation of plastics: A comprehensive review. *Biotechnol. Adv.* **2008**, *26*, 246–265. [CrossRef]
38. Lau, Y.M.; Deen, N.G.; Kuipers, J.A.M. Development of an image measurement technique for size distribution in dense bubbly flows. *Chem. Eng. Sci.* **2013**, *94*, 20–29. [CrossRef]
39. Yazdian, F.; Shojaosadati, S.A.; Nosrati, M.; Pesaran Hajiabbas, M.; Malek Khosravi, K. On-Line Measurement of Dissolved Methane Concentration During Methane Fermentation in a Loop Bioreactor. *Iran. J. Chem. Chem. Eng.* **2009**, *28*, 85–93.
40. Yazdian, F.; Shojaosadati, S.A.; Fatemi, S. Study of Growth Kinetic Models of a Methanotroph Bacterium Growing on Natural Gas. *J. Chem. Pet. Eng.* **2009**, *43*. [CrossRef]
41. Šimčík, M.; Mota, A.; Ruzicka, M.C.; Vicente, A.; Teixeira, J. CFD simulation and experimental measurement of gas holdup and liquid interstitial velocity in internal loop airlift reactor. *Chem. Eng. Sci.* **2011**, *66*, 3268–3279. [CrossRef]
42. Wallen, L.L.; Rohwedder, W.K. Poly-beta-hydroxyalkanoate from activated sludge. *Environ. Sci. Technol.* **1974**, *8*, 576–579. [CrossRef]
43. Koller, M. Switching from petro-plastics to microbial polyhydroxyalkanoates (PHA): The biotechnological escape route of choice out of the plastic predicament? *EuroBiotech J.* **2019**, *3*, 32–44. [CrossRef]

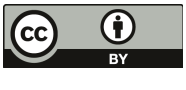

bioengineering

MDPI

Review

Bioprocess Engineering Aspects of Sustainable Polyhydroxyalkanoate Production in Cyanobacteria

Donya Kamravamanesh [1,2], Maximilian Lackner [2,3] and Christoph Herwig [1,*]

[1] Institute of Chemical, Environmental and Bioscience Engineering, Research Area Biochemical Engineering, Technische Universität Wien, 1060 Vienna, Austria; donya.kamravamanesh@tuwien.ac.at
[2] Lackner Ventures and Consulting GmbH, Hofherr Schrantz Gasse 2, 1210 Vienna, Austria; kontakt@drlackner.com
[3] Institute of Industrial Engineering, University of Applied Sciences FH Technikum Wien, Höchstädtplatz 6, 1200 Vienna, Austria
* Correspondence: christoph.herwig@tuwien.ac.at; Tel.: +43-1-58801-166400

Received: 22 November 2018; Accepted: 15 December 2018; Published: 18 December 2018

Abstract: Polyhydroxyalkanoates (PHAs) are a group of biopolymers produced in various microorganisms as carbon and energy reserve when the main nutrient, necessary for growth, is limited. PHAs are attractive substitutes for conventional petrochemical plastics, as they possess similar material properties, along with biocompatibility and complete biodegradability. The use of PHAs is restricted, mainly due to the high production costs associated with the carbon source used for bacterial fermentation. Cyanobacteria can accumulate PHAs under photoautotrophic growth conditions using CO_2 and sunlight. However, the productivity of photoautotrophic PHA production from cyanobacteria is much lower than in the case of heterotrophic bacteria. Great effort has been focused to reduce the cost of PHA production, mainly by the development of optimized strains and more efficient cultivation and recovery processes. Minimization of the PHA production cost can only be achieved by considering the design and a complete analysis of the whole process. With the aim on commercializing PHA, this review will discuss the advances and the challenges associated with the upstream processing of cyanobacterial PHA production, in order to help the design of the most efficient method on the industrial scale.

Keywords: polyhydroxyalkanoate (PHA), bioprocess design; carbon dioxide; cyanobacteria; upstream processing

1. Introduction

Petroleum-based polymers are relatively inert, versatile, and durable; therefore, they have been used in industry for more than 70 years [1]. However, they bear negative properties such as CO_2 emissions from incineration, toxicity from additives, and accumulated toxic substances in the environment, particularly in marine as microplastics, recalcitrance to biodegradation, and massive waste accumulation into the marine environment and the landfills [2,3]. With the limited fossil fuel resources and the environmental impact associated with the products, the research for an alternative seems essential in order to reduce our dependencies on non-renewable resources [4,5].

Biodegradable polymers, due to their eco-friendly nature, offer one of the best solutions to environmental problems caused by synthetic polymers [5]. Polyhydroxyalkanoates (PHAs) are a class of naturally occurring polymers produced by microorganisms [1,6,7], among which poly (3-hydroxybutyrate) (PHB) is the most studied biodegradable polymer that accumulates in bacteria in the form of inclusion bodies as carbon reserve material when cells grow under stress conditions [5,8]. PHB with a high crystallinity represents properties similar to synthetic polyesters and also to polyolefins such as polypropylene [6,9,10]. In addition, due to biocompatibility and

biodegradability, PHB possesses extensive interesting functions and can replace fossil-based plastics in many applications [7]. However, the low elongation and break and the brittleness of PHB are limitations that can be overcome using other PHA, like blends of copolymers such as polyhydroxyvalerate (PHV) and poly (3-hydroxybutric acid-co-3-hydroxyvaleric acid) (PHBV). The copolymer can either be directly biosynthesized under varying cultivation conditions or be chemically produced in vitro. Apart from short-chain length PHA, there are medium- and long-chain-length polymers which can help to tailor the material properties [11]. The strategies to overcome these limitations are studied in various wild-type and recombinant cyanobacteria, reviewed by Lackner et al. and Balaji et al. [11,12].

Today, PHB is commercially produced by heterotrophic bacteria, such as *Cupriavidus necator* (*C. necator*), and recombinant *Escherichia coli* (*E. coli*) [6,13,14]. High production cost, when compared with petroleum-based polymers, is one major challenge for extensive production and commercialization of PHB [5]. Major contributors to the overall cost being the expensive substrates, continuous oxygen supply, equipment depreciation, high energy demand, and chemicals used for downstream processing [15–17].

Attention has been focused to reduce the production cost, mostly by selecting more economically feasible and efficient carbon substrates for PHB production such as whey, hemicellulose, sugar cane, agricultural wastes, and molasses [5,18–20]. In this context, PHB production using cyanobacteria from more sustainable resources, such as CO_2, has gained importance. Cyanobacteria are an ideal platform for the production of biofuels and bulk chemicals through efficient and natural CO_2 fixation [21].

Other reviews have mainly discussed the potential of cyanobacteria for PHA production, cultivation conditions, and cyanobacterial metabolism, as well as the applications and industrial prospects of the synthesis of this biopolymer [22–26]. Minimization of the PHA production cost can only be achieved by considering the design and a complete analysis of the whole process [27]. In this work, the authors will discuss the bioprocess engineering aspects that focus on upstream processing and advances of sustainable PHA production from cyanobacteria, concentrating primarily on the unit operations of the upstream processing. The authors believe that a proper-time resolved quantification of the process will aid in a better understanding for process manipulation and optimization of industrial production.

2. Cyanobacteria: The Future Host in Biotechnology

Cyanobacteria are gram-negative bacteria with a long evolutionary history and are the only prokaryotes capable of plant-like oxygenic photosynthesis [28]. Unlike heterotrophic organisms, cyanobacteria require only greenhouse gas CO_2 and sunlight, along with minimal nutrients for growth, eliminating the cost of carbon source and complex media components [28]. Cyanobacteria are equipped with superior photosynthetic machinery, showing higher biomass production rates compared to plants and can convert up to 3–9% of the solar energy into biomass [28,29]. Moreover, in contrast to plants, cultivation of cyanobacteria requires less land area, therefore cyanobacteria do not compete for arable land used for agriculture [30]. Some cyanobacteria can produce PHB, when essential nutrients for growth, such as nitrogen and phosphorus, is limiting. From an economic point of view, however, photosynthetic PHB production in cyanobacteria has two major disadvantages: little productivity and slow growth [25]. Therefore, in order to promote photosynthetic PHB production on an industrially relevant scale, the productivity needs to improve significantly. Productivity is defined as the amount of PHA produced by unit volume in unit time [27]. In spite of all the efforts done, so far, very few reports have shown an actual improvement in the cyanobacterial PHB production process, while there are various challenges associated with cultivation, engineering and large-scale production of autotrophic cyanobacterial biomass.

3. Challenges in Cyanobacterial Bioprocess Technology

Figure 1 represents a bioprocess development chain for cyanobacterial PHA production consisting of strain and bioprocess developments and the downstream processing. The workflow shows the

strain selection, strain improvement, process understanding, and strategies for scale-up and then down-stream processing, representing the separation and purification of the final product. In order to obtain an optimal scalable bioprocess and in-depth understanding of the bioprocess kinetics, the following points have to be known. First, the holistic knowledge of enzymatic and metabolic pathways of the PHB biosynthesis in cyanobacteria. Second, the selection or development of the optimal strain with maximum productivity. Third, the selection of inexpensive substrate and optimization of media components for the particular production strain. Fourth, the design of the bioreactor system and the optimization of process parameters for scale-up, using the statistical design of experiments (DoE). Fifth, the usage of past data and advanced mathematical models for monitoring and control. Lastly, the development of novel strategies for PHB recovery with a minimum cost of energy and chemical requirement. This review will mainly focus on the bioprocess engineering aspects of photosynthetic PHB production providing an overview of the PHB production process chain starting from a single cell.

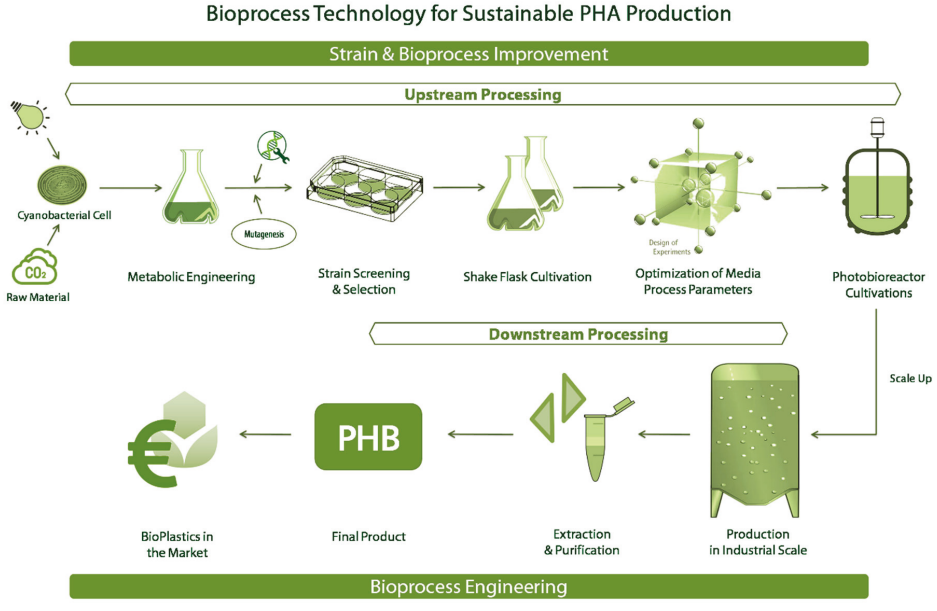

Figure 1. Represents the work-flow in bioprocess technology for the production of polyhydroxyalkanoates (PHAs) using cyanobacteria as the host system.

3.1. Process Design and Optimization

3.1.1. Existing Wild-Type Strains and Their Reported PHB Content

Cyanobacteria are indigenously the only organisms that produce PHA biopolymers using oxygenic photosynthesis [24]. Cyanobacteria grow mainly under autotrophic conditions, nevertheless, supplementation of sugars or organic acids in some species increases growth and PHB accumulation [24], which contributes to the production cost. To date, a few cyanobacterial strains have been identified for photosynthetic PHB accumulation. Table 1 presents the wild-type cyanobacterial strains, their PHB content in dry cell weight (DCW), and the carbon source used for the production.

As is indicated in Table 1, the PHB production process using CO_2 as the only carbon source shows a lower product content than using organic acids or sugars as substrate.

Table 1. Examples of wild-type cyanobacterial strains, with reported poly (3-hydroxybutyrate) (PHB) content, the carbon source, and growth conditions used for the production of the polymer.

Cyanobacteria	PHB Content (% DCW)	Substrate	Production Condition	Polymer Composition	Reference
Synechocystis sp. PCC 6803	38	Acetate	P limitation and gas exchange limitation [1]	PHB	[31]
Synechocystis sp. PCC 6714	16	CO_2	N [2] and P [3] limitation	PHB	[32]
Spirulina platensis	6.0	CO_2	Not given	PHB	[33]
Spirulina platensis UMACC 161	10	acetate and CO_2	N starvation	PHB	[34]
Spirulina maxima	7–9	CO_2	N and P limitation	PHB	[35]
Gloeothece sp. PCC 6909	9.0	acetate	Not given	Not specified	[36]
Nostoc moscorum Agardh	60	acetate and valerate	N deficiency	PHB-co-PHV	[37]
Nostoc moscorum	22	CO_2	P starvation	PHB	[38]
Alusira fertilisima CCC444	77	fructose and valerate	N deficiency	PHB-co-PHV	[39]
Alusira fertilisima CCC444	85	citrate and acetate	P deficiency	PHB	[40]
Synechocystis PCC 7942	3	CO_2	N limitation	PHB	[41]
Synechocystis PCC 7942	25.6	acetate	N limitation	PHB	[41]
Synechocystis sp. CCALA192	12.5	CO_2	N limitation	PHB	[42]
Anabaena Cylindrica	<0.005	CO_2	Balanced growth	PHB	[43]
Anabaena cylindrica	2.0	propionate	N limitation	PHB + PHV	[43]
Synechococcus elongatus	17.2	CO_2 and sucrose	N deficiency	Not specified	[44]
Caltorix scytonemicola TISTR 8095	25	CO_2	N deficiency	PHB	[45]

[1] gas exchange limitation = limitation of gas transfer to the culture vessel. [2] N = nitrogen. [3] P = phosphorus.

3.1.2. More Competent Cyanobacterial Cell Lines

Cyanobacteria are considered a sustainable and alternative host for PHB production due to their photoautotrophic nature [46]. Despite the fact that cyanobacterial PHB has been the subject of research for many years, it has not found its way to the market. One of the main challenges for cyanobacterial products to enter the market is that cyanobacterial strains are not yet optimized as cell factories for industrial processes. Intensive research has been done over the past 20 years for cyanobacterial strain improvement, research that has aimed to increase PHB productivity, mainly by overexpression of PHB biosynthetic genes. However, these attempts have rarely shown success regarding increased volumetric or specific polymer content for commercial production of cyanobacterial PHB. Recently, Katayama et al. reviewed the production of bioplastic compounds using genetically modified and metabolically engineered cyanobacteria [47]. In this study, we provide a list of genetically modified cyanobacteria with their PHB content and the tools used for the metabolic engineering of the strain.

3.1.3. Genetic Engineering of Cyanobacteria for PHB Production

Being prokaryotic, cyanobacteria possess a relatively simple genetic background which eases their manipulation [48]. Most cyanobacterial studies on metabolic engineering and PHB biosynthesis have been conducted with a limited number of model strains, of which *Synechocystis* sp. PCC 6803 is the most widely studied species for cyanobacterial research. The research, which has been done for decades on photosynthesis and the genome annotations, has resulted in a wide range of metabolic engineering tools and extensive biological insight for this species [48,49]. PHB production in cyanobacteria occurs mainly via three biosynthetic steps, where two molecules of acetyl-CoA form one molecule of acetoacetyl-CoA using the enzyme 3-ketothiolase encoded with the *phaA* gene [50]. Later, acetoacetyl-CoA is reduced by PhaB to hydroxybutyryl-CoA, utilizing NADPH as an electron donor [51]. In the end, the PHA synthase comprises of PhaC and PhaE polymerizes (R)-3-hydroxybutyryl-CoA to PHB [50,52]. Table 2 summarizes the efforts to overcome the bottlenecks in PHB biosynthetic pathway in cyanobacteria.

Table 2. Strategies to increase PHB biosynthesis yield.

Cyanobacterial Strain (Recombinant)	PHB Content (% DCW)	Genetic Tool Used	Production Conditions	References
Synechococcus sp. PCC 7942	1.0	Defective in glycogen synthesis	CO_2	[53]
Synechococcus sp. PCC 7942	26	Introducing PHA biosynthetic genes from *C. necator*	Acetate and nitrogen limitation	[41]
Synechocystis sp. PCC 6803	26	Overexpression of native *pha* genes	CO_2 and nitrogen deprivation	[46]
Synechocystis sp. PCC 6803	11	Introducing PHA biosynthetic genes from *C. necator*	Acetate and nitrogen limitation	[54]
Synechocystis sp. PCC 6803	14	Overexpression of PHA synthase	Direct photosynthesis	[55]
Synechocystis sp. PCC 6803	12	Increasing acetyl-CoA levels	CO_2	[56]
Synechococcus sp. PCC 7002	4.5	Introduction of GABA Shunt	CO_2	[57]
Synechocystis sp.	35	Optimization of acetoacetyl-CoA reductase binding site	CO_2	[58]
Synechocystis sp. PCC 6803	7.0	Transconjugant cells harboring expression vectors carrying *pha* genes	CO_2	[59]

Metabolic engineering of cyanobacteria with the aim to increase PHB content was also done by introducing the PHA synthase gene from *C. necator* into *Synechhocytis* sp. PCC 6803 [54]. The resulting recombinant *Synechhocytis* sp. PCC 6803 showed increased PHA synthase activity; the total PHB content, however, did not increase [47,54]. For cyanobacterial strain *Synechocystis* sp. PCC 6803, up to 35% (DCW) PHB was obtained using phaAB overexpression and 4 mM acetate [46]. However, the specific production rates in this case also did not show a significant improvement either. Recently, the overexpression of the acetoacetyl-CoA reductase gene in *Synechocystis* was found to increase the productivity of R-3-hydroxybutyrate from CO_2 to up to 1.84 g L^{-1} [58]. The highest volumetric productivity reported in this case was 263 mg L^{-1} d^{-1}.

3.1.4. Randomly Mutated Strains with Improved PHB Content

As an alternative approach to genetic engineering, random mutagenesis can be done for the generation of a mutant library with improved phenotypes. Mutagenesis can be done by exposing the cells of interest to a mutagenic source in order to induce random mutations into the genome. This can, for instance, completely knock-out a gene function [60] or increase enzymatic activity. UV irradiation is the most frequently used mutagen, which leads to transversion in the genome. Furthermore, ethidium bromide and ethyl-methanesulfonate are used as chemical mutagens [60,61]. A major disadvantage of using random mutagenesis is the need for intensive screening to select the mutant with desired phenotypes. The cyanobacterial strain *Synechocystis* sp. PCC 6714 has a great potential as photosynthetic PHB production organism. It has shown up to 17% (DCW) PHB content under nitrogen and phosphorus limiting conditions [32]. In addition to PHB, the strain also accumulates glycogen during the early phase of nitrogen limitation [62]. The random mutagenesis approach used for *Synechocystis* sp. PCC 6714 showed an increase in productivity of up to 2.5-folds resulting in 37 ± 4% (DCW) PHB for the best mutant [63]. The UV-mutation lead to an amino acid change in the phosphate system transport protein (PstA), resulting in higher efficiency of photosynthesis and CO_2 uptake rate for the mutant MT_a24 [63].

3.1.5. CRISPR/Cas Based Genome Editing in Cyanobacteria

Cyanobacteria are promising platforms for the production of biofuels and bio-based chemicals, however, the metabolic engineering of cyanobacteria poses various challenges [64]. CRISPR/Cas technology has enabled genome modification of cyanobacteria with gene substitution, marker-less point mutations, and gene knockouts and knock-ins with improved efficiency [65]. So far, the CRISPRi system has been used to downregulate the production of PHA and glycogen production in order

to increase fluxes towards other carbon storage compounds of interest [66], such as succinate [64]. However, the CRISPRi based gene editing to overexpress PHB biosynthetic genes has not been reported. While the CRISPR-based editing allows the creation of marker-less knockouts and knock-ins. Thus, in the future, the cyanobacterial strains produced might be considered commercially sustainable and safe for outdoor cultivations and CO_2 sequestration.

3.2. Process Design and Bioprocess Improvement Strategies

Nutrient deficiency or stress, mainly in terms of nitrogen or phosphorus limitation, stimulates the accumulation of PHB in cyanobacteria. Besides the strain engineering and improvement approach, various reports have discussed other factors, which can facilitate superior growth and productivity in cyanobacteria. Herein, the most important routes for improvement of PHB production in cyanobacteria are listed.

3.2.1. Media and Cultivation Conditions

Like all other bioprocesses, PHB production from cyanobacteria is mainly influenced by the cultivation parameters and nutrient supply. The importance of defined cultivation conditions used to obtain highly productive process for cyanobacteria and microalgae has been previously discussed [32,67,68]. Cyanobacterial growth requires a high concentration of essential nutrients, such as nitrogen, phosphorus, sulfur, potassium, magnesium, iron, and some traces of micromolecules. The supply of nutrients like nitrogen and phosphorus in limiting concentration is important for the production of PHB. Therefore, media optimization plays an important role to maximize the PHB productivity and lower production costs. Regarding optimized nitrogen concentration in the media, it was shown by Coelho et al. that 0.05 g L^{-1} nitrogen in the media results in the production of up to 30.7% (DCW) of PHB in *Spirulina* sp. LEB 18. Further optimization of nitrogen content to 0.22 g L^{-1} in the media increased the PHB content in spirulina sp. LEB 18 to 44.2% (DCW) [69]. However, the impact of nitrogen optimization on the volumetric or specific productivities were not reported in both cases. The optimization of media components, nitrogen, and phosphorus in the case of *Synechocystis* sp. PCC 6714 increased volumetric as well as specific production rates, both in the case of biomass growth and PHB content [62].

Besides media components, other key parameters influencing growth and PHB production in cyanobacteria are cultivation conditions, such as temperature, pH, light intensity, or light/dark cycles. Furthermore, production of the copolymers can be tailor-made by using co-substrates and varying the cultivation conditions, such as temperature and pH [70]. Various studies have used the statistical design of experiments (DoEs) in order to optimize the media as well as the cultivation conditions [31,32,71]. The DoEs are used to minimize the error in determining the influential parameters, allowing systematic and efficient variation of all factors [72]. Table 3 summarizes the cultivation parameters and the nutrient limitation used for cyanobacterial PHB synthesis.

Table 3. Reported cultivation parameters and media limitation used for photoautotrophic PHB production in wild-type cyanobacterial strains.

Cyanobacterial Strain	Limiting Component	Temperature °C	pH	Light Condition	PHB Content % (DCW)	Cultivation Time (Days)	Volume (L)	References
Synechocystis sp. PCC 6803	N and P starvation	28–32	7.5–8.5	dark/light cycle	11	10	0.05	[31]
Synechocystis sp. PCC6803	N starvation	30	n.p	light	4.1	7	n.p	[73]
Synechocystis sp. PCC6803	N limitation	28	n.p	18:6	8	30	0.8	[74]
Synechocystis sp. PCC 6714	N and P limitation	28	8.5	light	16.4	16	1	[32]
Synechocystis salina CCALA192	Optimized BG-11 media [4]	n.p [5]	8.5	light	6.6	21	200	[23]
Phormidium sp. *TISTR 8462*	N limitation	28	7.5	light	14.8	12	n.p	[75]
Calothrix scytonemicola TISTR 8095	N deprivation	28	7.5	light	25.4	12	n.p	[75]
Nostoc muscorum	Growth associated [6]	25	8.5	14:10	8.6	21	0.05	[76]
Nostoc muscorum	P depletion	22	n.p	light	10.2	19	n.p	[38]
Spirulina sp. LEB 18	Defined media [7]	30	n.p	12:12	30.7	15	1.8	[77]
Aulosira fertilissima	P limitation	28	8.5	14:10	10	4	0.05	[40]
Anabaena sp.	n.p	25	8	14:10	2.3	n.p	0.1	[78]

[4] Optimized BG-11 media = the optimized BG-11 media contains 0.45 g L^{-1} $NaNO_3$ and leads to a self-limitation of the culture. [5] n.p = not provided. [6] Growth associated = the production of PHA was associated with growth and no media limitation was given. [7] Defined media = concentration of nitrate, phosphate and sodium bicarbonate was optimized.

Two primary challenges of entering cyanobacterial PHB into the market are the concern of the sustainability of the production process and the high production costs of fresh water and nutrients. One solution could be to use waste streams like agricultural effluents with high nitrogen and phosphorus contents. Therefore, the production of the polymer is accompanied by the removal of nutrients from the water. On the other hand, the undefined substrate may raise new challenges that then need to be resolved [79]. Various reports have shown production of cyanobacterial PHB using waste streams. Troschl et al. have summarized the list of cyanobacterial strains cultivated on agro-industrial waste streams and anaerobic digestants to produce PHB [23]. One example is the cultivation of the diazotrophic cyanobacterial strain *Aulosira fertilisima* under a circulatory aquaculture system that resulted in increased dissolved oxygen levels during the cultivation period and the complete removal of nutrients, such as ammonia, nitrite, and phosphate, within 15 days of cultivation, yielding an average PHB content of 80–92 g m^{-3} [80]. This report, along with other previously shown studies [79,81–84], clearly shows the potential of cyanobacterial PHB production for wastewater treatment facilities.

3.2.2. PHB Production Using Mixed Photosynthetic Consortia

Another approach used for PHB production is the feast-famine strategy, which uses a mixed consortium of algae and cyanobacteria [85–88]. During this regime, the feast operation consists of a mixed culture of cyanobacterial consortium cultivated in a sequencing batch reactor (SBR) without aeration using acetate as a carbon source and light as an energy source [86]. During the famine phase, the NADH or the NADPH reserves of the cell is consumed using the oxygen produced by the algae cells present in the consortia leading to accumulation of around 20% (DCW) PHA [89]. Furthermore, maximum polymer content of 60% (DCW) of PHA was produced by a photosynthetic mixed culture in a permanent feast regime using high light intensity [86]. The anaerobic dark energy generation's capability of cyanobacteria is already been known [90]. Some cyanobacteria have also been known for their fermentation capability at the expense of their carbohydrate reserves [91]. The axenic dark feast conditions facilitated the acetate uptake, increasing the productivity significantly (up to 60%) (DCW), as the famine phase was eliminated [85,86]. The anaerobic fermentation of cyanobacteria to produce PHB has a potential, while the need for sterilization and aeration is eliminated, reducing also the energy costs. However, the source and cost of the substrate used remains a cost driver issue.

3.2.3. PHB Production Using Mixed Feed Systems

Production of PHAs in cyanobacteria can occur during phototrophic growth, using CO_2 as a sole carbon source and light energy, and also during heterotrophy, when using sugar supplementation. It has been estimated that the carbon substrate in a large-scale manufacturing context would constitute approximately 37% of the total production costs [27,92]. However, in order to cope with the low phototrophic PHB productivity in cyanobacteria, various studies have used supplementation of other carbon sources. The mini-review by Singh and Mallick has summarized the wild-type and recombinant cyanobacterial strains, their PHA content, and the substrate used for the biosynthesis of the biopolymer [24]. However, in most reported cases [34,46,93–97] of heterotrophic PHB production, the biomass concentrations produced are less than 1 g L^{-1} and increases in volumetric productivities are not described. Even though the PHB productivity increases in terms of biopolymer content (%DCW) using mixed feed systems, the use of external carbon substrates increases the production costs and also raises the question of the economic feasibility of PHB production from cyanobacteria. As long as heterotrophic organisms produce PHB at much higher rates than cyanobacteria, the only sense for commercialization of cyanobacterial PHB would be the sustainability. Therefore, research must focus on improving the phototrophic PHB production with the aim of increasing CO_2 uptake rates of cyanobacteria, with the support of viable bioprocess technology tools.

3.2.4. CO_2 Sequestration

CO_2 is a major greenhouse gas; its emission into the atmosphere has gradually increased in the past decades, causing global warming and its associated problems [98]. Carbon contributes to all organic compounds and is the main constituent of cyanobacterial and all biomass, amounting to up to 65% of DCW [79]. The industrial production of PHB that uses CO_2 feedstocks helps reduce the environmental impacts of CO_2 emission. Various studies have shown that an increase in CO_2 concentration during a cyanobacterial cultivation may increase the production of carbon reserve compounds, such as PHB. Markou et al. showed that an increase in carbon content leads to the production of carbon reserve compounds, such as lipids and PHAs [79]. The increase in the concentration of the carbon source also increased biopolymer accumulation in cyanobacterial strain *Spirulina* sp. LEB 18 [77]. However, what has not been discussed in the literature thus far are the effects of the day-night cycle on the CO_2 uptake rate and the productivity of carbon reserve compounds in cyanobacteria. Since CO_2 fixation occurs during the light phase, the total productivity and CO_2 sequestration rate will be lower in outdoor cultivations. During the dark phase, CO_2 utilization is minimized and the productivities are lowered and some carbon reserve molecules, such as glycogen, degrade. Other methods would need to be used to temporarily sequester CO_2 as a carbonate species during nighttime, which could then be utilized by cyanobacteria when the light is available again [99].

4. Production Strategies

The economic efficiency of any production process is indicated by the productivity, which comprises of growth rates, specific production rates, and the biomass concentration of the culture. Therefore, the economic efficiency of the production process will increase only when the mentioned parameters are improved. Once the strain and cultivation parameters are selected and optimized for the production process, the process performance can be considered and analyzed.

4.1. Cultivation Modes

Cyanobacteria producing PHA have been classified into two groups based on the culture conditions required for efficient polymer synthesis: group one requires a limitation of an essential media component for PHA synthesis; the second has no requirement for nutrient limitation for the accumulation of the polymer [100]. For industrial production of PHB, the second group is favorable for growth as it is accompanied by polymer synthesis.

In general, cultivation of cyanobacteria for the production of PHB can be done using various cultivation modes. The most common approach is using batch cultivation, in which the production of PHB is induced by a limiting nutrient or, in an ideal case, the production of the polymer becomes growth dependent. For the batch cultivation with the group one cyanobacteria, the concentration of nitrogen and phosphorus in the media play the key-role facilitating biomass growth, and their limitation trigger PHB synthesis. Thus, in such a process the cell growth is maintained without nutrient limitation, until the desired concentration is reached. Then, an essential limitation allows for efficient polymer accumulation. So far, a few studies have focused on optimizing the nutrients for the batch production of PHB in large-scale; others mainly have been done in flasks. Batch cultivation of *Synechocystis* sp. PCC 6803 using a nitrogen concentration of half of the optimal BG-11 media, showed 180 mg L^{-1} PHB from CO_2 [74]. The maximum PHB content of 125 mg L^{-1} was obtained for the non-sterile batch cultivation of *Synechocystis* sp. CCALA192 in a 200-L tubular photobioreactor [42]. Moreover, PHB was produced using optimized media in a one-liter tank reactor for the wild-type cyanobacterial strain *Synechocystis* sp. PCC 6714 obtained 640 mg L^{-1} of polymer [62].

The other common strategy for the cyanobacterial PHB production is using the SBR mode of operation, where growth and production occur in different reactors. In the growth vessel, media components are provided in abundance to facilitate maximum biomass production. In the induction photobioreactor, one or more media components are limited facilitating PHB biosynthesis. During

the induction, residual biomass concentration remains more or less constant, while cell concentration increases only by intracellular polymeric accumulation [101]. In order to facilitate higher productivities, both reactors can operate as chemostats. Thus far, no reports of cyanobacterial PHB production in SBR or chemostat mode have been described.

4.2. Cultivation Systems

Another challenge in commercial cyanobacterial production is associated with biomass production. There are three main production systems used for large-scale cultivation of microalgae and cyanobacteria. The most basic approach for the cultivation of photosynthetic organisms is the use of large natural locations, which is mostly done for microalgae such as *Dunaliella*. Releasing into natural locations is regarded as a deliberate release into the environment, since there are no effective protective measures to prevent the microalgae from entering the surroundings [60]. The other approach is the use of open raceway pond systems, which has been commonly applied worldwide. When these raceway ponds are used outdoors, the cultivation are regarded as a deliberate release, so the spread of genetically modified organisms cannot be excluded in this case [60]. Even though these systems are economically feasible, the maintenance of monocultures and improving productivity are the main bottlenecks associated with such cultivations. The use of an open pond system has so far been reported in a wastewater treatment facility, containing fish pond discharge that uses the cyanobacterial strain *Aulosira fertilissima*, which shows a PHB productivity of up to 92 g m^{-3} [80]. The third system is the sophisticated, closed production system: photobioreactors (PBR). These systems can be both placed in greenhouses to obtain more defined cultivation conditions or be installed outdoors. PBR systems are more flexible for the needs of the cultivation process and the desired species. The industrial-scale production of photoautotrophic cyanobacterial PHB has not been widely reported in photobioreactors. The various photobioreactor systems used to cultivate cyanobacteria is given by Koller et al. [102]. Yet Troschl et al. has described the cultivation of *Synechocystis salina* CCALA192 in a 200-L tubular photobioreactor for the production of PHB from CO_2 [23]. The maximum PHB productivity obtained under nitrogen limitation was 6.6% (DCW), while the volumetric and specific productivities were not reported in this case. Moreover, a mixed consortium of wastewater born cyanobacteria was cultivated in a 30-L PBR, showing a maximum productivity of 104 mg L^{-1} under phosphorus limitation [103].

5. Process Monitoring and Control

Today the most commonly used method for accurate determination of PHAs in bacterial cultivations is gas chromatography (GC) [104] or high-performance liquid chromatography (HPLC) [105,106]. These methods involve hydrolysis, subsequent methanolysis, or propanolysis of the PHAs in whole cells, in the presence of sulfuric acid and chloroform [107]. These extraction methods are laborious, time-consuming, and the optimum time of harvest might be lost due to the time needed for the analysis. Other methods for PHA analysis include gravimetric, infrared spectroscopy of chemically extracted PHB, fluorimetry, and cell carbon analysis [107–109]. It is necessary to develop viable analytics to help the development of an efficient commercial production process that enables monitoring and control of production, along with a rapid feedback on the state of the process.

Fourier transform infrared (FTIR) spectroscopy has been applied to determine the chemical composition of cyanobacteria with major cellular analytes, such as proteins, lipids, polysaccharide, nucleic acids, and PHAs [107,110]. It has been shown that FTIR spectroscopy can monitor water-soluble extracellular analytes in fermentation systems, as well as being an indirect method to determine the stage of fermentation by monitoring the physiological state of the cells [111]. Various studies have shown the potential of FTIR spectroscopy for determination of intracellular PHA contents in various microorganisms [107,112]. In the same direction, Jarute et al. have introduced an automated approach for on-line monitoring of the intracellular PHB in a process with recombinant *E. coli*, which uses stopped-flow attenuated total reflection FTIR spectroscopy [113]. In the case of cyanobacteria, there exists no such studies reporting on-line or at-line determination of intracellular carbon compounds,

such as PHAs and glycogen. The measurements used and the parameters controlled in microalgae processes are specific in-line probes, such as pO_2, pCO_2, pH, and temperature. In cyanobacterial industrial processes, spectroscopic measurement techniques, such as FTIR, can be used for monitoring, controlling the production, and determining the time of harvest. The on-line determination can also identify the limitation time and the limiting components based on the cell physiology, thus helping to make the cyanobacterial PHA production robust and manageable.

6. Production Scenarios

In order to compete with synthetic and other starch-based polymers in the market, the cost of cyanobacterial PHB needs to be reduced significantly. Yet, no economic analysis has been done to estimate the production costs of phototrophic PHB production. It has been reported that the cost of PHB production from heterotrophic organisms is in the range of 2–5 € kg^{-1} [114]. This value is still much higher than the estimated cost of petrochemical-based mass polymers like PE, PP, or PET, which is around 1.2 € kg^{-1} [114] and less. Taking into account the much lower time space yield and the biomass productivity in cyanobacteria and complications associated with the downstream processing, the cost associated with the production of PHB in cyanobacteria could be higher than that of heterotrophic microorganisms (>5 € kg^{-1}). Typically, more than 4.3 kg of sugar is needed to produce 1 kg of PHB [85]. Nevertheless, higher yields of product per substrate consumed have also been reported, showing values of 3.1 kg sucrose/kg PHB and of 3.33 kg glucose/kg of the polymer [15,115]. In this context, the substrate costs can be avoided by photoautotrophically produced PHB by cyanobacteria. However, the lower productivities of cyanobacteria will still increase the costs significantly. Among the main factors contributing to the cost of PHA production are equipment-related costs, such as direct-fixed-capital-dependent items, overheads, and some labor-dependent factors, which considerably increase with a decrease in productivity [27,101]. Therefore, for the production of the same amount of PHA per year, the process with lower productivity requires larger equipment [27,116]. To that end, one approach could be to reduce the costs associated with the building of photobioreactors. This can be accomplished by simplifying the design and the material used for the production of photobioreactors and their energy consumption [22]. Another alternative to increase the size of the facility or reactor while also reducing production costs is to use open pond raceways and wastewater born cyanobacteria instead of fresh water strains. However, it should be taken into account that the increase in volume will directly increase the effort associated with the downstream processing [25].

Moreover, it has been shown that using industrial flue gases may reduce the production cost of cyanobacterial biomass to around 2.5 € kg^{-1}, while using wastewater can decrease the costs further, to less than 2 € kg^{-1} [22,117]. Therefore, as already discussed, wastewater streams with high carbon, nitrogen, and phosphorus that are mix-fed with CO_2 from industrial flue gases, can be used to make the PHB production from cyanobacteria more efficient. Furthermore, producing several chemicals from the same microalgae feedstock could potentially make the production of multiple commodity chemicals from a biological resource economically viable [92].

7. The Remaining Challenges in Photosynthetic PHB Production

Current industrial PHA production processes rely mostly on the availability of agricultural resources, which are unsustainable (compare the food versus fuel discussion with first-generation biofuels) and leave a large ecological footprint [65].

In the case of cyanobacterial, PHA production research has mainly focused on genetic engineering to increase productivity, which mainly reports as higher % DCW polymer content. The studies have rarely reported an increase in photosynthetic efficiency or an increase in the specific growth rates and production rates. So far, very few studies have shown the use of wastewater-open pond systems for the production of PHAs. For a recent review of PHA production, see Koller et al. [118].

8. Outlook

Currently, the global research efforts directed towards individual aspects of cyanobacterial PHA production mainly focus on improved strains and recovery processes. Although various challenges are associated with the efficiency of the cyanobacterial PHA productivity and the extraction and purification of PHAs, optimization of each step separately will waste considerable effort and result in overall sub-optimality [27]. With respect to commercialization and scale-up of the cyanobacterial PHA production, the view of the whole processes needs to be considered. More attention towards sustainable and viable upstream processing may help to reach an economic PHA production point. Cyanobacterial PHA production, from an economic point of view, will only make sense if a continuous process can be achieved, especially using waste streams as a carbon source and for the media. The process can then be coupled with the bioremediation of agricultural and industrial effluents. Thus far, some wild-type and improved cyanobacterial strains are reported with PHB content which is mostly cultivated under controlled, defined, and sterile lab conditions. For production in industrial scale that is done under unsterile conditions, only *Nostoc moscorum* as an example is reported. Other strains are not tested or can hardly tolerate the harsh outdoor conditions. Although we have emphasized the importance of optimized media and cultivation conditions on PHA productivity, sustainable and viable commercial processes conducted under unsterile conditions using waste streams and open systems are required. Research needs to focus on screening for more robust strains, such as wastewater born mixed-cultures that can tolerate fluctuations in cultivation conditions like pH, temperature, salinity, and media composition. Furthermore, the durable strains for which production of PHB is associated with biomass growth and therefore the time-spaced yield will be improved.

PHA shows both the advantages of biobased carbon content and full biodegradability. In addition, cyanobacterial PHA can be more sustainable and more cost effective in the marine environment and when compared to PHA from carbohydrate fermentation. It can be a carbon-negative material, making the process not only attractive for PHA converters and users, but also for CO_2 emitters, like power stations. There are plenty of medium-size CO_2 point sources, e.g., biogas production facilities, where the CO_2 could be used in an adjacent cyanobacterial PHA factory erected on the non-arable land. Preferably, a biorefinery approach would be executed, where valuable compounds such as phytohormones and pigments are extracted from the cyanobacteria; then. PHA and biomass is anaerobically digested in a biogas plant, yielding a cost-effective and fully integrated process.

It is expected that over the next two decades there will be a shift toward more recycling of fossil-based and conventional plastics, with an accompanying reduction in material variety to facilitate collection, processing, and reuse. Moreover, we will see a maturing of the bioplastics industry, with more applications being developed with bioplastics, other than "gimmick" giveaways and small household and kitchen tools. Due to the unique and interesting property set of PHA, it can be anticipated that these materials, particularly PHB and its copolymers such as PHBV, will gain significance.

Author Contributions: D.K. and C.H. designed this study; D.K. carried out the research and wrote this manuscript, with the support of M.L. and C.H; the study was initiated by M.L. and C.H.; C.H. supervised this project; D.K., M.L., and C.H. have several years of practical research experience with PHB production from cyanobacteria focused on strain improvement, bioprocess optimization, and scale-up.

Funding: This research was funded by the authors' institutions.

Acknowledgments: The authors would like to thank the Vienna Business Agency for supporting the funding of this work.

Conflicts of Interest: The authors declare no conflict of interest.

References

1. De Koning, G.J.M. *Prospects of Bacterial Poly[(R)-3-(Hydroxyalkanoates)]*; Technische Universiteit Eindhoven: Eindhoven, The Netherlands, 1993.

2. Keshavarz, T.; Roy, I. Polyhydroxyalkanoates: Bioplastics with a green agenda. *Curr. Opin. Microbiol.* **2010**, *13*, 321–326. [CrossRef] [PubMed]
3. Lackner, M. Bioplastics. In *Kirk-Othmer Encyclopedia of Chemical Technology*; John Wiley & Sons, Inc.: Hoboken, NJ, USA, 2015.
4. Tan, G.-Y.; Chen, C.-L.; Li, L.; Ge, L.; Wang, L.; Razaad, I.; Li, Y.; Zhao, L.; Mo, Y.; Wang, J.-Y. Start a Research on Biopolymer Polyhydroxyalkanoate (PHA): A Review. *Polymers* **2014**, *6*, 706–754. [CrossRef]
5. Getachew, A.; Woldesenbet, F. Production of biodegradable plastic by polyhydroxybutyrate (PHB) accumulating bacteria using low cost agricultural waste material. *BMC Res. Notes* **2016**, *9*, 509. [CrossRef] [PubMed]
6. Madison, L.L.; Huisman, G.W. Metabolic Engineering of Poly(3-Hydroxyalkanoates): From DNA to Plastic. *Microbiol. Mol. Biol. Rev.* **1999**, *63*, 21–53. [PubMed]
7. Ten, E.; Jiang, L.; Zhang, J.; Wolcott, M.P. 3—Mechanical Performance of polyhydroxyalkanoate (PHA)-based biocomposites. In *Biocomposites*; Misra, M., Pandey, J.K., Mohanty, A.K., Eds.; Woodhead Publishing: Sawston, UK, 2015; pp. 39–52.
8. Galia, M.B. Isolation and analysis of storage compounds. In *Handbook of Hydrocarbon and Lipid Microbiology*; Timmis, K.N., Ed.; Springer: Berlin, Germany, 2010.
9. Barham, P.J.; Organ, S.J. Mechanical properties of polyhydroxybutyrate-hydroxybutyrate-hydroxyvalerate copolymer blends. *J. Mater. Sci.* **1994**, *29*, 1676–1679. [CrossRef]
10. Harding, K.G.; Dennis, J.S.; Blottnitz, H.; Harrison, S.T. Environmental analysis of plastic production processes: Comparing petroleum-based polypropylene and polyethylene with biologically-based poly-beta-hydroxybutyric acid using life cycle analysis. *J. Biotechnol.* **2007**, *130*, 57–66. [CrossRef] [PubMed]
11. Lackner, M.; Markl, E.; Grünbichler, H. Cyanobacteria for PHB Bioplastics Production: A Review. *Nov. Tech. Nutr. Food Sci.* **2018**, *2*, 4.
12. Balaji, S.; Gopi, K.; Muthuvelan, B. A review on production of poly β hydroxybutyrates from cyanobacteria for the production of bio plastics. *Algal Res.* **2013**, *2*, 278–285. [CrossRef]
13. Grothe, E.; Chisti, Y. Poly (ß-hydroxybutyric acid) thermoplastic production by Alcaligenes latus: Behavior of fed-batch cultures. *Bioprocess Biosyst. Eng.* **2000**, *22*, 441–449. [CrossRef]
14. Schubert, P.; Steinbüchel, A.; Schlegel, H.G. Cloning of the Alcaligenes eutrophus genes for synthesis of poly-beta-hydroxybutyric acid (PHB) and synthesis of PHB in *Escherichia coli*. *J. Bacteriol.* **1988**, *170*, 5837–5847. [CrossRef] [PubMed]
15. Nonato, R.; Mantelatto, P.; Rossell, C. Integrated production of biodegradable plastic, sugar and ethanol. *Appl. Microbiol. Biotechnol.* **2001**, *57*, 1–5. [PubMed]
16. Koller, M.; Salerno, A.; Reiterer, A.; Malli, H.; Malli, K.; Kettl, K.H.; Narodoslawsky, M.; Schnitzer, H.; Chiellini, E.; Braunegg, G. Sugar cane as feedstock for biomediated polymer production. In *Sugarcane: Production, Cultivation and Uses*; Nova Publishers: Hauppauge, NY, USA, 2012; pp. 105–136.
17. Steinbüchel, A. PHB and Other Polhydroxyalkanoic Acids. In *Biotechnology Set*, 2nd ed.; Wiley: Hoboken, NJ, USA, 2008; pp. 403–464.
18. Gurieff, N.; Lant, P. Comparative life cycle assessment and financial analysis of mixed culture polyhydroxyalkanoates production. *Bioresour. Technol.* **2007**, *98*, 3393–3403. [CrossRef] [PubMed]
19. Reis, M.A.M.; Serafim, L.S.; Lemos, P.C.; Ramos, A.M.; Aguiar, F.R.; Loosdrecht, M.C.M. Production of polyhydroxyalkanoates by mixed microbial cultures. *Bioprocess Biosyst. Eng.* **2003**, *25*, 377–385. [CrossRef] [PubMed]
20. Alias, Z.; Tan, I.K. Isolation of palm oil-utilising, polyhydroxyalkanoate (PHA)-producing bacteria by an enrichment technique. *Bioresour. Technol.* **2005**, *96*, 1229–1234. [CrossRef] [PubMed]
21. Oliver, N.J.; Rabinovitch-Deere, C.A.; Carroll, A.L.; Nozzi, N.E.; Case, A.E.; Atsumi, S. Cyanobacterial metabolic engineering for biofuel and chemical production. *Curr. Opin. Chem. Biol.* **2016**, *35*, 43–50. [CrossRef] [PubMed]
22. Costa, J.A.V.; Moreira, J.B.; Lucas, B.F.; Braga, V.D.S.; Cassuriaga, A.P.A.; Morais, M.G.D. Recent Advances and Future Perspectives of PHB Production by Cyanobacteria. *Ind. Biotechnol.* **2018**, *14*, 249–256. [CrossRef]
23. Troschl, C.; Meixner, K.; Drosg, B. Cyanobacterial PHA Production—Review of Recent Advances and a Summary of Three Years' Working Experience Running a Pilot Plant. *Bioengineering* **2017**, *4*, 26. [CrossRef] [PubMed]

24. Singh, A.K.; Mallick, N. Advances in cyanobacterial polyhydroxyalkanoates production. *FEMS Microbiol. Lett.* **2017**, *364*, fnx189. [CrossRef] [PubMed]
25. Drosg, B.; Fritz, I.; Gattermayer, F.; Silvestrini, L. Photo-autotrophic Production of Poly(hydroxyalkanoates) in Cyanobacteria. *Chem. Biochem. Eng. Q.* **2015**, *29*, 145–156. [CrossRef]
26. Koller, M.; Marsalek, L. Cyanobacterial Polyhydroxyalkanoate Production: Status Quo and Quo Vadis? *Curr. Biotechnol.* **2015**, *4*, 464–480. [CrossRef]
27. Choi, J.; Lee, S.Y. Factors affecting the economics of polyhydroxyalkanoate production by bacterial fermentation. *Appl. Microbiol. Biotechnol.* **1999**, *51*, 13–21. [CrossRef]
28. Lau, N.-S.; Matsui, M.; Al Abdullah, A.-A. Cyanobacteria: Photoautotrophic Microbial Factories for the Sustainable Synthesis of Industrial Products. *BioMed Res. Int.* **2015**, *2015*, 754934. [CrossRef] [PubMed]
29. Dismukes, G.C.; Carrieri, D.; Bennette, N.; Ananyev, G.M.; Posewitz, M.C. Aquatic phototrophs: Efficient alternatives to land-based crops for biofuels. *Curr. Opin. Biotechnol.* **2008**, *19*, 235–240. [CrossRef] [PubMed]
30. Case, A.E.; Atsumi, S. Cyanobacterial chemical production. *J. Biotechnol.* **2016**, *231*, 106–114. [CrossRef] [PubMed]
31. Panda, B.; Jain, P.; Sharma, L.; Mallick, N. Optimization of cultural and nutritional conditions for accumulation of poly-β-hydroxybutyrate in *Synechocystis* sp. PCC 6803. *Bioresour. Technol.* **2006**, *97*, 1296–1301. [CrossRef] [PubMed]
32. Kamravamanesh, D.; Pflügl, S.; Nischkauer, W.; Limbeck, A.; Lackner, M.; Herwig, C. Photosynthetic poly-β-hydroxybutyrate accumulation in unicellular cyanobacterium *Synechocystis* sp. PCC 6714. *AMB Express* **2017**, *7*, 143. [CrossRef] [PubMed]
33. Campbell, J.; Stevens, S.E.; Balkwill, D.L. Accumulation of poly-beta-hydroxybutyrate in *Spirulina platensis*. *J. Bacteriol.* **1982**, *149*, 361–363. [PubMed]
34. Toh, P.S.Y.; Jau, M.H.; Yew, S.P.; Abed, R.M.M.; Sidesh, K. Comparison of polyhydroxyalkanoates biosynthesis, mobilization and the effects on cellular morphology in Spirulina Platensis and *Synechocystis* sp. UNIWG. *J. Biosci.* **2008**, *19*, 21–38.
35. De Philippis, R.; Sili, C.; Vincenzini, M. Glycogen and poly-β-hydroxybutyrate synthesis in *Spirulina maxima*. *Microbiology* **1992**, *138*, 1623–1628. [CrossRef]
36. Stal, L.J.; Heyer, H.; Jacobs, G. Occurrence and Role of Poly-Hydroxy-Alkanoate in the Cyanobacterium Oscillatoria Limosa. In *Novel Biodegradable Microbial Polymers*; Dawes, E.A., Ed.; Springer: Dordrecht, The Netherlands, 1990; pp. 435–438.
37. Bhati, R.; Mallick, N. Production and characterization of poly(3-hydroxybutyrate-co-3-hydroxyvalerate) co-polymer by a N2-fixing cyanobacterium, *Nostoc muscorum* Agardh. *J. Chem. Technol. Biotechnol.* **2012**, *87*, 505–512. [CrossRef]
38. Haase, S.M.; Huchzermeyer, B.; Rath, T. PHB accumulation in *Nostoc muscorum* under different carbon stress situations. *J. Appl. Phycol.* **2012**, *24*, 157–162. [CrossRef]
39. Samantaray, S.; Mallick, N. Production of poly (3-hydroxybutyrate-co-3-hydroxyvalerate) co-polymer by the diazotrophic cyanobacterium *Aulosira fertilissima* CCC 444. *J. Appl. Phycol.* **2014**, *26*, 237–245. [CrossRef]
40. Samantaray, S.; Mallick, N. Production and characterization of poly-β-hydroxybutyrate (PHB) polymer from *Aulosira fertilissima*. *J. Appl. Phycol.* **2012**, *24*, 803–814. [CrossRef]
41. Takahashi, H.; Miyake, M.; Tokiwa, Y.; Asada, Y. Improved accumulation of poly-3-hydroxybutyrate by a recombinant cyanobacterium. *Biotechnol. Lett.* **1998**, *20*, 183–186. [CrossRef]
42. Troschl, C.; Meixner, K.; Fritz, I.; Leitner, K.; Romero, A.P.; Kovalcik, A.; Sedlacek, P.; Drosg, B. Pilot-scale production of poly-β-hydroxybutyrate with the cyanobacterium *Synechocytis* sp. CCALA192 in a non-sterile tubular photobioreactor. *Algal Res.* **2018**, *34*, 116–125. [CrossRef]
43. Lama, L.; Nicolaus, B.; Calandrelli, V.; Manca, M.C.; Romano, I.; Gambacorta, A. Effect of growth conditions on endo- and exopolymer biosynthesis in *Anabaena cylindrica* 10 C. *Phytochemistry* **1996**, *42*, 655–659. [CrossRef]
44. Mendhulkar, V.D.; Laukik, A.S. Synthesis of Biodegradable Polymer Polyhydroxyalkanoate (PHA) in Cyanobacteria Synechococcus elongates Under Mixotrophic Nitrogen- and Phosphate-Mediated Stress Conditions. *Ind. Biotechnol.* **2017**, *13*, 85–93. [CrossRef]
45. Monshupanee, T.; Nimdach, P.; Incharoensakdi, A. Two-stage (photoautotrophy and heterotrophy) cultivation enables efficient production of bioplastic poly-3-hydroxybutyrate in auto-sedimenting cyanobacterium. *Sci. Rep.* **2016**, *6*, 37121. [CrossRef] [PubMed]

46. Khetkorn, W.; Incharoensakdi, A.; Lindblad, P.; Jantaro, S. Enhancement of poly-3-hydroxybutyrate production in *Synechocystis* sp. PCC 6803 by overexpression of its native biosynthetic genes. *Bioresour. Technol.* **2016**, *214*, 761–768. [CrossRef] [PubMed]
47. Katayama, N.; Iijima, H.; Osanai, T. Production of Bioplastic Compounds by Genetically Manipulated and Metabolic Engineered Cyanobacteria. In *Synthetic Biology of Cyanobacteria*; Zhang, W., Song, X., Eds.; Springer: Singapore, 2018; pp. 155–169.
48. Koksharova, O.; Wolk, C. Genetic tools for cyanobacteria. *Appl. Microbiol. Biotechnol.* **2002**, *58*, 123–137. [PubMed]
49. Wilde, A.; Dienst, D. Tools for Genetic Manipulation of Cyanobacteria. In *Bioenergetic Processes of Cyanobacteria: From Evolutionary Singularity to Ecological Diversity*; Peschek, G.A., Obinger, C., Renger, G., Eds.; Springer: Dordrecht, The Netherlands, 2011; pp. 685–703.
50. Hauf, W.; Watzer, B.; Roos, N.; Klotz, A.; Forchhammer, K. Photoautotrophic Polyhydroxybutyrate Granule Formation Is Regulated by Cyanobacterial Phasin PhaP in *Synechocystis* sp. Strain PCC 6803. *Appl. Environ. Microbiol.* **2015**, *81*, 4411–4422. [CrossRef] [PubMed]
51. Taroncher-Oldenburg, G.; Nishina, K.; Stephanopoulos, G. Identification and analysis of the polyhydroxyalkanoate-specific β-ketothiolase and acetoacetyl coenzyme A reductase genes in the cyanobacterium *Synechocystis* sp. strain PCC6803. *Appl. Environ. Microbiol.* **2000**, *66*, 4440–4448. [CrossRef] [PubMed]
52. Hein, S.; Tran, H.; Steinbuchel, A. Synechocystis sp. PCC6803 possesses a two-component polyhydroxyalkanoic acid synthase similar to that of anoxygenic purple sulfur bacteria. *Arch. Microbiol.* **1998**, *170*, 162–170. [CrossRef] [PubMed]
53. Suzuki, E.; Ohkawa, H.; Moriya, K.; Matsubara, T.; Nagaike, Y.; Iwasaki, I.; Fujiwara, S.; Tsuzuki, M.; Nakamura, Y. Carbohydrate metabolism in mutants of the cyanobacterium *Synechococcus elongatus* PCC 7942 defective in glycogen synthesis. *Appl. Environ. Microbiol.* **2010**, *76*, 3153–3159. [CrossRef] [PubMed]
54. Sudesh, K.; Taguchi, K.; Doi, Y. Effect of increased PHA synthase activity on polyhydroxyalkanoates biosynthesis in *Synechocystis* sp. PCC6803. *Int. J. Biol. Macromol.* **2002**, *30*, 97–104. [CrossRef]
55. Lau, N.-S.; Foong, C.P.; Kurihara, Y.; Sudesh, K.; Matsui, M. RNA-Seq Analysis Provides Insights for Understanding Photoautotrophic Polyhydroxyalkanoate Production in Recombinant *Synechocystis* sp. *PLoS ONE* **2014**, *9*, e86368. [CrossRef] [PubMed]
56. Carpine, R.; Du, W.; Olivieri, G.; Pollio, A.; Hellingwerf, K.J.; Marzocchella, A.; Branco dos Santos, F. Genetic engineering of *Synechocystis* sp. PCC6803 for poly-β-hydroxybutyrate overproduction. *Algal Res.* **2017**, *25*, 117–127. [CrossRef]
57. Zhang, S.; Qian, X.; Chang, S.; Dismukes, G.C.; Bryant, D.A. Natural and Synthetic Variants of the Tricarboxylic Acid Cycle in Cyanobacteria: Introduction of the GABA Shunt into *Synechococcus* sp. PCC 7002. *Front. Microbiol.* **2016**, *7*, 1972. [CrossRef] [PubMed]
58. Wang, B.; Xiong, W.; Yu, J.; Maness, P.-C.; Meldrum, D.R. Unlocking the photobiological conversion of CO_2 to (*R*)-3-hydroxybutyrate in cyanobacteria. *Green Chem.* **2018**, *20*, 3772–3782. [CrossRef]
59. Hondo, S.; Takahashi, M.; Osanai, T.; Matsuda, M.; Hasunuma, T.; Tazuke, A.; Nakahira, Y.; Chohnan, S.; Hasegawa, M.; Asayama, M. Genetic engineering and metabolite profiling for overproduction of polyhydroxybutyrate in cyanobacteria. *J. Biosci. Bioeng.* **2015**, *120*, 510–517. [CrossRef] [PubMed]
60. Jaeger, L.D. *Strain Improvement of Oleaginous Microalgae*; Wageningen University: Wageningen, The Netherlands, 2015; p. 200.
61. Lee, B.; Choi, G.-G.; Choi, Y.-E.; Sung, M.; Park, M.S.; Yang, J.-W. Enhancement of lipid productivity by ethyl methane sulfonate-mediated random mutagenesis and proteomic analysis in *Chlamydomonas reinhardtii*. *Korean J. Chem. Eng.* **2014**, *31*, 1036–1042. [CrossRef]
62. Kamravamanesh, D.; Slouka, C.; Limbeck, A.; Lackner, M.; Herwig, C. Increased carbohydrate production from carbon dioxide in randomly mutated cells of cyanobacterial strain *Synechocystis* sp. PCC 6714: Bioprocess understanding and evaluation of productivities. *Bioresour. Technol.* **2019**, *273*, 277–287. [CrossRef] [PubMed]
63. Kamravamanesh, D.; Kovacs, T.; Pflügl, S.; Druzhinina, I.; Kroll, P.; Lackner, M.; Herwig, C. Increased poly-β-hydroxybutyrate production from carbon dioxide in randomly mutated cells of cyanobacterial strain *Synechocystis* sp. PCC 6714: Mutant generation and characterization. *Bioresour. Technol.* **2018**, *266*, 34–44. [CrossRef] [PubMed]

64. Li, H.; Shen, C.R.; Huang, C.-H.; Sung, L.-Y.; Wu, M.-Y.; Hu, Y.-C. CRISPR-Cas9 for the genome engineering of cyanobacteria and succinate production. *Metab. Eng.* **2016**, *38*, 293–302. [CrossRef] [PubMed]
65. Behler, J.; Vijay, D.; Hess, W.R.; Akhtar, M.K. CRISPR-Based Technologies for Metabolic Engineering in Cyanobacteria. *Trends Biotechnol.* **2018**, *36*, 996–1010. [CrossRef] [PubMed]
66. Yao, L.; Cengic, I.; Anfelt, J.; Hudson, E.P. Multiple Gene Repression in Cyanobacteria Using CRISPRi. *ACS Synth. Biol.* **2016**, *5*, 207–212. [CrossRef] [PubMed]
67. Pruvost, J.; Van Vooren, G.; Le Gouic, B.; Couzinet-Mossion, A.; Legrand, J. Systematic investigation of biomass and lipid productivity by microalgae in photobioreactors for biodiesel application. *Bioresour. Technol.* **2011**, *102*, 150–158. [CrossRef] [PubMed]
68. García-Malea, M.C.; Acién, F.G.; Del Río, E.; Fernández, J.M.; Cerón, M.C.; Guerrero, M.G.; Molina-Grima, E. Production of astaxanthin by *Haematococcus pluvialis*: Taking the one-step system outdoors. *Biotechnol. Bioeng.* **2009**, *102*, 651–657. [CrossRef] [PubMed]
69. Martins, R.G.; Goncalves, I.S.; de Morais, M.G.; Costa, J.A.V. Bioprocess Engineering Aspects of Biopolymer Production by the Cyanobacterium Spirulina Strain LEB 18. *Int. J. Polymer Sci.* **2014**, *2014*, 895237. [CrossRef]
70. Samantaray, S.; Mallick, N. Role of cultural variables in tailoring poly (3-hydroxybutyrate-co-3-hydroxyvalerate) copolymer synthesis in the diazotrophic cyanobacterium *Aulosira fertilissima* CCC 444. *J. Appl. Phycol.* **2015**, *27*, 197–203. [CrossRef]
71. Silva, C.S.P.; Silva-Stenico, M.E.; Fiore, M.F.; de Castro, H.F.; Da Rós, P.C.M. Optimization of the cultivation conditions for *Synechococcus* sp. PCC7942 (cyanobacterium) to be used as feedstock for biodiesel production. *Algal Res.* **2014**, *3*, 1–7. [CrossRef]
72. Ooijkaas, L.P.; Wilkinson, E.C.; Tramper, J.; Buitelaar, R.M. Medium optimization for spore production of coniothyrium minitans using statistically-based experimental designs. *Biotechnol. Bioeng.* **1999**, *64*, 92–100. [CrossRef]
73. Wu, G.; Wu, Q.; Shen, Z. Accumulation of poly-β-hydroxybutyrate in cyanobacterium *Synechocystis* sp. PCC6803. *Bioresour. Technol.* **2001**, *76*, 85–90. [CrossRef]
74. Carpine, R.; Olivieri, G.; Hellingwerf, K.; Pollio, A.; Pinto, G.; Marzocchella, A. Poly-β-hydroxybutyrate (PHB) Production by Cyanobacteria. *New Biotechnol.* **2016**, *33*, S19–S20. [CrossRef]
75. Kaewbai-Ngam, A.; Incharoensakdi, A.; Monshupanee, T. Increased accumulation of polyhydroxybutyrate in divergent cyanobacteria under nutrient-deprived photoautotrophy: An efficient conversion of solar energy and carbon dioxide to polyhydroxybutyrate by *Calothrix scytonemicola* TISTR 8095. *Bioresour. Technol.* **2016**, *212*, 342–347. [CrossRef] [PubMed]
76. Sharma, L.; Mallick, N. Accumulation of poly-beta-hydroxybutyrate in Nostoc muscorum: Regulation by pH, light-dark cycles, N and P status and carbon sources. *Bioresour. Technol.* **2005**, *96*, 1304–1310. [CrossRef] [PubMed]
77. Coelho, V.C.; da Silva, C.K.; Terra, A.L.; Costa, J.A.V.; de Morais, M.G. Polyhydroxybutyrate production by *Spirulina* sp. LEB 18 grown under different nutrient concentrations. *Afr. J. Microbiol. Res.* **2015**, *9*, 1586–1594.
78. Gopi, K.; Balaji, S.; Muthuvelan, B. Isolation Purification and Screening of Biodegradable Polymer PHB Producing Cyanobacteria from Marine and Fresh Water Resources. *Iran. J. Energy Environ.* **2014**, *5*, 94–100. [CrossRef]
79. Markou, G.; Vandamme, D.; Muylaert, K. Microalgal and cyanobacterial cultivation: The supply of nutrients. *Water Res.* **2014**, *65*, 186–202. [CrossRef] [PubMed]
80. Samantaray, S.; Nayak, K.J.; Mallick, N. Wastewater utilization for poly-β-hydroxybutyrate production by the cyanobacterium *Aulosira fertilissima* in a recirculatory aquaculture system. *Appl. Environ. Microbiol.* **2011**, *77*, 8735–8743. [CrossRef] [PubMed]
81. Bhati, R.; Mallick, N. Carbon dioxide and poultry waste utilization for production of polyhydroxyalkanoate biopolymers by *Nostoc muscorum* Agardh: A sustainable approach. *J. Appl. Phycol.* **2016**, *28*, 161–168. [CrossRef]
82. Chaiklahan, R.; Chirasuwan, N.; Siangdung, W.; Paithoonrangsarid, K.; Bunnag, B. Cultivation of Spirulina platensis using pig wastewater in a semi-continuous process. *J. Microbiol. Biotechnol.* **2010**, *20*, 609–614. [CrossRef] [PubMed]
83. Phang, S.M.; Miah, M.S.; Yeoh, B.G.; Hashim, M.A. Spirulina cultivation in digested sago starch factory wastewater. *J. Appl. Phycol.* **2000**, *12*, 395–400. [CrossRef]

84. Olguín, E.J.; Galicia, S.; Mercado, G.; Pérez, T. Annual productivity of Spirulina (Arthrospira) and nutrient removal in a pig wastewater recycling process under tropical conditions. *J. Appl. Phycol.* **2003**, *15*, 249–257. [CrossRef]
85. Kourmentza, C.; Plácido, J.; Venetsaneas, N.; Burniol-Figols, A.; Varrone, C.; Gavala, H.N.; Reis, M.A.M. Recent Advances and Challenges towards Sustainable Polyhydroxyalkanoate (PHA) Production. *Bioengineering* **2017**, *4*, 55. [CrossRef] [PubMed]
86. Fradinho, J.C.; Reis, M.A.M.; Oehmen, A. Beyond feast and famine: Selecting a PHA accumulating photosynthetic mixed culture in a permanent feast regime. *Water Res.* **2016**, *105*, 421–428. [CrossRef] [PubMed]
87. Fradinho, J.C.; Oehmen, A.; Reis, M.A. Photosynthetic mixed culture polyhydroxyalkanoate (PHA) production from individual and mixed volatile fatty acids (VFAs): Substrate preferences and co-substrate uptake. *J. Biotechnol.* **2014**, *185*, 19–27. [CrossRef] [PubMed]
88. Arias, D.M.; Fradinho, J.C.; Uggetti, E.; García, J.; Oehmen, A.; Reis, M.A.M. Polymer accumulation in mixed cyanobacterial cultures selected under the feast and famine strategy. *Algal Res.* **2018**, *33*, 99–108. [CrossRef]
89. Fradinho, J.C.; Domingos, J.M.; Carvalho, G.; Oehmen, A.; Reis, M.A. Polyhydroxyalkanoates production by a mixed photosynthetic consortium of bacteria and algae. *Bioresour. Technol.* **2013**, *132*, 146–153. [CrossRef] [PubMed]
90. Stal, L.J.; Moezelaar, R. Fermentation in cyanobacteria1. *FEMS Microbiol. Rev.* **1997**, *21*, 179–211. [CrossRef]
91. Stal, L.; Krumbein, W. Metabolism of cyanobacteria in anaerobic marine sediments. In Proceedings of the 2. Colloque International de Bacteriologie Marine, Brest, France, 1–4 October 1984; pp. 1–5.
92. Rahman, A.; Putman, R.J.; Inan, K.; Sal, F.A.; Sathish, A.; Smith, T.; Nielsen, C.; Sims, R.C.; Miller, C.D. Polyhydroxybutyrate production using a wastewater microalgae based media. *Algal Res.* **2015**, *8*, 95–98. [CrossRef]
93. Sharma, L.; Kumar Singh, A.; Panda, B.; Mallick, N. Process optimization for poly-beta-hydroxybutyrate production in a nitrogen fixing cyanobacterium, *Nostoc muscorum* using response surface methodology. *Bioresour. Technol.* **2007**, *98*, 987–993. [CrossRef] [PubMed]
94. Mallick, N.; Sharma, L.; Kumar Singh, A. Poly-beta-hydroxybutyrate accumulation in *Nostoc muscorum*: Effects of metabolic inhibitors. *J. Plant Physiol.* **2007**, *164*, 312–317. [CrossRef] [PubMed]
95. Mallick, N.; Gupta, S.; Panda, B.; Sen, R. Process optimization for poly(3-hydroxybutyrate-co-3-hydroxyvalerate) co-polymer production by *Nostoc muscorum*. *Biochem. Eng. J.* **2007**, *37*, 125–130. [CrossRef]
96. Bhati, R.; Samantaray, S.; Sharma, L.; Mallick, N. Poly-β-hydroxybutyrate accumulation in cyanobacteria under photoautotrophy. *Biotechnol. J.* **2010**, *5*, 1181–1185. [CrossRef] [PubMed]
97. Panda, B.; Sharma, L.; Mallick, N. Poly-β-hydroxybutyrate accumulation in *Nostoc muscorum* and *Spirulina platensis* under phosphate limitation. *J. Plant Physiol.* **2005**, *162*, 1376–1379. [CrossRef] [PubMed]
98. Google Scholar. Earth System Research Laboratory. 2017. Available online: https://esrl.noaa.gov/ (accessed on 15 April 2017).
99. Eberly, J.O.; Ely, R.L. Photosynthetic accumulation of carbon storage compounds under CO_2 enrichment by the thermophilic cyanobacterium *Thermosynechococcus elongatus*. *J. Ind. Microbiol. Biotechnol.* **2012**, *39*, 843–850. [CrossRef] [PubMed]
100. Lee, S.Y. Bacterial polyhydroxyalkanoates. *Biotechnol. Bioeng.* **1996**, *49*, 1–14. [CrossRef]
101. Lee, S.Y. Plastic bacteria? Progress and prospects for polyhydroxyalkanoate production in bacteria. *Trends Biotechnol.* **1996**, *14*, 431–438. [CrossRef]
102. Koller, M.; Khosravi-Darani, K.; Braunegg, G. *Advanced Photobioreactor Systems for the Efficient Cultivation of Cyanobacteria, in Photobioreactors Advancements, Applications and Research*; Tsang, Y.F., Ed.; Nova Science Publishers: New York, NY, USA, 2017; pp. 35–90.
103. Arias, D.M.; Uggetti, E.; García-Galán, M.J.; García, J. Production of polyhydroxybutyrates and carbohydrates in a mixed cyanobacterial culture: Effect of nutrients limitation and photoperiods. *New Biotechnol.* **2018**, *42*, 1–11. [CrossRef] [PubMed]
104. Riis, V.; Mai, W. Gas chromatographic determination of poly-?-hydroxybutyric acid in microbial biomass after hydrochloric acid propanolysis. *J. Chromatogr.* **1988**, *445*, 285–289. [CrossRef]
105. Karr, D.B.; Waters, J.K.; Emerich, D.W. Analysis of Poly-beta-Hydroxybutyrate in *Rhizobium japonicum* Bacteroids by Ion-Exclusion High-Pressure Liquid Chromatography and UV Detection. *Appl. Environ. Microbiol.* **1983**, *46*, 1339–1344. [PubMed]

106. Koller, M.; Rodríguez-Contreras, A. Techniques for tracing PHA-producing organisms and for qualitative and quantitative analysis of intra- and extracellular PHA. *Eng. Life Sci.* **2015**, *15*, 558–581. [CrossRef]
107. Kansiz, M.; Billman-Jacobe, H.; McNaughton, D. Quantitative determination of the biodegradable polymer Poly(beta-hydroxybutyrate) in a recombinant *Escherichia coli* strain by use of mid-infrared spectroscopy and multivariative statistics. *Appl. Environ. Microbiol.* **2000**, *66*, 3415–3420. [CrossRef] [PubMed]
108. Degelau, A.; Scheper, T.; Bailey, J.E.; Guske, C. Fluorometric measurement of poly-β hydroxybutyrate in Alcaligenes eutrophus by flow cytometry and spectrofluorometry. *Appl. Microbiol. Biotechnol.* **1995**, *42*, 653–657. [CrossRef]
109. Stenholm, H.; Song, S.; Eriksen, N.T.; Iversen, J.J.L. Indirect Estimation of Poly-β-Hydroxybutyric Acid by Cell Carbon Analysis. *Biotechnol. Tech.* **1998**, *12*, 451–454. [CrossRef]
110. Naumann, D.; Helm, D.; Labischinski, H. Microbiological characterizations by FT-IR spectroscopy. *Nature* **1991**, *351*, 81–82. [CrossRef] [PubMed]
111. Schuster, K.C.; Mertens, F.; Gapes, J.R. FTIR spectroscopy applied to bacterial cells as a novel method for monitoring complex biotechnological processes. *Vib. Spectrosc.* **1999**, *19*, 467–477. [CrossRef]
112. Randriamahefa, S.; Renard, E.; Guérin, P.; Langlois, V. Fourier transform infrared spectroscopy for screening and quantifying production of PHAs by Pseudomonas grown on sodium octanoate. *Biomacromolecules* **2003**, *4*, 1092–1097. [CrossRef] [PubMed]
113. Jarute, G.; Kainz, A.; Schroll, G.; Baena, J.R.; Lendl, B. On-line determination of the intracellular poly(beta-hydroxybutyric acid) content in transformed *Escherichia coli* and glucose during PHB production using stopped-flow attenuated total reflection FT-IR spectrometry. *Anal. Chem.* **2004**, *76*, 6353–6358. [CrossRef] [PubMed]
114. Song, J.H.; Murphy, R.J.; Narayan, R.; Davies, G.B.H. Biodegradable and compostable alternatives to conventional plastics. *Philos. Trans. R. Soc. B Biol. Sci.* **2009**, *364*, 2127–2139. [CrossRef] [PubMed]
115. Gerngross, T.U. Can biotechnology move us toward a sustainable society? *Nat. Biotechnol.* **1999**, *17*, 541. [CrossRef] [PubMed]
116. Choi, J.-I.; Lee, Y.S. Process analysis and economic evaluation for poly (3-hydroxybutyrate) production by fermentation. *Bioprocess Eng.* **1997**, *17*, 335–342. [CrossRef]
117. Acién, F.G.; Fernández, J.M.; Magán, J.J.; Molina, E. Production cost of a real microalgae production plant and strategies to reduce it. *Biotechnol. Adv.* **2012**, *30*, 1344–1353. [CrossRef] [PubMed]
118. Koller, M. Advances in Polyhydroxyalkanoate (PHA) Production. *Bioengineering* **2017**, *4*, 88. [CrossRef] [PubMed]

bioengineering

MDPI

Review

Recent Advances in the Use of Polyhydroyalkanoates in Biomedicine

Alejandra Rodriguez-Contreras

Department of Materials Science and Metallurgical Engineering, Universitat Politècnica de Catalunya (UPC), Escola d'Enginyeria de Barcelona Est (EEBE), Eduard Maristany 10-14, 08930 Barcelona, Spain; sandra8855@hotmail.com; Tel.: +34-651-569-562

Received: 20 August 2019; Accepted: 10 September 2019; Published: 12 September 2019

Abstract: Polyhydroxyalkanoates (PHAs), a family of natural biopolyesters, are widely used in many applications, especially in biomedicine. Since they are produced by a variety of microorganisms, they possess special properties that synthetic polyesters do not have. Their biocompatibility, biodegradability, and non-toxicity are the crucial properties that make these biologically produced thermoplastics and elastomers suitable for their applications as biomaterials. Bacterial or archaeal fermentation by the combination of different carbohydrates or by the addition of specific inductors allows the bioproduction of a great variety of members from the PHAs family with diverse material properties. Poly(3-hydroxybutyrate) (PHB) and its copolymers, such as poly(3-hydroxybutyrate-co-3-hydroxyvalerate) (PHVB) or poly(3-hydroxybutyrate-co-4-hydroxybutyrate) (PHB4HB), are the most frequently used PHAs in the field of biomedicine. PHAs have been used in implantology as sutures and valves, in tissue engineering as bone graft substitutes, cartilage, stents for nerve repair, and cardiovascular patches. Due to their good biodegradability in the body and their breakdown products being unhazardous, they have also been remarkably applied as drug carriers for delivery systems. As lately there has been considerable and growing interest in the use of PHAs as biomaterials and their application in the field of medicine, this review provides an insight into the most recent scientific studies and advances in PHAs exploitation in biomedicine.

Keywords: polyhydroxyalkanoates; biomedicine; biomaterials; Poly(3-hydroxybutyrate); tissue engineering; wound healing; delivery system; poly(3-hydroxybutyrate-co-3-hydroxyvalerate) (PHVB); poly(3-hydroxybutyrate-co-4-hydroxybutyrate)

1. Introduction

Synthetic plastics are used in many different applications, as they are a family of versatile materials. However, there is a global awareness of the environmental impact of these fossil-based polymers. At the same time, there is growing recognition that organic matter of biological origin can be a worthy alternative [1]. In this regard, natural polymers or biopolymers show many advantages relative to petrochemical materials, as they are biodegradable and produced from renewable sources. Furthermore, due to their similarity to the native natural environment, their biopolymer functions show good biological performance and adaptability, and adequate body reaction [2]. This makes them very attractive for their application not only in biomedicine but also in other fields such as pharmacology and biotechnology [1]. In biomedicine as the theoretical branch of medicine that applies the principles of biology, biochemistry, and biophysics to medical research and practice, the combination of synthetic and natural polymers is frequently used [3–6].

Polyhydroxyalkanoates (PHAs) are a big family of naturally produced polyesters. Chemically, they are linear polymers composed of hydroxyalkanoate units as their basic structure (Figure 1a).

These biopolymers are accumulated within the cytoplasm of diverse microorganisms under conditions of nutrient depletion and in the presence of an excess of carbon source [7–9]. They appear as granules and function as carbohydrate and energy storage (Figure 1c). PHAs can be produced by biotechnological processes via bacterial and archaeal fermentation. The members of the PHA family differ widely in their structure and properties (Figure 1a,d,e) depending on the producing microorganism, biosynthesis conditions, and type of carbon source used in the production process [8–10]. In general, PHAs are thermoplastic or elastomeric, and their sufficiently high molecular mass provides them with properties similar to those of conventional petrochemical polymers (Figure 1d) [11–14]. More specifically, they can be classified depending on their monomeric composition: short-chain-length PHA (*scl*-PHA), consisting of 3 to 5 carbon atoms per monomer; medium-chain-length PHA (*mcl*-PHA), with 6 to 14 carbon atoms; and the rather rare group of long-chain-length PHA (*lcl*-PHA), which presents more than 14 carbon atoms [15,16]. The vast majority of microorganisms synthesize either *scl*-PHAs containing primarily 3-hydroxybutyrate (3HB) units or *mcl*-PHAs containing 3-hydroxyhexanoate (3HHx), 3-hydroxyoctanoate (3HO), 3-hydroxydecanoate (3HD), and 3-hydroxydodecanoate (3HHD) as the major monomers [7,15]. While *scl*-PHAs are crystalline and feature typical thermoplastic properties, *mcl*-PHA resins resemble elastomers and latex-like materials with typically low glass transition temperature and lower molecular mass if compared to *scl*-PHA [15,17,18].

Poly(3-hydroxybutyrate) (PHB) is the most frequently occurring PHA member and is a linear, unbranched homopolymer consisting of (R)-3-hydroxybutyric acid units. When extracted from bacterial biomass, PHB tends to crystallize [19]. Although its applications are limited mainly by its high crystallinity and brittleness, which reduce its flexibility and ductility, PHB can be modified by simply physical blending or chemical alteration to fine-tune its mechanical properties [10,20]. Another strategy to modify its mechanical properties is by copolymerization via bacterial fermentation using different precursors (Figure 1d). For instance, a common PHB copolymer, poly(3-hydroxybutyrate-co-3-hydroxyvalerate) (PHBV), is characterized as less crystalline and more flexible than PHB itself [21], and its properties can be varied according to the 3-hydroxyvalerate (3HV) content in the structure (Figure 1d) [22]. PHBV is usually produced by adding valeric acid to the fermentation medium [23]. Poly(3-hydroxybutyrate-co-4-hydroxybutyrate) (PHB4HB) copolymer is another of the most well-known members of the PHA family. With higher 4-hydroxybutyric acid (4HB) content, PHA is more elastomeric and with outstanding elongation at break (Figure 1d) [24]. These PHAs members together with poly(3-hydroxybutyrate-co-3-hydroxyvalerate-co-3-hydroxyhexanoate) (PHBVHHx) represent the most commonly applied PHAs in biomedicine [25].

Current research on PHAs focuses on subjects such as gaining a better understanding of the mechanisms related to their biosynthesis, or how to modulate PHAs properties for different applications. The development of natural and recombinant microorganisms to efficiently produce PHAs and the finding of alternative raw materials that lead their production to more competitive costs are also important research topics [26,27].

PHAs show major advantages compared with traditional synthetic polymers. However, it is because of their biodegradability, biocompatibility, and non-toxicity that they are especially appealing materials for biomedical applications. Furthermore, an additional benefit is their unchanged local pH value during degradation. This makes them well tolerated by cells and the immune system compared to other polymers clinically used such as poly(lactide-co-glycolide) (PLGA), poly(ε-caprolactone) (PCL), poly(glycolic acid) (PGA), and poly(lactic acid) (PLA) [20]. In the last decades, there has been an increase in PHAs exploitation in biomedicine. Therefore, this review is an attempt to summarize the most important advances published in the last few years on the use of microbially originated PHAs used in this field.

a)

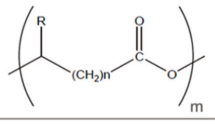

n	R	Polymer name
	Hydrogen	Poly(3-hydroxypropionate)
	Methyl	Poly(3-hydroxybutyrate)
1	Ethyl	Poly(3-hydroxyvalerate)
	Propyl	Poly(3-hydroxyhexanoate)
	Pentyl	Poly(3-hydroxyoctanate)
2	Hydrogen	Poly(4-hydroxybutyrate)
3	Hydrogen	Poly(5-hydroxyvalerate)

b)

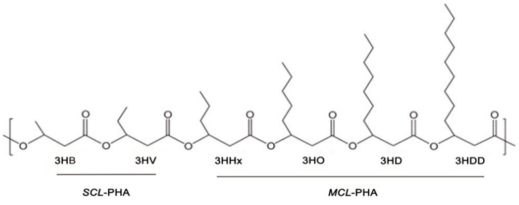

c)

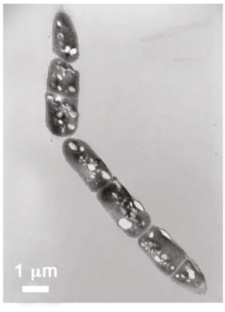

d)

Properties	PHB	P(3HB-3HV) for 4 – 95% (mol/mol) 3HV	PP
Molecular mass (10^5 g/mol)	1 – 8	3	2.2 – 7
Density (kg/m^3)	1.25	1.20	0.905
T_m (°C)	171 – 182	75 – 172	176
Crystallinity degree (X_c) (%)	80	55 – 70	70
T_g (°C)	4 – 10	-13 – +8	-10
O_2 Permeability [(cm^3/(m^{2}atm)]	45	n. d.	1700
UV Resistance	Good	Good	Bad
Resistance to solvents	Bad	Bad	Good
Tensile strength (Mpa)	40	25 – 30	38
Elongation to break (%)	6	8 – 1200	400
Young's modulus (GPa)	3.5	2.9 (3% 3HV); 0.7 (25% 3HV)	1.7
Biodegradability	Yes	Yes	No

e)

Parameter	Values for					
	PHB	P(3HB-3% 3HV)	P(3HB-20%3HV)	P4HB	P(3HB-16%4HB)	P(3HO-3HHx)
Melting temperature (T_m) (°C)	177	170	145	60	152	61
Glass transition temperature (T_g) (°C)	4	-	-1	-50	-8	-36
Tensile strength (MPa)	40	38	32	104	26	9
Young´s modulus (GPa)	3.5	2.9	1.2	149	-	0.008
Elongation at break (%)	6	-	50	1000	444	380

Figure 1. (**a**) Chemical structure of the polyhydroxyalkanoates (PHA) biopolymer family, the monomer number m range from 100 to 30,000 [12]. (**b**) Some commonly synthesized scl-PHA monomers (scl-HA) and mcl-PHA monomers (mcl-HA). 3HB: 3-hydroxybutyrate, 3HV: 3-hydroxyvalerate, 3HHx: 3-hydroxyhexanoate, 3HO: 3-hydroxyoctanoate, 3HD: 3-hydroxydecanoate, 3HDD: 3-hydroxydodecanoate. (**c**) Transmission electron microscopy micrograph of *Bacillus megaterium* uyuni S29 after 4 h of fermentation showing PHB granules as refractile inclusion bodies [28]. (**d**) Some physical, thermal, chemical, and mechanical properties of PHB and poly(3-hydroxybutyrate-co-3-hydroxyvalerate) (PHBV) compared to those of the petrol-based polypropylene (PP) [12,29]. (**e**) Table of properties of some PHAs members and copolymers [12,29].

2. Tissue Engineering

Tissue engineering is an interdisciplinary field of research focused on the creation of vital tissues by a combination of biomaterials, cells, and bioactive molecules, aiming to repair damaged or diseased tissues and organs [30]. Tissues can be classified as hard tissue substitutes, such as bone and cartilage, or soft tissues, such as vascular and skin grafts [31]. The biomaterial used must have two crucial features

to function as tissue repairer: to possess mechanical properties for supporting the organ during new tissue regeneration, and enhanced surface topography to allow efficient cell adhesion and proliferation. In this regard, engineered scaffolds are designed to closely mimic the topography, spatial distribution, and chemical environment corresponding to the native extracellular matrix of the intended tissue in order to support cell growth and differentiation [32]. PHAs constitute a great alternative for tissue engineering due to their versatility regarding their mechanical properties, combined with great biocompatibility with minimal tissue toxicity and degradability. Thus, PHAs have been exploited for the replacement and healing of both hard and soft tissues in tissue engineering to repair cartilage, cardiovascular tissues, skin, bone marrow, and nerve conduits [22,33–35].

2.1. Hard Tissue

2.1.1. Bone Tissue Engineering

Bone tissue engineering refers to the regeneration of new bone by providing mechanical support while inducing cell growth. For this application, hydroxyapatite (HA), inorganic substances, hydrogels, and even other biocompatible polymers are used to blend with PHAs to optimize their compressive elastic modulus and maximum stress. For instance, Degli Esposti et al. [36] very recently published the exploitation of a mixture of PHB with HA particles for the development of bio-resorbable porous scaffolds for bone tissue regeneration. The osteoinductivity and osteoconductivity of the bioactive scaffolds were attained mainly due to the incorporation of HA. By combining $CaCO_3$-mineralized piezoelectric with PHB- and PHBV-based scaffolds, Chernozem et al. [37] elaborated PHA biocomposites that provided biodegradability and stimulated bone tissue repair. The presence of mineral led to a pronounced apatite-forming behavior of the biodegradable PHAs scaffolds, and this turned out to stimulate the growth of the bone tissue. A more complex system is the one produced by Meischel et al. [38], who evaluated the response of bone to PHA composite implants in the femora of growing rats. Composites were constituted by PHB with zirconium dioxide, Herafill® (calcium sulfate, calcium carbonate, triglycerides, and gentamicin; produced by Hereus), and Mg-alloy WZ21. Longitudinal observation of the bone reaction at the implant site and resorption of the implanted pins were monitored, and the results showed that PHB composited with zirconium dioxide and 30% Herafill possessed the highest values of bone accumulation. The authors concluded that the mechanical properties (elastic modulus, tensile strength, and strain properties) of PHB composites in these conditions were close to that of bone.

Hydrogels can be used to create scaffolds with a well-interconnected porous structure. However, they provide poor mechanical stability and very low bioactivity, failing to create suitable constructs for bone tissue engineering. In order to improve the mechanical stability of hydrogels, Sadat et al. [39] developed a scaffold system based on combining a mix of biodegradable PHB and HA with a protein-based hydrogel in a single tri-layered scaffold. These scaffolds provided high strength, had the ability to encapsulate cells, and enhanced bone cell adaptability (Figure 2a).

In their study, Ding et al. [40] mixed the natural polyester PHB with the synthetic polyester PCL. They fabricated PHB/PCL/58S sol-gel bioactive glass hybrid scaffolds by electrospinning of the polymers and inorganic substances. The combination of the high stiffness of PHB, the flexibility of PCL, and the bioactivity of 58S bioactive glass in one single fibrous structure showed potential for using in bone tissue engineering integration. The composite enhanced the primary biological response of osteoblast-like cells and their viability, and significantly increased alkaline phosphatase enzyme activity.

2.1.2. Cartilage

Tissue engineering of cartilage provides promising strategies for the regeneration of damaged articular cartilage. There are significant challenges, since current surgical procedures are unable to restore normal cartilage function. It is important to create an alternative that matches the long-term

mechanical stability and durability of this native hard tissue [41]. Some recent studies demonstrated that the use of PHAs can be a solution. Ching et al. [41] produced diverse blends of PHB with poly(3-hydroxyoctanoate) (P3HO) as biodegradable polymer scaffolds. By studding different ratios of both polymers, they optimized their structure, stiffness, degradation rates, and biocompatibility. At a polymer rate (PHB/P3HO) of 1:0.25, the blend closely mimicked the collagen fibrillar meshwork of native cartilage and attained the stiffness of native articular cartilage (Figure 2b). They concluded that by fine tuning the ultrastructure and mechanical properties using different blends, these two polymers allowed the production of a cartilage repair kit for clinical use and the reduction of the risk of developing secondary osteoarthritis. More recently, Toloue et al. [42] evaluated the mechanical properties and cell viability of a mix of PHB with 3% chitosan reinforced with alumina as a scaffold for cartilage reparation. The presence of alumina nanowires significantly increased the tensile strength of PHB and PHB/chitosan scaffolds. In vitro studies showed that chondrocyte cells spread more on the composite than on pure PHB scaffolds. The authors concluded that the electrospun scaffold of PHB with chitosan and 3% alumina had the potential to be applied in cartilage tissue engineering.

2.2. Soft Tissue

2.2.1. Cardiac Tissue Engineering

Cardiac tissue engineering is currently a prime focus of research because of an enormous clinical need. *Mcl*-PHAs have demonstrated exceptional properties for cardiac tissue engineering applications. They are more elastic than other members of their family, showing an elastomeric nature, higher glass transition temperatures, and the potential to integrate with the myocardial network and be conjugated with bioactive molecules, such as vascular endothelial growth factor, to further increase cellular attachment, viability, and proliferation [18].

Guo et al. [35] summarized the recent use of P4HB as a promising biomaterial for applications in cardiac tissue engineering such as congenital heart defects, heart valves, and vascular grafts. The versatile material is also used in other applications as an absorbable monofilament for sutures, and hernia, tendon, and ligament repair, among others. Bagdadi et al. [43] used P3HO as a potential material for cardiac tissue engineering. They fabricated P3HO-based multifunctional cardiac patches with mechanical properties that were close to those of cardiac muscle. Furthermore, they were shown to be as good as collagen in terms of cell viability, proliferation, and adhesion. Likewise, Constantinides et al. [18] used *mcl*-PHAs for this application. They first produced the *mcl*-PHAs by bacterial fermentation with *Pseudomonas mendocina* CH50 using glucose as the sole carbon source under nitrogen limiting conditions. Then, the obtained *mcl*-PHAs were reinforced with PCL (5%) to produce thin films. The blended structures were implanted in post mortem murine heart in situ. The composites demonstrated possessing a great potential for maximizing tissue regeneration in myocardial infarction. Besides this study, there was research using PHBVHHx [25] in the form of membranes and PHB4HB [44] for the production of cardiac patches. These studies were carried out with stem cells of different origin.

Valvular heart diseases are the third leading cause of cardiovascular disease. Thus, heart valve tissue engineering (HVTE) has appeared as an important strategy to treat these disorders. Ideally, a designed construct should withstand the native dynamic mechanical environment, guide the regeneration of the diseased tissue, and more importantly, have the ability to grow with the patient's heart [45]. Xue et al. [45] summarized different types of synthetic biodegradable elastomers that have been explored for HVTE. Referring to a published work of Chen et al. [46], they specify that this class of elastomers, the PHAs, are generally stronger than polyurethane-based elastomers and more suitable to work under dynamic conditions such as those of cardiovascular tissue.

2.2.2. Wound Healing

The need for novel materials in the effective regeneration of injured skin is a serious concern in reconstructive medicine [47]. Many natural (collagen, alginic acid, hyaluronic acid, chitosan, fucoidan) and synthetic (teflon, polyurethanes, methyl methacrylate) polymers are being used in the preparation of artificial dressing materials for wound healing applications [48]. This complex application requires that the biomaterial fulfills the functions of healthy skin, which has an antimicrobial effect, promotes moist wound environment, permits gaseous exchange, provides mechanical protection, and is sufficiently elastic to fit the wound shape [47]. The PHA family of biopolymers has also extended in this novel medical area. One major factor inhibiting natural wound-healing processes is bacterial infection, especially in chronic wounds [49]. There are studies on wound healing with antibiotic delivery systems and applying PHAs as a remedy. For instance, Marcano et al. [49] optimized the micro/nano-structure of a wound dressing in order to obtain a more efficient antibiofilm protein-release profile for biofilm inhibition and/or detachment. Thus, they developed a three-dimensional (3D) substrate based on asymmetric PHA membranes to entrap an antibiofilm protein (Figure 2c). Similarly, the team of Volova [47] constructed wound dressings from PHB4HB membranes for skin wound repair and evaluated their effectiveness in experiments with laboratory animals. The nonwoven membranes of PHB4HB carried the culture of allogenic fibroblasts. The use of the biopolymer reduced inflammation, enhanced the angiogenic properties of the skin, and facilitated the wound healing process.

2.2.3. PHAs for Organ Tissues

PHBVHHx is considered a promising PHA member for the growth of stem cells, and certain studies utilized it as biomaterial for the preparation of three-dimensional supportive scaffolds for organ tissue. In some works [50,51], PHBVHHx films and scaffolds were developed and loaded with mesenchymal stem cells from human umbilical cord (UC-MSCs) to recover injured liver. Biopolymer scaffolds were transplanted into liver-injured mice, and the results demonstrated that the PHA scaffold significantly promoted the recovery of injured liver and could be used for liver tissue engineering. In the case of the work by Li et al. [50], differences between PHBVHHx and some other commonly used biopolymers such as PLA, PHB4HB, and PHBHHx were examined by loading them with stem cells into their scaffolds (Figure 2d). They concluded that the PHBVHHx structures exhibited the highest cell attachment and, when loaded with mesenchymal stem cells, significantly improved the recovery of injured liver.

PHAs have also been used in tendon healing. In order to improve the initial biomechanical repair strength of tendon tears at risk of failure, Tashjian et al. [52] produced a bioresorbable scaffold to reinforce the suture-tendon interface in rotator cuff repairs. A study of cyclic and ultimate failure properties of PHA mesh was conducted, obtaining better mechanical results than in the control condition (without the reinforcement).

As a hard tissue, Findrik et al. [31] exploited a blend of PLA and PHB to use it as a tubular substitute for urethra replacement. They dealt with the combination of both polymers to provide stabile conditions during the engineering of the replacement by adjusting material degradation and viscosity. By using a 3D printing process, a cubic sample representing basic scaffold structures and a tubular one serving as urethra substitution were designed.

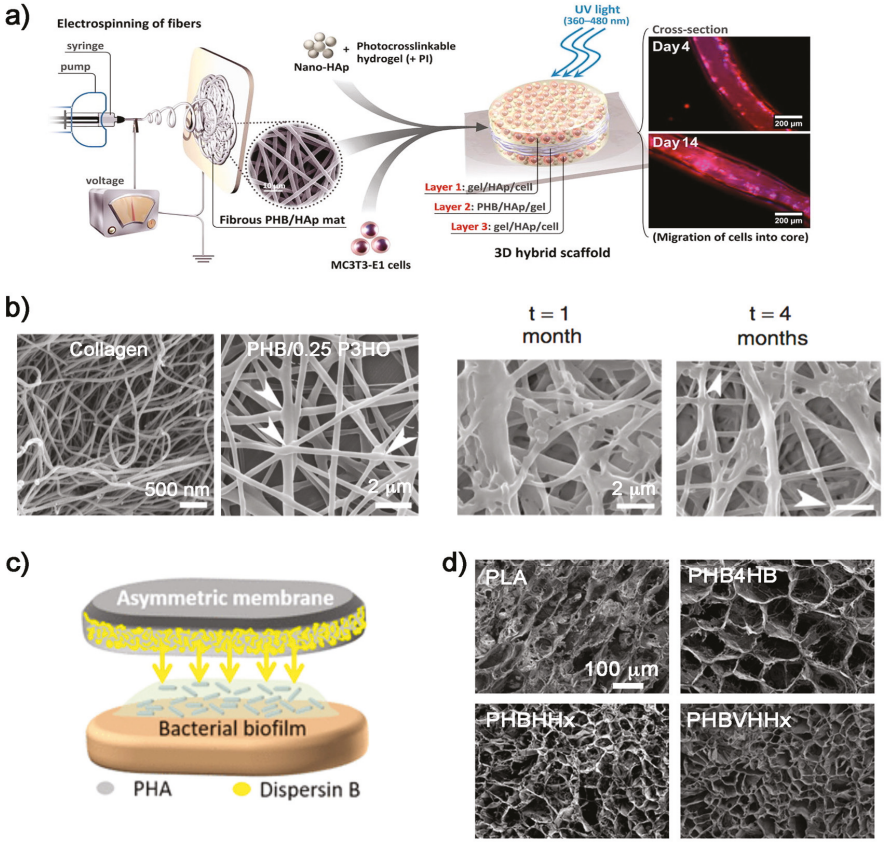

Figure 2. PHAs for tissue engineering: (**a**) Scheme of the published study of Sadat-Shojai et al. [39] where a cell-laden tri-layered scaffold of PHB with hydroxyapatite (HA) was performed to enhance bone regeneration in vivo. (**b**) Scanning electron microscopy (SEM) micrographs of PHB/P3HO scaffolds where the electrospun fibers with a ratio blend of 1:0.25 provided structures more similar to collagen natural fibers. Biopolymeric fibers after hydrolytic degradation [41]. (**c**) Scheme of the asymmetric PHA membranes entrapping an anti-biofilm protein (dispersin B) for wound healing [49]. (**d**) SEM micrographs of biopolymers scaffolds from Li et al. [50]. The biopolymer structures displayed different pore sizes where stem cells were loaded into, and the PHBVHHx ones exhibited the highest cell attachment.

3. Drug Delivery Systems

One of the key reasons for the common use of the PHA biopolymer family as drug carriers is their biodegradability under different environments. A vast number of microorganisms secrete extracellular PHA-hydrolyzing enzymes (PHA depolymerases and other enzymes) to degrade PHA polymers into oligomers and monomers, which subsequently act as nutrients inside the cells [53–55]. PHAs typically degrade by hydrolytic and bacterial depolymerase mechanisms over 52-plus weeks in vivo [56]. Furthermore, there are studies that compare PHAs biodegradability with that of other synthetic or semisynthetic polymers. Gil-Castell et al. [57] compared the durability of PLGA, polydioxanone (PDO), polycaprolactone (PCL), and PHB scaffolds. Results showed that for long-term applications, PCL and PHB were more appropriate materials than PLGA and PDO, which could be used in short-term applications. Regarding their biodegradability in ultra-pure water and phosphate buffer solution

at 37 °C, the PHB molar mass progressively decreased, reaching almost 50% after 650 days of immersion. However, PHAs' biodegradability depends on different factors such as the composition of the biopolymer, its stereo regularity, crystallinity (degradability decreases as the overall crystallinity increases), molecular mass (biopolymers are generally biodegraded more rapidly when their molecular mas is lower), and environmental conditions (temperature, moisture level, pH, and nutrient supply) [58]. This makes this biopolymer family especially appealing for delivery systems, since the controllable retarding properties of systems based on PHAs can be modulated mainly by their molecular mass and copolymer composition. Moreover, PHAs have already demonstrated a significant impact on the drug bioavailability, better encapsulation, and less toxicity of biodegradable polymers [59].

In the literature, several reviews of the use of PHAs as carriers in biomedine can be found. They embrace the shape of particles, spheres, micelles, liposomes, vesicles, or capsules as therapeutic delivery carriers. For instance, Masood et al. [60] reviewed the current implications of encapsulation of anticancer agents within PHAs, PLGA, and cyclodextrin-based nanoparticles to precisely target the tumor site. The recent scientific developments in the preparation of functionalized PHAs, PHA-drug and PHA-protein conjugates, multifunctional PHA nanoparticles, and micelles as well as biosynthetic PHA particles for drug delivery were reviewed by Michalak et al. [61]. The recent advances of using PHA-based nano-vehicles as therapeutic delivery carriers were summarized by Li and Loh [59]. Pramual et al. [62] developed and investigated nanoparticles of PHAs as carriers of a hydrophobic photosensitizer for photodynamic therapy. Besides these reviews, a patent has been published on the fabrication of a delivery system comprising *scl*-PHA nanoparticles having an anticancer drug encapsulated for oral administration [63]. Also, a similar study on the production of PHB and PHB/poly(ethylene glycol) (PEG)-based microparticles loaded with antitumor drugs by the spray-drying technique was recently published [64]. Apart from these, there are not many more new studies in which PHAs spherical shape structures are considered for drug delivery.

Manero's group has been working in the exploitation of PHAs in biomedicine, and they have recently published some studies focused on the application of PHAs as therapeutic delivery carriers. They produced antibiotic (doxycycline)-loaded micro- and nano-particles of PHB with different methodologies [65]. The produced carriers were capable of diffusing the active principle from the material to the media, creating a bacteria-free protective region. Later, new strategies for combining the antibacterial properties of doxycycline-loaded PHB micro- and nano-spheres on titanium (Ti) were developed to obtain implant surfaces with antibacterial activity [66]. Furthermore, they studied a novel approach to benefit the synergistic effects of antifouling PEG together with doxycycline-loaded PHB spheres (Figure 3a,b).

The use of PHAs for delivery systems has been studied with different structures. For instance, Lee et al. [67] developed a system of drug-containing PHA fibers that can be electrospun directly onto a metal stent in order to form a biocompatible coating (Figure 3c). PHAs have been used as matrixes to construct release formulations of antibiotic delivery, providing them with antimicrobial, antifungal, anti-biofilm, anti-inflammatory and virucidal properties dependent on the conjugated/enclosed therapeutic agent. Manero's group has exploited PHAs matrixes as coatings with an antibacterial delivery effect [68–70]. Aiming to obtain antimicrobial surfaces to prevent implant infections, they studied different strategies for developing antibacterial coatings on Ti and Tantalum (Ta). The surface of the biometals was coated with different PHAs (PHB, PHBV, and PHB4HB) using a dip-coating technique. Water-in-oil PHAs emulsions with the bioactive agents were produced to use them as coating fluids. The systems designed for drug delivery not only proved to assure the elimination of the first stage of bacterial biofilm formation (bacterial adhesion), but also their proliferation, since the biopolymer coating with antibiotic was able to degrade with time under physiological conditions, thus guaranteeing a controlled drug release over time (Figure 3d).

Complex systems for drug delivery, such as the one published by Timin et al. [71], have also been developed. In this example, the authors deposited polymer and hybrid microcapsules, which were used as drug carriers, onto polymer microfiber scaffolds of PCL, PHB, and PHB doped with the conductive

polyaniline (PANi). The immobilization of the microcapsules (loaded with bioactive molecules) onto the scaffold surfaces enabled multimodal triggering by physical and biological stimuli, providing the controllable release of the drug from the scaffolds. PHB and PHB-PANi scaffolds promoted the adhesion of mesenchymal stem cells compared to that of the PCL scaffolds. With this methodology, they provided a way to incorporate bioactive compounds onto polymer scaffolds, which makes these multimodal materials suitable for personalized drug therapy and bone tissue engineering.

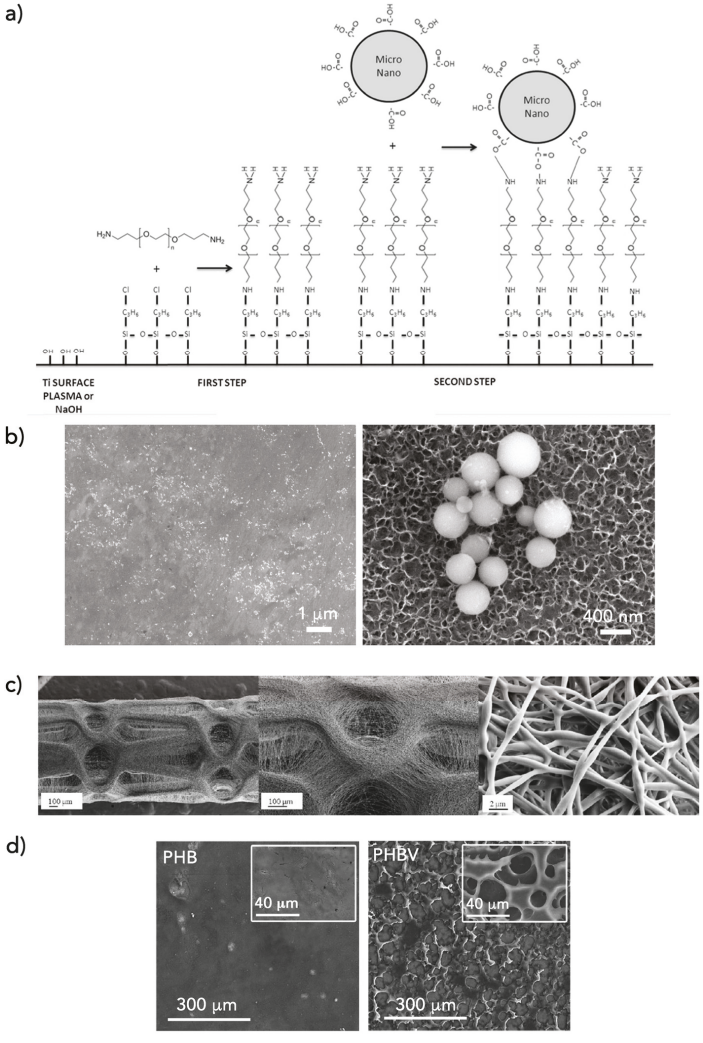

Figure 3. PHAs as drug delivery systems. (**a**) Scheme of the chemical reaction for adhesion of PHB micro- and nano-spheres on Ti surfaces: activation of the Ti surfaces (by plasma or NaOH treatment), silanization with the alkoxysilane 3-chloropropyltriethoxysilane (CPTES), covalent bounding with difunctionalized poly(ethylene glycol) (PEG), and covalent bonding with doxycycline-loaded PHB-spheres. (**b**) Field emission scanning electron microscopy micrographs of Ti surfaces with doxycycline-loaded spheres of PHB [66]. (**c**) SEM images of direct coatings of paclitaxel loaded P(3HB-co-95 mol% 4HB) nanofibers onto a metal stent (40×, 100×, and 5000×) [67]. (**d**) FESEM images at different magnifications of PHB and PHBV matrixes that totally coated Ti surfaces [69].

4. Conclusions

In the field of biomedicine, biopolymers show many advantages that make them superior to synthetic polymers, predominately because of their natural origin. PHAs represent a big family of biologically produced polymers that show common properties such as biocompatibility, biodegradability, and non-toxicity. These properties together with the ease of PHAs for tuning and adapting their mechanical properties, either by combination with other substances or by copolymerization in the biotechnological production process, make them very attractive for their application in different sectors, especially biomedicine. In the last few years, PHAs have been studied to be used in tissue engineering for hard and soft tissue replacement, and as therapeutic delivery carriers. According to the studies presented in this review and the successful results discussed, given the versatile properties that can be provided by PHAs and the need to continue improving biomedical solutions, PHAs will most likely continue to be investigated as an appealing alternative, penetrating the biomedical market in a not-too-distant future.

Funding: This review received no external funding.

Conflicts of Interest: The author declares no conflict of interest.

References

1. Rodríguez-Contreras, A. Concepts and Recent Advances on Biopolymers for Biomedical Applications: Special Mention to the PHAs Family. *Adv. Biotechnol.* **2019**, *IV*, 1–27.
2. Mavelil-Sam, R.; Pothan, L.A.; Thomas, S. Polyssacharide and Protein Bsed Aerogels: An Introductory Outlook. In *Biobased Aerogels: Polysaccharide and Protein-Based Materials*; Thomas, S., Pothan, L.A., Mavelil-Sam, R., Eds.; Royal Society of Chemistry: London, UK, 2018.
3. Won, J.-E.; El-Fiqi, A.; Jegal, S.-H.; Han, C.-M.; Lee, E.-J.; Knowles, J.C.; Kim, H.-W. Gelatin-apatite bone mimetic co-precipitates incorporated within biopolymer matrix to improve mechanical and biological properties useful for hard tissue repair. *J. Biomater. Appl.* **2013**, *28*, 1213–1225. [CrossRef] [PubMed]
4. Augustine, R. Skin bioprinting: A novel approach for creating artificial skin from synthetic and natural building blocks. *Prog. Biomater.* **2018**, *7*, 77–92. [CrossRef] [PubMed]
5. Park, H.-H.; Ko, S.-C.; Oh, G.-W.; Heo, S.-J.; Kang, D.-H.; Bae, S.-Y.; Jung, W.-K. Fabrication and characterization of phlorotannins/poly (vinyl alcohol) hydrogel for wound healing application. *J. Biomater. Sci. Polym. Ed.* **2018**, *29*, 972–983. [CrossRef] [PubMed]
6. Caddeo, S.; Mattioli-Belmonte, M.; Cassino, C.; Barbani, N.; Dicarlo, M.; Gentile, P.; Baino, F.; Sartori, S.; Vitale-Brovarone, C.; Ciardelli, G. Newly-designed collagen/polyurethane bioartificial blend as coating on bioactive glass-ceramics for bone tissue engineering applications. *Mater. Sci. Eng. C* **2019**, *96*, 218–233. [CrossRef] [PubMed]
7. Lee, S.Y. Bacterial polyhydroxyalkanoates. *Biotechnol. Bioeng.* **1996**, *49*, 1–14. [CrossRef]
8. Valappil, S.P.; Peiris, D.; Langley, G.J.; Herniman, J.M.; Boccaccini, A.R.; Bucke, C.; Roy, I. Polyhydroxyalkanoate (PHA) biosynthesis from structurally unrelated carbon sources by a newly characterized Bacillus spp. *J. Biotechnol.* **2007**, *127*, 475–487. [CrossRef] [PubMed]
9. Chen, G. *Plastics from Bacteria: Natural Functions and Applications*, *Microbiology Monographs*; Chen, G.G.-Q., Ed.; Springer: Berlin/Heidelberg, Germany, 2010; Volume 14.
10. Chen, G.-Q. A microbial polyhydroxyalkanoates (PHA) based bio- and materials industry. *Chem. Soc. Rev.* **2009**, *38*, 2434–2446. [CrossRef]
11. Koller, M. Production of Poly Hydroxyalkanoate (PHA) biopolyesters by extremophiles? *MOJ Polym. Sci.* **2017**, *1*, 69–85.
12. Sudesh, K.; Abe, H.; Doi, Y. Synthesis, structure and properties of polyhydroxyalkanoates: Biological polyesters. *Prog. Polym. Sci.* **2000**, *25*, 1503–1555. [CrossRef]
13. Yadav, P.; Yadav, H.; Shah, V.G.; Shah, G.; Dhaka, G. Biomedical Biopolymers, their Origin and Evolution in Biomedical Sciences: A Systematic Review. *J. Clin. Diagn. Res.* **2015**, *9*, ZE21–ZE25. [CrossRef] [PubMed]

14. Koller, M. Polyhydroxyalkanoate Biosynthesis at the Edge of Water Activity-Haloarchaea as Biopolyester Factories. *Bioengineering* **2019**, *6*, 34. [CrossRef] [PubMed]
15. Reddy, C.S.K.; Rashmi Ghai, R.; Kalia, V.C. Polyhydroxyalkanoates: An overview. *Bioresour. Technol.* **2003**, *87*, 137–146. [CrossRef]
16. Koller, M. Chemical and Biochemical Engineering Approaches in Manufacturing Polyhydroxyalkanoate (PHA) Biopolyesters of Tailored Structure with Focus on the Diversity of Building Blocks. *Chem. Biochem. Eng. Q.* **2019**, *32*, 413–438. [CrossRef]
17. Koller, M.; Salerno, A.; Dias, M.; Reiterer, A.; Braunegg, G. Modern Biotechnological Polymer Synthesis: A Review. *Food Technol. Biotechnol.* **2010**, *48*, 255–269.
18. Constantinides, C.; Basnett, P.; Lukasiewicz, B.; Carnicer, R.; Swider, E.; Majid, Q.A.; Srinivas, M.; Carr, C.A.; Roy, I. In Vivo Tracking and 1H/19F Magnetic Resonance Imaging of Biodegradable Polyhydroxyalkanoate/Polycaprolactone Blend Scaffolds Seeded with Labeled Cardiac Stem Cells. *ACS Appl. Mater. Interfaces* **2018**, *10*, 25056–25068. [CrossRef]
19. Fei, T.; Cazeneuve, S.; Wen, Z.; Wu, L.; Wang, T. Effective recovery of poly-β-hydroxybutyrate (PHB) biopolymer from Cupriavidus necator using a novel and environmentally friendly solvent system. *Biotechnol. Prog.* **2016**, *32*, 678–685. [CrossRef]
20. Koller, M. Biodegradable and Biocompatible Polyhydroxy-alkanoates (PHA): Auspicious Microbial Macromolecules for Pharmaceutical and Therapeutic Applications. *Molecules* **2018**, *23*, 362. [CrossRef]
21. Köse, G.T.; Kenar, H.; Hasırcı, N.; Hasırcı, V. Macroporous poly(3-hydroxybutyrate-co-3-hydroxyvalerate) matrices for bone tissue engineering. *Biomaterials* **2003**, *24*, 1949–1958. [CrossRef]
22. Grigore, M.E.; Grigorescu, R.M.; Iancu, L.; Ion, R.-M.; Zaharia, C.; Andrei, E.R. Methods of synthesis, properties and biomedical applications of polyhydroxyalkanoates: A review. *J. Biomater. Sci. Polym. Ed.* **2019**, *30*, 695–712. [CrossRef]
23. Berezina, N. Enhancing the 3-hydroxyvalerate component in bioplastic PHBV production by Cupriavidus necator. *Biotechnol. J.* **2012**, *7*, 304–309. [CrossRef] [PubMed]
24. Rahayu, A.; Zaleha, Z.; Yahya, A.R.M.; Majid, M.I.A.; Amirul, A.A. Production of copolymer poly(3-hydroxybutyrate-co-4-hydroxybutyrate) through a one-step cultivation process. *World J. Microbiol. Biotechnol.* **2008**, *24*, 2403–2409. [CrossRef]
25. Shijun, X.; Junsheng, M.; Jianqun, Z.; Ping, B. In vitro three-dimensional coculturing poly3-hydroxybutyrate-co-3-hydroxyhexanoate with mouse-induced pluripotent stem cells for myocardial patch application. *J. Biomater. Appl.* **2016**, *30*, 1273–1282. [CrossRef] [PubMed]
26. Zheng, Y.; Chen, J.-C.; Ma, Y.-M.; Chen, G.-Q. Engineering biosynthesis of polyhydroxyalkanoates (PHA) for diversity and cost reduction. *Metab. Eng.* **2019**. [CrossRef] [PubMed]
27. Brigham, C.J.; Riedel, S.L. The Potential of Polyhydroxyalkanoate Production from Food Wastes. *Appl. Food Biotechnol.* **2019**, *6*. [CrossRef]
28. Rodriguez-Contreras, A.; Koller, M.; Miguel, M.-d.S.D.; Calafell, M.; Braunegg, G.; Marqués-Calvo, M.S. Novel Poly[(R)-3-hydroxybutyrate]-producing bacterium isolated from a Bolivian hypersaline lake. *Food Technol. Biotechnol.* **2013**, *51*, 123–130.
29. Akaraonye, E.; Keshavarz, T.; Roy, I. Production of polyhydroxyalkanoates: The future green materials of choice. *J. Chem. Technol. Biotechnol.* **2010**, *85*, 732–743. [CrossRef]
30. Waghmare, V.S.; Wadke, P.R.; Dyawanapelly, S.; Deshpande, A.; Jain, R.; Dandekar, P. Starch based nanofibrous scaffolds for wound healing applications. *Bioact. Mater.* **2018**, *3*, 255–266. [CrossRef] [PubMed]
31. Findrik Balogová, A.; Hudák, R.; Tóth, T.; Schnitzer, M.; Feranc, J.; Bakoš, D.; Živčák, J. Determination of geometrical and viscoelastic properties of PLA/PHB samples made by additive manufacturing for urethral substitution. *J. Biotechnol.* **2018**, *284*, 123–130. [CrossRef] [PubMed]
32. Lizarraga-Valderrama, L.R.; Taylor, C.S.; Claeyssens, F.; Haycock, J.W.; Knowles, J.C.; Roy, I. Unidirectional neuronal cell growth and differentiation on aligned polyhydroxyalkanoate blend microfibres with varying diameters. *J. Tissue Eng. Regen. Med.* **2019**. [CrossRef] [PubMed]

33. Butt, F.I.; Muhammad, N.; Hamid, A.; Moniruzzaman, M.; Sharif, F. Recent progress in the utilization of biosynthesized polyhydroxyalkanoates for biomedical applications—Review. *Int. J. Biol. Macromol.* **2018**, *120*, 1294–1305. [CrossRef] [PubMed]
34. Singh, A.K.; Srivastava, J.K.; Chandel, A.K.; Sharma, L.; Mallick, N.; Singh, S.P. Biomedical applications of microbially engineered polyhydroxyalkanoates: An insight into recent advances, bottlenecks, and solutions. *Appl. Microbiol. Biotechnol.* **2019**, *103*, 2007–2032. [CrossRef] [PubMed]
35. Kai, G.; Martin, D.P. Chapter 7: Poly-4-hydroxybutyrate (P4HB) in Biomedical Applications and Tissue Engineering. In *Biodegradable Polymers, Volume 2: New Biomaterials Advancement and Challenges*; Chu, C.-C., Ed.; Nova Sience: Hauppauge, NY, USA, 2015; pp. 199–231.
36. Degli Esposti, M.; Chiellini, F.; Bondioli, F.; Morselli, D.; Fabbri, P. Highly porous PHB-based bioactive scaffolds for bone tissue engineering by in situ synthesis of hydroxyapatite. *Mater. Sci. Eng. C* **2019**, *100*, 286–296. [CrossRef] [PubMed]
37. Chernozem, R.V.; Surmeneva, M.A.; Shkarina, S.N.; Loza, K.; Epple, M.; Ulbricht, M.; Cecilia, A.; Krause, B.; Baumbach, T.; Abalymov, A.A.; et al. Piezoelectric 3-D Fibrous Poly(3-hydroxybutyrate)-Based Scaffolds Ultrasound-Mineralized with Calcium Carbonate for Bone Tissue Engineering: Inorganic Phase Formation, Osteoblast Cell Adhesion, and Proliferation. *ACS Appl. Mater. Interfaces* **2019**, *11*, 19522–19533. [CrossRef] [PubMed]
38. Meischel, M.; Eichler, J.; Martinelli, E.; Karr, U.; Weigel, J.; Schmöller, G.; Tschegg, E.K.; Fischerauer, S.; Weinberg, A.M.; Stanzl-Tschegg, S.E. Adhesive strength of bone-implant interfaces and in-vivo degradation of PHB composites for load-bearing applications. *J. Mech. Behav. Biomed. Mater.* **2016**, *53*, 104–118. [CrossRef] [PubMed]
39. Sadat-Shojai, M.; Khorasani, M.-T.; Jamshidi, A. A new strategy for fabrication of bone scaffolds using electrospun nano-HAp/PHB fibers and protein hydrogels. *Chem. Eng. J.* **2016**, *289*, 38–47. [CrossRef]
40. Ding, Y.; Li, W.; Müller, T.; Schubert, D.W.; Boccaccini, A.R.; Yao, Q.; Roether, J.A. Electrospun Polyhydroxybutyrate/Poly(ε-caprolactone)/58S Sol–Gel Bioactive Glass Hybrid Scaffolds with Highly Improved Osteogenic Potential for Bone Tissue Engineering. *ACS Appl. Mater. Interfaces* **2016**, *8*, 17098–17108. [CrossRef]
41. Ching, K.Y.; Andriotis, O.G.; Li, S.; Basnett, P.; Su, B.; Roy, I.; Tare, R.S.; Sengers, B.G.; Stolz, M. Nanofibrous poly(3-hydroxybutyrate)/poly(3-hydroxyoctanoate) scaffolds provide a functional microenvironment for cartilage repair. *J. Biomater. Appl.* **2016**, *31*, 77–91. [CrossRef]
42. Toloue, E.B.; Karbasi, S.; Salehi, H.; Rafienia, M. Evaluation of Mechanical Properties and Cell Viability of Poly (3-Hydroxybutyrate)-Chitosan/Al(2)O(3) Nanocomposite Scaffold for Cartilage Tissue Engineering. *J. Med. Signals Sens.* **2019**, *9*, 111–116. [CrossRef]
43. Bagdadi, A.V.; Safari, M.; Dubey, P.; Basnett, P.; Sofokleous, P.; Humphrey, E.; Locke, I.; Edirisinghe, M.; Terracciano, C.; Boccaccini, A.R.; et al. Poly(3-hydroxyoctanoate), a promising new material for cardiac tissue engineering. *J. Tissue Eng. Regen. Med.* **2018**, *12*, e495–e512. [CrossRef]
44. Ma, Y.-X.; Mu, J.-S.; Zhang, J.-Q.; Bo, P. Myocardial Patch Formation by Three-Dimensional 3-Hydroxybutyrate-co-4-Hydroxybutyrate Cultured with Mouse Embryonic Stem Cells. *J. Biomater. Tissue Eng.* **2016**, *6*, 629–634. [CrossRef]
45. Xue, Y.; Sant, V.; Phillippi, J.; Sant, S. Biodegradable and biomimetic elastomeric scaffolds for tissue-engineered heart valves. *Acta Biomater.* **2017**, *48*, 2–19. [CrossRef]
46. Chen, Q.; Liang, S.; Thouas, G.A. Elastomeric biomaterials for tissue engineering. *Prog. Polym. Sci.* **2013**, *38*, 584–671. [CrossRef]
47. Shishatskaya, E.I.; Nikolaeva, E.D.; Vinogradova, O.N.; Volova, T.G. Experimental wound dressings of degradable PHA for skin defect repair. *J. Mater. Sci. Mater. Med.* **2016**, *27*, 165. [CrossRef] [PubMed]
48. Sezer, A.D.; Cevher, E. Biopolymers as Wound Healing Materials: Challenges and New Strategies. In *Biomaterials Applications for Nanomedicine*; Rosario, P., Ed.; IntechOpen Limited: London, UK, 2011; pp. 383–414.
49. Marcano, A.; Bou Haidar, N.; Marais, S.; Valleton, J.-M.; Duncan, A.C. Designing Biodegradable PHA-Based 3D Scaffolds with Antibiofilm Properties for Wound Dressings: Optimization of the Microstructure/Nanostructure. *ACS Biomater. Sci. Eng.* **2017**, *3*, 3654–3661. [CrossRef]

50. Li, P.; Zhang, J.; Liu, J.; Ma, H.; Liu, J.; Lie, P.; Wang, Y.; Liu, G.; Zeng, H.; Li, Z.; et al. Promoting the recovery of injured liver with poly (3-hydroxybutyrate-co-3-hydroxyvalerate-co-3-hydroxyhexanoate) scaffolds loaded with umbilical cord-derived mesenchymal stem cells. *Tissue Eng Part A* **2015**, *21*, 603–615. [CrossRef] [PubMed]
51. Su, Z.; Li, P.; Wu, B.; Ma, H.; Wang, Y.; Liu, G.; Zeng, H.; Li, Z.; Wei, X. PHBVHHx scaffolds loaded with umbilical cord-derived mesenchymal stem cells or hepatocyte-like cells differentiated from these cells for liver tissue engineering. *Mater. Sci. Eng. C* **2014**, *45*, 374–382. [CrossRef]
52. Tashjian, R.; Kolz, C.; Suter, T.; Henninger, H. Biomechanics of Polyhydroxyalkanoate Mesh-Augmented Single-Row Rotator Cuff Repairs. *Am. J. Orthop.* **2016**, *45*, E527–E533.
53. Yutaka, T.; Buenaventurada, C. Degradation of Microbial Polyesters. *Biotechnol. Lett.* **2004**, *26*, 1181–1189.
54. Rodríguez-Contreras, A.; Calafell-Monfort, M.; Marqués-Calvo, M.S. Enzymatic degradation of poly(3-hydroxybutyrate) by a commercial lipase. *Polym. Degrad. Stab.* **2012**, *97*, 2473–2476. [CrossRef]
55. Rodríguez-Contreras, A.; Calafell-Monfort, M.; Marqués-Calvo, M.S. Enzymatic degradation of poly(3-hydroxybutyrate-co-4-hydroxybutyrate) by commercial lipases. *Polym. Degrad. Stab.* **2012**, *97*, 597–604. [CrossRef]
56. Misra, S.K.; Valappil, S.P.; Roy, I.; Boccaccini, A.R. Polyhydroxyalkanoate (PHA)/Inorganic Phase Composites for Tissue Engineering Applications. *Biomacromolecules* **2006**, *7*, 2249–2258. [CrossRef]
57. Gil-Castell, O.; Badia, J.D.; Bou, J.; Ribes-Greus, A. Performance of Polyester-Based Electrospun Scaffolds under In Vitro Hydrolytic Conditions: From Short-Term to Long-Term Applications. *Nanomaterials* **2019**, *9*, 786. [CrossRef]
58. Errico, C.; Bartoli, C.; Chiellini, F.; Chiellini, E. Poly(hydroxyalkanoates)-Based Polymeric Nanoparticles for Drug Delivery. *J. Biomed. Biotechnol.* **2009**, *2009*, 10. [CrossRef]
59. Li, Z.; Loh, X.J. Recent advances of using polyhydroxyalkanoate-based nanovehicles as therapeutic delivery carriers. *Nanomed. Nanobiotechnology* **2017**, *9*, e1429. [CrossRef]
60. Masood, F. Polymeric nanoparticles for targeted drug delivery system for cancer therapy. *Mater. Sci. Eng. C* **2016**, *60*, 569–578. [CrossRef]
61. Michalak, M.; Kurcok, P.; Hakkarainen, M. Polyhydroxyalkanoate-based drug delivery systems. *Polym. Int.* **2017**, *66*, 617–622. [CrossRef]
62. Pramual, S.; Assavanig, A.; Bergkvist, M.; Batt, C.A.; Sunintaboon, P.; Lirdprapamongkol, K.; Svasti, J.; Niamsiri, N. Development and characterization of bio-derived polyhydroxyalkanoate nanoparticles as a delivery system for hydrophobic photodynamic therapy agents. *J. Mater. Sci. Mater. Med.* **2016**, *27*, 40. [CrossRef]
63. Masood, F.; Chen, P.; Yasin, T.; Hameed, A. Novel Delivery System for Anticancer Drug Based on Short-Chain-Length Polyhydroxyalkanoate Nanoparticles. U.S. Patent US2015/0118293A1, 30 April 2015.
64. Murueva, A.V.; Shershneva, A.M.; Abanina, K.V.; Prudnikova, S.V.; Shishatskaya, E.I. Development and characterization of ceftriaxone-loaded P3HB-based microparticles for drug delivery. *Dry. Technol.* **2019**, *37*, 1131–1142. [CrossRef]
65. Rodríguez-Contreras, A.; Canal, C.; Calafell-Monfort, M.; Ginebra, M.-P.; Julio-Moran, G.; Marqués-Calvo, M.-S. Methods for the preparation of doxycycline-loaded phb micro- and nano-spheres. *Eur. Polym. J.* **2013**, *49*, 3501–3511. [CrossRef]
66. Rodríguez-Contreras, A.; Marqués-Calvo, M.S.; Gil, F.J.; Manero, J.M. Modification of titanium surfaces by adding antibiotic-loaded PHB spheres and PEG for biomedical applications. *J. Mater. Sci. Mater. Med.* **2016**, *27*, 124. [CrossRef]
67. Lee, Y.-F.; Sridewi, N.; Ramanathan, S.; Sudesh, K. The Influence of Electrospinning Parameters and Drug Loading on Polyhydroxyalkanoate (PHA) Nanofibers for Drug Delivery. *Int. J. Biotechnol. Wellness Ind.* **2015**, *4*, 103–113.
68. Rodríguez-Contreras, A.; Rupérez, E.; Marqués-Calvo, M.S.; Manero, J.M. Chapter 7—PHAs as matrices for drug delivery. In *Materials for Biomedical Engineering*; Holban, A.-M., Grumezescu, A.M., Eds.; Elsevier: Amsterdam, The Netherlands, 2019; pp. 183–213.
69. Rodríguez-Contreras, A.; García, Y.; Manero, J.M.; Rupérez, E. Antibacterial PHAs coating for titanium implants. *Eur. Polym. J.* **2017**, *90*, 66–78. [CrossRef]

70. Rodríguez-Contreras, A.; Guillem-Marti, J.; Lopez, O.; Manero, J.M.; Ruperez, E. Antimicrobial PHAs coatings for solid and porous Tantalum implants. *Colloids Surf. B Biointerfaces* **2019**, *182*, 110317. [CrossRef]
71. Timin, A.S.; Muslimov, A.R.; Zyuzin, M.V.; Peltek, O.O.; Karpov, T.E.; Sergeev, I.S.; Dotsenko, A.I.; Goncharenko, A.A.; Yolshin, N.D.; Sinelnik, A.; et al. Multifunctional Scaffolds with Improved Antimicrobial Properties and Osteogenicity Based on Piezoelectric Electrospun Fibers Decorated with Bioactive Composite Microcapsules. *ACS Appl. Mater. Interfaces* **2018**, *10*, 34849–34868. [CrossRef]

bioengineering

MDPI

Review

Biomedical Processing of Polyhydroxyalkanoates

Dario Puppi *, Gianni Pecorini and Federica Chiellini *

Department of Chemistry and Industrial Chemistry, University of Pisa, UdR INSTM – Pisa, Via G. Moruzzi 13, 56124 Pisa, Italy; gianni.pecorini21@gmail.com

* Correspondence: dario.puppi@unipi.it (D.P.); federica.chiellini@unipi.it (F.C.)

Received: 30 October 2019; Accepted: 25 November 2019; Published: 29 November 2019

Abstract: The rapidly growing interest on polyhydroxyalkanoates (PHA) processing for biomedical purposes is justified by the unique combinations of characteristics of this class of polymers in terms of biocompatibility, biodegradability, processing properties, and mechanical behavior, as well as by their great potential for sustainable production. This article aims at overviewing the most exploited processing approaches employed in the biomedical area to fabricate devices and other medical products based on PHA for experimental and commercial applications. For this purpose, physical and processing properties of PHA are discussed in relationship to the requirements of conventionally-employed processing techniques (e.g., solvent casting and melt-spinning), as well as more advanced fabrication approaches (i.e., electrospinning and additive manufacturing). Key scientific investigations published in literature regarding different aspects involved in the processing of PHA homo- and copolymers, such as poly(3-hydroxybutyrate), poly(3-hydroxybutyrate-*co*-3-hydroxyvalerate), and poly(3-hydroxybutyrate-*co*-3-hydroxyhexanoate), are critically reviewed.

Keywords: polyhydroxyalkanoates processing; electrospinning; additive manufacturing; selective laser sintering; fused deposition modeling; computer-aided wet-spinning

1. Introduction

The always increasing interest on polyhydroxyalkanoates (PHA) for biomedical applications stems from their well-ascertained biocompatibility and biodegradability in physiological environments [1]. In addition, their microbial synthesis by means of sustainable processes with potential for large-scale industrial production [2], together with a better processing versatility and superior mechanical properties in comparison with other polymers from natural resources, make PHA unique polymer candidates for advanced research and development approaches.

From a chemical point of view, PHA are aliphatic polyesters with a variable number of carbon atoms in the monomeric unit (Figure 1). They are generally classified as short-chain length (SCL)-PHA when they consist of monomers C3-C5 in length, and medium-chain length (MCL)-PHA when they consist of monomers C6–C14 in length [3]. SCL-PHA consist of monomeric units of 3-hydroxybutyrate (3HB), 4-hydroxybutyrate (4HB), or 3-hydroxyvalerate (HV). MCL-PHA consist of monomeric units of 3-hydroxyhexanoate (HHx), 3-hydroxyoctanoate (HO), 3-hydroxydecanoate (HD), 3-hydroxydodecanoate (HDD), 3-hydroxytetradecanoate (HTD), or even longer-chain comonomer units [4]. In general, SCL-PHA have high crystallinity degree and behave as a stiff and brittle material, while MCL-PHA have reduced crystallinity and increased flexibility showing elastomeric properties. The length of the pendant groups of the monomer units plays a key role in the resulting polymer physical properties, so that SCL-PHA copolymers with ethyl side groups can show elongation at break values varying in the range 5–50% depending in comonomers units ratio [5]. In addition, copolymers consisting of both SCL- and MCL-subunits can have properties between those of the two states. While

most bacteria accumulate PHA granules of only one type, i.e., SCL or MCL, bacteria accumulating SCL-MCL-PHA copolymers were also isolated [6].

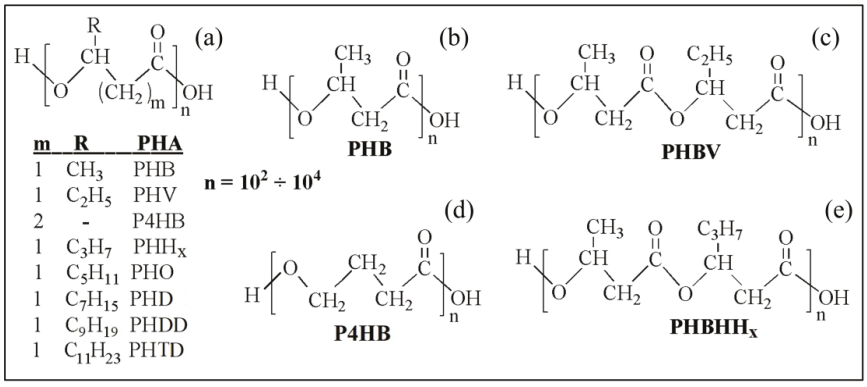

Figure 1. (**a**) General chemical structure of polyhydroxyalkanoates (PHA); chemical structure of (**b**) poly(3-hydroxybutyrate) (PHB), (**c**) poly(3-hydroxybutyrate-*co*-3-hydroxyvalerate) (PHBV), (**d**) poly(4-hydroxybutyrate) (P4HB), and (**e**) poly(3-hydroxybuyrate-*co*-3-hydroxyexanoate) (PHBHHx).

Poly(3-hydroxybutyrate) (PHB), which was the first discovered PHA in the 1920s [7], together with its copolymers poly(3-hydroxybutyrate-*co*-3-hydroxyvalerate) (PHBV), represent the most investigated microbial polyesters in the biomedical area thanks to the thermoplastic behavior, mechanical properties suitable for load-bearing applications, and versatile synthesis methods [8,9]. Novel microbial synthesis procedures have allowed the biomedical investigation of PHA with a wide range of molecular structures, in terms of molecular weight, length of alkyl side group, and ratio of comonomer units, as a means to develop materials with physical properties tailored to specific applications [10,11]. A widely investigated example in this context is represented by poly(3-hydroxybuyrate-*co*-3-hydroxyexanoate) (PHBHHx), which shows tunable elasticity by varying HHx percentage, exploitable for different applications, such as engineering tissues with much different stiffness (e.g., bone, cartilage, nerve, and blood vessel) [12]. Thanks to its low crystallinity, poly(4-hydroxybutyrate) (P4HB) has higher flexibility, ductility, and processing properties in comparison to PHB, which have been exploited to develop biomedical devices for soft tissue repair [13]. P4HB products currently on the clinical market include, among others, GalaFLEX®, a surgical mesh of knitted fibers [14], TephaFLEX®sutures, meshes, tubes, and thin films [15], MonoMax®sutures [16], Phantom Fiber™ sutures and BioFiber®Surgical Mesh [17].

PHA versatility in terms of processing approaches and conditions has allowed the investigation and application of a wide range of fabrication techniques relevant to biomedical research and industrial application. As it will be discussed in detail in the following sections, techniques based on different working principles have been successfully employed to process PHA, either in the form of a melt or a solution, and shape them at different scale length levels. Techniques with an old industrial history, such as melt spinning and blow extrusion, are currently employed to produce implantable medical devices made from PHA that are available on the market. Other approaches industrially employed in the case of commodity use polymers, such as solvent casting and injection molding, or under development for porous polymer structures fabrication, such as freeze drying and phase separation methods, have been also optimized for PHA processing. In this context, this review article is aimed at summarizing PHA processing properties in relationship to the requirements of the different techniques developed so far for their processing, as well as at critically overviewing key literature on this topic. Emphasis is dedicated to cutting edge advancement reported in literature on electrospinning and additive manufacturing application to PHA processing.

2. Physical and Processing Properties of PHA

As previously mentioned, the side group length significantly affects PHA crystallinity, mechanical behavior, as well as processing properties. PHB has a glass transition temperature (T_g) ~0 °C, melting temperature (T_m) ~180 °C, crystallinity degree in the range 60–80%, and degradation temperature (T_{deg}) ~220 °C. The narrow window between T_m and T_{deg}, typically requires the use of plasticizers for PHB melt processing in order to prevent polymer decomposition, which can occur at temperatures above 150 °C, as well as to enhance melt strength and elasticity [13,18]. By increasing the molar percentage of HV in copolymers, T_m can be decreased down to 130 °C and crystallinity to 35%, without marked effect on T_g and T_{deg}, thus widening processing temperature window and enhancing melt processability. Analogously, in the case of PHBHHx, T_m can be decreased down to 54 °C and crystallinity to 15%. Values of Young modulus and elongation at break reported in literature for PHBV (0.5–3.5 GPa, 5–50%) and PHBHHx (0.1–0.5 GPa, 5–850%) are generally different than those reported for PHB (0.9–4.0 GPa, 5–20%). As a consequence of the absence of alkyl side groups along the macromolecular chain, P4HB has much lower T_g, (~ −50°C), T_m (55–70 °C), and crystallinity (<40%) than PHB, resulting in enhanced melt processability, lower stiffness, and much larger elongation at break. These differences justify the successful application of different melt processing techniques for the fabrication of biomedical products currently available on the market, as discussed in the next section. Copolymers of 3HB and 4HB monomeric units, poly(3-hydroxybutyrate-*co*-4-hydroxybutyrate) (P3HB-*co*-4HB), show thermal and morphological parameters, as well as mechanical and processing properties, in between those of the two relevant homopolymers [19].

SCL-PHA are soluble only in a few organic solvents, including chloroform, dichloromethane, dimethyl formamide, tetrahydrofuran, and dioxane. In addition, their solubilization can require high temperatures or sonication to form a homogeneous solution at concentrations suitable for processing techniques commonly used in the biomedical field (e.g., solvent casting, phase separation, and electrospinning) [20]. This aspect is particularly significant in the case of PHB often resulting in suspensions rather than homogeneous solutions when mixed with organic solvents.

The theoretical and practical aspects of the most exploited processing techniques in the biomedical field, as well as of advanced fabrication approaches based on electrospinning [21] and additive manufacturing [22], are overviewed in the following section. Schematic representations of various techniques commonly employed for PHA biomedical processing are reported in Figure 2. They include techniques to fabricate 3D molded objects (e.g., injection molding), films (e.g., blow extrusion), continuous fibers (e.g., wet-spinning), nanoparticles (e.g., double emulsion), as well as a number of processing approaches to obtain a porous structure. The latter are due to a widespread interest raised within the scientific and clinical communities for the development of biodegradable scaffolds with a porous architecture tailored to tissue regeneration strategies.

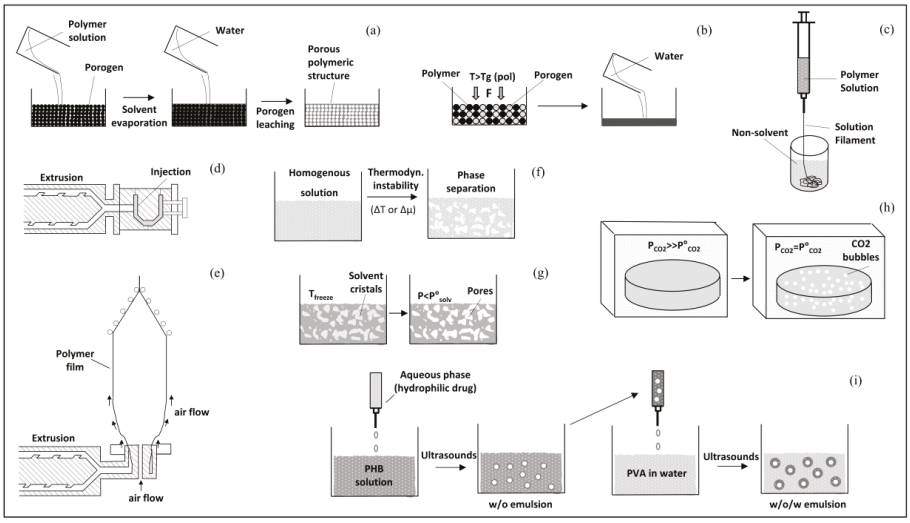

Figure 2. Schematic representation of techniques commonly employed for PHA processing in the biomedical area (modified from [23]). (**a**) Solvent casting-particle leaching process: a polymer solution is cast into a mold filled with porogen particles, the solvent is allowed to evaporate and the porogen is finally water-leached out; (**b**) melt molding-particulate leaching: a powder mixture of polymer and porogen is placed in a mold and heated above the polymer T_g while a pressure (F) is applied, the porogen is then water-leached out; (**c**) representative fiber spinning technique, i.e., wet-spinning: a polymeric solution is extruded directly into a coagulation bath leading to the formation of a continuous polymer fiber by non-solvent-induced phase inversion; (**d**) injection molding: a polymeric material is melt-extruded and injected into a mold; (**e**) film extrusion: a polymeric material is melt-extruded in the form of a tubular film by using a circular die and air pressure; (**f**) phase separation: a thermodynamic instability is established in a homogeneous polymer solution that separates into a polymer-rich and a polymer-poor phase; (**g**) freeze drying: a polymer solution is cooled down leading to the formation of solvent ice crystals, then a pressure lower than the equilibrium vapor pressure of the solvent (P_{solv}) is applied; (**h**) gas foaming: a chemical or physical blowing agent is mixed with the polymeric material, typically during extrusion (in the case depicted in figure a polymeric sample is exposed to high pressure CO_2 allowing saturation of the gas in the polymer and the subsequent gas pressure reduction causes the nucleation of CO_2 bubbles); (**i**) double emulsion for particles preparation: an aqueous phase containing a drug is added to a polymer solution, a water-in-oil (w/o) emulsion is obtained through sonication and added to a second aqueous phase, to form a w/o/w emulsion, particles are then separated by centrifugation, after organic solvent evaporation under stirring, and possibly resuspended in an aqueous phase.

3. Biomedical Processing of PHA

Given the thermoplastic behavior and solubility in organic solvents of this class of polyesters, various approaches have been investigated for processing PHA into systems with different potential biomedical applications. Representative tailored processing strategies to obtain PHA-based constructs with a morphology engineered at different scale levels are described in the following, as seen in Figure 3. A particular focus is given to electrospinning and additive manufacturing, which represents the most advanced processing approaches with great potential for biomedical industry translation. Electrospinning is the technique of election for fabricating PHA nanofibers organized into 3D assemblies with structural features mimicking those of the native tissues' extracellular matrix. This aspect together with other inherent advantages, including high surface to volume ratio of ultrafine fiber systems and processing versatility for drug-loading, make electrospinning of PHA suitable for a wide array

of biomedical applications, as discussed more in depth in Section 3.1. Moreover, combining the sustainable production potential of PHA with the high technological level of additive manufacturing, in terms of reproducibility, automation degree, and control on composition and structure at different length scales, is inspiring a growing body of current literature that can have a tremendous impact on the biomedical industry.

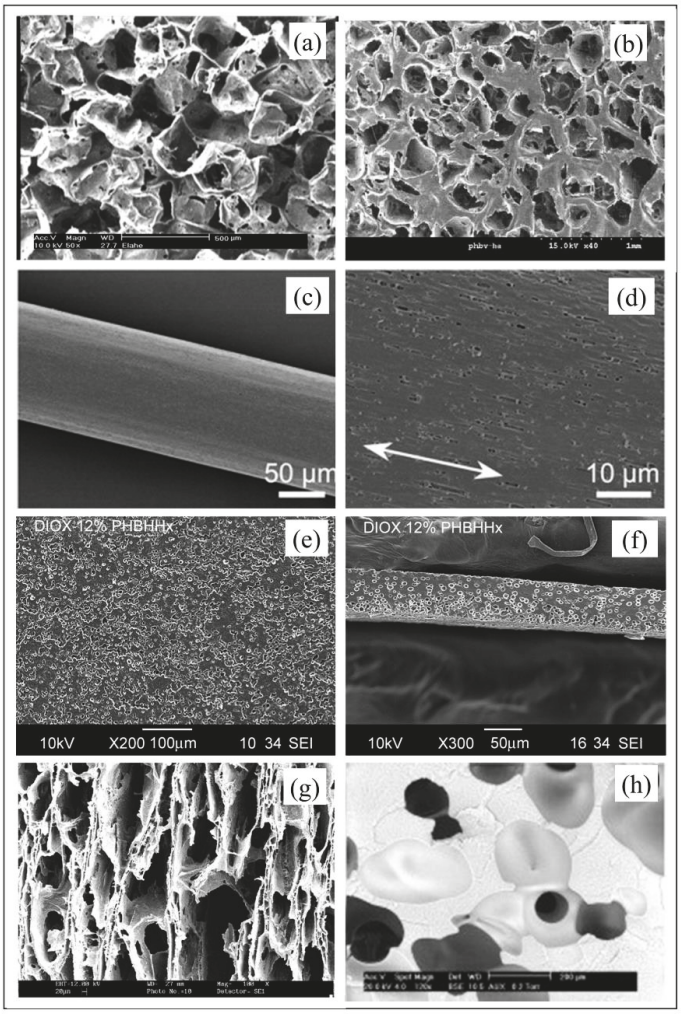

Figure 3. Scanning electron microscopy (SEM) analysis of PHA morphology after processing: (**a**) PHB porous structure by solvent casting/particulate leaching (scale bar 500 µm; reproduced from [24]); (**b**) PHBV/hydroxyapatite (HA) porous structure by melt molding/particulate leaching (scale bar 1 mm; reproduced from [25]); (**c**) low and (**d**) high magnification analysis of PHBV fiber fabricated by melt-spinning, and subjected to isothermal crystallization and 10 times one-step-drawing at room temperature (reproduced from [26]); (**e**) top view and (**f**) cross-section of PHBHHx film prepared by phase inversion of a 1,4 dioxane solution through immersion in water (reproduced from [27]); (**g**) PHBV scaffold by means of emulsion freezing/freeze drying technique (scale bar 20 µm; reproduced from [28]); (**h**) PHBV porous morphology obtained by gas foaming (scale bar 200 µm; reproduced from [29]).

Solvent casting represents one of the most straightforward approaches to process PHA into two-dimensional (2D) membranes. For instance, Basnett et al. [24] developed films based on poly(3-hydroxyoctanoate) (PHO) blended with PHB by dissolving the two polymers in chloroform at different weight ratios (80:20, 50:50 or 20:80) for a total concentration of 5% wt. The solutions were mixed by sonication, cast into a glass petri dish, and then air dried for one week to obtain films of 180–220 μm thickness. Drying in an atmosphere saturated with the solvent is often employed to achieve slow solvent evaporation and avoid internal stress formation. Combination of solvent casting with salt leaching is an effective means to obtain a PHA porous structure. As an example, Masaeli et al. [30] added NaCl particles (200–250 μm) to chloroform solutions of PHB and, after solvent evaporation and vacuum drying, submitted the solid to extensive water washing for five days. The resulting salt-leached membranes have a thickness of around 500 μm and a porosity of around 90% (Figure 3a). Advantages of this processing approach is the ease of fabrication, the possibility to vary the pore's size over a large range, as well as to control pore size and porosity independently. The main limitation is that only small thicknesses can be achieved due to difficulty in removing salt particles along thick sections. In addition, membrane shape is given by the mold, and obtaining customized geometries requires designing and fabricating ad-hoc molds.

Melt molding can be alternatively employed to fabricate thin PHA membranes, possibly in combination with salt leaching for developing porous architectures. After filling a mold with polymer and porogen particles, the system is heated above polymer T_g, while applying pressure to the powder. Once the polymer particles are fused together, the mold is removed and the porogen is leached out. As an example, PHBV/hydroxyapatite (HA) powder (9:1 w/w) was mixed with NaCl particles (100~300 μm) at a 1:17 weight ratio and then cast in a mold at 180 °C [25]. After leaching out salt particles, through water washing, and drying it under a vacuum, PHBV scaffolds exhibited an interconnected, porous network with pore sizes ranging from several microns to around 400 μm (Figure 3b). This processing approach holds some advantages and disadvantages of solvent casting-based techniques, such as the independent control of pore shape and porosity, the ease of fabrication, the limited design freedom in terms of membrane shape and thickness. Moreover, while it avoids the use of organic solvents that can be harmful for biological systems, it requires high temperature processing with the related risks of thermal degradation and energy costs.

Fiber spinning techniques, i.e., melt-, dry-, and wet-spinning, were recently investigated to process PHBV into single fibers or tridimensional (3D) fibrous macroporous scaffolds. They involve the extrusion of a polymer as a melt, in the case of melt-spinning, or dissolved in a solvent and then extruded in air or directly into a coagulation bath, in the case of dry- or wet-spinning, respectively. Depending on the technique employed, the final applications, and other product requirements, the fibers are submitted to different post-processing treatments (e.g., drying, washing, and drawing) or assembled into 3D fibrous systems. In the case of melt spinning, different methods have been investigated to overcome PHA processing shortcomings, such as adhesion, high brittleness, and low melt strength, related to slow crystallization rate, large spherulite size, and secondary crystallization [31]. Blending with organic or inorganic particles acting as nucleating agents, graft copolymerization, or fiber stretching are effective means to control and optimize the crystal structure and crystallization behavior of PHBV. For instance, PHBV fibers with around 1 GPa tensile strength were prepared by quenching during melt spinning, followed by isothermal crystallization near the T_g, and one-step-drawing at room temperature (Figure 3c) [26]. As previously mentioned, melt spinning is commercially employed for producing monofilaments or multifilaments made of P4HB (T_m ~60 °C) that are used as sutures or further processed using conventional textile processes, such as braiding, knitting, and weaving, to produce scaffolds and surgical meshes [14,15]. In particular, P4HB monofilament sutures show superior tensile strength characteristics than polydioxanone and polypropylene sutures. Wet-spinning technique has been investigated to overcome the aforementioned shortcomings related to thermal processing of PHA. For instance, Alagoz et al. [32] extruded a chloroform solution of PHBV into a coagulation bath of methanol. The fibers produced were kept in methanol overnight at −4 °C for

solidification, then placed into a cylindrical Teflon mold, and dried in a vacuum oven. The resulting scaffolds had a diameter of 4 mm, height of 2 mm, interconnected porosity of 75%, average fiber diameter of 90 μm, and pore size of 250 μm.

Injection molding and film extrusion are also used to process PHA into 2D or 3D objects with potential application in the biomedical industry. These techniques involve processing the polymer in a screw extruder, pumping the melt through a die. The melt is either injected in a mold, or axially drawn and radially expanded in the form of a thin-walled tube to obtain a continuous film. Injection molding can be also combined with the particulate leaching strategy, or integrated with blowing agents that are blended with the raw polymer and activated upon heating to form a porous structure [33]. A range of melt extrusion grade formulations based on PHB or PHBV blended with additives, other polymers, and/or inorganic fillers, have been developed to enhance the material toughens processability, as well as to reduce costs. They are currently available on the market for applications other than medical ones. Examples are injection molding and film blowing grade PHA formulations approved for food contact that are marketed by Telles and TianAn [34]. Although the employment of these melt processing approaches to biomedical research is limited, the trademark TephaFLEX®by Tepha Inc. includes, besides the previously cited sutures produced by melt spinning, P4HB surgical tubes and films made by injection molding and blow extrusion, respectively [15].

Phase separation approaches are widely investigated for the preparation of porous PHA systems. They generally rely on establishing a thermodynamic instability in a polymer solution, through changes of physical conditions (e.g., temperature) or chemical composition (e.g., non-solvent addition), to induce a separation into two phases at different composition. Li et al. [35] obtained a nanofibrous network through phase separation by lowering the temperature of a PHB/chloroform/dioxane ternary mixture, with the resulting formation of a gel, which was then water-washed and freeze dried. This method was suitable also for the preparation of nanofibrous systems made of PHB blended with either PHBHHx or P4HB, whose tensile modulus, strength, and elongation at break could be modulated by varying the blend composition. Similarly, Tsujimoto et al. [36] obtained a microporous PHBHHx architecture by quenching a homogeneous polymer/DMSO solution that was prepared at 85 °C. Injectable formulations based on PHA can be prepared by dissolving the polymer in an organic solvent considered as not-toxic. This strategy is based on polymer film formation upon solution injection as a consequence of solvent dilution by the aqueous body fluids. Dai et al. [27] injected in the intra-abdominal position of rats formulations of PHBHHx dissolved in different solvents, i.e., N-methyl pyrrolidone, dimethylacetamide, 1,4-dioxane, dimethyl sulfoxide, and 1,4-butanolide. In particular, they found that PHBHHx films with a porous structure were formed when the solution came into contact with aqueous fluids because of a non-solvent-induced phase inversion process (Figure 3d). The wet-spinning methods described in this article also rely on a phase separation process induced by immersion into a polymer non-solvent [37].

Freeze drying is another processing approach investigated to fabricate porous PHA systems starting from a polymeric solution. As demonstrated by Sultana and Wang [28,38,39], porous scaffolds based on PHBV alone or in blends with poly(l-lactic acid) (PLLA), possibly loaded with HA, can be fabricated through an emulsion freezing/freeze drying process. In detail, the process involves adding an acetic acid aqueous phase to a polymer solution in order to obtain an emulsion that is then frozen and lyophilized. After sublimation, solvent (e.g., chloroform) and water phase crystals leave behind an anisotropic highly porous structure (Figure 3e). In the case of composite development, HA particles are added to the water phase before emulsion formation.

Foaming of PHA can be achieved by means of the employment of physical or chemical blowing agents, typically during melt extrusion. In the case of employment of physical agents, such as supercritical CO_2, pressurized machinery with a more complex technology for gas pumping, screw extrusion, and pressure profile control is required [29]. Either exothermic (e.g., azodicarbonamide [40]) or endothermic chemical blowing agents (e.g., sodium bicarbonate and citric acid [41]) can be employed, the first ones releasing N_2, the others releasing CO_2. Epoxy-functionalized

chain extenders and post-extrusion water-quenching have been proposed as effective means to enhance PHA foaming by increasing melt strength and controlling crystallization kinetics [42]. Although the great progress achieved on relevant processing aspects, foaming is not often used in the biomedical field since, despite the technological complexity, pores interconnectivity and surface porosity, which are a key requirement for most applications, are not easily obtained with this approach (Figure 3f).

Formulation of nanoparticles, microspheres, and microcapsules made from PHA has been widely investigated to develop biodegradable systems able to deliver pharmacologically active agents to a specific site of action, at the therapeutically optimal rate and dose regime [43]. Depending on drug hydrophilic/lipophilic behavior and the particle morphological requirements, different formulation methods can be employed, such as polymerization and nanoparticle formation in-situ, modified double emulsion-solvent evaporation, and oil-in-water emulsion-solvent evaporation [44]—as well as the dialysis method [45]. For instance, standard double-emulsion protocols for PHB nanoparticles preparation involve i) adding an aqueous phase, containing a drug and possibly an emulsifier, to an organic polymer solution under vigorous stirring or sonication ii) adding the obtained water-in-oil (w/o) emulsion to a second aqueous phase containing a hydrophilic polymer, e.g., poly(vinyl alcohol) (PVA), to form a w/o/w emulsion, iii) stirring until complete organic solvent evaporation, centrifugation, and resuspension in an aqueous phase. Folate-conjugated PHB nanoparticles loaded with an anti-cancer drug were recently prepared by following this method [46].

3.1. Electrospinning

Electrospinning is the most employed technique for the production, on a lab and industrial scale, of polymeric nanofibers and nanofibrous meshes suitable for different applications, such as patches for tissue engineering and wound repair, nanostructured systems for drug release, filtration membranes, and protective and high-tech clothes [47]. This technique is based on an electrostatically-driven process that involves feeding a polymeric solution through a capillary into a high voltage electric field. The liquid drop is deformed, under the action of electrostatic forces and surface tension, assuming a shape similar to that of a cone. At a critical value of the applied voltage, a thin fluid jet is ejected at the apex of the cone and accelerated towards a grounded or oppositely-charged electrode, typically a flat metallic plate (Figure 4a). The stretching forces acting on the jet and the contemporary solvent evaporation, amplified by the violent whipping and splitting the jet undergoes during its travel, lead to the formation of fibers with a diameter in the range of a few micrometers down to tens of nanometers. The electrospun fibers can be collected in the form of nonwoven, yarn, 3D assemblies, and patterned structures, depending on the electrode/counter-electrode configuration [48].

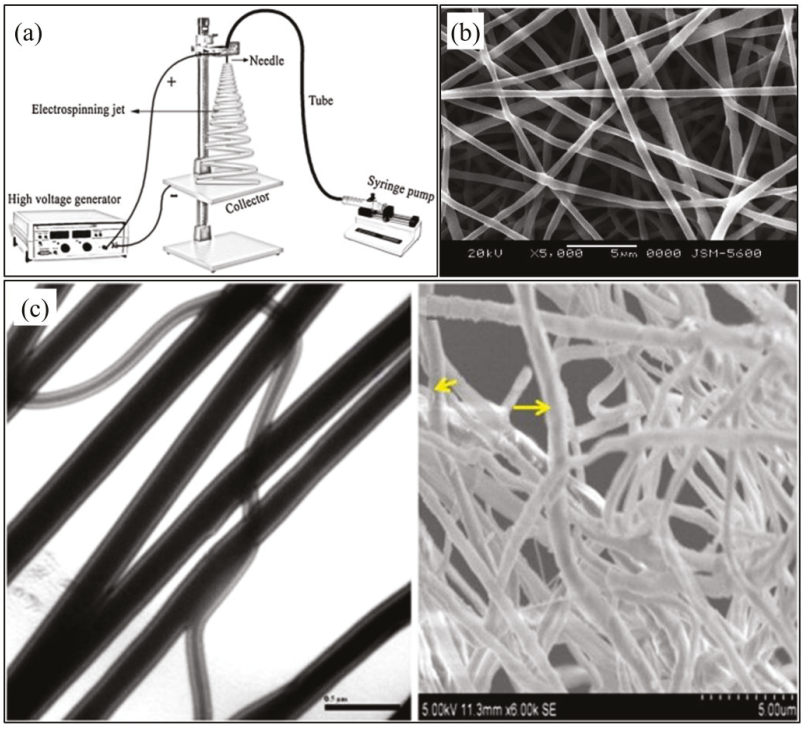

Figure 4. (**a**) Schematic representation of electrospinning set up (reproduced from [49]); (**b**) SEM micrograph of electrospun PHBHHx/ poly(d,l-lactic acid) (PDLLA) blend fiber mesh (reproduced from [50]); (**c**) TEM (left) and SEM (right) micrographs of PHB/gelatin core/sheath coaxial fibers (scale bars 0.5 μm and 5 μm, respectively; yellow arrows indicate the polymeric core/sheath structure; reproduced from [51]).

The great interest by the biomedical science and engineering community on electrospinning is justified by its tremendous potential for the development of nanostructured systems designed for advanced tissue engineering and drug release applications. Indeed, electrospun nanofiber assemblies highly mimic the nanostructure of native extracellular matrix, thus providing cells with a 3D nanofibrous environment which allows them to better maintain their phenotypic shape and establish natural behavior patterns, in comparison to what observed in 2D cell culture and 3D macroporous architectures [52]. In addition, the simplicity and inexpensive nature of the fabrication setup making possible its scale up, and the high design freedom of fibers assembly architecture and composition, together with the versatility in the development of tailored drug-loading methods for functionalizing polymeric nanofibers with a wide variety of therapeutics, have led to a fast growing amount of literature published on electrospinning for drug release [53].

One of the first articles on electrospinning of PHA was published in 2006 and described an investigation of the relationship between processing parameters and electrospun fiber assembly morphology, as observed by means of SEM [54]. The study resulted in the development of a set of scaffolds made of PHB, PHBV, or their blend (75:25, 50:50, or 25:75 weight ratio) with average fiber diameter of few microns. High magnification SEM analysis showed that PHB/PHBV blend fibers had a rough surface, which was explained by the authors with a phase inversion process related to the rapid evaporation of chloroform, employed as a solvent. These scaffolds sustained the growth in vitro of mouse fibroblasts and human osteoblasts, at higher levels than analogous cast-films [55]. Electrospun PHB meshes were also recently shown to be a suitable substrate for human mesenchymal

stem cells (MSCs) adhesion, proliferation, and differentiation [56,57]. As systematically investigated by Zhu et al. [58], the variation of PHBV concentration in the starting solution significantly influenced the morphology of the resulting fibers, likely because of an effect on chain entanglement during electrospinning [59]. They were able to change the electrospun structure by gradually increasing polymer concentration, from beaded to string-on-beads morphology, and then to uniform fibrous mesh, with a relevant increase of surface hydrophobicity, as a consequence of the increased roughness.

As reviewed by Sanhueza et al. [21], a current research trend is devoted to electrospinning PHA blended with other synthetic or natural polymers, with the aim of tuning the properties of the resulting fibers or endowing them with intrinsic bioactivity. Cheng et al. [50] processed PHBHHx and poly(d,l-lactic acid) (PDLLA) dissolved in chloroform mixed with dimethylformamide (DMF) (80/20 w/w) to increase the solution electrical conductivity. In particular, they showed that by increasing the PDLLA weight percentage from 25 to 50 or 75%, the tensile modulus was decreased and the elongation at break increased, while the biodegradation rate was higher, due to the more amorphous morphology of PDLLA in comparison to the semicrystalline nature of PHBHHx. The possibility of tuning PHBV meshes mechanical properties through blending with MCL-PHA was also recently shown. Indeed, electrospun meshes crystallinity, tensile strength, and modulus decreased, while the elongation at break increased, by blending PHBV with poly(3-hydroxyoctanoate-*co*-3-hydroxyhexanoate) (PHOHHx) (25% wt.), which is an amorphous MCL-PHA with elastomeric properties at room temperature. PHB blending with poly(l-lactide-*co*-ε-caprolactone) led to fiber diameter decreasing and hydrophobicity increasing, without any resulting effect on electrospun mesh mechanical properties [60]. An acetyl triethyl citrate/poly(vinyl acetate) blend was employed as a plasticizer and compatibilizer to improve the miscibility between PHB and poly(propylene carbonate) [61]. The resulting blend was electrospun into meshes with decreased crystallinity and T_m in comparison to PHB meshes. Nagiah et al. [51,62] investigated the modulation of the properties of PHB/gelatin membranes designed for skin tissue engineering, by adopting different electrospinning strategies. Indeed, by simultaneously electrospinning the two polymers with two separated syringes, processing a blend of the two polymers, or employing a coaxial electrospinning approach, they developed membranes composed by single gelatin fibers and PHB fibers, PHB/gelatin blend fibers, or biphasic fibers composed by a PHB core and a gelatin sheath, respectively (Figure 4c). The different fibers' composition and architecture resulted in significant differences in mechanical properties, wettability, and proliferation of human dermal fibroblasts and keratinocytes cultured in vitro on the membranes. Zhinjiang et al. [63] demonstrated that a variation of PHB/cellulose ratio in a starting chloroform/DMF mixture significantly affected the biodegradation rate, as well as the wettability and mechanical properties of the resulting electrospun blend nanofibers. Blend fibers made of PHB/chitosan blends with different weight ratio were also electrospun by using trifluoroacetic acid, as a common solvent [64]. The addition of chitosan resulted in increased wettability and biodegradation rate, as well as decreased tensile strength. The possibility of tuning in a wide range of the tensile strength and elongation at break of zein/P3HB-*co*-4HB blend meshes by electrospinning was also recently shown by varying the weight ratio between the two polymers. Different chemical modification strategies have been also adopted to improve cell adhesion onto electrospun PHA meshes, e.g., epoxy functionalization [65] and polysaccharide-grafting [66,67]. Other PHA fibers functionalization approaches include combination with antibacterial particles (e.g., silver [68] and zinc oxide [69] nanoparticles) or electrosprayed osteoconductive ceramics (e.g., HA nanoparticles [70]), as well as grafting with carbon nanotubes mechanical-reinforcing fillers [71].

A large body of literature has been dedicated to investigate and modulate electrospun PHA fibers organization and topography, as a means to control cell behavior and mesh mechanical properties. Yiu et al. [72] carried out a significant comparative study on the influence of topographic morphology of PHBHHx membranes fabricated by compression-molding, solvent-casting or electrospinning, on human MSCs adhesion, proliferation, and differentiation in vitro. Differently to what was observed in the two other kinds of membrane, MSCs showed a specific orientation on the electrospun fibrous meshes, exploitable for guided tissue regeneration and co-culturing of cells with orientation specificity

(e.g., nerve, muscle and ligament cells). Aligned PHBV fibers systems can be fabricated by employing a rotating cylinder as fibers collector and auxiliary electrode [73]. Various studies have shown that fibers' alignment can significantly influence physical-chemical, mechanical, and biological properties of the resulting membrane. For instance, an article reported enhanced wettability for PHBV aligned fibers in comparison to PHBV randomly-oriented fibers [74]. In addition, tensile testing revealed that the aligned PHBV fibers membranes were stronger in the longitudinal direction, but weaker in the transverse direction, in comparison to non-woven PHBV meshes showing instead an isotropic behavior. Fibers alignment resulted also in a different morphology of human osteosarcoma SaOS-2 cells that elongated when cultured in vitro. Similarly, Wang et al. [75] observed higher tensile modulus and strength, as well as increased MSCs elongation and differentiation, when electrospun PHBHHx fibers were aligned along their axes (Figure 5). The relationship between fibers' alignment and mechanical properties was further investigated by a recent study reporting on electrospinning of PHB, P3HB-*co*-4HB, PHBV, and PHBHHx [76]. In all cases, fibers' alignment resulted in enhanced tensile mechanical properties with an overall effect on surface properties. The employment of a rotating fiber collector has been also widely investigated for the production of non-woven meshes with a tubular geometry investigated, as suitable nerve conduits [77] or blood vessel scaffolds [78].

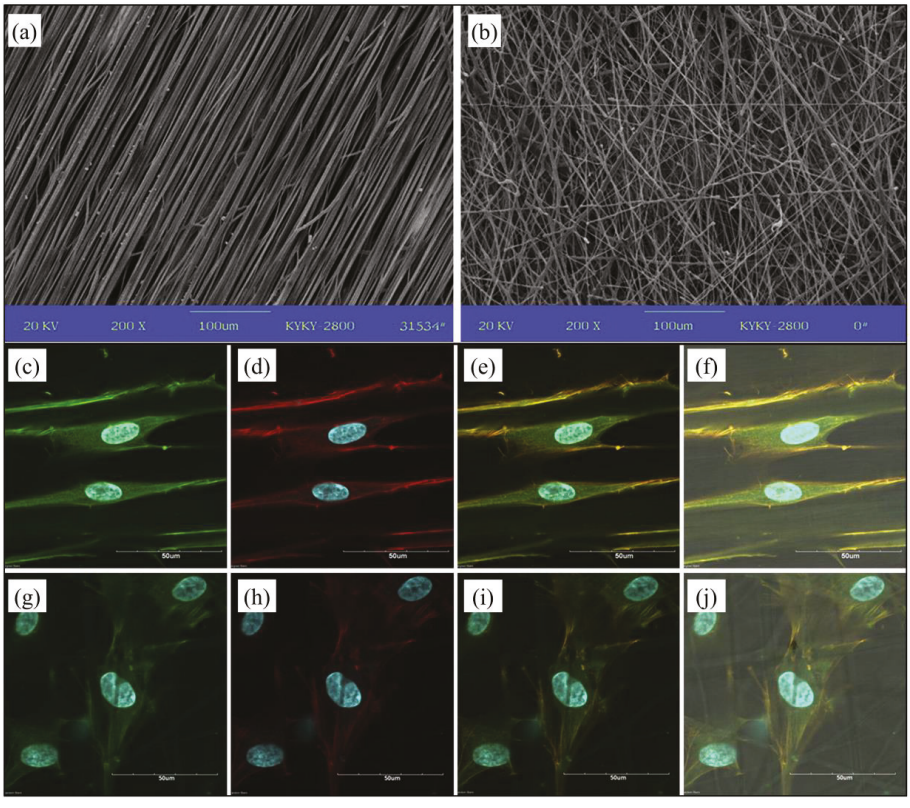

Figure 5. SEM micrographs of electrospun PHBHHx meshes composed by (**a**) aligned fibers or (**b**) randomly-oriented fibers (scale bar: 100 μm); confocal laser scanning microscopy images of MSCs cultured for three days on PHBHHx meshes composed by (**c**–**f**) aligned fibers or (**g**–**j**) randomly-oriented fibers (adhesion complexes (vinculin) in green, actin in red and nuclei in blue; scale bar in (**a**) and (**b**) 100 μm, scale bar in (**c**–**j**) 50 μm; reproduced from [75]).

3.2. Additive Manufacturing

As described in this section, various additive manufacturing approaches have been successfully applied to process different PHA, mainly into 3D porous scaffolds (Figure 6). Additive manufacturing was defined by ASTM as "the process of joining materials to make objects from 3D model data, usually layer upon layer" [79]. Additive manufacturing techniques are based on a computer-controlled design and fabrication process involving a sequential delivery of materials and/or energy to build up 3D layered objects. The geometrical and dimensional details, as well as other product specifications, such as density and composition gradients, are defined in a digital file which is then converted into a numerical control programming language, which specifies the motion of automated manufacturing tools. This approach enables advanced control over composition, shape, and dimensions of the object, in terms of design freedom and resolution. An advantage of additive manufacturing peculiar to the biomedical field is the possibility of deriving the 3D model data from medical imaging techniques commonly used for diagnostic purposes, such as computer tomography and magnetic resonance imaging. In this way, the anatomical features of biological tissues and organs can be reproduced through the fabrication process [80].

The various additive manufacturing techniques developed so far enable the processing of a wide range of materials by applying different approaches. Indeed, laser-based techniques are based on directing a beam or projection of light either to a photosensitive resin that is selectively photopolymerized, like in the case of stereolithography [81], or to a powder bed that is selectively sintered or fused, in the case of selective laser sintering (SLS) [82]. In the case of binder jetting, also referred to as 3D printing, a liquid binder, typically a polymer solvent, is deposited on a powder bed, which is selectively dissolved and fused upon solvent evaporation [83]. In extrusion-based techniques, a polymer in the form of a melt [84] or a solution/suspension [85] is extruded under controlled environmental conditions and selectively deposited onto a building stage. Fused deposition modeling (FDM) is a widely investigated example of melt-extrusion technique involving the extrusion and controlled deposition of a polymeric filament at a temperature above its T_g. Computer-aided wet-spinning (CAWS) involves the controlled extrusion and deposition of a polymeric solution or suspension directly into a coagulation bath to achieve polymer solidification through a non-solvent-induced phase-inversion process.

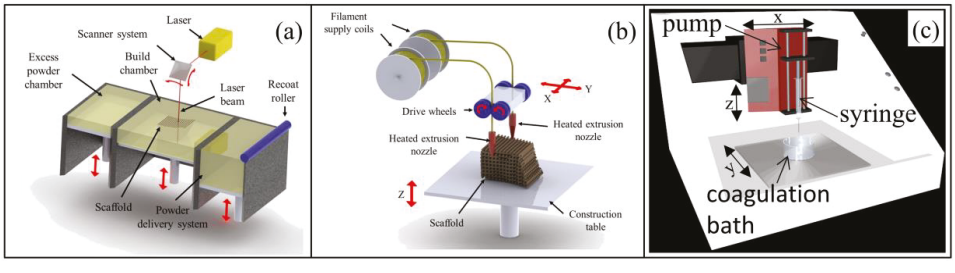

Figure 6. Schematic representation of additive manufacturing techniques applied to PHA processing: (**a**) selective laser sintering (SLS) and (**b**) fused deposition modeling (FDM) (reproduced from [80]); (**c**) computer-aided wet-spinning (CAWS) (reproduced from [86]).

Selective laser sintering (SLS) was the first reported additive manufacturing technique to be employed for PHA processing (Figure 6a). In particular, different articles described the fabrication of 2D and 3D constructs with a predefined shape and interconnected porous architecture, through automated sintering of PHB particles, without any significant change in polymer chemical composition and thermal properties [87–89]. Duan et al. [90–92] published a few articles showing that PHBV scaffolds loaded with calcium phosphate (Ca–P) nanoparticles could be fabricated by processing nanocomposite microspheres previously prepared by means of an emulsion-solvent evaporation

method (Figure 7a). They also showed that the scaffolds could be functionalized with the recombinant human bone morphogenetic protein-2 growth factor that was bound to a heparin coating applied on the surface. Although, this set of PHA scaffolds showed high fidelity on the macroscopic scale to the virtual model geometrical features, a low topographical resolution, was observed under SEM analysis (Figure 7c–f). This morphological feature, distinctive of SLS, is a consequence of an incomplete coalescence of polymeric particles during sintering due to the low laser energy employed to prevent thermal decomposition.

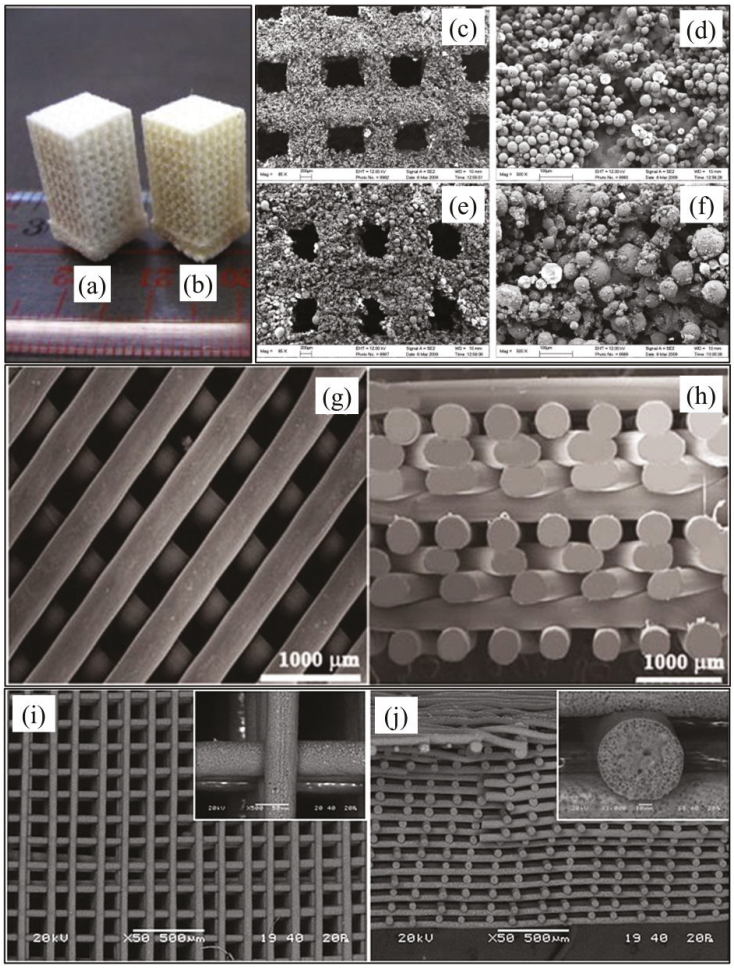

Figure 7. Additive manufactured PHA scaffolds: photograph of (**a**) PHBV and (**b**) CaP-loaded PHBV scaffolds by SLS, and relevant SEM micrographs of (**c**,**d**) PHBV and (e, f) CaP-loaded PHBV scaffolds (scale bars in (**c**) and (**e**) 200 µm, in (**d**) and (**f**) 100 µm; reproduced from [90]); SEM micrographs of (**g**) top view and (**h**) cross-section PHBV/PCL scaffolds by FDM (reproduced from [93]); SEM micrographs of (**i**) top-view and (**j**) cross-section of PHBHHx scaffolds by CAWS (inserts are high magnification micrographs, reproduced from [94]).

Fused deposition modeling (FDM) feasibility for processing PHA and exploiting their thermoplastic behavior has been assessed by a number of research activities (Figure 6b). However,

the employment of FDM is still delayed in comparison to what achieved with other aliphatic polyesters, (e.g., PLLA), as a consequence of the limited thermal stability of PHA as well as their low melt elasticity and strength. For this reason, blending with other polymers or plasticizers is needed for successful PHA processing by FDM. Kosorn et al. [93] developed scaffolds made of poly(ε-caprolactone) (PCL)/PHBV blends with different weight ratios between the two polymers (75:25, 50:50, and 25:75) (Figure 7g,h). They demonstrated that the synergistic effect of increase in PHBV ratio and surface low-pressure plasma treatment significantly increased the proliferation and chondrogenic differentiation of porcine chondrocytes cultured in vitro in combination with the scaffolds. Blending with commercial monomeric plasticizers based on esters of citric acid (Citroflex®) was recently shown to be an effective means for FDM processing of PHB/PDLLA/plasticizer blends (60/25/15 wt.) into dog bone shape samples for tensile test [95]. Selection of the optimal plasticizer allowed a remarkable increase in elongation at break (from 5 to 187%) as well as a reduction of warping effects in the printed part upon solidification. The development of filaments made of maleic anhydride-grafted PHA loaded with palm fibers [96], wood flour [97], or multi-walled carbon nanotubes [98] was also recently reported in literature.

Computer-aided wet-spinning (CAWS) represents a successful example of hybrid additive manufacturing technique applied for the processing of PHA. CAWS approach involves the extrusion of a chloroform or tetrahydrofuran suspension of PHBHHx directly into a non-solvent bath (e.g., ethanol) to fabricate a device with a layer-layer process (Figure 6c). Under optimal conditions, the phase inversion process governing polymer solidification leads to the formation of a microporosity in the polymeric matrix integrated with the macroporous network created by the controlled deposition process (Figure 7i,j) [85,99]. PHBHHx scaffolds with different shape and porous architecture, resulting in varied mechanical response, can be fabricated by changing the design model and the processing conditions [94]. Indeed, anatomical PHBHHx scaffolds with the shape and dimensions of a critical size segment of a New Zealand rabbit's radius model, and endowed with a longitudinal macrochannel for optimal bone regeneration conditions, were recently developed [100]. This kind of PHBHHx scaffolds, possibly in the form of a blend with PCL [101], were demonstrated to sustain the in vitro adhesion and proliferation of MC3T3-E1 murine preosteoblast cells. CAWS approach was also recently implemented with a rotating mandrel, as a fiber collector during polymer coagulation, to fabricate small-caliber biodegradable stents made of either PHBHHx or PCL [102]. Tubular constructs with different porous architectures were developed by controlling the synchronized motion of the deposition needle and the rotating mandrel.

4. Conclusions and Future Perspectives

Thanks to their thermoplastic behavior and suitable rheological properties when dissolved or suspended in proper organic solvents, processing of PHA has been investigated by adopting a number of tailored technological approaches. Indeed, the wide processing versatility given by the great variety, in terms of macromolecular structure and morphology, offered by PHA, makes this class of biodegradable polymers one of the most investigated in the biomedical field, especially when a load-bearing role is required. These aspects, together with the promising perspectives for PHA sustainable development [103], are propelling a fast growing research on relevant processing approaches to specific biomedical requirements. Both techniques with a long-history of industrial use, such as melt-spinning and foaming, and emerging techniques currently in the phase of being industrially-implemented, i.e., electrospinning and additive manufacturing, are applied for biomedical processing of PHA. The next frontier could be represented by the combination of different processing approaches to integrate in a single PHA device the high resolution down to the micro/nanoscale given by techniques like electrospinning and electrospraying, with the advanced control at the macroscale guaranteed by automated additive manufacturing approaches.

Acknowledgments: The financial support of the University of Pisa PRA-2018-23 project entitled "Functional Materials" is gratefully acknowledged.

Conflicts of Interest: The authors declare no conflict of interest.

References

1. Puppi, D.; Chiellini, F.; Dash, M.; Chiellini, E. Biodegradable polymers for biomedical applications. In *Biodegradable Polymers: Processing, Degradation & Applications*; Felton, G.P., Ed.; Nova Science Publishers: New York, NY, USA, 2011; pp. 545–560.
2. Koller, M. Advances in polyhydroxyalkanoate (PHA) production. *Bioengineering* **2017**, *4*, 88. [CrossRef] [PubMed]
3. Nomura, C.T.; Tanaka, T.; Gan, Z.; Kuwabara, K.; Abe, H.; Takase, K.; Taguchi, K.; Doi, Y. Effective enhancement of short-chain-length−medium-chain-length polyhydroxyalkanoate copolymer production by coexpression of genetically engineered 3-ketoacyl-acyl-carrier-protein synthase iii (fabh) and polyhydroxyalkanoate synthesis genes. *Biomacromolecules* **2004**, *5*, 1457–1464. [CrossRef] [PubMed]
4. Chen, S.; Liu, Q.; Wang, H.; Zhu, B.; Yu, F.; Chen, G.-Q.; Inoue, Y. Polymorphic crystallization of fractionated microbial medium-chain-length polyhydroxyalkanoates. *Polymer* **2009**, *50*, 4378–4388. [CrossRef]
5. Yang, Q.; Wang, J.; Zhang, S.; Tang, X.; Shang, G.; Peng, Q.; Wang, R.; Cai, X. The properties of poly(3-hydroxybutyrate-co-3-hydroxyhexanoate) and its applications in tissue engineering. *Curr. Stem Cell Res. Ther.* **2014**, *9*, 215–222. [CrossRef] [PubMed]
6. Yoshie, N.; Inoue, Y. Chemical composition distribution of bacterial copolyesters. *Int. J. Biol. Macromol.* **1999**, *25*, 193–200. [CrossRef]
7. Lemoigne, M. Produits de deshydration et de polymerisation de l'acide b-oxobutyrique. *Bull. Soc. Chem. Biol.* **1926**, *8*, 770–782.
8. Nigmatullin, R.; Thomas, P.; Lukasiewicz, B.; Puthussery, H.; Roy, I. Polyhydroxyalkanoates, a family of natural polymers, and their applications in drug delivery. *J. Chem. Technol. Biotechnol.* **2015**, *90*, 1209–1221. [CrossRef]
9. Rodriguez-Contreras, A. Recent advances in the use of polyhydroyalkanoates in biomedicine. *Bioengineering* **2019**, *6*, 82. [CrossRef]
10. Morelli, A.; Puppi, D.; Chiellini, F. Polymers from renewable resources. *J. Renew. Mater.* **2013**, *1*, 83–112. [CrossRef]
11. Koller, M. Biodegradable and biocompatible polyhydroxy-alkanoates (PHA): Auspicious microbial macromolecules for pharmaceutical and therapeutic applications. *Molecules* **2018**, *23*, 362. [CrossRef]
12. Chen, G.-Q.; Wu, Q. The application of polyhydroxyalkanoates as tissue engineering materials. *Biomaterials* **2005**, *26*, 6565–6578. [CrossRef] [PubMed]
13. Manavitehrani, I.; Fathi, A.; Badr, H.; Daly, S.; Negahi Shirazi, A.; Dehghani, F. Biomedical applications of biodegradable polyesters. *Polymers* **2016**, *8*, 20. [CrossRef] [PubMed]
14. Galatea Surgical Scaffolds. Available online: https://www.galateasurgical.com/ (accessed on 30 October 2019).
15. Tepha Medical Devices. Available online: https://www.tepha.com (accessed on 30 October 2019).
16. B. Braun Italia. Available online: https://www.bbraun.it (accessed on 30 October 2019).
17. Wright Medical Group N.V. Available online: http://www.wright.com (accessed on 30 October 2019).
18. Leroy, E.; Petit, I.; Audic, J.L.; Colomines, G.; Deterre, R. Rheological characterization of a thermally unstable bioplastic in injection molding conditions. *Polym. Degrad. Stab.* **2012**, *97*, 1915–1921. [CrossRef]
19. Miranda De Sousa Dias, M.; Koller, M.; Puppi, D.; Morelli, A.; Chiellini, F.; Braunegg, G. Fed-batch synthesis of poly(3-hydroxybutyrate) and poly(3-hydroxybutyrate-co-4-hydroxybutyrate) from sucrose and 4-hydroxybutyrate precursors by burkholderia sacchari strain dsm 17165. *Bioengineering* **2017**, *4*, 36. [CrossRef]
20. Madkour, M.H.; Heinrich, D.; Alghamdi, M.A.; Shabbaj, I.I.; Steinbüchel, A. PHA recovery from biomass. *Biomacromolecules* **2013**, *14*, 2963–2972. [CrossRef]
21. Sanhueza, C.; Acevedo, F.; Rocha, S.; Villegas, P.; Seeger, M.; Navia, R. Polyhydroxyalkanoates as biomaterial for electrospun scaffolds. *Int. J. Biol. Macromol.* **2019**, *124*, 102–110. [CrossRef]
22. Puppi, D.; Chiellini, F. Additive manufacturing of PHA. In *Handbook of Polyhydroxyalkanoates*; Koller, M., Ed.; CRC Press: Boca Raton, FL, USA, 2020.
23. Puppi, D.; Chiellini, F.; Piras, A.M.; Chiellini, E. Polymeric materials for bone and cartilage repair. *Prog. Polym. Sci.* **2010**, *35*, 403–440. [CrossRef]

24. Basnett, P.; Ching, K.Y.; Stolz, M.; Knowles, J.C.; Boccaccini, A.R.; Smith, C.; Locke, I.C.; Keshavarz, T.; Roy, I. Novel poly(3-hydroxyoctanoate)/poly(3-hydroxybutyrate) blends for medical applications. *React. Funct. Polym.* **2013**, *73*, 1340–1348. [CrossRef]
25. Baek, J.-Y.; Xing, Z.-C.; Kwak, G.; Yoon, K.-B.; Park, S.-Y.; Park, L.S.; Kang, I.-K. Fabrication and characterization of collagen-immobilized porous PHBV/HA nanocomposite scaffolds for bone tissue engineering. *J. Nanomater.* **2012**, *2012*, 171804. [CrossRef]
26. Tanaka, T.; Fujita, M.; Takeuchi, A.; Suzuki, Y.; Uesugi, K.; Ito, K.; Fujisawa, T.; Doi, Y.; Iwata, T. Formation of highly ordered structure in poly[(r)-3-hydroxybutyrate-co-(r)-3-hydroxyvalerate] high-strength fibers. *Macromolecules* **2006**, *39*, 2940–2946. [CrossRef]
27. Dai, Z.-W.; Zou, X.-H.; Chen, G.-Q. Poly(3-hydroxybutyrate-co-3-hydroxyhexanoate) as an injectable implant system for prevention of post-surgical tissue adhesion. *Biomaterials* **2009**, *30*, 3075–3083. [CrossRef] [PubMed]
28. Sultana, N.; Khan, T.H. In vitro degradation of PHBV scaffolds and nHA/PHBV composite scaffolds containing hydroxyapatite nanoparticles for bone tissue engineering. *J. Nanomater.* **2012**, *2012*, 190950. [CrossRef]
29. Le Moigne, N.; Sauceau, M.; Benyakhlef, M.; Jemai, R.; Benezet, J.-C.; Rodier, E.; Lopez-Cuesta, J.-M.; Fages, J. Foaming of poly(3-hydroxybutyrate-co-3-hydroxyvalerate)/organo-clays nano-biocomposites by a continuous supercritical co2 assisted extrusion process. *Eur. Polym. J.* **2014**, *61*, 157–171. [CrossRef]
30. Masaeli, E.; Morshed, M.; Rasekhian, P.; Karbasi, S.; Karbalaie, K.; Karamali, F.; Abedi, D.; Razavi, S.; Jafarian-Dehkordi, A.; Nasr-Esfahani, M.H.; et al. Does the tissue engineering architecture of poly(3-hydroxybutyrate) scaffold affects cell-material interactions? *J. Biomed. Mater. Res. Part A* **2012**, *100*, 1907–1918. [CrossRef] [PubMed]
31. Xiang, H.; Chen, Z.; Zheng, N.; Zhang, X.; Zhu, L.; Zhou, Z.; Zhu, M. Melt-spun microbial poly(3-hydroxybutyrate-co-3-hydroxyvalerate) fibers with enhanced toughness: Synergistic effect of heterogeneous nucleation, long-chain branching and drawing process. *Int. J. Biol. Macromol.* **2019**, *122*, 1136–1143. [CrossRef]
32. Alagoz, A.S.; Rodriguez-Cabello, J.C.; Hasirci, V. PHBV wet-spun scaffold coated with ELR-REDV improves vascularization for bone tissue engineering. *Biomed. Mater.* **2018**, *13*, 055010. [CrossRef]
33. Raeisdasteh Hokmabad, V.; Davaran, S.; Ramazani, A.; Salehi, R. Design and fabrication of porous biodegradable scaffolds: A strategy for tissue engineering. *J. Biomater. Sci. Polym. Ed.* **2017**, *28*, 1797–1825. [CrossRef]
34. Ashter, S.A. 7-processing biodegradable polymers. In *Introduction to Bioplastics Engineering*; Ashter, S.A., Ed.; William Andrew Publishing: Oxford, UK, 2016; pp. 179–209.
35. Li, X.-T.; Zhang, Y.; Chen, G.-Q. Nanofibrous polyhydroxyalkanoate matrices as cell growth supporting materials. *Biomaterials* **2008**, *29*, 3720–3728. [CrossRef]
36. Tsujimoto, T.; Hosoda, N.; Uyama, H. Fabrication of porous poly(3-hydroxybutyrate-co-3-hydroxyhexanoate) monoliths via thermally induced phase separation. *Polymers* **2016**, *8*, 66. [CrossRef]
37. Puppi, D.; Piras, A.M.; Chiellini, F.; Chiellini, E.; Martins, A.; Leonor, I.B.; Neves, N.; Reis, R. Optimized electro- and wet-spinning techniques for the production of polymeric fibrous scaffolds loaded with bisphosphonate and hydroxyapatite. *J. Tissue Eng. Regen. Med.* **2011**, *5*, 253–263. [CrossRef]
38. Sultana, N.; Wang, M. Fabrication of HA/PHBV composite scaffolds through the emulsion freezing/freeze-drying process and characterisation of the scaffolds. *J. Mater. Sci. Mater. Med.* **2007**, *19*, 2555–2561. [CrossRef] [PubMed]
39. Sultana, N.; Wang, M. PHBV/PLLA-based composite scaffolds fabricated using an emulsion freezing/freeze-drying technique for bone tissue engineering: Surface modification andin vitrobiological evaluation. *Biofabrication* **2012**, *4*, 015003. [CrossRef] [PubMed]
40. Liao, Q.; Tsui, A.; Billington, S.; Frank, C.W. Extruded foams from microbial poly(3-hydroxybutyrate-co-3-hydroxyvalerate) and its blends with cellulose acetate butyrate. *Polym. Eng. Sci.* **2012**, *52*, 1495–1508. [CrossRef]
41. Wright, Z.C.; Frank, C.W. Increasing cell homogeneity of semicrystalline, biodegradable polymer foams with a narrow processing window via rapid quenching. *Polym. Eng. Sci.* **2014**, *54*, 2877–2886. [CrossRef]
42. Ventura, H.; Laguna-Gutiérrez, E.; Rodriguez-Perez, M.A.; Ardanuy, M. Effect of chain extender and water-quenching on the properties of poly(3-hydroxybutyrate-co-4-hydroxybutyrate) foams for its production by extrusion foaming. *Eur. Polym. J.* **2016**, *85*, 14–25. [CrossRef]

43. Shrivastav, A.; Kim, H.-Y.; Kim, Y.-R. Advances in the applications of polyhydroxyalkanoate nanoparticles for novel drug delivery system. *Biomed. Res. Int.* **2013**, *2013*, 581684. [CrossRef]
44. Barouti, G.; Jaffredo, C.G.; Guillaume, S.M. Advances in drug delivery systems based on synthetic poly(hydroxybutyrate) (co)polymers. *Prog. Polym. Sci.* **2017**, *73*, 1–31. [CrossRef]
45. Errico, C.; Bartoli, C.; Chiellini, F.; Chiellini, E. Poly(hydroxyalkanoates)-based polymeric nanoparticles for drug delivery. *J. Biomed. Biotechnol.* **2009**, *2009*, 571702. [CrossRef]
46. Althuri, A.; Mathew, J.; Sindhu, R.; Banerjee, R.; Pandey, A.; Binod, P. Microbial synthesis of poly-3-hydroxybutyrate and its application as targeted drug delivery vehicle. *Bioresour. Technol.* **2013**, *145*, 290–296. [CrossRef]
47. Persano, L.; Camposeo, A.; Tekmen, C.; Pisignano, D. Industrial upscaling of electrospinning and applications of polymer nanofibers: A review. *Macromol. Mater. Eng.* **2013**, *298*, 504–520. [CrossRef]
48. Teo, W.E.; Ramakrishna, S. A review on electrospinning design and nanofibre assemblies. *Nanotechnology* **2006**, *17*, R89–R106. [CrossRef] [PubMed]
49. Almuhamed, S.; Bonne, M.; Khenoussi, N.; Brendle, J.; Schacher, L.; Lebeau, B.; Adolphe, D.C. Electrospinning composite nanofibers of polyacrylonitrile/synthetic na-montmorillonite. *J. Ind. Eng. Chem.* **2016**, *35*, 146–152. [CrossRef]
50. Cheng, M.-L.; Chen, P.-Y.; Lan, C.-H.; Sun, Y.-M. Structure, mechanical properties and degradation behaviors of the electrospun fibrous blends of phbhhx/pdlla. *Polymer* **2011**, *52*, 1391–1401. [CrossRef]
51. Nagiah, N.; Madhavi, L.; Anitha, R.; Anandan, C.; Srinivasan, N.T.; Sivagnanam, U.T. Development and characterization of coaxially electrospun gelatin coated poly (3-hydroxybutyric acid) thin films as potential scaffolds for skin regeneration. *Mater. Sci. Eng. C* **2013**, *33*, 4444–4452. [CrossRef] [PubMed]
52. Puppi, D.; Zhang, X.; Yang, L.; Chiellini, F.; Sun, X.; Chiellini, E. Nano/microfibrous polymeric constructs loaded with bioactive agents and designed for tissue engineering applications: A review. *J. Biomed. Mater. Res. B Appl. Biomater.* **2014**, *102*, 1562–1579. [CrossRef] [PubMed]
53. Puppi, D.; Chiellini, F. 12-drug release kinetics of electrospun fibrous systems. In *Core-Shell Nanostructures for Drug Delivery and Theranostics*; Focarete, M.L., Tampieri, A., Eds.; Woodhead Publishing: Sawston, UK; Cambridge, UK, 2018; pp. 349–374.
54. Sombatmankhong, K.; Suwantong, O.; Waleetorncheepsawat, S.; Supaphol, P. Electrospun fiber mats of poly(3-hydroxybutyrate), poly(3-hydroxybutyrate-co-3-hydroxyvalerate), and their blends. *J. Polym. Sci. Part B Polym. Phys.* **2006**, *44*, 2923–2933. [CrossRef]
55. Sombatmankhong, K.; Sanchavanakit, N.; Pavasant, P.; Supaphol, P. Bone scaffolds from electrospun fiber mats of poly(3-hydroxybutyrate), poly(3-hydroxybutyrate-co-3-hydroxyvalerate) and their blend. *Polymer* **2007**, *48*, 1419–1427. [CrossRef]
56. Ramier, J.; Grande, D.; Bouderlique, T.; Stoilova, O.; Manolova, N.; Rashkov, I.; Langlois, V.; Albanese, P.; Renard, E. From design of bio-based biocomposite electrospun scaffolds to osteogenic differentiation of human mesenchymal stromal cells. *J. Mater. Sci. Mater. Med.* **2014**, *25*, 1563–1575. [CrossRef]
57. Grande, D.; Ramier, J.; Versace, D.L.; Renard, E.; Langlois, V. Design of functionalized biodegradable PHA-based electrospun scaffolds meant for tissue engineering applications. *New Biotechnol.* **2017**, *37*, 129–137. [CrossRef]
58. Zhu, S.; Yu, H.; Chen, Y.; Zhu, M. Study on the morphologies and formational mechanism of poly(hydroxybutyrate-co-hydroxyvalerate) ultrafine fibers by dry-jet-wet-electrospinning. *J. Nanomater.* **2012**, *2012*, 525419. [CrossRef]
59. Puppi, D.; Piras, A.M.; Detta, N.; Dinucci, D.; Chiellini, F. Poly(lactic-co-glycolic acid) electrospun fibrous meshes for the controlled release of retinoic acid. *Acta Biomater.* **2010**, *6*, 1258–1268. [CrossRef] [PubMed]
60. Daranarong, D.; Chan, R.T.H.; Wanandy, N.S.; Molloy, R.; Punyodom, W.; Foster, L.J.R. Electrospun polyhydroxybutyrate and poly(L-lactide-*co*-ε-caprolactone) composites as nanofibrous scaffolds. *Biomed. Res. Int.* **2014**, *2014*, 741408. [CrossRef] [PubMed]
61. El-Hadi, A.M. Improvement of the miscibility by combination of poly(3-hydroxy butyrate) phb and poly(propylene carbonate) ppc with additives. *J. Polym. Environ.* **2017**, *25*, 728–738. [CrossRef]
62. Nagiah, N.; Madhavi, L.; Anitha, R.; Srinivasan, N.T.; Sivagnanam, U.T. Electrospinning of poly (3-hydroxybutyric acid) and gelatin blended thin films: Fabrication, characterization, and application in skin regeneration. *Polym. Bull.* **2013**, *70*, 2337–2358. [CrossRef]

63. Zhijiang, C.; Yi, X.; Haizheng, Y.; Jia, J.; Liu, Y. Poly(hydroxybutyrate)/cellulose acetate blend nanofiber scaffolds: Preparation, characterization and cytocompatibility. *Mater. Sci. Eng. C* **2016**, *58*, 757–767. [CrossRef]
64. Sadeghi, D.; Karbasi, S.; Razavi, S.; Mohammadi, S.; Shokrgozar, M.A.; Bonakdar, S. Electrospun poly(hydroxybutyrate)/chitosan blend fibrous scaffolds for cartilage tissue engineering. *J. Appl. Polym. Sci.* **2016**, *133*. [CrossRef]
65. Ramier, J.; Boubaker, M.B.; Guerrouache, M.; Langlois, V.; Grande, D.; Renard, E. Novel routes to epoxy functionalization of PHA-based electrospun scaffolds as ways to improve cell adhesion. *J. Polym. Sci. Part A Polym. Chem.* **2014**, *52*, 816–824. [CrossRef]
66. Lemechko, P.; Ramier, J.; Versace, D.L.; Guezennec, J.; Simon-Colin, C.; Albanese, P.; Renard, E.; Langlois, V. Designing exopolysaccharide-graft-poly(3-hydroxyalkanoate) copolymers for electrospun scaffolds. *React. Funct. Polym.* **2013**, *73*, 237–243. [CrossRef]
67. Versace, D.-L.; Ramier, J.; Babinot, J.; Lemechko, P.; Soppera, O.; Lalevee, J.; Albanese, P.; Renard, E.; Langlois, V. Photoinduced modification of the natural biopolymer poly(3-hydroxybutyrate-co-3-hydroxyvalerate) microfibrous surface with anthraquinone-derived dextran for biological applications. *J. Mater. Chem. B* **2013**, *1*, 4834–4844. [CrossRef]
68. Versace, D.-L.; Ramier, J.; Grande, D.; Andaloussi, S.A.; Dubot, P.; Hobeika, N.; Malval, J.-P.; Lalevee, J.; Renard, E.; Langlois, V. Versatile photochemical surface modification of biopolyester microfibrous scaffolds with photogenerated silver nanoparticles for antibacterial activity. *Adv. Healthc. Mater.* **2013**, *2*, 1008–1018. [CrossRef]
69. Rodríguez-Tobías, H.; Morales, G.; Ledezma, A.; Romero, J.; Saldívar, R.; Langlois, V.; Renard, E.; Grande, D. Electrospinning and electrospraying techniques for designing novel antibacterial poly(3-hydroxybutyrate)/zinc oxide nanofibrous composites. *J. Mater. Sci.* **2016**, *51*, 8593–8609. [CrossRef]
70. Ramier, J.; Bouderlique, T.; Stoilova, O.; Manolova, N.; Rashkov, I.; Langlois, V.; Renard, E.; Albanese, P.; Grande, D. Biocomposite scaffolds based on electrospun poly(3-hydroxybutyrate) nanofibers and electrosprayed hydroxyapatite nanoparticles for bone tissue engineering applications. *Mater. Sci. Eng. C* **2014**, *38*, 161–169. [CrossRef] [PubMed]
71. Mangeon, C.; Mahouche-Chergui, S.; Versace, D.L.; Guerrouache, M.; Carbonnier, B.; Langlois, V.; Renard, E. Poly(3-hydroxyalkanoate)-grafted carbon nanotube nanofillers as reinforcing agent for PHAs-based electrospun mats. *React. Funct. Polym.* **2015**, *89*, 18–23. [CrossRef]
72. Yu, B.-Y.; Chen, P.-Y.; Sun, Y.-M.; Lee, Y.-T.; Young, T.-H. Response of human mesenchymal stem cells (hMSCs) to the topographic variation of poly(3-hydroxybutyrate-co-3-hydroxyhexanoate) (PHBHHx) films. *J. Biomater. Sci. Polym. Ed.* **2012**, *23*, 1–26. [CrossRef]
73. Tong, H.-W.; Wang, M. Electrospinning of aligned biodegradable polymer fibers and composite fibers for tissue engineering applications. *J. Nanosci. Nanotechnol.* **2007**, *7*, 3834–3840. [CrossRef]
74. Tong, H.-W.; Wang, M.; Lu, W.W. Electrospun poly(hydroxybutyrate-co-hydroxyvalerate) fibrous membranes consisting of parallel-aligned fibers or cross-aligned fibers: Characterization and biological evaluation. *J. Biomater. Sci. Polym. Ed.* **2011**, *22*, 2475–2497. [CrossRef]
75. Wang, Y.; Gao, R.; Wang, P.-P.; Jian, J.; Jiang, X.-L.; Yan, C.; Lin, X.; Wu, L.; Chen, G.-Q.; Wu, Q. The differential effects of aligned electrospun phbhhx fibers on adipogenic and osteogenic potential of mscs through the regulation of pparγ signaling. *Biomaterials* **2012**, *33*, 485–493. [CrossRef]
76. Volova, T.; Goncharov, D.; Sukovatyi, A.; Shabanov, A.; Nikolaeva, E.; Shishatskaya, E. Electrospinning of polyhydroxyalkanoate fibrous scaffolds: Effects on electrospinning parameters on structure and properties. *J. Biomater. Sci. Polym. Ed.* **2014**, *25*, 370–393. [CrossRef]
77. Arslantunali, D.; Dursun, T.; Yucel, D.; Hasirci, N.; Hasirci, V. Peripheral nerve conduits: Technology update. *Med. Devices (Auckl.)* **2014**, *7*, 405–424.
78. Awad, N.K.; Niu, H.; Ali, U.; Morsi, Y.S.; Lin, T. Electrospun fibrous scaffolds for small-diameter blood vessels: A review. *Membranes* **2018**, *8*, 15. [CrossRef]
79. Standard F2792-12a. *Standard terminology for additive manufacturing technologies (Withdrawn 2015)*; ASTM International: West Conshohocken, PA, USA, 2012.
80. Mota, C.; Puppi, D.; Chiellini, F.; Chiellini, E. Additive manufacturing techniques for the production of tissue engineering constructs. *J. Tissue Eng. Regen. Med.* **2015**, *9*, 174–190. [CrossRef] [PubMed]

81. Chartrain, N.A.; Williams, C.B.; Whittington, A.R. A review on fabricating tissue scaffolds using vat photopolymerization. *Acta Biomater.* **2018**, *74*, 90–111. [CrossRef] [PubMed]
82. Williams, J.M.; Adewunmi, A.; Schek, R.M.; Flanagan, C.L.; Krebsbach, P.H.; Feinberg, S.E.; Hollister, S.J.; Das, S. Bone tissue engineering using polycaprolactone scaffolds fabricated via selective laser sintering. *Biomaterials* **2005**, *26*, 4817–4827. [CrossRef] [PubMed]
83. Butscher, A.; Bohner, M.; Hofmann, S.; Gauckler, L.; Müller, R. Structural and material approaches to bone tissue engineering in powder-based three-dimensional printing. *Acta Biomater.* **2011**, *7*, 907–920. [CrossRef] [PubMed]
84. Turner, B.N.; Strong, R.; Gold, S.A. A review of melt extrusion additive manufacturing processes: I. Process design and modeling. *Rapid Prototyp. J.* **2014**, *20*, 192–204. [CrossRef]
85. Puppi, D.; Chiellini, F. Wet-spinning of biomedical polymers: From single-fibre production to additive manufacturing of three-dimensional scaffolds. *Polym. Int.* **2017**, *66*, 1690–1696. [CrossRef]
86. Puppi, D.; Morelli, A.; Bello, F.; Valentini, S.; Chiellini, F. Additive manufacturing of poly(methyl methacrylate) biomedical implants with dual-scale porosity. *Macromol. Mater. Eng.* **2018**, *303*, 1800247. [CrossRef]
87. Oliveira, M.F.; Maia, I.A.; Noritomi, P.Y.; Nargi, G.C.; Silva, J.V.L.; Ferreira, B.M.P.; Duek, E.A.R. Construção de scaffolds para engenharia tecidual utilizando prototipagem rápida. *Matéria* **2007**, *12*, 373–382. [CrossRef]
88. Pereira, T.F.; Silva, M.A.C.; Oliveira, M.F.; Maia, I.A.; Silva, J.V.L.; Costa, M.F.; Thiré, R.M.S.M. Effect of process parameters on the properties of selective laser sintered poly(3-hydroxybutyrate) scaffolds for bone tissue engineering. *Virtual Phys. Prototyp.* **2012**, *7*, 275–285. [CrossRef]
89. Pereira, T.F.; Oliveira, M.F.; Maia, I.A.; Silva, J.V.L.; Costa, M.F.; Thiré, R.M.S.M. 3d printing of poly(3-hydroxybutyrate) porous structures using selective laser sintering. *Macromol. Symp.* **2012**, *319*, 64–73. [CrossRef]
90. Duan, B.; Wang, M.; Zhou, W.Y.; Cheung, W.L.; Li, Z.Y.; Lu, W.W. Three-dimensional nanocomposite scaffolds fabricated via selective laser sintering for bone tissue engineering. *Acta Biomater.* **2010**, *6*, 4495–4505. [CrossRef] [PubMed]
91. Duan, B.; Wang, M. Customized Ca–P/PHBV nanocomposite scaffolds for bone tissue engineering: Design, fabrication, surface modification and sustained release of growth factor. *J. R. Soc. Interface* **2010**, *7*, S615–S629. [CrossRef] [PubMed]
92. Duan, B.; Cheung, W.L.; Wang, M. Optimized fabrication of Ca–P/PHBV nanocomposite scaffolds via selective laser sintering for bone tissue engineering. *Biofabrication* **2011**, *3*, 015001. [CrossRef] [PubMed]
93. Kosorn, W.; Sakulsumbat, M.; Uppanan, P.; Kaewkong, P.; Chantaweroad, S.; Jitsaard, J.; Sitthiseripratip, K.; Janvikul, W. PCL/PHBV blended three dimensional scaffolds fabricated by fused deposition modeling and responses of chondrocytes to the scaffolds. *J. Biomed. Mater. Res. B Appl. Biomater.* **2017**, *105B*, 1141–1150. [CrossRef] [PubMed]
94. Mota, C.; Wang, S.Y.; Puppi, D.; Gazzarri, M.; Migone, C.; Chiellini, F.; Chen, G.Q.; Chiellini, E. Additive manufacturing of poly[(r)-3-hydroxybutyrate-co-(r)-3-hydroxyhexanoate] scaffolds for engineered bone development. *J. Tissue Eng. Regen. Med.* **2017**, *11*, 175–186. [CrossRef]
95. Menčík, P.; Přikryl, R.; Stehnová, I.; Melčová, V.; Kontárová, S.; Figalla, S.; Alexy, P.; Bočkaj, J. Effect of selected commercial plasticizers on mechanical, thermal, and morphological properties of poly(3-hydroxybutyrate)/poly(lactic acid)/plasticizer biodegradable blends for three-dimensional (3d) print. *Materials* **2018**, *11*, 1893. [CrossRef]
96. Wu, C.-S.; Liao, H.-T.; Cai, Y.-X. Characterisation, biodegradability and application of palm fibre-reinforced polyhydroxyalkanoate composites. *Polym. Degrad. Stab.* **2017**, *140*, 55–63. [CrossRef]
97. Wu, C.-S.; Liao, H.-T. Fabrication, characterization, and application of polyester/wood flour composites. *J. Polym. Eng.* **2017**, *37*, 689–698. [CrossRef]
98. Wu, C.S.; Liao, H.T. Interface design of environmentally friendly carbon nanotube-filled polyester composites: Fabrication, characterisation, functionality and application. *Express Polym. Lett.* **2017**, *11*, 187–198. [CrossRef]
99. Puppi, D.; Mota, C.; Gazzarri, M.; Dinucci, D.; Gloria, A.; Myrzabekova, M.; Ambrosio, L.; Chiellini, F. Additive manufacturing of wet-spun polymeric scaffolds for bone tissue engineering. *Biomed. Microdevices* **2012**, *14*, 1115–1127. [CrossRef]
100. Puppi, D.; Pirosa, A.; Morelli, A.; Chiellini, F. Design, fabrication and characterization of tailored poly[(r)-3-hydroxybutyrate-*co*-(r)-3-hydroxyexanoate] scaffolds by computer-aided wet-spinning. *Rapid Prototyp. J.* **2018**, *24*, 1–8. [CrossRef]

101. Puppi, D.; Morelli, A.; Chiellini, F. Additive manufacturing of poly(3-hydroxybutyrate-co-3-hydroxyhexanoate) /poly(ε-caprolactone) blend scaffolds for tissue engineering. *Bioengineering* **2017**, *4*, 49. [CrossRef] [PubMed]
102. Puppi, D.; Pirosa, A.; Lupi, G.; Erba, P.A.; Giachi, G.; Chiellini, F. Design and fabrication of novel polymeric biodegradable stents for small caliber blood vessels by computer-aided wet-spinning. *Biomed. Mater.* **2017**, *12*, 035011. [CrossRef] [PubMed]
103. Koller, M.; Maršálek, L.; de Sousa Dias, M.M.; Braunegg, G. Producing microbial polyhydroxyalkanoate (PHA) biopolyesters in a sustainable manner. *New Biotechnol.* **2017**, *37*, 24–38. [CrossRef]

MDPI
St. Alban-Anlage 66
4052 Basel
Switzerland
Tel. +41 61 683 77 34
Fax +41 61 302 89 18
www.mdpi.com

Bioengineering Editorial Office
E-mail: bioengineering@mdpi.com
www.mdpi.com/journal/bioengineering

MDPI
St. Alban-Anlage 66
4052 Basel
Switzerland

Tel: +41 61 683 77 34
Fax: +41 61 302 89 18

www.mdpi.com

ISBN 978-3-03928-641-6